Reversal of Centrosome Amplification to Reduce Oncogenicity of Metastatic Uveal Melanoma

by
Kim Jadwiga Fabian-Kolpanowicz

PhD Thesis in Biomedical and Life Sciences

Lancaster University
Faculty of Health and Medicine
Biomedical Life Sciences

May 2023

Declaration

I declare that the content of this thesis is my own work and has not been submitted by myself in substantially the same form for the award of a higher degree elsewhere. Any sections of the thesis which have been published have been clearly identified.

Kim J Fabian-Kolpanowicz

Acknowledgements

Firstly, I am sincerely grateful for the help and opportunities provided by my supervisor Dr. Andrew Fielding. Thank you for all of your input and encouragement with experiments, and for being so enthusiastic about the results I showed you. Thank you additionally for your patient and understanding approach, which was so helpful. I'm also indebted to my secondary supervisor Dr. Elaine Taylor, for providing a useful and experienced perspective to the process, as well as some excellent advice on my thesis. I must also thank the Mort lab for their collaboration with FUCCI cell lines, especially to Dr. Richard Mort for taking the time to advise me regarding image analysis. None of this work would have been possible without the generous funding from North West Cancer Research: thank you.

Next I'd like to thank my lab mates: Dr. Amanda Thomas, Dr. Marine Aublette and Lauryn Buckley-Benbow. My PhD started in a slightly lonely lab and it was welcome to gain some good company! Thank you for the cheers when experiments went right, and for the commiserations and suggestions when they went wrong.

My experience at Lancaster would have been all the poorer without the company of the other PhD students in the department, thank you for the light relief from work during entertaining lunch room chats. Special thanks to Dr. James Tollitt, Dr. Marine Aublette and Jack Martin for the (sometimes crazy) runs, bouldering and trips to the pub. I'm also thankful for the friendship of fellow tea enthusiast Wayne Gould, especially for all of those socially distanced walks in the midst of Covid restrictions.

Thank you to my family: my mum, dad, Nell and Danusia for cheering me on. You always believed in me, even when I didn't. Thank you to my boyfriend, Jordan Simcoe, for making that long drive between Loughborough and Lancaster so many times! Looking forwards to seeing you at the weekends kept me going whenever I was having a bad week, and it's been so nice to finally live together once I started writing up.

Lastly, thank you to my cat, Kitty, for keeping me company in the office and trying to edit my thesis by walking all over the keyboard. His edits were not included in the final text.

List of Figures

Figure 1-1. Diagram of centrosome structure. 2
Figure 1-2. Centrosome duplication cycle. 3
Figure 1-3. Routes to centrosome amplification. 9
Figure 1-4. Potential coping mechanisms for cells with centrosome amplification. 13
Figure 1-5. Diagram of Uveal Melanoma molecular subgroups. 17
Figure 1-6. A summary of the oncogenic and targetable features of cells with centrosome amplification. 18
Figure 2-1. Example images of the Trackmate cell tracking process. 26
Figure 3-1. Origins of Mel270, OMM2.3 and OMM2.5 cells. 44
Figure 3-2. Investigation into centrosome amplification in uveal melanoma cells. 48
Figure 3-3. OMM2.3 and OMM2.5 cells, but not Mel270 cells, display high levels of centrosome amplification. 50
Figure 3-4. RNA integrity measured by Agilent Bioanalyser 2100. 52
Figure 3-5. RNA sequencing of uveal melanoma cells. 54
Figure 3-6. Volcano plot of longlist genes. 56
Figure 3-7. Ct variation in potential reference genes. 61
Figure 3-8. Comparison of RNA-Seq results to qPCR results. 62
Figure 3-9. Mel270, OMM2.3 and OMM2.5 cells express wild type p53. 63
Figure 3-10. Expression of shortlist genes in NCI-60 cells with and without CA. 64
Figure 4-1. Validation of knock down of PLK4 and KIFC1 by reverse siRNA transfection 73
Figure 4-2. Optimisation of staining panel for siRNA screen. 75
Figure 4-3. Optimisation of seeding density for siRNA screen. 76
Figure 4-4. Optimisation of image acquisition for siRNA screen. 78
Figure 4-5. Comparison of image analysis workflows 81
Figure 4-6. Workflow of siRNA screen. 83
Figure 4-7. Results from the siRNA screen 85
Figure 4-8. Knockdown of Aurora A or HSP90B1 reduces CA score in OMM2.3 cells. 87
Figure 4-9. Aurora A and HSP90B1 mRNA expression in siAuroraA and siHSP90B1 treated OMM2.3 cells. 88
Figure 5-1. Aurora A and HSP90B1 protein expression in Mel270, OMM2.3 and OMM2.5 cells. 101
Figure 5-2. Cell cycle populations of siAuroraA and siHSP90B1 treated OMM2.3 cells. 103
Figure 5-3. Protein recovery of Aurora A and HSP90B1 after siRNA treatment. 106

Figure 5-4. Matched mRNA and protein expression of Aurora A and HSP90B1 after siRNA treatment. 109
Figure 5-5. FUCCI-CLIF: Live imaging scratch-immunofluorescence assay with H2B-FUCCI2a transfected cells. 112
Figure 5-6. Mean straight line speed of FUCCI2a-OMM2.3 cells. 114
Figure 5-7. Migration of OMM2.3 cells with and without centrosome amplification. 116
Figure 6-1. Possible routes to reversal of centrosome amplification. 125
Figure 6-2. Multiparametric data available from FUCCI-CLIF analysis 129
Figure 6-3. Proposed model for development and reversal of centrosome amplification. 132

List of Tables

Table 2-1. Primary antibodies used for immunofluorescence staining. 23
Table 2-2. Secondary antibodies used for immunofluorescence staining. 23
Table 2-3. Primers used for PCR assays. 30
Table 2-4. Primers used for TP53 sequencing. 33
Table 2-5. Cycling conditions for p53 sequencing primers. 34
Table 2-6. Primary antibodies used for western blotting. 38
Table 2-7. Secondary antibodies used for western blotting. 39
Table 2-8. Blocking and diluent solutions used for western blotting. 39
Table 3-1. RNA extracts for sequencing. 51
Table 3-2. A list of shortlisted genes to be included in an siRNA screen to identify drivers of centrosome amplification in OMM2.3 cells. 60
Table 4-1. Image acquisition settings tested for siRNA screen. 77
Table 4-2. Methods to count nuclei and pericentrin foci. 79
Table 5-1. Comparison of G2 populations in siRNA treated cells as determined by cyclin B1 immunofluorescence staining and propidium iodide flow cytometry. 104

List of Abbreviations

+ve - Positive

°C - Degrees Celsius

µg - Micrograms

µL - Microlitres

µm - Micrometre

µM - Micromolar

A - Amps

ACTB - Actin B

ALS - Alisertib

AML - Acute myeloid leukaemia

ANKRD26 - Ankyrin Repeat Domain Containing 26

ANOVA - Analysis of variance

APC - Anaphase promoting complex

APS - Ammonium persulfate

AURKA - Aurora A

BANCR - BRAF-Activated Non-Protein Coding RNA

BAP1 - BRCA1 associated protein-1

BCA - Bicinchonic acid

BET - Bromodomain and Extra-Terminal motif

bp - Base pair

BRAF - B-Raf Proto-Oncogene, Serine/Threonine Kinase

BSA - Bovine serum albumen

C.I. - Confidence interval

C2CD3 - C2 Domain Containing 3 Centriole Elongation Regulator

CA - Centrosome amplification

Ca^{2+} - Calcium ion

CAMK2A - Calcium/Calmodulin Dependent Protein Kinase II Alpha

CAMK2D - Calcium/Calmodulin Dependent Protein Kinase II Delta

CAPNS1 - Calpain Small Subunit 1

CCNB1 - Cyclin B1

CCND1 - Cyclin D1

Cdh1 - Fizzy And Cell Division Cycle 20 Related 1, *also known as FZR1*

CDK1 - Cyclin dependent kinase 1

CDK2 - Cyclin dependent kinase 2

CDK5RAP2 - CDK5 Regulatory Subunit Associated Protein 2

cDNA - copy DNA

Cdt1 - Chromatin licensing and DNA replication factor 1

CEP120 - Centrosomal protein of 120 kDa

CEP135 - Centrosomal protein of 135 kDa

CEP152 - Centrosomal protein of 152 kDa

CEP63 - Centrosomal protein of 63 kDa

CEP97 - Centrosomal protein of 97 kDa

CHK2 - Checkpoint kinase 2

CK1α - Casein kinase 1α

CLEM - Correlative light and electron microscopy

cm - Centimetre

C-Nap1 - Centrosomal protein of 250 kDa

CP110 - Centriolar coiled-coil protein of 110 kDa

CPAP - Centromere protein J

Ct - Threshold cycle

CYSLTR2 - Cysteinyl Leukotriene Receptor 2

D3-UM - Disomy 3 uveal melanoma

DA - Distal appendage

DAM - Distal appendage matrix

DAPI - 4',6-diamidino-2-phenylindole

DEG - Differentially expressed gene

DMSO - Dimethyl sulfoxide

DNA - deoxyribonucleic acid

DNase - Deoxyribonuclease

dsDNA - Double stranded DNA

DTT - Dithiothreitol

E2F1 - E2F Transcription Factor 1

ECM - Extracellular matrix

EDTA - Ethylenediaminetetraacetic acid

Eg5 - Kinesin-related motor protein Eg5, *also known as KIF11*

EIF1AX - Eukaryotic Translation Initiation Factor 1A X-Linked

ER - Endoplasmic reticulum

FAM83D - Family With Sequence Similarity 83 Member D

FBS - Foetal bovine serum

FBXW5 - F-Box And WD Repeat Domain Containing 5

FIJI - Fiji is just ImageJ

FOXA1 - Forkhead box protein A1

FOXM1 - Forkhead box protein M1

FOXP1 - Forkhead box protein P1

FPKM - Fragments per kilobase of transcript per million mapped reads

FUCCI - Fluorescent ubiquitin based cell cycle indicator

FUCCI-CLIF - FUCCI-Correlative Live imaging and Immunofluorescence

Fwd - Forwards

g - Gravitational force

G1 - Gap 1 phase

G2 - Gap 2 phase

GADD45a - Growth Arrest And DNA Damage Inducible Alpha

GAPDH - Glyceraldehyde-3-Phosphate Dehydrogenase

gDNA - Genomic DNA

Gem - Geminin

GFP - Green fluorescent protein

GNA11 - G Protein Subunit Alpha 11

GNAQ - G Protein Subunit Alpha Q

GO - Gene ontology

H2B - Histone H2B

HER2 - Human epidermal growth factor receptor 2

HSP90 - Heat shock protein 90

HSP90AA1 - Heat Shock Protein 90 Alpha Family Class A Member 1

HSP90AA2 - Heat Shock Protein 90 Alpha Family Class A Member 2

HSP90AB1 - Heat Shock Protein 90 Alpha Family Class B Member 1

HSP90B1 - Heat Shock Protein 90 Beta Family Member 1

HSPA6 - Heat Shock Protein Family A member 6

HSPA7 - Heat Shock Protein Family A member 7

HSPA8 - Heat Shock Protein Family A member 8

IARC - International Agency for Research on Cancer

iGRP94 - GRP94 Inhibitor-1

IL-8 - Interleukin 8

IP3 - Inositol 1,4,5-trisphosphate

IU - International unit

kb - Kilobase

kDa - Kilodalton

KID - Kinesin Family Member 22, *also known as KIF22*

KIFC1 - Kinesin Family Member C1

M - Mitosis

M - Molar

M3-UM - Monosomy 3 uveal melanoma

mAmp - Milliamps

MAPK - Mitogen-activated protein kinase

MDM2 - Mouse double minute 2 homolog

mg - Milligrams

MGW - Molecular grade water

mL - Millilitres

mM - Millimolar

mRNA - Messenger RNA

MSLS - Mean straight line speed

MT - Microtubule

MTS - [3-(4,5-dimethylthiazol-2-yl)-5-(3-carboxymethoxyphenyl)-2-(4-sulfophenyl)-2H-tetrazolium]

MYC - MYC Proto-Oncogene, BHLH Transcription Factor

NaN3 - Sodium azide

NaOH - Sodium hydroxide

NCI - National Cancer Institute

NEK2A - NIMA Related Kinase 2

ng - Nanogram

NIN - Ninein

nm - Nanometre

nM - Nanomolar

NPM1 - Nucleophosmin 1

nt - Nucleotide

OFD1 - Oral-Facial-Digital Syndrome 1 Protein

OFD2 - Oral-Facial-Digital Syndrome 2 Protein

p21 - Cyclin Dependent Kinase Inhibitor 1A, *also known as CDKN1A*

p53/TP53 - Cellular tumour antigen p53

padj - Adjusted p value

PAGE - Polyacrylamide gel electrophoresis

PBS - Phosphate buffered saline

PCM - Pericentriolar material

PCR - Polymerase chain reaction

pHH3 - Phospho-histone H3

PI - Propidium iodide

PIDD1 - p53-induced death domain-containing protein 1

PIK3 - Phosphoinositide 3-kinase

PLCB4 - Phospholipase C Beta 4

PLK1 - Polo like kinase 1

PLK4 - Polo like kinase 4

POC5 - Protein of centriole 5

PPP1R14C - Protein Phosphatase 1 Regulatory Inhibitor Subunit 14C

PPP4R2 - Protein Phosphatase 4 Regulatory Subunit 2

PRKACB - Protein Kinase CAMP-Activated Catalytic Subunit Beta

QC - Quality control

qPCR - Quantitative PCR

Rac1 - Rac Family Small GTPase 1

Ran-BP1 - RAN Binding Protein 1

Rap1 - Ras-related protein 1

Rev - Reverse

RIN - RNA integrity score

RNA - Ribonucleic acid

RNase - Ribonuclease

RNA-Seq - RNA sequencing

ROI - Region of interest

ROS - Reactive oxygen species

rpm - Revolutions per minute

RPMI - Roswell Park Memorial Institute

RPS11 - Ribosomal Protein S11

S - Synthesis phase

SAK - Serine/threonine-protein kinase PLK4

SAS-4 - Spindle assembly abnormal protein 4

SAS-6 - Spindle assembly abnormal protein 6 homolog

SCF - Skp1–Cullin–F-box protein

SD - Standard deviation

SDA - Subdistal appendage

SDS - Sodium dodecyl sulfate

SF3B1 - Splicing Factor 3b Subunit 1

siAA - Aurora A siRNA

siCon - Control siRNA

siH - HSP90B1 siRNA

siKIFC1 - KIFC1 siRNA

siRNA - Small interfering ribonucleic acid

Skp2 - S-phase kinase-associated protein 2

SNP - Single nucleotide polymorphism

SPICE1 - Spindle And Centriole Associated Protein 1

SRFF2 - Serine and arginine rich splicing factor 2

SRPR - Signal recognition particle receptor

ssRNA - Single stranded RNA

STIL - SCL-interrupting locus, *also known as SIL*

STR - Short tandem repeat

TACC2 - Transforming Acidic Coiled-Coil Containing Protein 2

TACC3 - Transforming Acidic Coiled-Coil Containing Protein 3

TAE - Tris-acetate-EDTA

TBST - Tris buffered saline Tween 20

TCGA - The cancer genome atlas

TEMED - Tetramethylethylenediamine

TRAP-1 - TNFR-associated protein 1

TTK - TTK protein kinase, *also known as MPS1*

UM - Uveal melanoma

USP33 - Ubiquitin specific peptidase 33

UTR - Untranslated region

UV - Ultraviolet

V - Volts

v/v - Volume for volume

-ve - Negative

w/v - Weight for volume

WDR62 - WD repeat domain 62

WT - Wild type

γ-TuRC - Gamma tubulin ring complex

Abstract

Centrosome amplification (CA), whereby cells have more than the normal number of centrosomes, is a common feature amongst aggressive cancers with a poor prognosis. CA drives oncogenic phenotypes such as increased invasiveness (via both cell-autonomous and non-cell-autonomous mechanisms) and chromosomal instability. In addition, CA can initiate tumourigenesis in flies and mice, and can drive advanced tumourigenic traits early on that promote disease progression. We hypothesise that reversal of CA may reverse CA-driven oncogenic phenotypes and therefore might be a new way to target aggressive cancers with a poor prognosis.

This thesis presents the use of three patient-matched uveal melanoma (UM) cell lines as a new model to study CA that has developed in a patient setting. Mel270 cells were derived from a primary tumour and have negligible CA. OMM2.3 and OMM2.5 cells were derived from distinct liver metastases from the same patient and have high levels of CA. Primary UM can be well managed, however ~50% patients develop metastatic disease, for which there is no curative treatment and 1 year survival rates are ~50%, so there is a need to develop new therapies to target metastatic UM.

Using RNA-Seq, genes that were differentially expressed in metastasis versus primary derived cells were selected for an siRNA screen to identify genes with a role in CA. Knockdown of either Aurora A or HSP90B1 induced a consistent reduction of CA in OMM2.3 cells. It is believed that Aurora A and HSP090B1 have independent effects on CA, as depleting either Aurora A or HSP90B1 using siRNAs did not affect the RNA or protein levels of the other. A new assay combining live imaging of migrating cells and immunofluorescence was developed and used, which we call FUCCI-CLIF (**F**luorescent **U**biquitination based **C**ell **C**ycle **I**ndicator - **C**orrelative **L**ive imaging and **I**mmuno**f**luorescence). FUCCI-CLIF provides insight into cell migration, cell cycle and CA status. Knockdown of Aurora A or HSP90B1 reduced migration as calculated by mean straight line speed. Further investigation indicated this was a non-cell-autonomous effect on cell migration.

Ultimately, the work presented suggests that depleting or inhibiting proteins required for CA in a cancer specific setting reverses CA and concomitantly reduces oncogenic properties of aggressive metastatic UM cells, and is therefore a much needed new potential therapeutic approach against metastatic UM.

Table of Contents

Declaration.....i

Acknowledgements.....ii

List of Figures.....iii

List of Tables.....v

List of Abbreviations.....vi

Abstract.....xv

Chapter 1. General Introduction 1

1.1. Centrosomes 2

1.2. Centrosome Replication Cycle 3

1.3. Centrosome Amplification 6

1.4. Routes to Centrosome Amplification 6

1.4.1. Centriole Over-duplication 6

1.4.2. Failed Cytokinesis 7

1.4.3. *De novo* Synthesis 7

1.4.4. Centriole Over-elongation 8

1.4.5. The Role of p53 in Centrosome Amplification 9

1.5. Oncogenic Characteristics Induced by Centrosome Amplification 10

1.5.1. Chromosomal Instability 10

1.5.2. Invasiveness 10

1.5.3. Defects in Asymmetric Divisions of Stem Cells 11

1.6. Cancer Development 11

1.7. Targeting Cells with Centrosome Amplification 12

1.7.1. Centrosome Amplification Coping Mechanisms 12

1.7.2. Centrosome Clustering 13

1.7.3. Reversal of Centrosome Amplification 14

1.7.4. Reversing Centrosome Amplification in Aggressive Tumour Types 14

1.7.5. Centrosome Amplification Signature 14
1.8. Uveal Melanoma 15
1.9. Aims 17
Chapter 2. Methods and Materials 20
2.1. Tissue Culture 21
2.1.1. General Tissue Culture 21
2.1.2. Cell Stock Cryopreservation and Revival 21
2.1.3. Cell Line Authentication and Mycoplasma Screens 21
2.1.4. Generation of H2B-FUCCI2a Cell Lines 22
2.2. Immunofluorescence Staining 22
2.3. Confocal Microscopy and Image Analysis 23
2.3.1. Initial Centrosome Amplification Incestigation 24
2.3.2. Centrosome Amplification Quantification in Mitotic Cells 24
2.3.3. Centrosome Amplification Score 24
2.3.4. Migration Analysis of H2B-FUCCI2a Cells 25
2.4. Transwell Assays 27
2.5. Extraction of RNA from Cell Pellets 27
2.5.1. Quality Control: Nanodrop and Agilent Bioanalyser 28
2.5.2. RNA Sequencing and Analysis 29
2.6. PCR 29
2.6.1. cDNA Synthesis 29
2.6.2. Primer Design 29
2.6.3. Conventrional PCR 30
2.6.4. qPCR 31
2.6.4.1. Master Mix Preparation 31
2.6.4.2. Thermocycling 31
2.6.4.3. Analysis 31
2.7. Sequencing TP53 in Uveal Melanoma Cell Lines 32

2.7.1. Genomic DNA Extraction 32
2.7.2. PCR Amplification of TP53 32
2.7.3. Sequencing 35
2.7.4. Sequence Analysis 35
2.8. Flow Cytometry 35
2.8.1. Cell Fixation 35
2.8.2. Propidium Iodide Staining and Flow Cytometry 35
2.8.3. Analysis 36
2.9. Western Blots 36
2.9.1. Hot Laemelli Lysis of Cells 36
2.9.2. BCA Assay 36
2.9.3. SDS-PAGE and Western Blot 37
2.9.3.1. Gel Preparation 37
2.9.3.2. Sample Preparation 37
2.9.3.3. Gel Electrophoresis 37
2.9.3.4. Western Blotting 37
2.9.3.5. Image Analysis 39
2.10. Aurora A and HSP90B1 Inhibitors 39
2.10.1. MTS Assay 40
2.11. siRNA Transfection 40
2.11.1. Forwards Transfection 40
2.11.2. Reverse Transfection 41
2.11.3. siRNA Screen 41
2.12. Statistical Analysis 42
Chapter 3. Characterisation of Centrosome Amplification in Patient Matched Primary and Metastatic Uveal Melanoma Cells Followed by Transcriptiomics Comparison to Identify Drivers of Centrosome Amplification 43
3.1. Introduction 44

3.1.1. Mel270, OMM2.3 and OMM2.5 Cells: A Patient Matched Cell Line Model of Uveal Melanoma Disease Progression 45
3.1.2. The Use of 'omics Technologies to Study Cancer 45
3.1.2.1. RNA Sequencing versus Proteomics 46
3.1.2.2. RNA Sequencing Workflow 46
3.1.3. Chapter Aims 47
3.2. Centrosome Amplification in Uveal Melanoma Cell Lines 47
3.3. RNA Sequencing 50
3.3.1. Preparation of Samples for RNA Sequencing 51
3.3.2. Differentially Expressed Genes 52
3.3.2.1. RNA Expression Correlation 55
3.4. Selecting Genes for an siRNA Screen 55
3.5. Confirmation of RNA Sequencing Results by qPCR 61
3.6. TP53 Sequencing 63
3.7. Wider Relevance of siRNA Screen 63
3.8. Chapter Discussion 64
Chapter 4. Knockdown of Aurora A or HSP90B1 Reduces Centrosome Amplification in OMM2.3 Cells 69
4.1. Introduction 70
4.1.1. Design Features of an siRNA Screen 70
4.1.2. Chapter Aims 71
4.2. Reverse siRNA Transfection 72
4.3. Imaging and Analysis Optimisation 73
4.3.1. Immunofluorescent Staining Panels 74
4.3.2. Seeding Density 75
4.3.3. Image Acquisition 76
4.4. Development of an Image Analysis Workflow 78
4.4.1. Common Steps in the Analysis Workflow 80
4.4.2. Comparison of Analysis Workflows 80

4.5. siRNA Screen to Identify Genes with a Role in Centrosome Amplification 82
4.5.1. Deconvolution of siRNA Pools 86
4.5.2. Selection of siRNAs for Aurora A and HSP90B1 by qPCR 88
4.6. Chapter Discussion 89
Chapter 5. Characterisation of Centrosome Amplification-reversed OMM2.3 Cells 97
5.1. Introduction 98
5.1.1. FUCCI Biosensors 98
5.2. Aurora A and HSP90B1 Protein Expression in Mel270, OMM2.3 and OMM2.5 Cells 99
5.3. Aurora A Knockdown increases G2, 4n+ and 8N populations in OMM2.3 Cells 102
5.4. Aurora A and HSP90B1 Protein Recovery After siRNA Knockdown 104
5.5. Matched mRNA and Protein Expression of Aurora A and HSP90B1 After siRNA Knockdown 107
5.6. Cell Migration in OMM2.3-H2B-FUCCI2a Cells After Aurora A or HSP90B1 Knockdown or Inhibition 110
5.6.1. FUCCI-Correlative Live and Immunofluorescent Microscopy Assay Development 110
5.6.2. Experimental Setup 113
5.6.3. siRNA Knockdown or Aurora A or HSP90B1 Reduces Mean Straight Line Speed of the Fastest Cells 113
5.6.4. Migration is Affected More by siRNA Knockdown of Aurora A than by Individual Centrosome Amplification Status of Cells 115
5.7. Chapter Discussion 117
Chapter 6. General Discussion 122
6.1. Recap of Study Aims and Findings 123
6.2. The Role of Aurora A in Centrosome Amplification 127
6.3. The Role of HSP90B1 in Centrosome Amplification 127
6.4. FUCCI-CLIF: A Novel Assay to Study Cell Behaviour 128
6.5. Therapeutic Potential of Targeting Aurora A or HSP90B1 129

6.6. Targeting Centrosome Amplification in Uveal Melanoma.....130

6.7. Proposed Model for Centrosome Amplification Reversal Through Aurora A or HSP90B1 Inhibition 131

6.8. Concluding Remarks.....132

References.....134

Appendices.....173

Chapter 1.

General Introduction

1.1. Centrosomes

Centrosomes are the dominant microtubule organising centres in animal cells (Blanco-Ameijeiras et al., 2022). They consist of two barrel shaped centrioles, held together at a perpendicular angle, which are surrounded by a matrix of proteins called the pericentriolar material (PCM) (Fry et al., 2017; Loncarek & Bettencourt-Dias, 2018). Centrioles are made from 27 γ-tubulin filaments, arranged into 9 bundles of three creating a 9-fold symmetry (Figure 1-1). A centrosome contains a mature mother centriole, and a newer daughter centriole that will have been newly synthesised during the previous cell cycle (Blanco-Ameijeiras et al., 2022). Mother centrioles are decorated with distal and subdistal appendage proteins. Centrosomes are a major hub for signal transduction in the cell (Nigg & Stearns, 2011), play a role in cell polarity (Nigg & Raff, 2009), and are responsible for organising the mitotic spindle in mitosis (Meraldi, 2016).

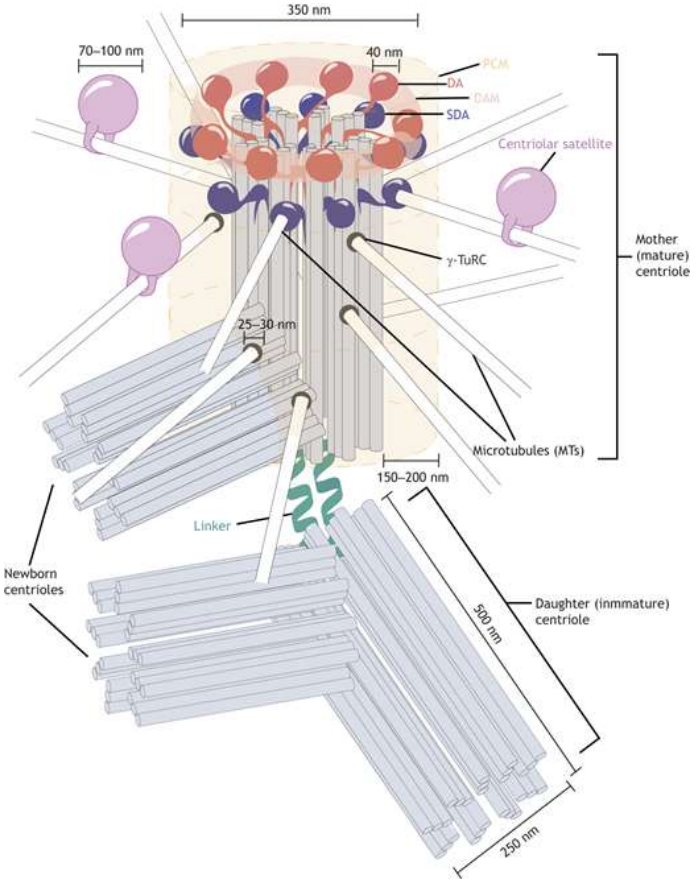

Figure 1-1. Diagram of centrosome structure.
Centrosomes have two main components: centrioles and pericentriolar material (PCM). Centrioles are made up of nine triplets of tubulin filaments, creating a 9-fold symmetry. The mother centriole has distal appendages (DA), a distal appendage matrix (DAM) and sub-distal appendages (SDA); the daughter centriole does not have these features. Pro-centrioles, also known as newborn centrioles, form perpendicular to the proximal end of existing centrioles. The mother and daughter centrioles are held together by interconnecting fibres, also known as linker proteins: C-NAP1 and Rootletin. The PCM is a dense collection of proteins, including γ-tubulin ring complexes (γ-TuRCs) and pericentrin. Image reproduced with permission from Blanco-Ameijeiras et al., 2022.

1.2. Centrosome Replication Cycle

Cells begin the cell cycle with one centrosome and, during the cell cycle, the centrosome must be replicated exactly once so that when the cell comes to divide, there are two centrosomes to organise a bipolar mitotic spindle (Figure 1-2). Centrosome replication is a tightly regulated process with five main steps: centriole disengagement, procentriole formation, procentriole elongation, centrosome maturation and centrosome separation (Blanco-Ameijeiras et al., 2022; Nigg & Holland, 2018).

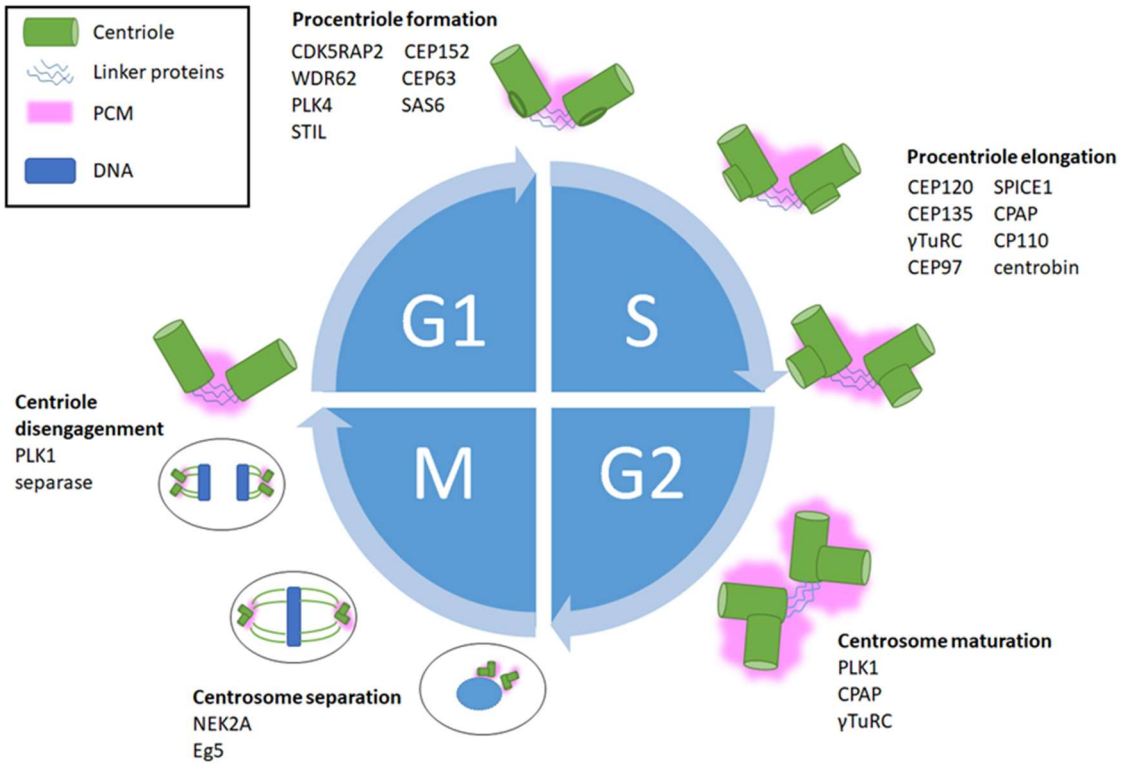

Figure 1-2. Centrosome duplication cycle.
As the cell exits mitosis, the two centrioles disengage so they are no longer directly connected and are instead held together by a proteinaceous linker. At G1/S, a single site on the proximal end of each mother centriole is established for the procentriole to form. Throughout S and G2, the procentriole elongates and eventually acquires PCM. The cell now has two centrosomes, each containing a mother and a daughter centriole. As the cell enters mitosis, the tether holding the two centrosomes together is disassembled, and the centrosomes migrate to either pole of the cell and form the mitotic spindle. The PCM is illustrated as an amorphous aggregate in this figure, however in reality the PCM is a highly ordered structure. From S phase onwards, the PCM is mainly organised around the mother centriole. As the centrosome cycle progresses, the PCM expands and the new daughter centriole gains PCM in G2, ready for the onset of mitosis. After mitosis, the volume of PCM decreases again. Key proteins required for the five steps of centrosome duplication are listed.

In late mitosis to G1, PLK1 and separase activity allows the two centrioles to disengage (Fu et al., 2015; Gönczy & Hatzopoulos, 2019). One mechanism by which this process is regulated is via the APC/C, which degrades the inhibitor of separase: securin (Hatano & Sluder, 2012). Though the centrioles are now disengaged, they are still loosely associated with each other

via linker proteins including rootletin and C-Nap1 (Bahe et al., 2005). Once disengaged, a ring of proteins, including CDK5RAP2, CEP152, WDR62, CEP63 and PLK4 localise at the proximal end of each mother centriole (Gönczy & Hatzopoulos, 2019; Kodani et al., 2015). The hierarchical assembly of CDK5RAP2, CEP152, WDR62 and CEP63 culminates in the localisation of CDK2 to the centrosome (Kodani et al., 2015). CDK2 has been implicated in the regulation of the centrosome duplication cycle, though the exact mechanisms are unclear. Work in *Xenopus* egg extracts demonstrated that loss of CDK2 activity impairs centriole disengagement and duplication, suggesting a positive regulation role (Hinchcliffe et al., 1999; Lacey et al., 1999). However another study has found that CDK2 deficiency lead to early centriole disengagement and duplication, suggesting that CDK2 is necessary to prevent early disengagement and duplication (Adon et al., 2010).

At the G1/S transition, APC/C is silenced and no longer degrades STIL and SAS-6, which can now increase in abundance to a critical level (Arquint & Nigg, 2016). STIL binds to PLK4 at the centriole and becomes phosphorylated. Phosphorylated STIL recruits SAS-6 which acts as a scaffold for procentriole formation (Dzhindzhev et al., 2014; Tang et al., 2011). The feedback between PLK4, STIL and SAS-6 culminate in a single point at the proximal end of the centriole becoming the site of procentriole formation (Takao et al., 2019). The SCF-FBXW5 complex is key in regulating levels of SAS6 to ensure that the scaffold forms at the correct time in the cell cycle, and that it only forms once (Puklowski et al., 2011). SCF-FBXW5 ubiquitinates SAS6 and targets it for proteasomal degradation. SCF-FBXW5 is itself inhibited by PLK4 phosphorylation. As S phase progresses, PLK4 autophosphorylates, targeting itself for degradation. This allows SCF-FBXW5 to become active, leading to SAS6 degradation. During M and G1, FBXW5 is degraded by the APC/C, allowing SAS6 levels to build for the next round of the centrosome duplication cycle.

Procentrioles continue to elongate throughout S/G2. Two proteins, CEP120 and SPICE1 localise to the elongating centriole and recruit CEP135 (Comartin et al., 2013). CEP135 acts as a bridge between SAS6 and CPAP, a key contributor to elongation (Y.-C. Lin et al., 2013; Y. N. Lin et al., 2013; Sharma et al., 2016). CPAP and CEP120 work with γ-tubulin ring complexes to add centriolar microtubules onto the SAS-6 scaffold (Dammermann et al., 2008; Y. N. Lin et al., 2013). Another key elongation protein is CP110, which is recruited to the centrosome by CEP97 and centrobin (Gudi et al., 2011; Spektor et al., 2007). CP110 forms a cap on the elongating centriole, under which tubulin dimers are added, and also negatively regulates centriole length (T. I. Schmidt et al., 2009). Levels of CP110 are controlled in an antagonistic manner by USP33 and SCF-cyclin F. USP33 is a de-ubiquitinating

enzyme with high expression levels in S and early G2 phase, and stabilises CP110 at centrosomes (J. Li et al., 2013). In G2, levels of cyclin F rise and SCF-cyclin F ubiquitinates CP110, targeting it for proteasome degradation (D'Angiolella et al., 2010).

Work in *Drosophila melanogaster* has demonstrated that centriole length is controlled by the rate and duration of elongation, such that centrioles grow at a comparatively slower rate during a longer period of elongation (Aydogan et al., 2018, 2020). This process is regulated by PLK4 abundance, the oscillation of which is controlled in part by CP110 and CEP97 oscillation (Aydogan et al., 2022). This regulation of centriole length depends on PLK4 levels rather than a direct sensing of length, leaving centrioles vulnerable to dysregulated elongation if PLK4 levels are perturbed.

Throughout G2, up until G1 of the next cell cycle, the newly formed centrosomes undergo a maturation process whereby PCM components are recruited and organised, appendage proteins are added and the centrosome is relicensed for duplication in the next cell cycle. PLK1 phosphorylates PCM components including pericentrin and, in *Drosophila melanogaster*, SAS-4 (CPAP orthologue) (K. Lee & Rhee, 2011; Ramani et al., 2018). This triggers expansion of the PCM, allowing for increased microtubule nucleation during mitosis (Piehl et al., 2004). The timing of this maturation process has been shown in *Drosophila* to be regulated, in part, by CDK1 which phosphorylates SAS-4 and creates a docking site for PLK1 (Novak et al., 2016). Alongside PCM expansion, appendage proteins are added to the daughter centriole, converting it into a mother centriole for the next cell cycle. TALPID3 and C2CD3 are two proteins that are essential for this process (L. Wang et al., 2018; X. Ye et al., 2014). OFD1 and OFD2, distal and subdistal appendage proteins respectively, play key roles in the hierarchical recruitment of other distal and subdistal appendage proteins (Kashihara et al., 2019; L. Wang et al., 2018).

At G2/M, the cell has two centrosomes tethered together by C-Nap1 and rootletin (Bahe et al., 2005; Yang et al., 2006). Centrosome separation begins in late G2 when NEK2A phosphorylates and displaces C-Nap1, causing the linker to dissemble. NEK2A activity is antagonised by PP1γ, this antagonistic relationship is regulated by Aurora A and PLK1 (Mardin et al., 2011). Eg5 motor protein activity is responsible for moving the centrosomes to either pole of the cell allowing centrosomes to form a bipolar spindle (Blangy et al., 1995; Hata et al., 2019).

1.3. Centrosome Amplification

Healthy cells begin interphase with one centrosome, which is duplicated once so there are two centrosomes by the beginning of mitosis. In many cancer cells, however, a phenomenon called centrosome amplification (CA) can be observed (Godinho & Pellman, 2014; Nigg, 2002). Cells with CA have more than the normal number of centrosomes. This has profound effects on the cell during interphase and mitosis, inducing oncogenic features such as increased invasiveness and chromosomal instability (Arnandis et al., 2018; Ganem et al., 2009; Godinho et al., 2014; Lingle et al., 2002) and indeed, at least in some circumstances, CA is sufficient to induce tumourgenesis (Basto et al., 2008; Levine et al., 2017).

1.4. Routes to Centrosome Amplification

Possible mechanisms that cause CA to arise include dysregulation of the centrosome duplication cycle, failed cytokinesis, de novo centrosome synthesis and fracturing of over-elongated centrioles (Figure 1-3) (Denu et al., 2018; Godinho & Pellman, 2014; Marteil et al., 2018). These routes to CA are not fully understood at the molecular level and numerous pathways may be involved, but many studies indicate that loss of normal p53 activity and overexpression of PLK4 are common features of cells displaying CA (Adon et al., 2010; Serçin et al., 2016; Shinmura et al., 2014; Wong et al., 2015).

1.4.1. Centriole Over-duplication

CA can occur as a result of centriole overduplication within a cell cycle, which is a consequence of dysregulation of the centrosome duplication cycle. As mentioned in an earlier section, the centrosome cycle is a tightly regulated process that relies of the correct spatio-temporal localisation of many proteins, regulated be various mechanisms including proteolysis and phosphorylation by CDKs. Dysregulation of this process by overexpression of certain centriolar components such as PLK4, CP110, CEP120 or CPAP, or disruption regulatory pathways can lead to excess centrosome duplication within a cell cycle under experimental conditions (D'Angiolella et al., 2010; J. Li et al., 2013; Y. N. Lin et al., 2013; Serçin et al., 2016; Shinmura et al., 2014).

Additionally, if cells are arrested in S or G2, the mechanisms that ensure centrosomes are only duplicated once during a cell cycle seem to fail, leading to additional rounds of centrosome duplication. Hydroxyurea treatment, which causes DNA replication stress and stalls cells in S phase, has been used to induce CA in a manner that depends on the CHK2

DNA damage response pathway (Balczon et al., 1995; T. Y. Chen et al., 2015; C. Y. Wang et al., 2015). Treatment with a CDK1 inhibitor, which arrests cells in late G2, resulted in centriole overduplication in a manner that was dependent on the centriole maturation and disengagement activity of PLK1 (Lončarek et al., 2010).

The contribution of overduplication to CA can be determined by measuring the ratio of mature centrioles to new daughter centrioles. Overduplication would lead to less than 50% of centrioles bearing a mature marker. This was measured in a panel of melanoma cell lines, and it was found that in those cells with CA, only 18% centrosomes co-stained for the mature marker leading the authors to conclude that CA had arisen from overduplication (Denu et al., 2018).

1.4.2. Failed Cytokinesis

Tetraploidy due to failed cytokinesis has been reported as a common step in cancer development, and can precede aneuploidy. These events generate cells with doubled centrosomes and may occur in response to dysregulated protein activity or DNA damage stress (Fujiwara et al., 2005; Ganem et al., 2007; Olaharski et al., 2006). Aurora A activity is involved in centrosome separation and mitotic progression (Mardin et al., 2011; Marumoto et al., 2003; Mori et al., 2007). Aurora A overexpression in a p53 null setting caused cytokinesis failure, leading to tetraploidy and CA in an in vitro setting (Meraldi et al., 2002). Cells with impaired an impaired p53/p21 response to DNA damage entered an aberrant mitosis which eventually failed, giving rise to cells with CA (Bunz et al., 1998).

Ploidy deregulation is a side effect of cytokinesis failure. 64% of cell lines with CA in the NCI-60 panel showed ploidy deregulation suggesting a potential link between failed cytokinesis and CA, though this observation only describes a correlation (Marteil et al., 2018).

1.4.3. *De novo* Synthesis

There are mechanisms within normal biology to synthesise centrosomes *de novo* in order to generate multi-ciliated cells (Zhao et al., 2013). Over expression of PLK4 or prolonged S phase arrest have been shown to lead to aberrant *de novo* centriole formation (Khodjakov et al., 2002; Lopes et al., 2015; Pannu et al., 2012). *De novo* synthesis has also been seen in response to surgical or laser removal of centrosomes in either G1 or G2 (Lončarek et al., 2010; Uetake et al., 2007). Whilst this *de novo* synthesis was in response to artificial centrosome removal, it demonstrated that that normal, untransformed cells have the ability to synthesise centrosomes *de novo* separately from a canonical pathway. Overexpression of CEP63 induced *de novo* synthesis of centrosomes (Löffler et al., 2011). It has been

hypothesised that the presence of centrosomes inhibits *de novo* synthesis through an unknown mechanism (Brownlee & Rogers, 2013). If this is the case, inhibition of this pathway would be necessary for the *de novo* pathway to contribute to the generation of cells with CA.

1.4.4. Centriole Over-elongation

A mechanism that has come to light more recently is the fracturing of over-elongated centrioles. This importance of this mechanism was revealed in a comprehensive study of CA in the NCI-60 panel of cell lines. Cell lines with high levels of CA had a larger proportion of overly elongated centrioles and inducing over-elongation by overexpression of CPAP induced CA in cell lines with initially low levels of CA (Marteil et al., 2018). These over-elongated centrioles potentially fragment, creating new centrioles, or enable ectopic formation of additional centrioles (Kohlmaier et al., 2009; Y. N. Lin et al., 2013; Marteil et al., 2018). Partially fragmented over-elongated centrioles have been observed in at least one clinical case of neoplasia, though no CA was observed in this case (Dittrich et al., 2019). A related observation in *Drosophila* is that a pericentrin-like-protein mutant resulted in fragmented centrioles and formed multipolar spindles (Martinez-Campos et al., 2004).

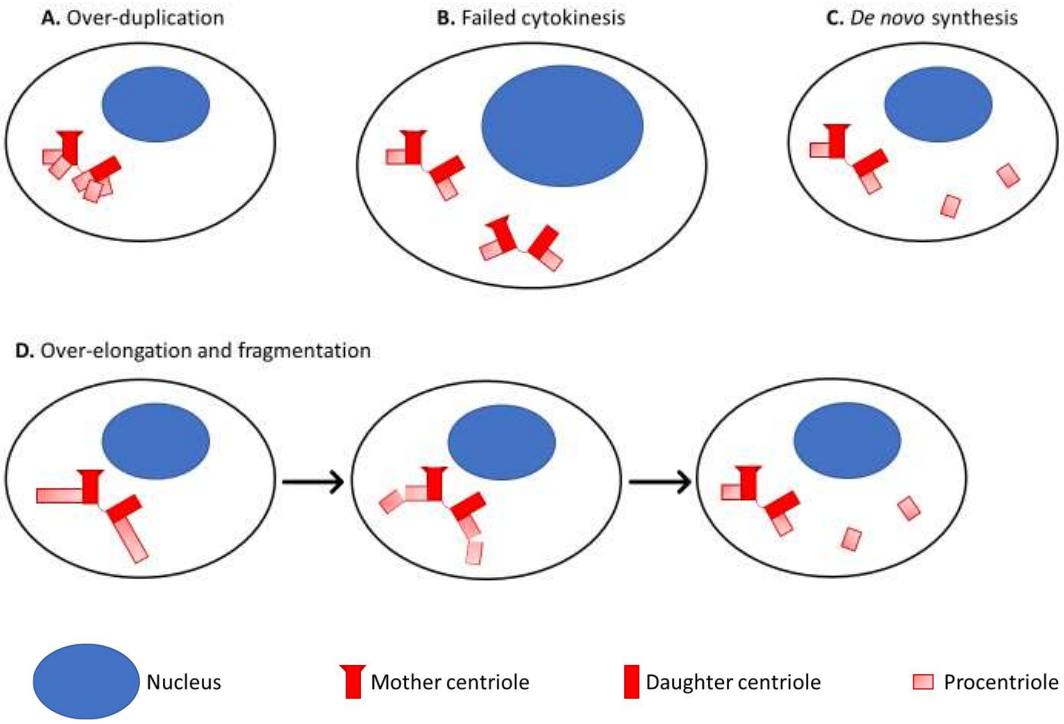

Figure 1-3. Routes to centrosome amplification.
A summary of four different routes to centrosome amplification covered in the text above: over-duplication (A), failed cytokinesis (B), *de novo* synthesis (C) and over-elongation (D).

1.4.5. The Role of p53 in Centrosome Amplification

The recent attention to CA stemmed from a study that linked loss of p53 to CA (Fukasawa et al., 1996). There has since been much discussion into the role of p53 and CA, as there seems to be an association between the two (Chan, 2011). Indeed, many studies into CA require a p53 null setting either for CA to persist or for the CA phenotypes to present themselves (Adon et al., 2010; Lopes et al., 2018; Marin Navarro et al., 2020; Serçin et al., 2016). However, comparing p53 and CA status of the NCI-60 panel revealed that almost half of the cell lines with mutant p53 did not have CA, and there was no significant difference in CA between cells with functional p53 and cells with mutated p53 (Marteil et al., 2018). Loss of p53 does not always lead to CA, as demonstrated in a study where *p53*$^{-/-}$ mice had normal centrosome number (Marthiens et al., 2013).

It seems that loss of p53 or p53 signalling is a common feature in cells with CA, but p53 loss alone is not necessarily enough to induce CA. Instead, loss of p53 activity may create a permissive setting to maintain CA and the proliferative ability of those cells with CA (Andreassen et al., 2001; Fava et al., 2017; Holland et al., 2012; Meraldi et al., 2002). A mechanistic link between CA and p53 activity has recently been identified, being dependant

on the distal appendage protein ANKRD26 and its ability to recruit PIDD1, a component of the PIDDosome. In a setting of clustered supernumerary centrosomes this leads to activation of the PIDDososme, cleaving the p53 inhibitor MDM2, resulting in p53/p21 dependent cell cycle arrest (Burigotto et al., 2021; Evans et al., 2021; Fava et al., 2017). Interestingly, a mutation in *ANKRD26* that abolishes its ability to recruit PIDD1 was found in 20 different human tumour samples, suggesting that this is a mutation that is positively selected for in cancers (Evans et al., 2021). However, the CA status of these tumours was not investigated.

1.5. Oncogenic Characteristics Induced by Centrosome Amplification

1.5.1. Chromosomal Instability

Having additional centrosomes can cause two types of error during cell division. Firstly, if the centrosomes are not regulated they may form a multipolar spindle. Proper DNA segregation becomes impossible, the multipolar cell division causes gross aneuploidy that causes daughter cells to die (Cosenza & Krämer, 2016). To negate this, cells with CA can employ a number of mechanisms to regulate their supernumerary centrosomes to allow formation of pseudo-bipolar spindles. The most common and widely studied of these mechanisms is centrosome clustering, where supernumerary centrosomes are gathered into just two poles, allowing formation of pseudo-bipolar spindles (Godinho et al., 2009). However, cells often undergo multipolar intermediates prior to successful clustering which can allow chromosomes to form merotelic kinetochore attachments. These merotelic attachments can cause chromosome missegregation, lagging of chromosomes during anaphase which allows DNA damage to occur, or shattering of chromosomes through a process called chromothripsis (Ganem et al., 2009; Marteil et al., 2018; C. Z. Zhang et al., 2015). This process can induce a much lower level of aneuploidy that daughter cells can withstand, but may also help to drive cancer progression (Cosenza & Krämer, 2016; Lingle et al., 2002).

1.5.2. Invasiveness

Cell-autonomous increased invasiveness due to CA is a result of the increased microtubule nucleating activity conferred by having extra centrosomes. The increase in microtubule nucleation leads to an increase in Rac1 activity through an unknown mechanism, which caused defects in cell-cell adhesion and induced formation of invasive cytoskeletal protrusions (Godinho et al., 2014). More recently it has also been shown that CA can cause non-cell-autonomous increased invasiveness. Cells with CA have increased levels of cytoplasmic reactive oxygen species (ROS) as a result of the cellular stress caused by CA. The

high levels of cytoplasmic ROS drives secretion of invasive factors, including IL-8. IL-8 increases paracrine HER2 signalling, increasing the invasive capacity of these neighbouring cells (Arnandis et al., 2018). Further insight into the mechanisms behind increased invasiveness due to CA has recently linked increased Rap1 activity to increased migration and invasion. Additionally, impaired cell-cell, enhanced cell-extracellular matrix (ECM) adhesion and altered expression of ECM remodelling proteins were observed in cells with CA (Prakash et al., 2022).

1.5.3. Defects in Asymmetric Divisions of Stem Cells

CA has been shown to have tumourigenic potential. CA in *Drosophila melanogaster* (induced by overexpression of SAK, the *D. melanogaster* homologue of PLK4) caused defects in the asymmetric mitoses of neuroblasts. The resulting symmetric mitoses increased the pool of neuroblasts in the brain tissue, and transplantation of brain tissue with CA into the abdomen of healthy wild type *D. melanogaster* caused tumours and metastases to form, whereas transplantation of healthy brain tissue had no effect (Basto et al., 2008).

1.6. Cancer Development

CA has been observed many different solid and haematological malignancies (Chan, 2011). There has been some debate as to whether CA is a cause or a consequence of cancer (Nigg, 2002). Hypothesised routes to CA indicate a "cancer setting" is required for CA to arise. However, artificial induction of CA has been sufficient to cause tumourigenesis in flies, as mentioned above, and mice (Basto et al., 2008; Levine et al., 2017).

Mouse studies have demonstrated that, whilst some tissues such as the liver and skin can tolerate CA, CA can increase initiation of tumour growth in a model of intestinal cancer and that CA is sufficient to trigger growth of lymphomas, squamous cell carcinomas and sarcomas (Levine et al., 2017; Vitre et al., 2015). Levine et al discuss that discrepancies between their study and other studies with PLK4-overexpression-induced CA, which don't see the tumourigenic effect, may be due to two factors. Firstly, the methods used to overexpress PLK4 vary, with other methods potentially causing too high a level of CA that cells couldn't survive, tolerate or responded to by silencing *PLK4*. Secondly, other studies may not have followed survival for long enough to observe an increase in tumour growth.

In ovo assays have recently been employed to highlight the early role in which CA may play in the development of cancer (Prakash et al., 2022). When grafted onto the chorioallantioc

membrane of a chicken, induction of CA in the non-tumourigenic breast epithelial cell line MCF10A was sufficient to drive migration and invasion through the chorionic epithelium and into the intermediate mesoderm. More strikingly, during the 5 day time-course of the assay, CA drove advanced tumourigenic characteristics such as haemorrhaging, necrosis and calcification at the graft/chorioallantioc membrane interface.

Either way, there is clear evidence that CA is a driver of oncogenic traits. This means that CA is a promising target for new cancer therapies. As well as increased centrosome number, cells with CA have also been observed to have elongated centrioles, have additional dense PCM and have extra centrioles, giving centrosomes a rosette-like appearance (Ganem et al., 2009; Marteil et al., 2018).

1.7. Targeting Cells with Centrosome Amplification

1.7.1. Centrosome Amplification Coping Mechanisms

Having extra centrosomes is detrimental for a dividing cell, with the potential for causing cell death either as a result of massive aneuploidy after a multipolar mitosis, or apoptosis following mitotic arrest (Farrukh et al., 2022). To avoid this fate, cells with CA can employ coping mechanisms to survive with extra centrosomes (Figure 1-4). The most commonly observed and well-studied coping mechanism in cancer cells with CA is centrosome clustering, where supernumerary centrosomes are clustered to form a pseudo-bipolar spindle (Basto et al., 2008; Choe et al., 2018; Farrukh et al., 2022; Quintyne et al., 2005; Sabat-Pośpiech et al., 2022). Another potential mechanism is centrosome inactivation, which has been observed in *Drosophila melanogaster* (both in the developing embryo and in a CA setting) and *Caenorhabditis elegans* (Basto et al., 2008; Magescas et al., 2019; Sibon et al., 2000). A third potential mechanism is centrosome loss, by extrusion or degradation. *Dictyostelium* can extrude excess centrosomes in cytoplasts (Gräf et al., 2003). Centrosome degradation, also called centrosome elimination or centrosome reduction, is observed in oogenesis (Gruss, 2018; Manandhar et al., 2005). More recently, centrosome loss has been seen in colorectal cancer cell lines in response to tetraploidisation, though the mechanism for this loss was not explored (Galofré et al., 2020).

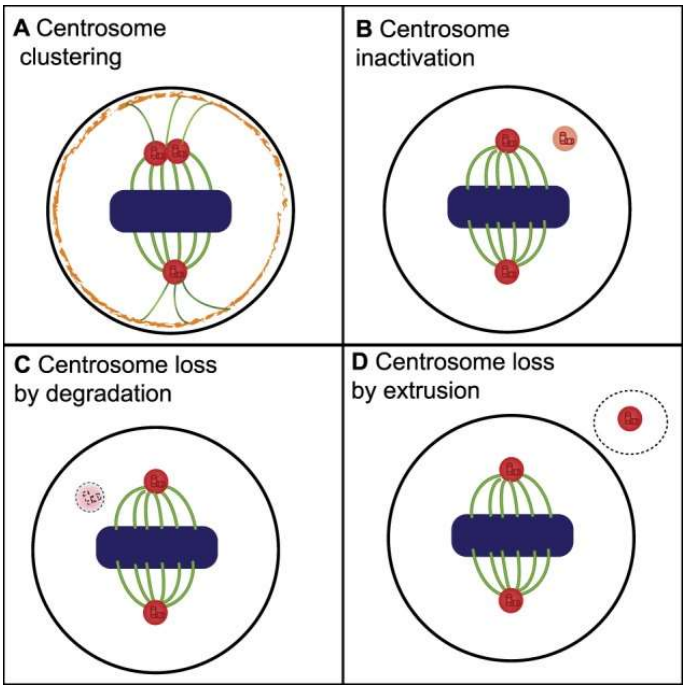

Figure 1-4. Potential coping mechanisms for cells with centrosome amplification.
Four different mechanisms that could be used by cells with CA when going through mitosis to avoid multipolar division and cell death. Out of clustering (A), deactivation (B), loss by degradation (C) and loss by extrusion (D), centrosome clustering is the most widely observed in cancer cells with CA. Image reproduced with permission from Sabat-Pośpiech et al., 2019.

The coping mechanisms or unusual behaviours of cell with CA can be targeted to develop cancer specific treatments. For example, cells with CA have an accumulation of autophagosomes, leading to increased levels of autophagy, making them more sensitive to autophagy inhibitors (Denu et al., 2019). The majority of current research has focussed on targeting centrosome clustering as a cancer therapy, with the reasoning that without centrosome clustering, cells with CA often undergo prolonged mitotic arrest followed by apoptosis or may divide more than two ways, generating non-viable daughter cells (Ganem et al., 2009; Sabat-Pośpiech et al., 2019).

1.7.2. Centrosome Clustering

One example of a protein that is a promising target to prevent centrosome clustering is KIFC1 (also known as HSET). KIFC1 is a protein in the kinesin-14 family that aids the clustering of centrosomes via its pole focusing activity (Kleylein-Sohn et al., 2012), involving the cross linking of microtubules (Kwon et al., 2008) and tethering of microtubule minus ends to centrosomes (She & Yang, 2017). Normal healthy cells do not rely as heavily on KIFC1 activity as cells with CA, as redundant functions of other kinesins mean that depleted KIFC1 activity can be compensated in healthy cells (Kleylein-Sohn et al., 2012; Mountain et

al., 1999). On the other hand, in cells with CA, KIFC1 is required to cluster centrosomes, so depleted KIFC1 activity causes cell death (Kwon et al., 2008).

However, although targeting centrosome clustering is a promising avenue, currently no agents targeting clustering have made it into clinical trials. Several small molecule inhibitors of KIFC1 have been developed which are effective at inducing multipolar spindles, however there seems to be a pharmacological issue with regards to cancer cell specific lethality (Sabat-Pośpiech et al., 2019; Watts et al., 2013; Wu et al., 2013; W. Zhang et al., 2016). Therefore, alternative approaches to target CA should be explored.

1.7.3. Reversal of Centrosome Amplification

An alternative approach to targeting cells with CA would be to find a way to reverse CA, with the rationale that this could reverse the oncogenic effects that CA causes. Another rationale for reversing CA is that, in some cases, cancer cells may be reliant on their additional centrosomes to compensate for defects in centrosome function, for example due to APC mutation. These cells would be vulnerable to a reversal of CA (Harrison et al., 2018). However, in order to reverse CA, it will be necessary to further understand the mechanisms that cause CA in cancer.

1.7.4. Reversing Centrosome Amplification in Aggressive Tumour Types

Cancers with high levels of CA often tend to be more aggressive types of cancer, for example a list of genes named “CA20”, made up of 20 genes that seem to be involved in CA, is an effective prognostic indicator of breast cancer survival (Ogden et al., 2017). Comparison of studies of a wide variety of cancers revealed that CA is associated with early disease reoccurrence, disease progression and poor survival (Chan, 2011). There is a requirement to find novel therapies to these aggressive cancers, which are also resistant to current treatment methods, e.g. triple negative breast cancer. Unpublished data from the Fielding lab has shown for the first time that CA is present in moderate levels in primary uveal melanoma, and high levels in metastatic uveal melanoma, which is a cancer that suffers from particularly poor treatment response.

1.7.5. Centrosome Amplification Signature

CA is a lucrative target for the development of new cancer therapies, given its cancer specific nature and functional role in cancer malignancy. Identification of cancers with CA that would be responsive to these new therapies could however be a limiting step, the current method of analysing immunohistochemical stained formalin-fixed paraffin embedded biopsies is time consuming and limited by the thickness of sections (Duensing, 2015; Patel et al., 2018).

The development of a transcriptomic signature that could identify CA would be beneficial to the implementation of such CA targeted therapies. Various mechanistic routes as to how CA can develop have been summarised in section 1.4. These mechanisms often rely on dysregulated expression of key proteins involved in centrosome duplication. It stands to reason that there may be a "centrosome amplification signature" of cells with CA, with certain genes commonly being over or under expressed compared to healthy cells. The development of a CA20 score took into account the expression of 20 genes encoding centrosome structural proteins and genes whose dysregulation have been implicated experimentally in the development of CA (Ogden et al., 2017). This score had prognostic value with regards to overall survival in breast cancer data-sets, however the ability of the CA20 score to predict CA status was not tested. Having said that, cancers with a high CA20 score have also been shown to display features associated with CA (De Almeida et al., 2019). In addition to the CA20 score, a number of oncogenes and tumour suppressors have been identified for their potential roles in CA (Fukasawa, 2007). Another approach that could be taken to identify a CA signature would be to compare 'omics data of cells with and without CA. The NCI-60 panel of cell lines could be a useful resource in this sense, as their CA status has been robustly quantified (Marteil et al., 2018).

1.8. Uveal Melanoma

Uveal melanoma (UM) is the most common intraocular cancer in adults, though at 2 - 8 cases per million it is a rare disease, which can make recruitment into clinical trials to test new treatments difficult (Rantala et al., 2019; Singh & Topham, 2003; Virgili et al., 2007). There are a number of different treatments for the primary disease, including brachytherapy, laser therapy, proton beam therapy and surgical removal of the tumour or whole eye (Nathan et al., 2015). Treatment strategy will depend on factors such as the size at discovery, patient age and tumour location, and usually provides good results with overall survival of treated patients being 69% after 5 years (Kujala et al., 2003). Unfortunately many patients will develop metastatic uveal melanoma, most often to the liver (Diener-West et al., 2005). Rates of metastasis have been reported to be 25 and 34% after 5 and 10 years respectively, however long term monitoring reveals that it can take many years for metastatic disease to present and that over 50% of UM cases will eventually result in metastatic disease (Diener-West et al., 2005; Kujala et al., 2003). Although genetic markers can help classify UM tumours as being more or less likely to metastasize (see below), the cellular mechanisms behind metastasis are poorly understood. Once metastases develop,

survival rates are poor with median survival being around 1 year (Rantala et al., 2019). As such, it is clear that research to improve understanding of metastatic UM and to identify and develop potential targets for treatment, is of desperate importance to UM patients.

Although UM and cutaneous melanoma both arise from melanocytes, they have a very different genetic profile. Whereas cutaneous melanoma is notorious for having a high mutational burden with a somatic mutation rate of 18 per Mb, UM has a much lower somatic mutation rate of burden of 1.1 per Mb (Bakhoum & Esmaeli, 2019). UM also lacks the key mutations that drive cutaneous melanoma, perhaps most significantly lacking *BRAF* mutations, and is instead characterised by a handful of key mutations. Mutually exclusive mutations in *GNAQ*, *GNA11*, *CYSLTR2* or *PLCB4*, all members of the same signalling pathway, have been identified as an early event in UM development, and have even been identified in benign nevi (Bakhoum & Esmaeli, 2019; Decatur et al., 2016). Mutually exclusive mutations in *BAP1*, *SF3B1*, *SRSF2* or *EIF1AX* occur later in tumour development and are thought to drive tumour progression (Bakhoum & Esmaeli, 2019; Decatur et al., 2016; Helgadottir & Höiom, 2016). In addition, it has long been recognised that loss of a copy of chromosome 3 or gains in 8q and 6p chromosomes are common features of uveal melanoma (Horsman et al., 1990; Horsthemke et al., 1992; Prescher et al., 1990, 1994). Since then, the disomy/ monosomy status of chromosome 3 (D3-UM/ M3-UM) has been used as a prognostic marker, with M3-UM being a strong indicator of the likelihood of an individual to develop metastases. However there is no difference in the prognosis of individuals with metastatic D3-UM vs metastatic M3-UM (Sandinha et al., 2005).

A recent TCGA 'omics study has further added to the picture of UM genetics, identifying 4 molecular subgroups of uveal melanoma which have different clinical outcomes (Figure 1-5) (Robertson et al., 2017). Subgroup 1 is characterised by disomy 3 status and a mutation in *EIF1AX* and has the best prognosis. Subgroup 2 is characterised by disomy 3 status and a mutation in *SF3B1* and has an intermediate prognosis. Subgroups 3 and 4 are characterised by monosomy 3 and *BAP1* mutation and are both associated with a poor prognosis, but differ in some of the pathways that are upregulated. Subgroup 3 has upregulated MAPK/PIK3, FOXA1/FOXM1 and E2F1 pathways. Subgroup 4 favours hypoxia, DNA damage repair and MYC pathways.

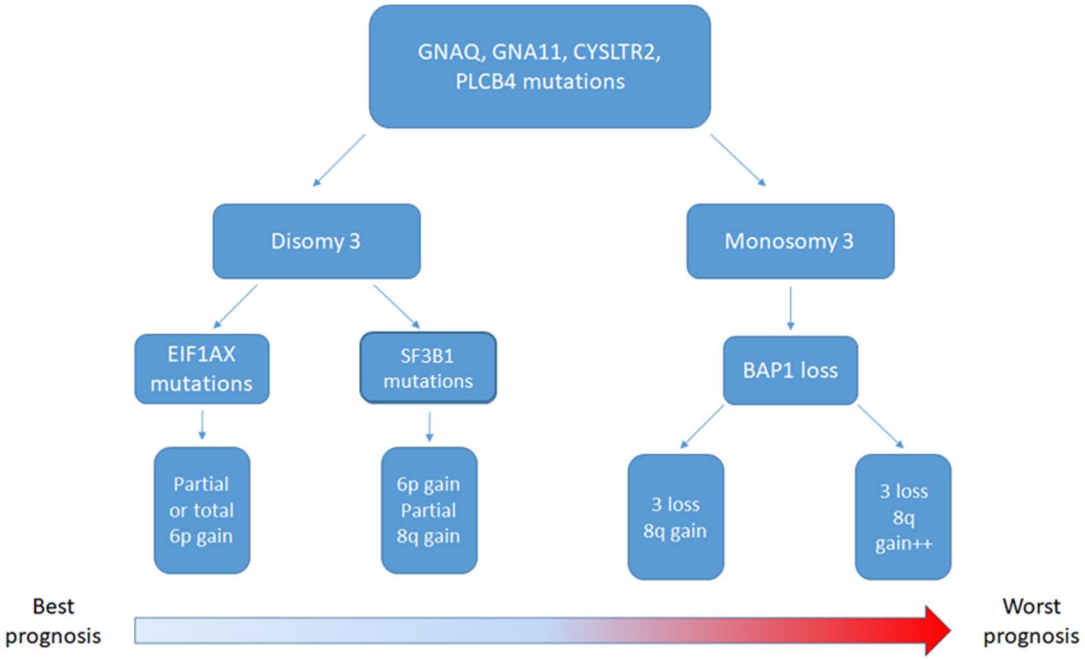

Figure 1-5. Diagram of Uveal Melanoma molecular subgroups.
Uveal melanoma can be split into four molecular subgroups with prognostic significance. There are ubiquitous yet mutually exclusive mutations in *GNAQ/GNA11*, *CYSLTR2* and *PLCB4*. Disomy 3 uveal melanomas can be further split by those that have *EIF1AX* mutations and partial or total 6p gain, and those that have *SF3B1* mutations, 6p gain and partial 8q gain. Monosomy 3 uveal melanomas have *BAP1* loss and either low or high levels of 8q gain

1.9. Aims

There is mounting evidence that CA is a driver of oncogenic traits such as increased invasiveness and chromosomal instability, and also that it may be an early driving event in the development of cancer (Arnandis et al., 2018; Ganem et al., 2009; Godinho et al., 2014; Levine et al., 2017; Prakash et al., 2022). As a feature of cancer cells not seen in normal healthy cells, CA is an attractive target for the development of cancer specific therapies. Current research has focussed primarily of targeting the coping mechanisms that cancer cells with CA employ to survive with additional centrosomes such as centrosome clustering, but no therapies have progressed to clinical trials to date (Figure 1-6) (Sabat-Pośpiech et al., 2019).

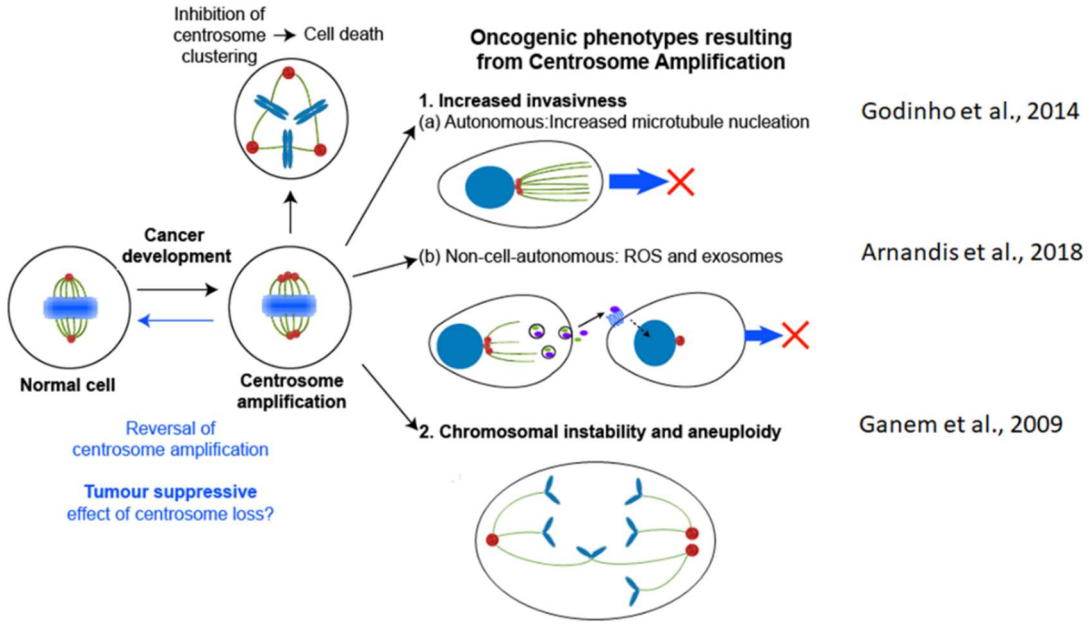

Figure 1-6. A summary of the oncogenic and targetable features of cells with centrosome amplification.
At some point during the process of cancer development, some cancer cells develop centrosome amplification. This drives oncogenic phenotypes such as increased autonomous invasion (1a), increased non-autonomous invasion (1b) and chromosomal instability and aneuploidy through merotelic kinetochore attachments and lagging chromosomes (2). Inhibition of centrosome clustering is an attractive therapeutic avenue, but no anti-clustering drugs have successfully been developed to date. We hypothesise that reversal of centrosome amplification could have tumour suppressive effects (blue text). Image adapted with permission from Sabat-Pośpiech et al., 2019.

The overall aims of this project will take a different approach to the task of targeting CA by exploring the possibility of reversing CA that has occurred naturally in a patient setting. The first aim is to identify the causes of CA in a patient-matched cell line model of primary and metastatic UM. Secondly, it will be tested if the identified expression changes can be manipulated to reverse CA. The third question is whether reversal of CA will have any therapeutic effects, in terms of a reduction in oncogenic features (particularly cell motility) associated with CA.

To do this, patient matched uveal melanoma cell lines will be used to form a model to study the development of CA. RNA sequencing analysis will be used to identify targets for an siRNA screen that can identify genes whose dysregulated expression may have led to increased CA. Assuming successful reversal of CA is achieved, the effects on cell migration will be assessed. The principal experimental aims in this thesis are:

- Measure CA in patient-matched cell lines derived from primary and metastatic UM (Chapter 3).
- Perform a comparative transcriptomic analysis of the primary and metastatic UM cell lines to identify expression changes that may have led to CA (Chapter 3).
- Select differentially expressed genes from RNA sequencing analysis for use in an siRNA screen (Chapter 3).
- Perform an siRNA screen in primary and metastatic UM cells to identify genes whose knockdown alters levels of CA (Chapter 4).
- Validate hits identified in the siRNA screen (Chapter 4).
- Characterise the effects of hit-knockdown on metastatic UM cells (Chapter 5).
- Develop a correlative live cell imaging and immuno-fluorescence assay to allow analysis of cell migration parameters in relation to centrosome status, at single-cell resolution (Chapter 5).

Chapter 2.

Methods and Materials

2.1. Tissue Culture

2.1.1. General Tissue Culture

Mel270, OMM2.3 and OMM2.5 cells were cultured in RPMI media (61870-010, Gibco) supplemented with 10% foetal calf serum (10500-064, Gibco), 50 IU/mL penicillin and 50 µg/mL streptomycin (15070-063, Gibco). H2B-FUCCI2a-Mel270, H2B-FUCCI2a-OMM2.3 and H2B-FUCCi2a-OMM2.5 cells were cultured in RPMI media supplemented with 10% foetal calf serum, 50 IU/mL penicillin, 50 µg/mL streptomycin and 0.2 µg/mL puromycin (A11138-03, Gibco). All cells were cultured at 37 °C with 5% CO_2 and passaged every 3-4 days as cultures neared confluence. To passage, cells were dissociated with 0.05% trypsin-EDTA (15400-054, Gibco) or TrypLE Express (12604-013, Gibco) and diluted as appropriate for each cell line in culture medium. Cells were counted using a Neubauer haemocytometer when necessary.

2.1.2. Cell Stock Cryopreservation and Revival

Low passage cultures were cryopreserved to create cell stocks. Confluent T75 flasks were dissociated as previously described and resuspended in their appropriate culture medium. Cells were pelleted (1000 rpm, 188 g, 3 min) and supernatant removed. Pellets were resuspended in residual supernatant (~100 µL) before resuspending in 3 mL freezing media per flask (appropriate culture media as described above, plus an additional 10% foetal calf serum and 10% DMSO). Cell suspension was dispensed into cryovials, with 1 mL cell suspension per vial. Vials were placed in an isopropanol chamber and frozen in a -80 °C freezer overnight before being transferred to liquid nitrogen for long term storage.

To revive frozen cells, vials were thawed promptly in 37 °C water bath and resuspended in 10 mL culture media. Resuspended cells were seeded into a T25 and cultured overnight before changing the culture media.

2.1.3. Cell Line Authentication and Mycoplasma Screens

At the beginning of the project, Mel270, OMM2.3 and OMM2.5 cell lines were sent off for STR profiling to confirm cell identity. Cells were pelleted (1000 rpm, 188 g, 3 min) and all supernatant removed. Pellets were washed with PBS (14200-075, Gibco) to remove residual media and re-pelleted (2000 rpm, 376g, 3 min). Supernatant was removed from pellets before shipping to Eurofins as per their instructions for STR profiling.

Mycoplasma screens were also carried out every 6 months. Screens were performed in house by Lisa Butler, a member of technical staff in the Division of Biomedical and Life

Sciences. For the assay, media from cells that were 70-80% confluent and that had been cultured 3-4 days without a media change was provided for use in a luciferase based mycoplasma detection assay.

2.1.4. Generation of H2B-FUCCI2a Cell Lines

Stable H2B-FUCCI2a cell lines were generated by Dr. Andrew Fielding and masters student Yue Hu using the PiggyBac transposon system. Cells were seeded into 6 well plates and left to grow for 24 hours before transfection. A number of ratios of Opti-MEM:GeneJuice:plasmid were tested to optimise transfection, the following ratios gave the best results. To transfect cells, 100 µL Opti-MEM media (31985-062, Gibco) was combined with 3 µL GeneJuice transfection reagent (70967-3, Merck) for each well and incubated for 5 minutes at room temperature. 1 µg pBH2BF2aIP and 1 µg pbHybase was added to the Opti-MEM and GeneJuice mix, pipetting up and down. This transfection mixture was incubated for 20 minutes at room temperature before being added dropwise to cells with 2 mL fresh media. Cells were left to grow for a further 24 hours before each well was passaged into a 10 cm plate. After another 24 hours growth, media was supplemented with 0.2 µg/mL puromycin. Cell treatment with puromycin continued until colonies formed, changing media every 3-4 days. Colonies were observed using confocal microscopy (Zeiss LSM880) to check for plasmid incorporation. Individual positive colonies were transferred to 6 well plates and grown to 70-90% confluence before being passaged to T75 flasks and subsequently freezing down.

2.2. Immunofluorescence Staining

Depending on experimental setup, cells were seeded onto glass coverslips (631-0149, VWR) or glass bottomed plates (P24-1.5P and P96-1.5P, Cellvis). To fix and permeabilise cells, media was removed and cells were rinsed twice, gently, with PBS (14040-133, Thermo Fisher Scientific) before adding ice cold methanol (M/3950/15, Fisher Scientific) to fully cover cells and incubated at -20 °C, 15 minutes. After fixation, methanol was removed and replaced with PBS to prevent cells from drying out. N.B. All following incubations were carried out at room temperature. Coverslips, when used, were transferred cell side up onto parafilm (I3080-5075, Starlab). Glass bottomed plates, when used, were placed on a gyratory rocker during incubations. Cells were blocked with 5% goat serum (16210-064, Gibco) in PBS for 1 hour. Serum was removed with a pipette before applying 1° antibody solutions diluted with 5% goat serum (Table 2-1) and incubating for 1 hour. 1° antibody was removed and cells

were gently rinsed three times with PBS before applying 2° antibody solution diluted in 5% goat serum (Table 2-2) and incubating protected from light for 1 hour. 2° antibody was removed and cells were gently washed three times with PBS. To mount coverslips, any excess PBS was removed gently with a lint free tissue before mounting onto glass slides using Mowiol (ref. 81381, Sigma) containing DAPI at 1 µg/mL. Mowiol was made up according to manufacturer's instructions. Slides were stored at 4 °C, protected from light. Cells on glass bottomed plates were counterstained using DAPI in PBS at 1µg/mL for 10 minutes. To store plates, wells were filled with PBS, sealed with parafilm and stored at 4 °C, protected from light.

Target	Host	Clonality	Supplier	Ref. code	Dilution
Pericentrin	Rabbit	Monoclonal	Abcam	ab4448	1/1000
α-Tubulin	Mouse	Monoclonal	Sigma	T6199	1/1000
α-Tubulin	Rat	Monoclonal	Millipore	MAB1864	1/1000
Centrin	Mouse	Monoclonal	Millipore	04-1624	1/1000
Cyclin B1	Mouse	Monoclonal	Millipore	05-373	1/1000
Phospho-histone H3	Mouse	Monoclonal	Abcam	ab14955	1/1000

Table 2-1. Primary antibodies used for immunofluorescence staining.

Target	Host	Clonality	Supplier	Ref. code	Dilution	Dye
Anti-Rabbit	Goat	Polyclonal	Invitrogen	A32732	1/500	Alexa Fluor Plus 555
Anti-Mouse	Goat	Polyclonal	Invitrogen	A32723	1/500	Alexa Fluor Plus 488
Anti-Rat	Goat	Polyclonal	Invitrogen	A21247	1/500	Alexa Fluor 647

Table 2-2. Secondary antibodies used for immunofluorescence staining.

2.3. Confocal Microscopy and Image Analysis

A Zeiss LSM880 confocal microscope and Zen software (version 14) were used to image fluorescently stained cells and to create FUCCI timelapse videos. Image acquisition settings and image analysis varied depending on experimental setup. Image analysis was performed using ImageJ (version 1.53q).

2.3.1. Initial Centrosome Amplification Investigation

For initial investigation into centrosome amplification (CA) in Mel270, OMM2.3 and OMM2.5 cells, slides were imaged using a Plan-Apochromat 20x/0.8 M27 objective, taking 4x4 tiled z-stacks. These images were analysed using the maximum intensity projection of the pericentrin channel and of the merged image. Mitotic cells were marked as regions of interest (ROI) and the ROIs saved as an overlay. The number of centrosomes was manually counted for each mitotic cell.

2.3.2. Centrosome Amplification Quantification in Mitotic Cells

To measure the level of CA in Mel270, OMM2.3 and OMM2.5 cells, z-stacks were taken of individual mitotic cells using a Plan-Apochromat 40x/1.4 Oil DIC M27 objective. Mitotic cells were identified in a methodical manner, scanning a coverslip from right to left, top to bottom. Centrosomes were counted manually using the merged, pericentrin and centrin z-stacks to identify bona fide centrosomes.

2.3.3. Centrosome Amplification Score

For the siRNA screen and subsequent experiments where a “CA score” was to be determined, several fields of view, most often 4, were taken per well using a Plan-Apochromat 20x/0.8 M27 objective, set to 0.8x zoom. To ensure centrosomes were in focus across a large field of view, the pinhole was opened to image a cross section of 15 µm.

To analyse images, a CA score was calculated using the formula (pericentrin foci – cyclin B1 positive cells)/nuclei. This calculates the number of centrosomes per cell. In healthy cells, there is one centrosome in G1/S and two centrosomes in G2/M. Cyclin B1 acts as a marker for cells in G2/M so by subtracting the number of cyclin B1 positive cells from the pericentrin foci, this accounts for any differences in cell cycle population between different siRNA treatments. To count pericentrin foci, cyclin B1 positive cells and nuclei, single channel images of pericentrin, cyclin B1 and DAPI stained cells were used, respectively.

To count pericentrin foci, a median blur filter kernel size 1 was applied and then find maxima was tested at different levels of prominence. “Find maxima” is able to identify local maxima within an image. Changing the prominence threshold alters the sensitivity of find maxima in picking out maxima from background noise within the image. Setting find maxima to a lower prominence allows it to pick out more subtle maxima. For each image, a prominence was selected that best counted pericentrin foci and the number of maxima identified was recorded.

To count nuclei, a median blur filer kernel size 5 was first applied. Then the image was thresholded with the maximum value set to 255 and the minimum value set manually so that every nucleus was selected. The resulting binary image then had “fill holes” and “watershed” applied before using “analyse particles” to count the nuclei. The analyse particle settings had size (micron^2) set to 50-infinity, circularity set to 0.00-1.00 and show: overlay masks. All options were selected apart from exclude on edges, record stats and in situ show. The number of particles was recorded.

The number of cyclin B1 positive cells was counted manually.

2.3.4. Migration Analysis of H2B-FUCCI2a Cells

Migration of FUCCI cells was carried out as a timelapse wound healing assay. Cells were seeded into a glass bottom 24 well plate (P24-1.5P, Cellvis) and grown to confluence. Before imaging, a wound was made using a p10 pipette tip. To allow for live imaging, cells were maintained at 37 °C and 5% CO_2 using the TempModule S1 (800-450000, Pecon) and CO_2 Module S1 (810-450001, Pecon) modules. Cells were imaged every 10 minutes using a Plan-Apochromat 20x/0.8 M27 objective in two fields of view per treatment. A Focus Controller 2 (Zeiss) was used to ensure cells stayed in focus over the time series.

Identification of nuclei was performed on the H2B channel using StarDist, an ImageJ plugin (U. Schmidt et al., 2018; Weigert et al., n.d.). Cell movement was identified as tracks using TrackMate, an ImageJ plugin (Figure 2-1) (Ershov et al., 2021). Depending on whether data was being collected for bulk migration analysis or tracking individual cells, different parameters were used. On the initial thresholding step, all spots were selected for both types of analysis. On the set filters on spots step, for bulk migration, spots with a quality of 0.74 and above were kept (default settings), this removes erroneous background segmentation that isn’t nuclei. For tracking individual cells, all spots were kept. For both types of analysis, the tracker used was the Simple LAP tracker with a linking max distance of 30 µm, gap-closing max distance of 30 µm and gap-closing max frame gap of 5, these setting are recommended by the TrackMate Stardist tutorial for tracking nuclei. On the set filters on tracks step, tracks with 100 or more spots were kept for bulk migration analysis. For tracking individual cells, all tracks were kept. The tracks and spots table outputs were exported to excel for further analysis.

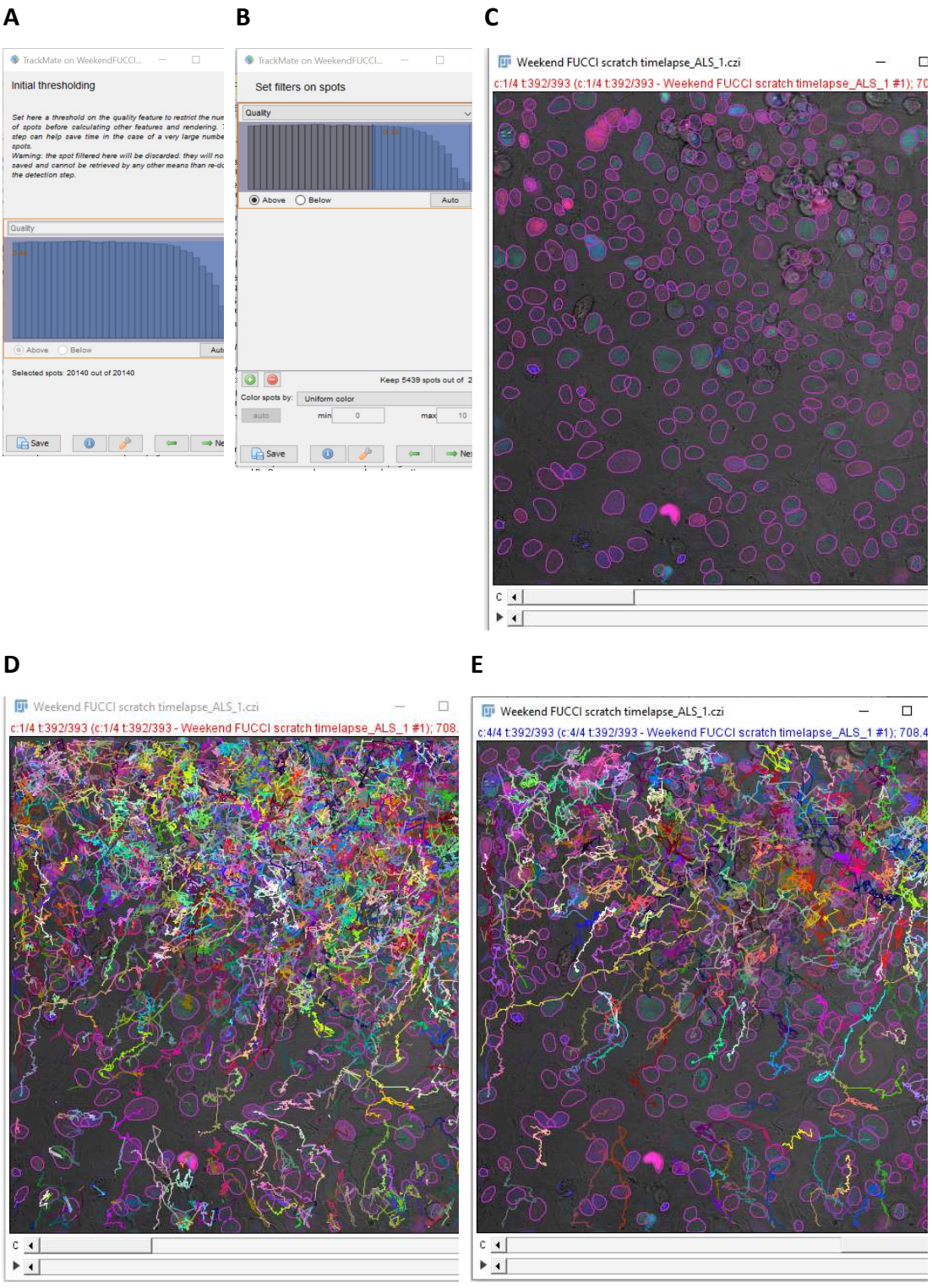

Figure 2-1. Example images of the Trackmate cell tracking process.
Trackmate was used to identify and track nuclei in cell migration experiments. All identified spots were kept at the initial thresholding step (A). Spots can be filtered based on a "quality" score (B). An example of nuclear segmentation by Trackmate (C). An example all the tracks identified by Trackmate before (D) and after (E) filtering for tracks that have ≥100 spots.

2.4. Transwell Assays

Transwell assays were used to compare the migration and invasion of cells with and without siRNA knockdown of Aurora A or HSP90B1. For the migration assay, 500,000 cells in serum free RPMI media were seeded onto transwell membranes (8.0 µm pore size, 353097, Corning, Fisher Scientific). Fully supplemented RPMI media was added outside of the insert to act as a chemoattractant. For the invasion assay, transwells were coated with Matrigel (354234, Corning, Fisher Scientific). Several Matrigel concentrations ranging from 3 to 10 mg/mL (diluted using serum free RPMI) were trialled, along with different volumes of Matrigel to change the overall thickness. The rest of the experimental setup was the same as the transwell migration assay described above. 45 µL of Matrigel at 3mg/mL initially appeared to permit invasion during optimisation, however this was not seen in the final experiment.

After 24 hours of growth, inserts were processed, fixed and stained for analysis. Cells that hadn't migrated/ invaded were removed by removing media from TC inserts and rinsing with PBS. Cells were fixed with 3.7% paraformaldehyde (R1026, Agar Scientific) and permeabilised with methanol before staining nuclei with DAPI in PBS at 1µg/mL. Entire inserts were imaged by taking a 6x6 tiled image using an EC Plan-Neopluar 10x/0.3 objective.

To count nuclei of cells that had migrated/ invaded, a circular region of interest was drawn covering the entire membrane. Nuclei were segmented using StarDist 2D (U. Schmidt et al., 2018; Weigert et al., n.d.). The model used was versatile (fluorescent nuclei), the normalise image option was activated, percentile low was set to 1.0, percentile high was set to 99.8 and the probability/score threshold was set to 0.5. Once nuclei were segmented, the image was thresholded on the default setting and the watershed function was applied. Segmented nuclei within the circle region of interest were counted using find maxima. As the image was binary after thresholding, the prominence selected has no effect on the number of maxima that are detected.

2.5. Extraction of RNA from Cell Pellets

Cells were grown in 35 mm plates overnight when extracting RNA for sequencing, otherwise seeding and growing conditions depended on the experiment. RNA was extracted from cells gently pelleted (5 minutes, 300 g) using QIAshredder columns (category number 79654) and QIAGEN RNeasy kit (category number 74134) according to manufacturer's protocol. Briefly, cells were first gently pelleted (5 minutes, 300 g), supernatant removed and then lysed using

the lysis buffer from the RNeasy kit and the QIAshredder columns. Lysed cells were loaded onto gDNA extraction columns to remove any genomic DNA from the samples. Lysate was then loaded onto RNeasy columns with a series of wash buffers before eluting RNA from the column using 30 µL DNase/RNase free water. Sample eluate was reloaded onto the column and centrifuged again to maximise yield. RNA extracts were quantified using a Nanodrop spectrophotometer on the ssRNA setting, using RNase free water as a blank, before being stored at -80 °C.

A number of steps were taken to ensure high quality of extracted RNA:

- Working area and equipment (pipettes, microcentrifuge, pens) were cleaned with RNase Zap (R2020, Sigma) prior to extraction.
- Addition of β-mercaptoethanol (63689, Sigma and 125470100, Arcol Organics) to buffer RLT was an optional step in the protocol that was followed. β-mercaptoethanol is a reducing agent and breaks disulfide bonds in RNases, preventing degradation of RNA.
- Throughout the extraction, to reduce carry over from collection tubes, flow through was carefully removed with a pipette before spinning collection tubes down and removing any residual flow through.
- To maximise the binding of RNA to the column membrane, samples were left for 1 minute to adsorb onto the membrane before carrying out any centrifugation steps.

2.5.1. Quality Control: Nanodrop and Agilent Bioanalyser

For good quality RNA sequencing, a certain quantity, purity and integrity of RNA is required. To ensure RNA samples sent off for sequencing met these requirements, they were checked using a Nanodrop spectrophotometer and Agilent 2100 Bioanalyser. Sample concentrations were ≥ 20 ng/µL and had A260/280 ≥ 2.0 and A260/230 ≥ 2.0 as measured by a Nanodrop. RNA integrity was measured using the Agilent 2100 Bioanalyser. RNA samples were diluted to within the Agilent 2100 Bioanalyser's quantitative range and then measured using the Agilent RNA 6000 Nano Kit (5067-1511, Agilent) according to the manufacturer's protocol on the "total eukaryotic RNA setting". Extracts were required to have an RNA integrity (RIN) score of ≥6.9 out of 10. All extracts surpassed this, with RINs ranging from 9.6 to 9.8.

2.5.2. RNA Sequencing and Analysis

For each cell line, 4 separate RNA samples were sent for sequencing. RNA sequencing was carried out by Novogene. Briefly, their process involved creating a cDNA library from submitted RNA samples, cDNA library quality control, Illumina sequencing, quality control and filtering of raw sequencing data, mapping to a reference genome using the TopHat2 algorithm (v2.0.12m mismatch = 2), expression quantification using HTSeq software on union mode (v0.6.1, -m union), and differential gene expression analysis using DESeq (v1.12.0, padj < 0.05). Additionally, because four replicates were sent per cell, advanced RNA-Seq correlation was calculated to measure the similarity between samples. RNA sequencing was performed with 150 bp paired end reads, with a sequencing depth of 20 million reads per sample.

2.6. PCR

2.6.1. cDNA Synthesis

cDNA was synthesised from RNA extracts to be used in qPCR reactions using iScript Reverse Transcription Supermix (1708841, BioRad) according to the manufacturer's protocol. An appropriate amount of RNA (usually 1 µg) was combined with 4 µL 5x supermix and enough nuclease free water to bring the total reaction volume to 20 µL. Reaction mixes were incubated in a thermocycler (Eppendorf 5332 Mastercycler Personal) with the following protocol: 5 minutes at 25 °C, 20 minutes at 46 °C, 1 minute at 95 °C and held at 4 °C. cDNA was stored at -20 °C.

2.6.2. Primer Design

Primer sequences were selected from literature or designed using https://eurofinsgenomics.eu/en/ecom/tools/pcr-primer-design/. Primers were tested using BLAST (Altschul et al., 1997) to ensure they recognised the correct sequence and to determine the expected product size. Primers were then analysed using NetPrimer, an online primer analysis tool by Premier Biosoft (http://www.premierbiosoft.com/NetPrimer/AnalyzePrimer.jsp). This allows for prediction of tertiary structures that may hinder good priming, as well as and identifying features such as GC content, base repeats and runs, and 3' vs 5' stability. A number of primers were usually tested in this manner for each assay, and the best one ordered to test in the lab (Table 2-3. Primers used for PCR assays.).

Assay	Fwd (5' – 3')	Rev (5' – 3')	Product size (base pairs)
Aurora A	CTGAGGAGGAACTGGCATCAA	ATTAGGTAGACTCTGGTAGCATCAT	297
HSP90B1	CAACGCTTCGGTCAGGGTAT	AGGGGGCATCCAAAACAAGT	341
PLK4	CCTTATCACCTCCTCCTT	CCAAGTCCTTCATTTGTAACC	142
KIFC1	ACTACAGTGCCACAGACA	CCTGATGTGCCAGACTTC	145
NEK2	TGCTTCGTGAACTGAAACATCC	CCAGAGTCAACTGAGTCACTACT	194
TTK	AGCAGCAACAGCATCAAATACT	GCTTGAACCTCCACTTCCTATC	136
CAMK2D	TCTTGACAACTATGCTGGCTACA	TAGAATCGGTGAAAATCCATCCCTT	357/297*
p21	TTAGCAGCGGAACAAGGAGT	GCCGAGAGAAAACAGTCCAG	224
ACTB	CACCCTCTACAATGAGCTGCGTGTG	ATAGCACAGCCTGGATAGCCACGTAC	157
GAPDH	CCACCCATGGCAAATTCCATGGCA	TCTAGACGGCAGGTCAGGTCCACC	597
CAPNS1	ATGGTTTTGGCATTGACACATG	GCTTGCCTGTGGTGTCGC	65
SRPR	CATTGCTTTTGCACGTAACCAA	ATTGTCTTGCATGCGGCC	69
RPS11	AAGCAGCCGACCATCTTTCA	CGGGAGCTTCTCCTTGCC	68

Table 2-3. Primers used for PCR assays.
*Depending on splice variant.

2.6.3. Conventional PCR

Conventional PCR was used to check that primers were working as expected: ensuring PCR products were the expected size; that PCR reactions were generating a single product; and to check that primer dimer products were not forming. For each reaction mix, 0.5 µL of 10 µM forward primer, 0.5 µL of 10 µM reverse primer, 12.5 µL OneTaq Quick-Load 2x Master Mix with Standard Buffer (NEB, M0486S) and 10.5 µL nuclease free water were added to PCR reaction tubes. 1 µL cDNA or 1 µL nuclease free water was added before transferring to a thermocycler. Samples were run on the following protocol: 30 seconds at 94 °C, 30x (15 seconds at 94 °C, 60 seconds at 50-60 °C depending on primers, 20 seconds at 68 °C), 5 minutes at 68 °C and held at 4 °C. PCR products were stored at 4 °C for short term (1 day) or -20 °C for long term storage.

Samples were run on 2% agarose gels made using agarose (BP160-500, Fisher Bioreagents) and 1x TAE buffer. 1x TAE buffer was made up as needed from 50x TAE buffer (2 M TRIS base, 1 M acetic acid, 100 mM EDTA, pH = 8, pH was altered using NaOH pellets). SYBR safe DNA gel stain (S33102, Invitrogen) was added to agarose gel once cool but before set at a

ratio of 3 µL SYBR safe to 50 mL agarose gel. Gels were run for approximately 1 hour at 100 v. Quick load 1kb plus ladder (N0469S, New England Biolabs) was loaded alongside samples as a molecular weight marker. Gels were visualized under UV light using a Biorad Chemidock MP imaging system.

2.6.4. qPCR

2.6.4.1. Master Mix Preparation

qPCR reaction mixes were prepared using iTaq Universal SYBR green master mix (1725121, Biorad). The recipe for one reaction was 5 µL 2x master mix, 0.5 µL forwards primer (10 µM), 0.5 µL reverse primer (10 µM), 3 µL nuclease free water and spiked with 1 µL cDNA. Reaction mix was loaded into 96 well PCR plates and then spiked. Samples were spiked in triplicate and each assay also had triplicate no template control wells. Plates were sealed with optically clear adhesive seals (MSB1001, Biorad). Plates were run on the same day as being prepared and were stored at 4 °C if not run immediately.

2.6.4.2. Thermocycling

Before running, plates were vortexed for 30 seconds and spun down on an Axygen mini plate spinner (CEN1012, Scientific Laboratory Supplies) for 30 seconds. Plates were run on a CFX96 real time PCR system (Biorad) under the following cycling conditions:

1. 95 °C for 30 seconds
2. 95 °C for 5 seconds
3. 60 °C for 30 seconds
4. Steps 2 and 3 repeated for a total of 40 cycles
5. Melt curve from 65 °C to 95 °C.

2.6.4.3. Analysis

Once plate runs had completed, amplification curves and melt curves were examined to make ensure that the PCR run was satisfactory, i.e. a single melt peak at the correct temperature. Relative expression of genes of interest was calculated using the $2^{-\Delta\Delta Ct}$ method. The reference gene was RPS11, and was selected amongst a panel of reference genes for having the most consistent expression between Mel270, OMM2.3 and OMM2.5 cells. The RPS11 assay was always run on the same plate as the gene of interest. When comparing gene expression in Mel270, OMM2.3 and OMM2.5 cells, Mel270 Cts were used to calculate ΔΔCts for OMM2.3 and OMM2.5. When comparing gene expression after siRNA treatment, mock treated samples were used instead.

2.7. Sequencing TP53 in Uveal Melanoma Cell Lines

2.7.1. Genomic DNA Extraction

Genomic DNA was extracted for PCR and sequencing of p53. 100,000 cells were pelleted before adding 500 µL QuickExtract solution (QE0905T, Lucigen) and vortexing to mix. Tubes were incubated at 65 °C for 6 minutes, vortexed, and incubated at 95 °C for 2 minutes. The resulting extract was measured using a Nanodrop spectrometer on the dsDNA setting. Extracts used had an A260/230 ratio >1.6 and an A260/280 ratio between 1.7 and 2.0.

2.7.2. PCR Amplification of TP53

PCR was performed to amplify regions of the TP53 gene, covering exons 2 to 11. The recipe for one reaction was 10 µL OneTaq Quick-Load 2x Master Mix with Standard Buffer, 0.8 µL 10 µM forwards primer, 0.8 µL 10 µM reverse primer, 6.4 µL milliQ water and 2 µL genomic DNA extract, which was equivalent to approximately 50 ng DNA per reaction. All primers except exon 2-3 were from the IARC p53 database (Bouaoun et al., 2016). The primers for exon 2-3 were from Gomes et al., 2012.

Cycling conditions were optimized so that only one PCR product of the correct size was produced (Table 2-4 and Table 2-5), this was checked by running PCR products on a 2% agarose gel containing SYBR safe DNA dye (see section 2.6.3).

For the exon 2-3 assay, additional products were formed. The correct product was excised from agarose gel under UV light and purified using a QiaQuick gel extraction kit (Qiagen, 28704) according to manufacturer's instructions, with minor adjustments. The excised bands were weighed in 1.5 mL tubes and then three volumes of buffer QG was added (100 mg ~ 100 µL). The gels were dissolved by incubating the tubes in a heat block at 50 °C for 12 minutes, vortexing occasionally to mix. One volume of isopropanol was added to the dissolved gels, mixed by pipetting and loaded onto QIAquick columns. All following centrifugation steps were carried out at 13,000 g. The columns were centrifuged for 1 minute and flow through was discarded. 500 µL buffer QG was loaded on to the columns, centrifuged for 1 minute and flow through was discarded. 500 µL buffer PE was loaded on to the columns, incubated at room temperature for 5 minutes, centrifuged for 1 minute and flow through was discarded. This step was repeated for a second time before transferring columns to a clean 1.5 mL tube and centrifuging for 1 minute to fully dry out membrane. Tubes containing columns were placed in a heat block at 45 °C for 5 minutes to remove any

residual alcohol. Columns were transferred to a clean 1.5 mL tube to elute DNA. To elute, 30 µL extraction buffer was loaded onto the columns, incubated at room temperature for 4 minutes and centrifuged for 1 minute.

Once PCR conditions had been optimized for all assays, 2 reactions were set up per cell line per assay. These two reactions were combined after PCR was completed. For all assays except exon 2-3, 8 µL PCR product was loaded onto an agarose gel and compared to a sample of known concentration to estimate DNA concentration. The remaining PCR product was diluted as appropriate and sent for sequencing. For assay exon 2-3, all of the PCR product was loaded onto an agarose gel and purified as written above. Samples were quantified on a nanodrop spectrophotometer, diluted as appropriate and sent for sequencing.

Assay	**Fwd (5' – 3')**	**Rev (5' – 3')**	**Product size (base pairs)**	**Cycling conditions**
Exon 2-3	GATCCCCACTTTTCCT CTTGC	CTCCAGGTCCCCAGC CCAA	297	3
Exon 4	TGAGGACCTGGTCCT CTGAC	AGAGGAATCCCAAAG TTCCA	412	B
Exon 5-6	TGTTCACTTGTGCCCT GACT	TTAACCCCTCCTCCCA GAGA	466	B
Exon 7	AGGCGCACTGGCCTC ATCTT	TGTGCAGGGTGGCAA GTGGC	176	1
Exon 8-9	TTGGGAGTAGATGGA GCCT	AGTGTTAGACTGGAA ACTTT	444	2
Exon 10	CAATTGTAACTTGAA CCATC	GGATGAGAATGGAA TCCTAT	259	D
Exon 11	AGACCCTCTCACTCAT GTGA	TGACGCACACCTATT GCAAG	244	B

Table 2-4. Primers used for TP53 sequencing.

Cycle name	Cycling conditions
B	1 cycle: 94 °C……..2 min 20 cycles: 94 °C….30 sec 63 °C….45 sec, -0.5 °C every 3 cycles 72 °C….1 min 30 cycles: 94 °C 60 °C….45 sec 72 °C….1 min 1 cycle: 72 °C…….10 min Hold at 10 °C
D	1 cycle: 94 °C……..2 min 20 cycles: 94 °C….30 sec 58.5 °C….45 sec, -0.5 °C every 3 cycles 72 °C….1 min 30 cycles: 94 °C 55 °C….45 sec 72 °C….1 min 1 cycle: 72 °C…….10 min Hold at 10 °C
1	1 cycle: 94 °C……..2 min 50 cycles: 94 °C….30 sec 65 °C….45 sec 72 °C….1 min 1 cycle: 72 °C…….10 min Hold at 10 °C
2	1 cycle: 94 °C……..2 min 50 cycles: 94 °C….30 sec 55 °C….45 sec 72 °C….1 min 1 cycle: 72 °C…….10 min Hold at 10 °C
3	1 cycle: 94 °C……..2 min 50 cycles: 94 °C….30 sec 58 °C….45 sec 72 °C….20 sec 1 cycle: 72 °C…….10 min Hold at 4 °C

Table 2-5. Cycling conditions for p53 sequencing primers.

2.7.3. Sequencing

PCR product purification and sequencing was carried out by Eurofins Genomics "TubeSeq" sequencing service. Prior to sample submission, DNA concentration was approximated by comparing band intensity samples of a known concentration run on the same gel. The remaining proportion of PCR product was diluted as necessary to achieve the correct concentration according to Eurofins' guidelines.

2.7.4. Sequence Analysis

Expected sequences for each PCR product were generated using NCBI nucleotide BLAST, querying the forwards primer, searching for the reverse primer in the graphics result, selecting the amplicon and downloading the selection as a FASTA file. Sequencing results for OMM2.3 and OMM2.5 were aligned with the expected sequence using Clustal Omega Multiple Sequence Alignment tool (ver 1.2.4). Peptide sequences derived from aligned OMM2.3 and OMM2.5 sequences were compared against the known p53 peptide sequences using Expasy.

2.8. Flow Cytometry

Flow cytometry analysis was performed on cells treated with pooled siRNA targeting Aurora A or HSP90B1 to quantify the effects on cell cycle populations.

2.8.1. Cell Fixation

Cells were transfected with siRNA as described in section 2.11.1. 72 hours after transfection, cells were ready for flow cytometry analysis. Before fixing, cells were trypsinised and resuspended before pelleting in a centrifuge (5 min, 300 g). Supernatant was removed and pellets were rinsed with PBS to remove all traces of serum, before centrifuging a second time to pellet cells (5 min, 300 g). Supernatant was removed and pellets were resuspended in residual PBS by gently flicking tubes. To fix, 3 mL ice cold 70% ethanol was added drop wise whilst flicking and shaking tubes to obtain fixed single cells. Fixed cells were stored at 4 °C and stained the same day.

2.8.2. Propidium Iodide Staining and Flow Cytometry

Fixed cells were centrifuged to pellet (5 min, 500 g). Supernatant was removed and pellets were resuspended in 2 mL PBS to rinse. Rinsed cells were centrifuged to pellet (5 min, 300 g). Supernatant was removed and pellets were resuspended in 500 µL FxCycle PI/RNase

staining solution (F10797, Invitrogen). Cells were incubated at room temperature for 30 minutes, protected from light. Samples were read on a flow cytometer (Beckman Coulter Cytoflex, CytExpert version 2.0.0.153). A gate was set up to select single cells and at least 20,000 cells were counted per sample.

2.8.3. Analysis

Data were analysed using CytExpert software (version 2.0.0.153). Forward scatter area was plotted against side scatter area to gate to remove debris. Propidium iodide area was plotted against propidium iodide width to gate for single cells. Then, for each cell line, a histogram of propidium iodide area against counts was plotted. The histogram for mock treated cells was used to gate for G1, S and G2 phases of the cell cycle. These gates were used to calculate the proportion of cells in each of these phases for the different siRNA treatments.

2.9. Western Blots

2.9.1. Hot Laemmli Lysis of Cells

To extract protein, cells were lysed using hot Laemmli lysis buffer made with 50mM TRIS (Melford, B2005), 10% glycerol (Melford, 2202), 2% SDS (Alfa Aesar, J63394), pH = 6.8. Before lysing, media was removed from cells and cells were washed twice with sterile PBS. To lyse, plates were placed on a heat block set to 105 °C with an appropriate volume (e.g. 150 µL for a confluent 6 cm dish) of Laemmli lysis buffer preheated to 105 °C and scraped with a cell scraper. Lysate was then transferred to a screw capped 1.5ml tube and heated in the heat block set to 105 °C for 10 minutes, vortexing approximately every 2 minutes. A small amount of diluted lysate was made (1/5 dilution in MilliQ Water) before storing the lysate and diluted lysate at −20 °C.

2.9.2. BCA Assay

Protein concentration of lysates was determined by measuring the 1/5 diluted samples using the colourimetric BCA assay (Thermo Scientific, category number 23227).
Protein standards, ranging from 25 - 2000 µg/mL albumin, were made up according to manufacturer's instructions and stored as single use aliquots at -20 °C.
10 µL of each standard and sample was loaded in triplicate into 96 well plates. 200 µL working reagent (1:50 mixture of reagent A and reagent B) was added to each well. A visual inspection was made to ensure sample and reagents were well mixed before incubating in the dark at 37 °C for 30 minutes. Absorbance was measured at a wavelength of 562 nm on a

plate reader. Protein concentration of sample lysates were then calculated using a standard curve created with blank adjusted means of the protein standards.

2.9.3. SDS-PAGE and Western Blot

2.9.3.1. Gel Preparation

To prepare gels, 10% acrylamide gels were poured (9.7 mL MGW, 5 mL TRIS (1.5 M, pH8.8), 5 mL 40% acrylamide/bis (37.5:1) (Arcos Organics, 33022 5000) 200 µL SDS, 100 µL 10% APS (Sigma, A3678-25G), 20 µL TEMED (Sigma, T9281) and topped with a stacking gel once set (3.17 mL MGW, 1.25 mL TRIS (0.5M, pH6.8), 0.5 mL acrylamide/bis (37.5:1), 50 µL SDS, 25 µL 10% APS, 5 µL TEMED). APS and TEMED were only added immediately before pouring gels.

2.9.3.2. Sample Preparation

Samples were diluted with 10x loading buffer (1M DTT (Melford, D1100-25.0), 1% (w/v) bromophenol blue (BDH Chemicals, 20017) in a ratio of 9 parts sample: 1 part 10x loading buffer. Samples plus 10x loading buffer were prepared to an appropriate concentration (depending on which target was being probed) by diluting with 1x loading buffer (50 mM TRIS pH 6.8, 2% SDS v/v, 10% glycerol v/v, 0.1 M DTT, 0.1% bromophenol blue w/v). Samples were prepared to a total volume of 30 µL or 15 µL depending on whether they were to be loaded into a 10 or 15 well gel, respectively. Diluted samples were then heated in a heat block at 100 °C for 5 minutes. After heating, samples were vortexed and briefly span down to remove droplets from lids.

2.9.3.3. Gel Electrophoresis

Gels were loaded into Bio-Rad electrophoresis tanks and filled with TRIS-glycine running buffer (25 nM TRIS, 192 mM glycine, 0.1% SDS, pH 8.3). Alongside samples, each gel was also loaded with a lane of 2 µL PageRuler Plus prestained protein ladder (Thermo Fisher, 26619). Gels were run at 45 mAmp per gel for approximately 40 minutes, using the bands of ladder to gauge when to stop. Gels were transferred onto a nitrocellulose membrane using the Biorad TurboBlot system (category number: 170-4270) and transferred using a BioRad Trans-Blot Turbo transfer system machine on the “mixed molecular weight” setting (1.3A, 25V, 7 minutes).

2.9.3.4. Western Blotting

All incubations were carried out at room temperature unless otherwise stated. Membranes were placed on a gyratory rocking machine for all incubations.

Membranes were stained briefly (30 seconds) with Ponceau stain to visualise protein bands and check for successful transfer. Membranes were cut into appropriate sections to probe

for targets of different molecular weight before rinsing in PBS to remove traces of Ponceau stain. Membranes were then blocked, stained with primary antibodies and stained with secondary antibodies. The blocking solution and antibody diluent varied depending on what primary antibody was being used to probe the membrane, details of these solutions can be found in Table 2-8.

Membrane sections were incubated for at least 1 hour in blocking solution. Blocking solution was completely removed before adding primary antibody solutions (Table 2-6). Primary antibody incubations were carried out overnight at 4 °C.

Primary antibody solutions were removed and stored at 4 °C or -20 °C, depending on whether antibody solutions had been prepared with NaN_3 (stored at 4 °C) or without NaN_3 (stored at -20 °C). Membrane sections underwent 3x 5 minute PBS washes before adding secondary antibody solution (Table 2-7). Secondary antibodies were diluted in 5% milk in PBS with the exception of HSP90B1 sections, where secondary antibodies were diluted in 2% BSA in TBST (Table 2-8). All remaining incubations were carried out protected from light. Secondary antibodies were incubated for 1 hour. Membrane sections underwent 3x 5 minute PBST (0.05% tween, Melford, P1362) washes before being stored in PBS. Membranes were stored at 4 °C in PBS, protected from light, until being imaged using a LiCOR Odyssey FC (700 and 800nm, 2 minute exposure). Membranes were usually imaged the same day as blotting is finished. Short term (up to 1 week), membranes were stored in PBS at 4 °C, protected from light. Long term, membranes were wrapped in clingfilm with a very small amount of PBS and stored at -20 °C.

Target	Host	Clonality	Supplier	Reference code	Dilution
α-Tubulin	Mouse	Monoclonal	Sigma	T6199	1/1000
KIFC1	Rabbit	Monoclonal	Abcam	ab172620	1/5000
Aurora A	Rabbit	Monoclonal	Abcam	ab52973	1/1000
HSP90B1	Rabbit	Monoclonal	Abcam	ab108606	1/500

Table 2-6. Primary antibodies used for western blotting.

Target	Host	Clonality	Supplier	Reference code	Dilution	Dye
Anti-Rabbit	Donkey	Polyclonal	Licor	926-32212	1/15000	IRDye 800CW
Anti-Mouse	Donkey	Polyclonal	Licor	926-68073	1/15000	IRDye 680RD

Table 2-7. Secondary antibodies used for western blotting.

Antibody	Blocking Solution	Primary Antibody Diluent	Secondary Antibody Diluent
α-Tubulin	PBS + 5% milk or TBST + 5% BSA	PBS + 5% milk or TBST + 5% BSA + 0.05% NaN_3	PBS + 5% milk
KIFC1	PBS + 5% milk	PBS + 5% milk	PBS + 5% milk
Aurora A	TBST + 5% BSA	TBST + 5% BSA + 0.05% NaN_3	PBS + 5% milk
HSP90B1	TBST + 2% BSA	TBST + 2% BSA + 0.05% NaN_3	TBST + 2% BSA

Table 2-8. Blocking and diluent solutions used for western blotting.

2.9.3.5. Image Analysis

Blots were analysed using ImageStudio Lite software (version 5.2.5). Signal intensity of bands were quantified and normalised by dividing with the signal of the loading control, α-tubulin.

2.10. Aurora A and HSP90B1 Inhibitors

Alisertib (ALS) (Selleckchem, MLN8237) and GRP94 Inhibitor-1 (iGRP94) (MedChemExpress, HY-112910/CD-0067933) were used to inhibit Aurora A and HSP90B1, respectively. An MTS assay (CellTitre 96® AQ_{ueous} One Solution Cell Proliferation Assay, Promega, G3580) was used to determine the appropriate concentrations to use. ALS and iGRP94 stocks were prepared to 10 mM in DMSO and stored at -80 °C. 100 nM ALS and 5 µM iGRP94 chosen concentrations for experiments.

2.10.1. MTS Assay

OMM2.3 cells were seeded at a density of 3000 cells/well in a 96 well plate. The following day, inhibitor was added at a range of concentrations from 20 µM to 1 nM in triplicate wells, plus a negative control condition with no inhibitor added. Cells were left to grow for 72 hours before carrying out the MTS assay according to manufacturer's instructions. Briefly, media was removed and replaced with 100 µL fresh media before adding 20 µL MTS to each well. Media and reagent were also added to triplicate wells with no cells to act as a blank. Cells were returned to the incubator for 2 hours before reading absorbance at 490 nm on a plate reader. Absorbance from triplicate wells was averaged, then the blank average was subtracted, then values were normalized to the negative control untreated wells.

2.11. siRNA Transfection

siRNA transfections were carried out using RNAiMax Lipofectamine reagent (Invitrogen, 56531). Stock siRNAs were stored at -20 °C at 10 µM or 20 µM. Both forwards and reverse transfection methods were used. For all siRNA experiments, mock and siCon conditions were also included. The mock condition was prepared exactly the same as experimental conditions with the exception that OptiMEM (Gibco, 31985-062) was added instead of siRNA. siCon was either a scrambled siRNA called AllStars negative control siRNA (Qiagen, SI03650318), or siGFP-22 which targets GFP. In the siRNA screen and deconvolution experiments, AllStars Death was used as a positive control of siRNA transfection. AllStars death leads to cell death upon successful transfection.

2.11.1. Forwards Transfection

A forwards siRNA transfection refers to transfection of cells that have already been plated out and grown for a short time. For a forwards transfection, cells were seeded and left to grow for 24 hours. The next day, cells were transfected with siRNA. The following volumes were used for a transfection in final volume of 550 µL with a final concentration of siRNA of 40 nM. Volumes were scaled up and down to accommodate multiple transfection conditions and different final volumes. 1.1 µL stock siRNA at 20 µM was diluted in 57.6 µL OptiMEM (Gibco, 31985-062). 0.88 µL RNAiMax was diluted in 8 µL OptiMEM. 8 µL diluted RNAiMax was added to diluted siRNA, mixed gently and incubated at room temperature for 20 minutes to form siRNA-lipid complexes. 430 µL unsupplemented RPMI was added to cells, followed by 65 µL siRNA-lipid complex and cells were returned to the incubator. 4 hours

after transfection, 55 µL FBS was added to cells. 24 hours after transfection, media was removed from cells and replaced with supplemented RPMI as outlined in section 2.1.1.

2.11.2. Reverse Transfection

A reverse siRNA transfection refers to transfection of cells that are seeded at the time of transfection. It is more suitable for high throughput procedures. The following volumes are used for one transfection in a 96 well plate with a final volume of 125 µL and a final siRNA concentration of 40 nM. Volumes of reagents were scaled depending on the number of reactions and the final volume. 0.15 µL RNAiMax was diluted in 2.85 µL OptiMEM. 0.5 µL siRNA at a stock concentration of 10 µM was diluted in 21.5 µL OptiMEM. This step was carried out directly into the tissue culture vessel that cells would be seeded into. 3 µL diluted RNAiMax was added to diluted siRNA and incubated for 20 minutes at room temperature to form siRNA-lipid complexes. At this point, cells were dissociated and resuspended in unsupplemented RPMI media. Cells were counted and diluted to the desired concentration and 87.5 µL diluted cell suspension was added to the tissue culture vessel containing the siRNA-lipid complex. Cells were returned to an incubator for 4 hours before adding FBS to a final concentration of 10%. 24 hours after transfection, media was removed from cell and replaced with supplemented RPMI as outlined in section 2.1.1.

2.11.3. siRNA Screen

The siRNA screen and related deconvolution experiments were carried out using the reverse transfection method. Four siRNAs were ordered from Qiagen for each gene target, spread across four plates (Appendix A). siRNAs were reconstituted in nuclease free water according to manufacturer's instructions. A fifth "pool plate" was created, pooling the different siRNAs into one well per gene target. A sixth "experimental plate" was created according to a plate plan, which randomised the location of pooled siRNA. It also introduced, for each cell line: six randomised mock wells; six randomised siCon-ve wells; and one siCon+ve well in a known position. The experimental plate was used to set up siRNA screens. Randomising the location of target siRNAs, mock and siCon-ve wells allowed subsequent imaging and analysis to be carried out blind. The individual siRNAs in the original four plates were used to carry out siRNA deconvolution after the initial siRNA screen. All plates were stored at -20 °C.

For both the screen and deconvolution experiments, 72 hours after transfection cells were fixed and stained as described in section 2.2. Cells were imaged and analysed as described in section 2.3.3.

2.12. Statistical Analysis

Statistical analysis was performed in GraphPad Prism (v9.3.1). Assumptions of parametric tests, such as gaussian distribution of data and equal variability of differences, were tested to ensure statistical models fitted the data. In cases where assumptions were not met, the appropriate non-parametric tests were used instead.

Chapter 3.

Characterisation of Centrosome Amplification in Patient Matched Primary and Metastatic Uveal Melanoma Cells Followed by Transcriptomics Comparison to Identify Drivers of Centrosome Amplification

3.1. Introduction

Centrosome amplification (CA) is a phenomenon that has been identified in many different types of cancer (Chan, 2011). Recently, our group completed the first study of CA in uveal melanoma (Sabat-Pośpiech et al., 2022). This revealed that CA was present in uveal melanoma tumours, early passage patient derived tumour cells and uveal melanoma cell lines. CA was associated with the more aggressive monosomy 3 subtype of uveal melanoma (Sabat-Pośpiech et al., 2022), which is in turn highly associated with metastasis (Gill et al., 2022; Prescher et al., 1996; Sandinha et al., 2005). In order to further study the development and functional consequences of CA in uveal melanoma, cell lines were selected. Mel270, OMM2.3 and OMM2.5 cell lines were attractive because they were a patient matched group of cell lines, derived from the primary tumour and two liver metastases (Figure 3-1).

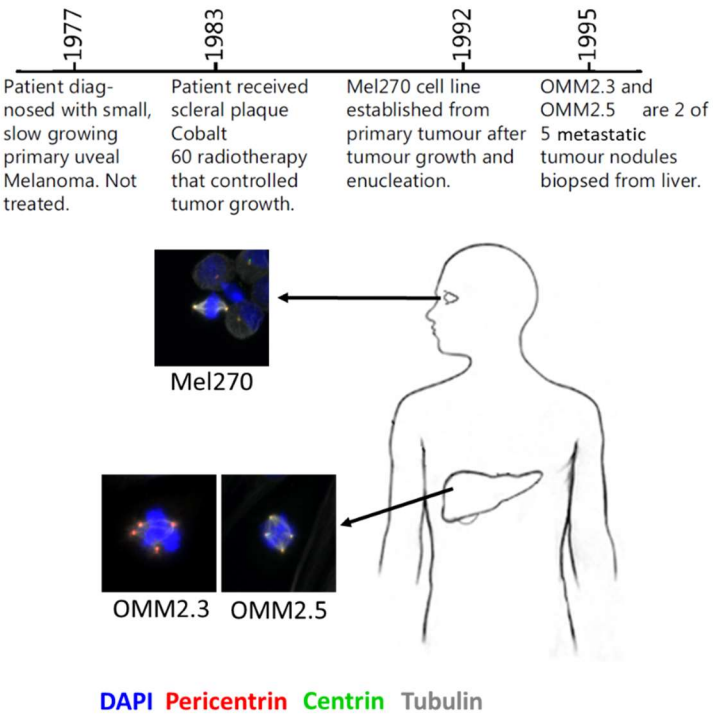

Figure 3-1. Origins of Mel270, OMM2.3 and OMM2.5 cells.
Mel270, OMM2.3 and OMM2.5 cells are the cell lines used in this study. They are patient matched cell lines derived from primary uveal melanoma and two distinct liver metastases. A timeline describes key dates in disease progression for the patient: diagnosis, radiotherapy, enucleation and liver biopsy. Both cell lines were established after the patient had received cobalt-60 plaque radiotherapy (P. W. Chen et al., 1997).

3.1.1. Mel270, OMM2.3 and OMM2.5 Cells: A Patient Matched Cell Line Model of Uveal Melanoma Disease Progression

Mel270, OMM2.3 and OMM2.5 are three uveal melanoma (UM) cell lines that have been used throughout this study. All three cell lines are patient matched, with Mel270 cells being derived from the primary tumour and OMM2.3 and OMM2.5 cells being derived from two distinct liver metastases (P. W. Chen et al., 1997). Preliminary work indicated that the two metastatic cell lines show high levels of CA, whereas Mel270 appeared to have lower levels of CA (Fielding, unpublished). This presented the possibility of a useful model to study CA in a naturally occurring setting of disease progression, as opposed to CA that had been artificially induced, such as in Löffler et al. 2011, Coelho et al. 2015 and Yoshino et al. 2020.

The first aim of this chapter was to characterise the UM cell panel in terms of CA, and establish how they may be used as a model to study CA. The second aim was to do an RNA-Seq experiment to compare the three cell lines to identify potential drivers of CA. Both of these aims provided the foundation for further work in this PhD.

To characterise cell lines, CA was measured using immuno-fluorescent labelling of centrosomes, confocal imaging and imaging analysis. Additionally, as a key potential regulator of CA, p53 was sequenced for the three cell lines. Subsequently, RNA-Seq was used to identify key changes in gene expression between the cell lines in the UM cell panel that may have contributed to the different CA states. Key differentially expressed genes identified by RNA-Seq were then validated using a second method, qPCR.

3.1.2. The Use of ‘omics Technologies to Study Cancer

“Omics” technologies are characterised by the identification and quantification of all of a particular molecule of interest within a sample. For example DNA sequence in genomics, RNA expression in transcriptomics, proteins in proteomics and metabolites in metabolomics. Over the past 20 years, the use of omics technologies to understand biological process has been ever increasing, providing large sets of data and insight into diseases such as cancer (Chakraborty et al., 2018; Heo et al., 2021; Karczewski & Snyder, 2018).

The choice of which ‘omics technology to use requires consideration of the disease that is being studied, what question is being asked, and what information will be provided. For this study, we wanted to identify what had driven the increased levels of CA in OMM2.3 and OMM2.5 cells compared to Mel270 cells. We hypothesised that it was due to altered gene expression, which could be measured at the level of RNA (transcriptomics/ RNA-Seq) or

protein expression (proteomics). Ultimately, RNA-Seq was the method that was deemed most appropriate.

3.1.2.1. RNA Sequencing versus Proteomics

Cancer is a disease that is driven by DNA mutations and dysregulated gene expression, and RNA sequencing, or RNA-Seq, is a method that can measure these changes. An advantage of RNA-Seq over proteomics is that RNA-Seq is able to detect transcripts over a wide range of levels, from very low to very high. Highly abundant proteins can mask the detection of proteins expressed to a low level in proteomic analysis (Dupree et al., 2020; Timp & Timp, 2020; Zubarev, 2013). Thus, the wide dynamic range of RNA-Seq compared to proteomics allows for greater coverage of what is being expressed in a cell. RNA-Seq, but not proteomics, can detect the expression on non-protein coding RNAs such as lncRNAs, which have emerged as important players in cancer progression (Aprile et al., 2023; Y. Fang & Fullwood, 2016; Yu et al., 2020). A major disadvantage of transcriptomics compared to proteomics is that RNA transcript doesn't necessarily translate into protein expression (Y. Guo et al., 2008; Schwanhüusser et al., 2011). Also, post translational modifications, that potentially regulate protein stability or activity, are missed (Aebersold et al., 2018; J. M. Lee et al., 2023). Therefore, some studies take a multi 'omics approach (Chaudhary et al., 2018; Feng et al., 2021; Heo et al., 2021; Robertson et al., 2017). That is beyond the scope of this study, however the protein levels of specific RNA-Seq results of interest can be determined by western blotting.

3.1.2.2. RNA Sequencing Workflow

The main steps of RNA-Seq are RNA extraction, cDNA library construction, RNA sequencing, mapping sequencing reads to reference genome and differential expression analysis. If desired, there are further analysis that can be taken. Examples of further analysis that can be performed are gene ontology (GO) enrichment analysis and protein-protein interaction analysis. Additionally, after mapping reads to a reference genome, there is also the opportunity to look for single nucleotide polymorphisms (SNPs) and indels, for alternative splicing analysis and for new transcript prediction. For this piece of work, RNA was extracted, its quality analysed and then sent to a company, Novogene, for the remaining steps.

The construction of a cDNA library has several steps itself. Novogene use a proprietary fragmentation buffer to randomly fragment the RNA. Random hexamers and reverse transcriptase are used to synthesise the first strand. Another proprietary buffer is used to synthesise the second strand by nick translation, which labels the cDNA (Green & Sambrook,

2022). The cDNA is purified, has an A-tail added to the 3' end and then sequencing adapters are ligated onto the ends. The cDNA library is enriched using PCR.

After sequencing, a key quality control step is to filter the raw reads so that only high quality reads remain, which improves the downstream analysis. Novogene removes the following reads:

- Reads with adaptor contamination.
- Reads where ≥10% nucleotides are uncertain.
- Reads where ≥50% of the read has base qualities of ≤20*.

*A base quality of 20 represents a 1 in 100 error rate. Quality scores are logarithmic, such that Q10 represents a 1 in 10 error rate and Q30 represents a 1/1000 error rate.

High quality RNA is required for the best RNA-Seq results. A Nanodrop spectrophotometer can be used to detect contamination by protein or extraction reagents. Contaminations impact on the ability to synthesise a high quality cDNA library, which in turn effects quality of subsequent sequencing (Kukurba & Montgomery, 2015). Another RNA quality measure is the RNA integrity number (RIN) score, generated by the Agilent Bioanalyser. Numerous factors contribute to the RIN score, including the ratio of 26s to 18s rRNA and the presence of small fragments of degraded RNA (Schroeder et al., 2006). A low RIN score effects the accuracy of subsequent RNA-Seq (E. A. Chen et al., 2014).

3.1.3. Chapter Aims

- Quantify centrosome amplification in Mel270, OMM2.3 and OMM2.5 cell lines.
- Extract high quality RNA from Mel270, OMM2.3 and OMM2.5 cells for RNA-Seq.
- RNA-Seq and analysis
- Determine appropriate reference gene for qPCR assays.
- Confirm selected RNA-Seq results using qPCR.
- Identify differentially expressed genes for further analysis in an siRNA screen.

3.2. Centrosome Amplification in Uveal Melanoma Cell Lines

To make initial observations of CA in Mel270, OMM2.3 and OMM2.5 cells, immunofluorescence experiments (see section 2.2 and 2.3.1) were set up using pericentrin as a centrosome marker (Figure 3-2). CA was observed in all three cell lines, however there appeared to be higher levels in the two metastatic cell lines, OMM2.3 and OMM2.5.

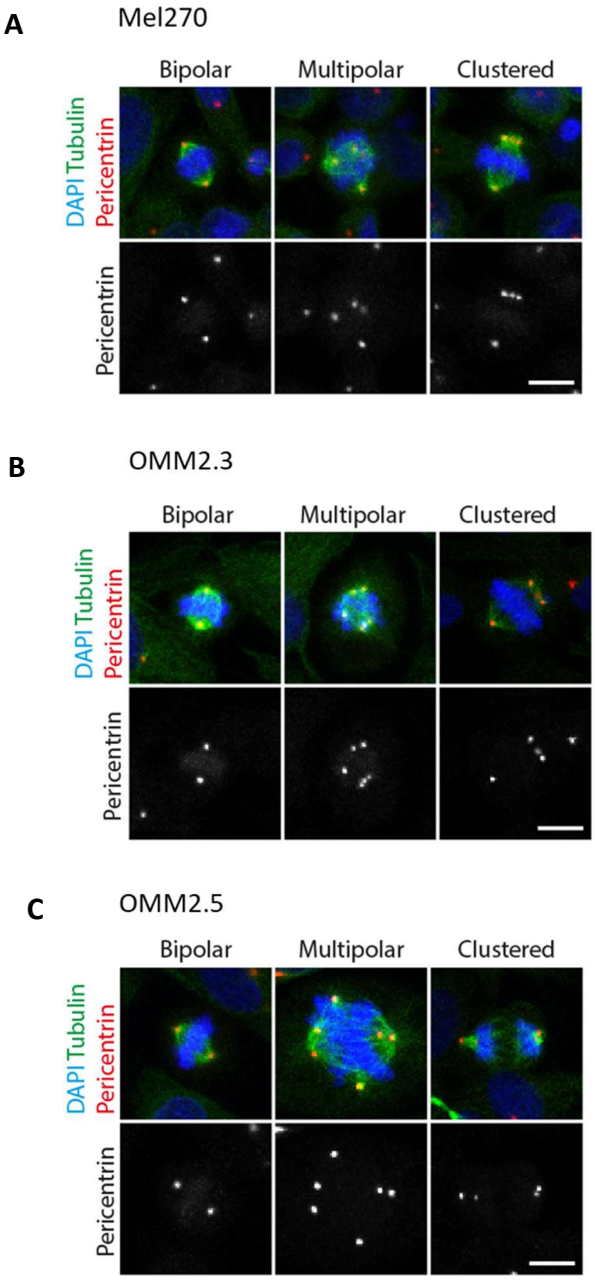

Figure 3-2. Investigation into centrosome amplification in uveal melanoma cells.
Mel270 (A), OMM2.3 (B) and OMM2.5 (C) cells fixed and processed for immunofluorescence, with cells stained for α-tubulin (green), pericentrin (red) and with DAPI (blue). Pericentrin was used as a marker for centrosomes, tubulin and DAPI helped to identify mitotic cells. Scale bars are 10 µm.

We sought to refine this analysis, in order to more accurately measure CA. The use of two labels to identify centrosomes is considered standard, some of these markers include γ-tubulin, CP110, CEP135 and centrin (M. Guo et al., 2023; Marteil et al., 2018; M. Wang, Rogers, et al., 2019). For this work, pericentrin and centrin were used as a dual marker to label bona fide centrosomes. Improvements were made to image acquisition, taking high resolution z-stacks of individual mitotic cells. This ensured no centrosomes were missed out

from the plane of focus, and made it easier to distinguish nearby centrosomes. Example images can be seen in Figure 3-3, panels A-C. Cells were imaged and analysed blind to avoid bias. Between 83 and 99 mitotic cells were analysed per cell line. As with the initial immunofluorescence work, CA was observed in all three cell lines. However, the percentage of mitotic cells with >2 centrosomes in OMM2.3 and OMM2.5 cells (33 and 25% respectively), was higher than in Mel270 cells where only 10% mitotic cells had >2 centrosomes (Figure 3-3, panel D). These values can be put into context with the level of CA seen in other cancer cell lines. In a 2018 study by Marteil et al., CA was measured in 53 cell lines from the NCI-60 panel, using comparable methods (z-stacks of mitotic cells with dual centrosome markers). Since low levels of CA can also be seen in non-cancerous cells, 5 non-cancerous cell lines were measured to calculate a "baseline" level of CA, below which a cell line would not be considered as having CA. This baseline was ≤13%, indicating the 10% seen in Mel270 could be considered as having low or negligible CA. Of the 53 NCI-60 cell lines that were measured, 28 had CA above the 13% baseline. If OMM2.3 and OMM2.5 cells were included with those 28 cell lines, they would have the 8th and 13th highest levels of CA respectively. All in all, these results showed that Mel270, OMM2.3 and OMM2.5 cells can be used as a model to study the development of CA as a cancer has progressed from primary (Mel270) to metastatic (OMM2.3 and OMM2.3) disease.

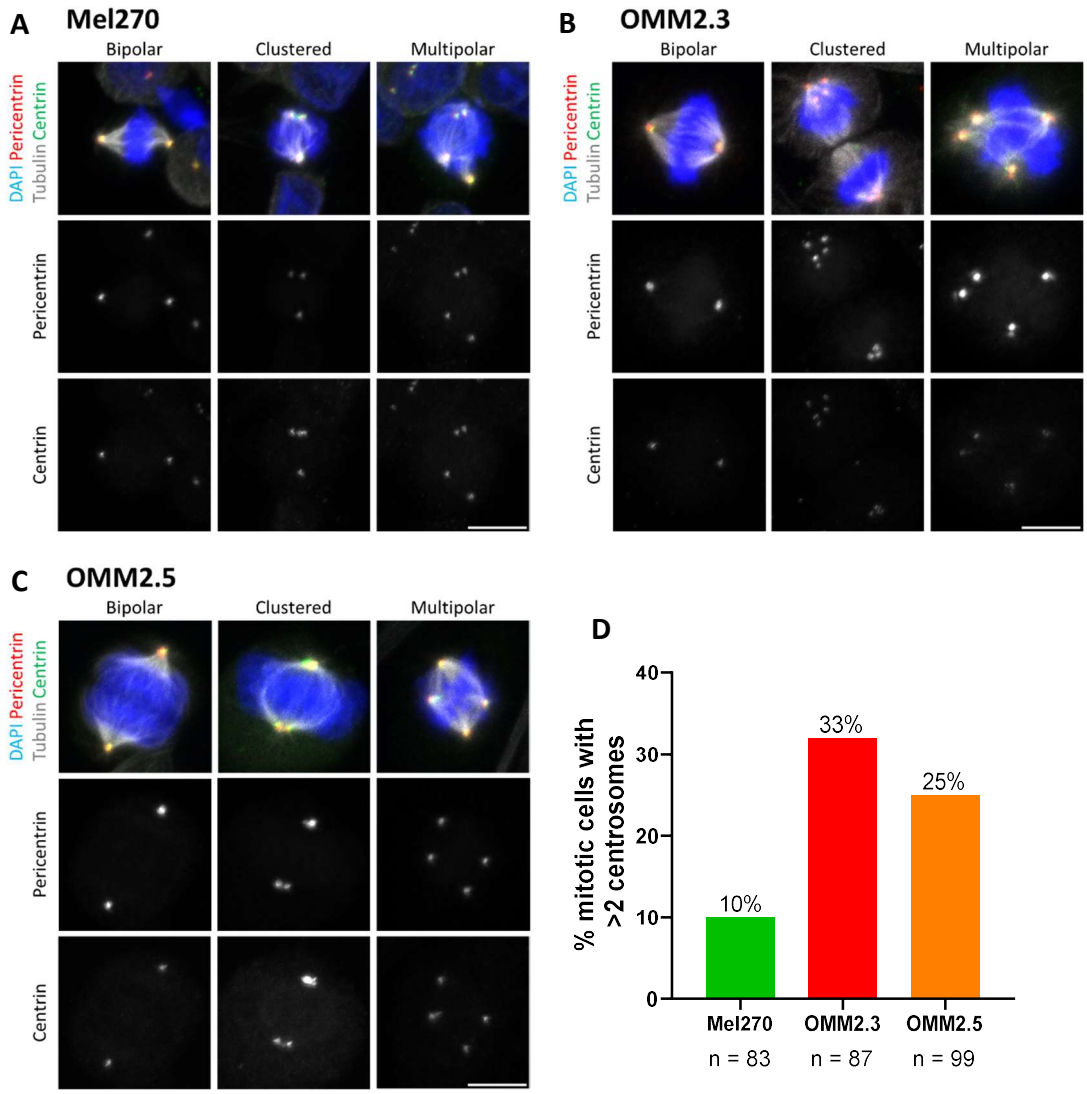

Figure 3-3. OMM2.3 and OMM2.5 cells, but not Mel270 cells, display high levels of centrosome amplification.
Maximum intensity projections of Mel270 (A), OMM2.3 (B) and OMM2.5 (C) cells stained for α-tubulin (grey), pericentrin (red), centrin (green) and with DAPI (blue). Pericentrin and centrin were used to label centrosomes, tubulin and DAPI were used to identify mitotic cells. The proportion of cells with >2 centrosomes (i.e. with centrosome amplification) was calculated for each cell line following blind image analysis (D). Scale bars are 10 µm.

3.3. RNA Sequencing

Having established the use of Mel270, OMM2.3 and OMM2.5 cells as a model to study CA, we chose RNA-Seq to probe gene expression differences and investigate changes that might play a role in the different levels of CA. From this RNA-Seq analysis, the aim was to select genes to be used in an siRNA screen to link changes in expression to functional changes in the development on CA in OMM2.3 and OMM2.5 cells. If a gene was overexpressed in the metastatic cell lines, we wanted to investigate whether siRNA knockdown of these genes in the metastatic cell lines could reverse the CA status of these cells. If a gene was

underexpressed in the metastatic cell lines, we wanted to investigate whether siRNA knockdown of these genes in Mel270 cells could induce an increased level of CA.

3.3.1. Preparation of Samples for RNA Sequencing

High quality RNA was extracted from each of the cell line using an optimised RNA extraction protocol (see section 2.5), in accordance with guidelines from Novogene. Four samples were sent off for each cell line. Other than four A260/230 ratios, which fell just short of recommendations, the RNA quantity, purity and integrity of the samples far surpassed the guideline requirements (Table 3-1 and Figure 3-4. RNA integrity measured by Agilent Bioanalyser 2100.). This resulted in very high quality RNA-Seq results, which is apparent from the various stages of QC that were performed before and after mapping to a reference genome (Appendix B and C).

Sample name	Extraction Date	Nucleic Acid Concentration (ng/µl)	A260	A280	260/280	260/230
Mel270 1	20/11/2018	661.8	16.55	7.94	2.08	2.04
Mel270 2	17/11/2018	291.0	7.28	3.46	2.10	2.15
Mel270 3*	23/11/2018	266.1	6.65	3.18	2.09	1.95
Mel270 4	26/11/2018	409.0	10.23	4.89	2.09	2.05
OMM2.3 1	20/11/2018	440.3	11.01	5.27	2.09	2.16
OMM2.3 2	18/12/2018	565.5	14.14	6.85	2.06	2.03
OMM2.3 3*	21/11/2018	261.8	6.55	3.12	2.10	1.99
OMM2.3 4*	19/12/2018	199.4	4.99	2.37	2.10	1.96
OMM2.5 1	21/11/2018	164.3	4.11	1.95	2.11	2.00
OMM2.5 2*	23/11/2018	162.9	4.07	1.93	2.11	1.96
OMM2.5 3	20/11/2018	302.4	7.56	3.61	2.09	2.11
OMM2.5 4	18/12/2018	567.6	14.19	6.83	2.08	2.19

Table 3-1. RNA extracts for sequencing.
RNA was extracted from the three UM cell lines (4 individual biological replicates of each cell line) using Qiagen RNeasy kit, with an optimised protocol. A summary of the 12 extracts that were chosen for RNA sequencing are presented in this table. Extracts were selected for their high purity (260/280 ≥ 2, 260/230 ≥ 2) and high concentration (≥ 20 ng/µL). *Samples with a 260/230 ratio below 2, but were deemed close enough to 2 to be acceptable.

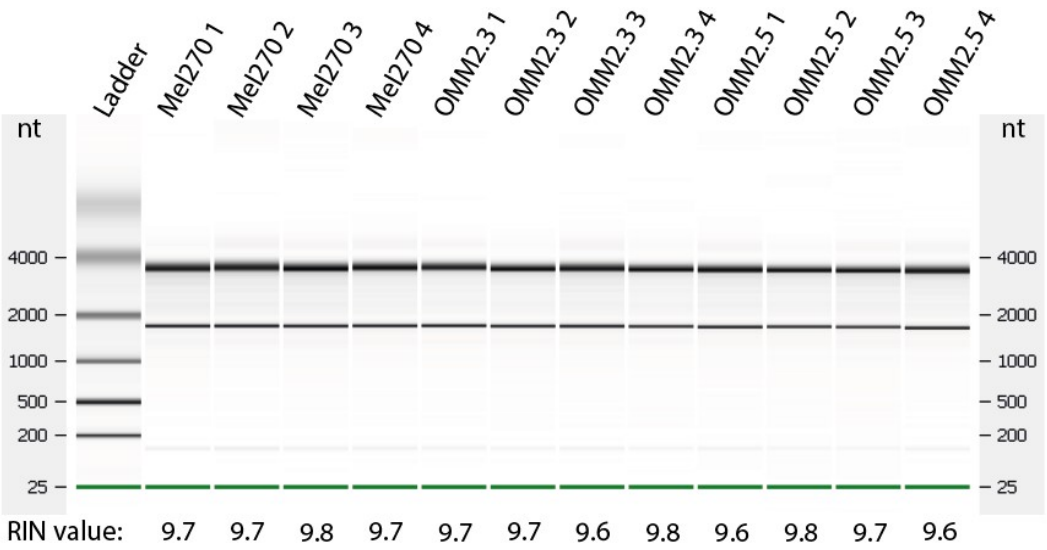

Figure 3-4. RNA integrity measured by Agilent Bioanalyser 2100.
A digitally created mock electrophoresis gel, representing the electropherogram trace of each RNA extract selected for RNA-Seq. The RNA integrity (RIN) score for each sample can be found below their lane in the mock gel.

The Agilent Bioanalyser 2100 generates an RNA integrity (RIN) score using a proprietary algorithm. The Agilent Bioanalyser 2100 measures RNA integrity by running dyed samples through capillary electrophoresis, detecting the different sizes and abundances of RNA fragments. This generates an electropherogram which can be used to create a mock gel for ease of analysis. High RNA integrity is indicated by clear bands on the mock gel at just below 4000 and 2000 for 28s and 18s rRNA respectively, and a lack of bands anywhere else (Schroeder et al., 2006). A RIN score of ≥0.8 was requested by Novogene for high quality RNA-Seq data. All 12 values for these samples far exceeded this with RIN scores of ≥9.6 (Figure 3-4).

3.3.2. Differentially Expressed Genes

A key result from the RNA-Seq analysis was the identification of differentially expressed genes (DEGs) using the DESeq algorithm. DESeq was used to normalize readcounts, compare gene expression between cell lines and generate an adjusted p value (padj) to determine differential gene expression.

A gene was considered to be a DEG if it had a padj of ≤0.05 ($-\log_{10}(0.05) = 1.3$). For OMM2.3 versus Mel270 cells, there were 9297 DEGs and for OMM2.5 versus Mel270, there were 7613 DEGs (Figure 3-5, panels A and B). For OMM2.3 versus OMM2.5 there were only 112 DEGs, indicating a similarity between those two cell lines (Figure 3-5, panel C). For the purposes of this research, it was the DEG lists for OMM2.3 versus Mel270 and OMM2.5

versus Mel270 that were of interest, as these would help to identify changes in gene expression that lead to increased CA in OMM2.3 and OMM2.5 cells compared to Mel270 cells.

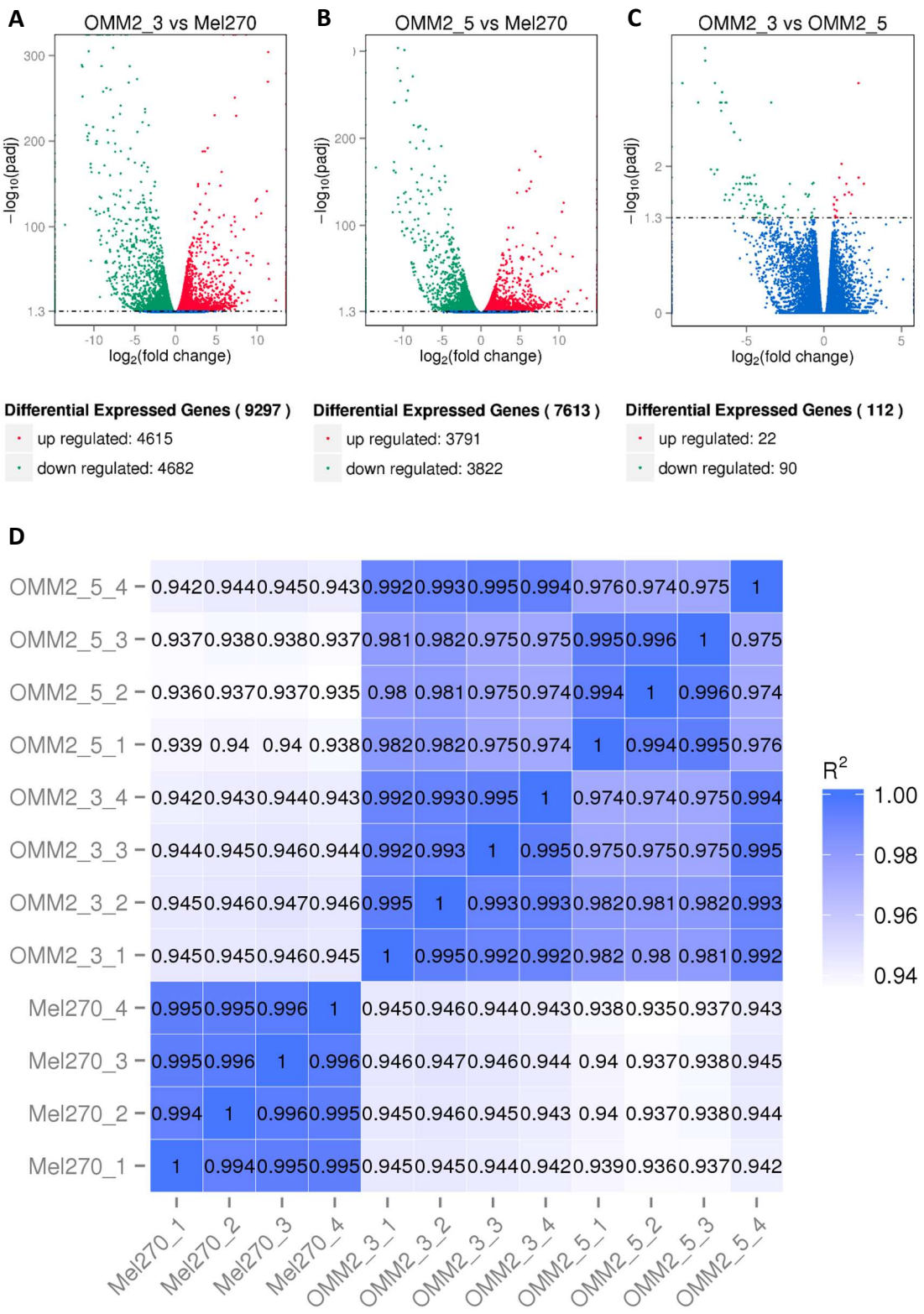

Figure 3-5. RNA sequencing of uveal melanoma cells.
Volcano plots of differentially expressed genes (DEGs) between OMM2.3 versus Mel270 (A), OMM2.5 versus Mel270 (B) and OMM2.3 verses OMM2.5 (C) identified through RNA-Seq and subsequent analysis. DEGs were identified using DESeq, with a padj of ≤0.05 ($-\log_{10}(0.05) = 1.3$) used as a cut off to label genes as being differentially expressed. Pearson correlation between each sample was also calculated for further comparison of sample similarity (D).

3.3.2.1. RNA Expression Correlation

Correlation between samples can be measured to check that biological replicates are similar to each other (Figure 3-5, panel D). For each sample combination, the $\log_{10}$(FPKM+1) of every gene was plotted against each other and the R^2 values have been displayed as a matrix. According to the Standards, Guidelines and Best Practices for RNA-Seq (V1.0, 2011) produced by the ENCODE Consortium, typical R^2 between biological replicates should be 0.92 – 0.98. In this case, the biological replicates are four separate RNA extracts for each cell line. The R^2 values between these are all very high, being >0.97. This gives confidence that the samples were collected in a reproducible manner. Despite the high number of DEGs between OMM2.3 or OMM2.5 cells versus Mel270 cells, there was also a high correlation of gene expression between cell lines, with the R^2 values between cell lines all being >0.93. This is because the cell lines were all derived from the same patient. The genetic similarity between these cell lines is an advantage of this model; the genes which are DEGs are more likely to be a result of disease progression, rather than natural biological variability that would be seen between different people.

3.4. Selecting Genes for an siRNA Screen

Our data identified thousands of genes as being differentially expressed in OMM2.3 and OMM2.5 cells when compared to Mel270 cells (see section 3.3.2). A targeted approach was taken to reduce this number to one that is more manageable for a screen. A list of 138 genes that were proposed to have roles in CA was compiled from existing literature. These included the list of genes identified in a review by Fukasawa 2007, the list of genes selected for the prognostic CA20 screen developed by Ogden et al., 2017, and genes involved in centriole elongation following the discovery of a link between centriole elongation and CA (Marteil et al., 2018). This list was then cross referenced with the list of DEGs, identified in this work, creating a longlist of 107 genes that were present in both lists (Figure 3-6, Appendix D). Genes were selected from this longlist in two ways to be included in an siRNA screen. Firstly, there were genes that were the biggest outliers from the longlisted genes when plotted as a volcano plot (Figure 3-6). These were *p21*, *TACC2*, *MYC*, *CCND1*, *Ran-BP1*, *HSP90B1*, *PPP4R2*, *HSPA6*, *PRKACB*, *PPP1R14C*, *CAMK2A*, *HSPA7*, *NIN* and *BANCR*. Secondly, there were a number of genes that were of particular interest due to their role in the emerging dogma surrounding CA or their potential for future therapies. *PLK4* was included as it encodes a key protein for centrosome duplication and its overexpression is a common method to artificially induce CA in an experimental setting (Coelho et al., 2015; Denu et al.,

2018; Gönczy & Hatzopoulos, 2019). *MDM2* was included as its upregulation would interfere with p53 stability, and loss of p53 activity has been implicated in the maintenance of CA (Fava et al., 2017; Fukasawa et al., 1996; Hou et al., 2019; Marin Navarro et al., 2020). *CCNB1* was included as it is key for mitotic progression, and failed mitosis is a potential route to CA (Brown et al., 2007; Meraldi et al., 2002; Schnittger & De Veylder, 2018). Several kinases were included, as kinases can successfully be targeted therapeutically (Bhullar et al., 2018). *Aurora A* (Marumoto et al., 2003), *NEK2* (Fry et al., 2012) and *PLK1* (K. Lee & Rhee, 2011; Ramani et al., 2018; Smith et al., 2011) were included as centrosomal kinases, whilst *TTK* was included as a mitotic kinase (Jelluma et al., 2008; Pike & Fisk, 2011). All of these genes, along with those biggest outliers from the volcano plot, were combined make up the shortlist of 23 genes to be tested in an siRNA screen (Table 3-2).

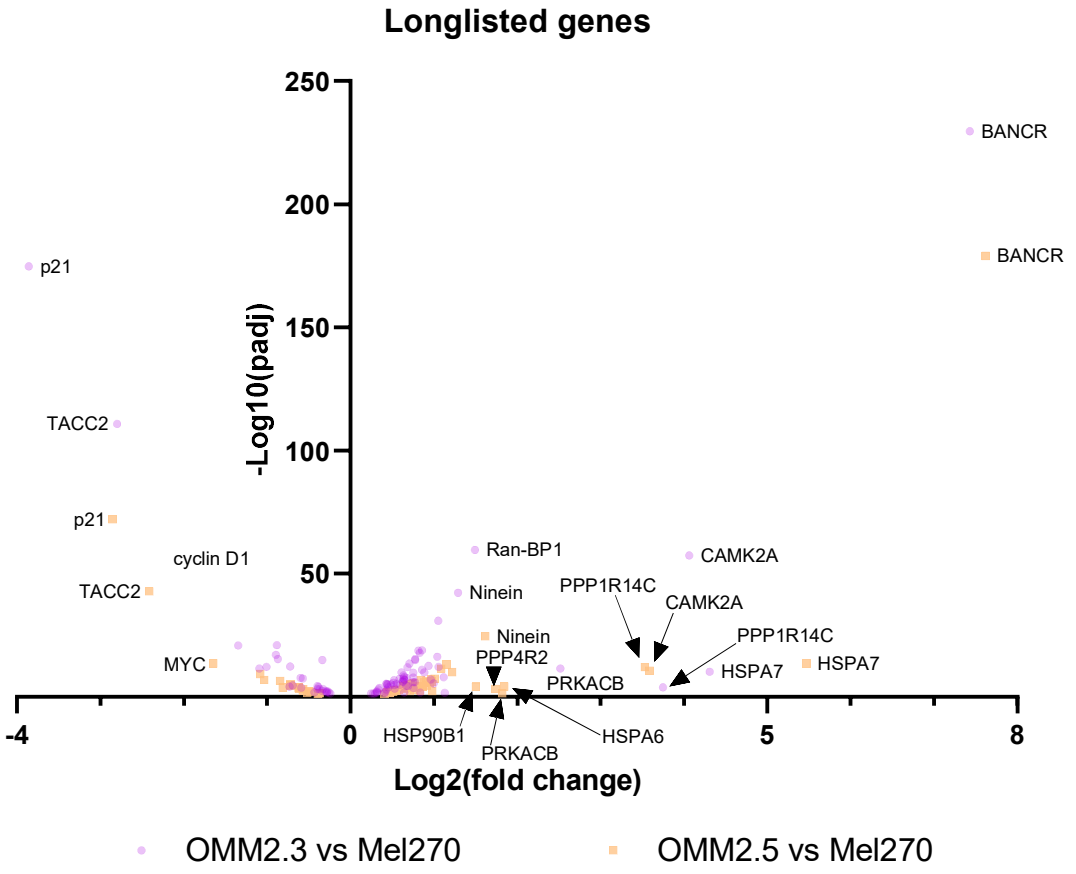

Figure 3-6. Volcano plot of longlist genes.
All longlist genes were DEGs, therefore have a padj ≤0.05. Plotting the hits on a volcano plot enabled identification of outlying genes with the highest $\log_2$(fold change), annotated with arrows. These genes, along with some other hits of special interest, made up the shortlist genes to be tested in an siRNA screen.

Interestingly, when comparing the DEG “hits” that made up the long list of 107 genes, genes were always dysregulated in the same “direction” for OMM2.3 and OMM2.5 cells. In other words, there were no results where a gene was upregulated in one cell line and down regulated in another. Additionally, when looking at the shortlisted genes (Table 3-2), all DEGs from the OMM2.5 vs. Mel270 comparison were also differentially expressed in OMM2.3 vs Mel270, but there were some DEGs from the OMM2.3 vs Mel270 comparison that were not differentially expressed in OMM2.5 vs Mel270.

Target		Log2(fold change) of readcount			
Ensembl ID	**Common Name**	**OMM2.3**	**OMM2.5**	**Proposed function in centrosome amplification**	**References**
ENSG00000087586	Aurora A	0.52375	0.52393	Regulation of centrosome duplication, centrosome maturation, centrosome separation in G2, and centrosome function in mitosis.	(Fukasawa, 2007; Ogden et al., 2017)
ENSG00000070808	CAMK2A	4.063	3.5837	Positive regulation of initiation of centrosome duplication.	(Fukasawa, 2007)
ENSG00000174799	CEP135	0.64654	0.47445	Recruitment of CPAP, essential for centriole elongation, to centrioles. Altered ratio of CEP135 isoforms can induce CA.	(Ganapathi Sankaran et al., 2019; Kodani et al., 2015; Y.-C. Lin et al., 2013)
ENSG00000136997	c-MYC	-0.8807	-1.6452	Overexpression has caused centriole overduplication.	(Duensing et al., 2010)
ENSG00000151849	CPAP	0.75515	0.73542	Overexpression has cause centriole over-elongation. Interacts with cytoplasmic tubulin to aid clustering of supernumerary centrosomes.	(Comartin et al., 2013; Y. N. Lin et al., 2013; Mariappan et al., 2019)
ENSG00000134057	Cyclin B	0.64374	0.64514	Regulation of centrosome separation in late G2 and centrosome function in mitosis via controlling PP1 and Eg5.	(Fukasawa, 2007)
ENSG00000110092	Cyclin D1	-1.3446	NDE	Positively regulates initiation of centrosome duplication.	(Fukasawa, 2007; Ogden et al., 2017)

ENSG00000166598	HSP90B1	0.99908	1.5069	An endoplasmic reticulum situated heat shock protein. Related to HSP90, which localises to the centrosome, stabilising PLK1 activity and centrosome structure, and is also required for recruitment of y-tubulin to overduplicated centrioles.	(Fukasawa, 2007; Lange et al., 2000; Prosser et al., 2009)
ENSG00000173110	HSPA6	1.1312	1.8429	Required for PCM assembly and function of centrosomes during mitosis. Protects centrosomes from heat induced damage.	(C.-T. Fang et al., 2019; Fukasawa, 2007; Hut et al., 2005)
ENSG00000225217	HSPA7	4.3077	5.4673	Required for PCM assembly and function of centrosomes during mitosis. Protects centrosomes from heat induced damage.	(C.-T. Fang et al., 2019; Fukasawa, 2007; Hut et al., 2005)
ENSG00000135679	MDM2	0.63543	0.85877	Positive regulation of centrosome duplication by promoting p53 degradation.	(Fukasawa, 2007; Ogden et al., 2017)
ENSG00000117650	NEK2	0.58986	0.58167	Regulation of centrosome separation in late G2, and centrosome maturation in association with PLK1.	(Fukasawa, 2007; Ogden et al., 2017)
ENSG00000100503	Ninein	1.292	1.6164	A subdistal centriole appendage, facilitates MT anchoring at the mother centriole.	(Kodani et al., 2013)
ENSG00000124762	p21	-3.8589	-2.8528	Induced by p53 dependent G2/M checkpoint, suppresses CDK2 activity. Low levels of p21 correlated with high levels of CA in oral squamous cell carcinoma.	(Cai et al., 2009; Fukasawa, 2007)

ENSG00000166851	PLK1	0.62838	0.45398	Regulation of centrosome duplication, separation and function.	(Fukasawa, 2007; Ogden et al., 2017)
ENSG00000142731	PLK4	0.64644	NDE	Regulation of initiation of centrosome duplication.	(Fukasawa, 2007)
ENSG00000198729	PPP1R14C	3.7487	3.5296	Regulation of centrosome separation by activating Nek2A and Aurora A.	(Fukasawa, 2007)
ENSG00000163605	PPP4R2	0.64888	1.7433	PPP4 recruits PCM to centrosome, role in activating MT nucleating ability of centrosome. Negative regulation of Cdk1.	(Fukasawa, 2007; Sumiyoshi et al., 2002; Toyo-oka et al., 2008)
ENSG00000142875	PRKACB	2.5181	1.8202	Regulation of centrosome function and mitotic spindle assembly in association with pericentrin.	(Fukasawa, 2007)
ENSG00000099901	Ran-BP1	1.4919	1.2209	Catalyses Ran-GTP to RanGDP, allowing Ran to control import and export of proteins from the nucleus, which plays a role in centrosome duplication regulation.	(Fukasawa, 2007)
ENSG00000138162	TACC2	-2.7992	-2.412	May act as a tumour suppressor, stabilise/ concentrate MTs at centrosomes. Localised by TTK.	(Dou et al., 2004; Fukasawa, 2007; Raff, 2002)
ENSG00000112742	TTK	0.62969	0.9662	Positive regulation of initiation of centrosome duplication.	(Fukasawa, 2007)
ENSG00000278910	BANCR	7.4301	7.6184	lncRNA associated with poor prognosis in UM.	(Robertson et al., 2017)

Table 3-2. A list of shortlisted genes to be included in an siRNA screen to identify drivers of centrosome amplification in OMM2.3 cells.

3.5. Confirmation of RNA Sequencing Results by qPCR

It is standard practice to validate RNA-Seq results using another method such as qPCR (Lovén et al., 2012). For the best qPCR results, an appropriate reference gene needs to be selected that will have limited variations in expression. *β-Actin (ACTB)*, *GAPDH*, *CAPNS1*, *SRPR* and *RPS11* were all reference genes that had been used in published work using Mel270, OMM2.3 and OMM2.5 cells (Bronkhorst et al., 2014; Heijkants et al., 2017; Maat et al., 2008). Each of these reference genes was tested using 11 different cDNAs made from Mel270, OMM2.3 and OMM2.5 RNA extracts (Figure 3-7). The cDNAs were synthesised using 1 µg RNA. Out of the 5 assays, the *RPS11* assay had the least variation in Ct between cDNAs with a standard deviation of 0.802, therefore *RPS11* was used as a reference gene for all further qPCR work in this thesis.

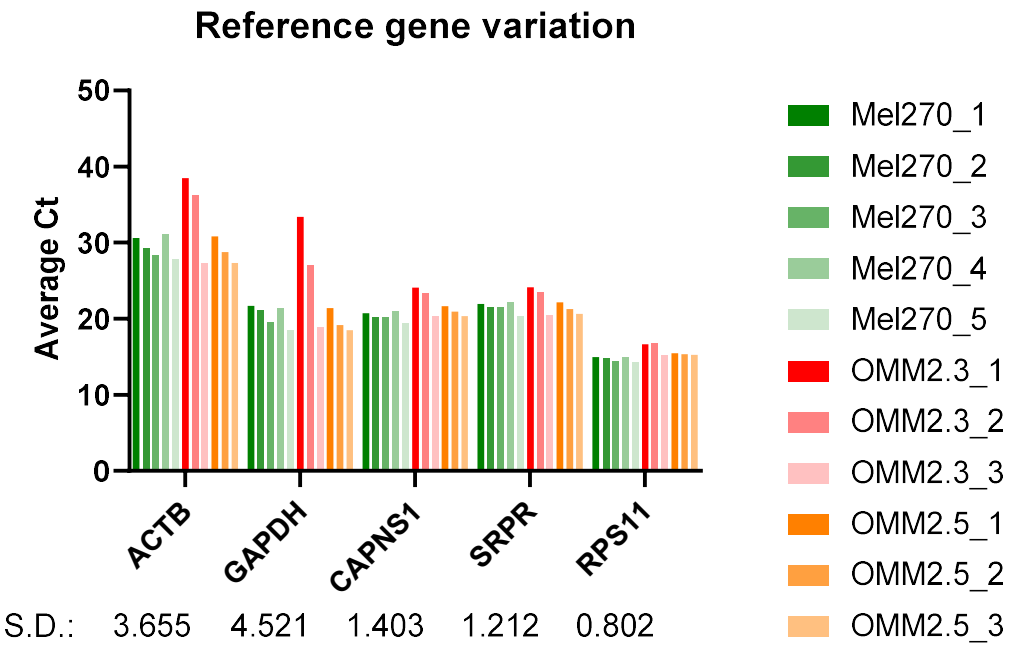

Figure 3-7. Ct variation in potential reference genes.
qPCR assays for β-Actin (ACTB), GAPDH, CAPNS1, SRPR and RPS11 were compared using 11 different cDNAs from Mel270, OMM2.3 and OMM2.5 cells. Assays were tested in triplicate wells. The standard deviation (S.D.) of the Ct value for each gene is displayed below the graph.

Four genes were selected for qPCR analysis from the shortlist of genes to be included in the siRNA screen: *NEK2*, *TTK*, *CAMK2D* and *p21*. These genes displayed a range of expression, as illustrated by their **F**ragments **P**er **K**ilobase of transcript per **M**illions of base pairs sequenced (FPKM) values. The FPKM value normalises read count (the number of reads that map to a

gene) for sequencing depth and gene length. Gene expression, gene length and sequencing depth all contribute to the read count, so normalising for sequencing depth and gene length to generate an FPKM value allows for comparison of gene expression between different genes and samples.

Between *NEK2*, *TTK*, *CAMK2D* and *p21* across the three cell lines, FPKMs ranged from ~10 to ~200. The pattern of expression as determined by qPCR was the same as that seen in the RNA-Seq results for all four genes (Figure 3-8). Most importantly, statistically significant differences between Mel270 and OMM2.3/OMM2.5 that were seen in the RNA-Seq results remained statistically significant in the qPCR assays.

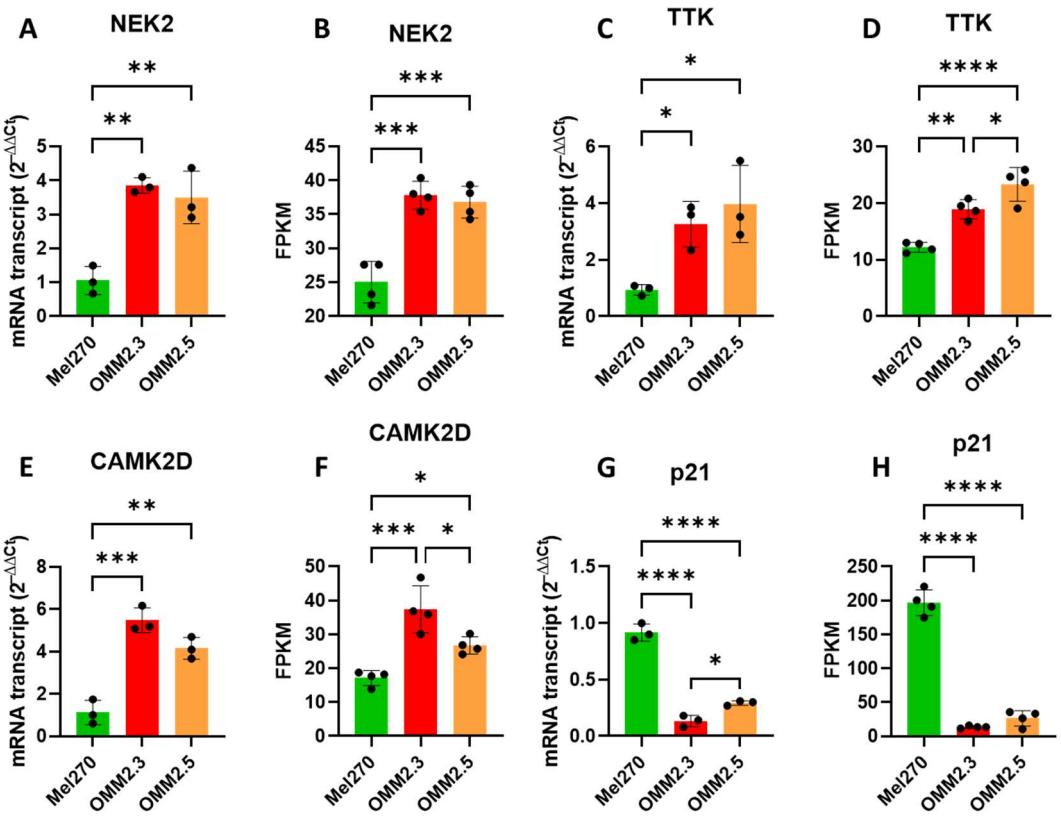

Figure 3-8. Comparison of RNA-Seq results to qPCR results.
Relative mRNA transcript of *NEK2* (A), *TTK* (C), *CAMK2D* (E) and *p21* (G) in Mel270, OMM2.3 and OMM2.5 cells. Alongside these results are the fragments per kilobase of transcript per million mapped reads (FPKM) values from RNA-Seq of *NEK2* (B), *TTK* (D), *CAMK2D* (F) and *p21* (H) for Mel270, OMM2.3 and OMM2.5 RNA extracts. N = 3 for qPCR assays, which were carried out in triplicate wells, and n = 4 for FPKM values. Means were compared using an ordinary one-way ANOVA and Tukey's multiple comparisons post hoc test (* = $p \leq 0.05$, ** = $p \leq 0.01$, *** = $p \leq 0.001$, **** = $p \leq 0.0001$).

3.6. TP53 Sequencing

The functional loss of p53, be it through mutation or downregulation, is believed to play a role in the maintenance of CA, as many studies require a p53 null setting for CA to persist (Adon et al., 2010; Lopes et al., 2018; Marin Navarro et al., 2020; Serçin et al., 2016). As *TP53* was not in the list of DEGs and its mutational status is unknown, we decided to sequence the *TP53* gene in OMM2.3 and OMM2.5 cells (Figure 3-9). Analysis of the sequencing results indicated that *TP53* is wild type in both cell lines.

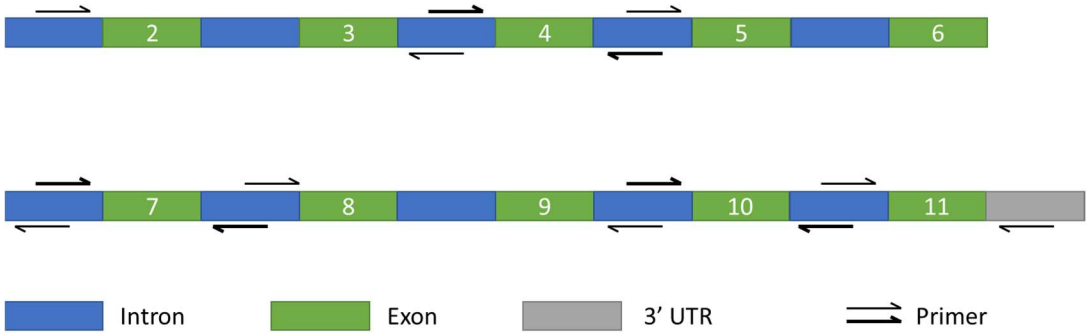

Figure 3-9. Mel270, OMM2.3 and OMM2.5 cells express wild type p53.
The mutational status of *TP53* in Mel270, OMM2.3 and OMM2.5 cells was unknown. PCR reactions were set up with primers spanning the protein coding exons, as indicated with the arrows in the figure above. PCR fragments were sequenced by Eurofins using sanger sequencing. The sequences were compared to wild type *TP53*. No mutations were found.

3.7. Wider Relevance of siRNA Screen

Our recent study discovered that CA is present in UM tumour tissue, particularly tumours that are at a high risk of metastasising (Sabat-Pośpiech et al., 2022). This lends relevance to the use of our patient-matched metastatic UM cell line model for the development of CA. Despite this, a caveat of using Mel270, OMM2.3 and OMM2.5 cells as a model is that they model just two instances of CA in one patient. As there are several plausible routes to CA, it is important to consider what the wider relevance of this work might be (Denu et al., 2018; Fujiwara et al., 2005; Khodjakov et al., 2002; Marteil et al., 2018; Pannu et al., 2012). For this reason, the expression of the 23 genes to be used in an siRNA screen was investigated in other cell lines. 53 cell lines from the NCI-60 panel have been categorised as either having CA or not having CA in a study by Marteil et al., 2018. Using data available on cBioPortal, mRNA Z-scores were collected for each of the 23 genes in each of the 53 cell lines. The mRNA Z-score compares mRNA expression of the chosen cell line to that of a reference population which, for the NCI-60 panel, is all profiled samples within that dataset. The mRNA Z-score of a gene for an individual cell line is calculated as the number of standard deviations away the gene's expression is from the mean of the reference population. In order to

compare the RNA-Seq data from this study to the mRNA Z-scores reported on cBioPortal, for each gene:

1. The average log_2(fold change) of "OMM2.3 vs Mel270" and "OMM2.5 vs Mel270" was calculated.
2. The average mRNA Z-score of all the NCI-60 cell lines with CA was calculated.
3. The average mRNA Z-score of all the NCI-60 cell lines without CA was calculated.

These values were plotted onto graphs, seen in Figure 3-10. There was a positive correlation between average log2(fold change) and average mRNA Z-scores for NCI-60 cells with CA (Spearman's rank correlation, r(20) = 0.6047, p =0.0029). Conversely, there was a negative correlation between average log2(fold change) and average mRNA Z-scores for NCI-60 cells without CA (Spearman's rank correlation, r(20) = -0.5189, p = 0.0133). Taken together, this indicates the genes selected for the siRNA screen generally have a similar pattern of over or under expression in other cell lines with CA. Therefore, results from an siRNA screen of these genes might be applicable in other cells with CA.

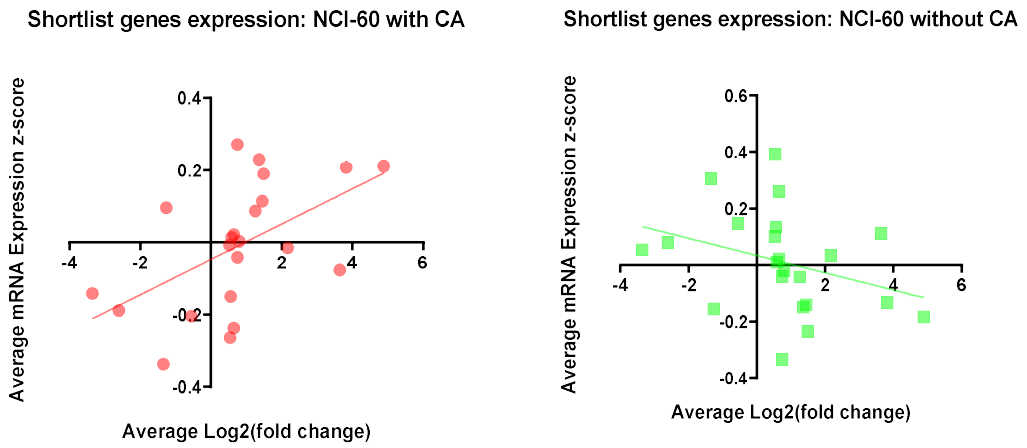

Figure 3-10. Expression of shortlist genes in NCI-60 cells with and without CA.
The expression of shortlisted genes in NCI-60 cell lines with (A) and without (B) CA has been compared against the average Log_2(fold change) of shortlisted genes in OMM2.3 vs Mel270 and OMM2.5 vs Mel270. Expression data for NCI-60 panel cell lines was gathered from cBioPortal.org. Spearman's rank correlation was computed to assess the relationship between average Log2 fold change and average mRNA expression z-score of NCI-60 cell lines either with or without CA. There was a positive correlation between the two variables when looking at NCI-60 cell lines with CA (A), r(20) = 0.6047, p = 0.0029. There was a negative correlation between the two variables when looking at NCI-60 cell lines without CA (B), r(20) = -0.5189, p = 0.0133.

3.8. Chapter Discussion

The first aim of this chapter was to quantify CA in Mel270, OMM2.3 and OMM2.5 cells to establish their use as a model to study CA, after having observed CA in patient derived UM.

We found that Mel270 had low levels of CA, whereas OMM2.3 and OMM2.5 cells had high levels of CA. This could be put into context of other cell lines that have CA – the CA observed in OMM2.3 and OMM2.5 cells was relatively high (Marteil et al., 2018).

The next aims of the chapter were to extract RNA from Mel270, OMM2.3 and OMM2.5 cells and use that RNA for RNA-Seq and analysis. The quality of the RNA used for sequencing was very high, which helps to improve RNA-Seq results (Kukurba & Montgomery, 2015).

After RNA-Seq and related DEG analysis, the next aim was to validate some of the RNA-Seq results. The method chosen was qPCR. An appropriate reference gene, *RPS11*, was selected out of a panel of 5 reference genes. Selection of good reference gene is important for reliable qPCR analysis, so this aim is useful for all subsequent qPCR in this PhD. 4 genes were selected from the DEG list to test: *p21*, *CAMK2D*, *NEK* and *TTK*. The qPCR results showed the same pattern of expression across Mel270, OMM2.3 and OMM2.5 cells compared to the RNA-Seq results. To see results that concur from two different methods gives more confidence in those findings. RNA-Seq and qPCR differ in the number of steps taken in the process, for example RNA-Seq requires some data to be filtered out, and generation of a cDNA library is a step that has the potential to generate some inaccuracies in the final data set. RNA-Seq is a good technique to assess the broad spectrum of gene expression, whereas qPCR is very good at accurately measuring the relative abundance of individual genes.

The primary question being asked of the RNA-Seq data was to find genes whose differential expression in OMM2.3 and OMM2.5 cells compared to Mel270 cells may have contributed to the high levels of CA seen in OMM2.3 and OMM2.5 cells. However, this dataset could also be used to ask other questions. OMM2.3 and OMM2.5 cells shared a very similar gene expression profile. When compared to Mel270 cells, OMM2.3 and OMM2.5 cells had 9297 and 7616 DEGs respectively. However, when comparing OMM2.3 and OMM2.5 together, there were only 112 genes. Another indication of the similarity between OMM2.3 and OMM2.5 is to look at the R^2 values for the correlation of gene expression. The primary purpose of looking at correlation between samples is to check that biological replicates are similar. The minimum value should be 0.92, all replicates in this work far exceeded that value and were generally above 0.99. The correlations between OMM2.3 and OMM2.5 samples were also very high, generally being above 0.97. In fact, even the correlations between Mel270 samples and OMM2.3 or OMM2.5 samples were still above the 0.92 threshold. Taken together with the high number of DEGs that were found between Mel270 and OMM2.3 or OMM2.5 cells, this would indicate that where gene expression is not

differential, it is very similar. Having RNA-Seq data of patient matched primary tumour- and metastatic tumour-derived cell lines is a useful resource to study the development of metastatic disease in uveal melanoma.

The RNA-Seq results were used to select genes to use in an siRNA screen to identify genes with a role in the development of CA in OMM2.3 and OMM2.5 cells. A targeted approach was taken to select these genes. First, a list of 138 genes was compiled using information that is already available in the literature. These genes all already had some indication of a role in CA. This list was compared against the DEGs that came from RNA-Seq analysis. Genes from the initial list that were also differentially expressed made a long list of 107 genes, from which 23 genes were shortlisted to be included in an siRNA screen. These genes were those with the highest change in expression, plus some other genes of specific interest. Another approach that could have been taken would have been a more discovery-based approach. This would involve selecting genes from the DEG list, regardless of their known function. One way to do this would be to select the genes with the highest $-Log_{10}$(padj), or the highest Log_2(fold change). The benefit of an approach like this is that it can lead to the discovery of new genes to be involved in a process, such as CA. The drawback is that there is an increased likelihood that none of the candidates will yield a positive result in the subsequent screen. Ideally, both a targeted approach and discovery-based approach would be used to select candidates for a screen. However, the resource and time intensive nature of this particular screen meant that the numbers of genes that could be included in a screen were limited.

The *TP53* gene has particular importance in cancer and more specifically CA research. The 1996 study by Fukasawa et al. heralded the modern interest in CA with the observation of "abnormally amplified centrosomes", specifically implicated by a loss in p53 protein. As such, p53 was initially the main focus of CA studies. Many subsequent studies into CA required a p53 null setting for CA to persist (Adon et al., 2010; Lopes et al., 2018; Marin Navarro et al., 2020; Serçin et al., 2016). A loss of p53 activity seems to be important for CA but it isn't the only part of the picture; loss of p53 is not always sufficient to induce CA, and when comparing the p53 status of cell lines with and without CA, there was no statistically significant difference (Marteil et al., 2018; Marthiens et al., 2013). Interestingly, *TP53* was not a DEG when comparing either OMM2.3 or OMM2.5 to Mel270 cells. The mutational status of p53 in these cell lines was not known so *TP53* was sequenced for all 3 cell lines, and this showed that p53 was wild type (WT) in all three cell lines (see section 3.6). It was useful to know the p53 status of these cells not only to put the CA into context, but also to inform the selection of potential p53 targeting drugs which work via different mechanisms. For

example, PRIMA-1 restores WT activity of mutant p53, whereas Nutlins restore p53 signalling via MDM2 inhibition (Bykov et al., 2002; Hou et al., 2019).

There was a lack of direct p53 dysfunction in Mel270, OMM2.3 and OMM2.5 cells, however the most downregulated gene in the long list was *p21*. p21 is a CDK inhibitor, regulating G1 and S phase cell cycle progression (Gartel & Radhakrishnan, 2005; L. Wang et al., 2021). p21 also acts as a downstream activator of p53, causing cell cycle arrest (Engeland, 2022; L. Wang et al., 2021). Overduplication of centrioles can trigger p53/p21 mediated cell cycle arrest, and knock down of p21 can increase the proliferative ability of cells with induced CA (Evans et al., 2021; Holland et al., 2012). Additionally, expression of the p53 inhibitor MDM2 was increased in OMM2.3 and OMM2.5 cells compared to Mel270 cells, which would have the effect of dampening any p53 response (Hou et al., 2019). Taken together, these results support the claim that disruption to p53 activity is required for maintenance of CA. It is probable those cell lines with both CA and WT p53 status in Marteil et al., 2018 had the p53 pathway disrupted in another was as seen with these UM cell lines in this work.

Another interesting result from RNA-Seq analysis was the fact that *PLK4* was only overexpressed in OMM2.3 cells, but not OMM2.5 cells, when compared with Mel270 cells. PLK4 activity is key to normal centriole duplication and PLK4 overexpression is often used as a method to artificially induce CA (Arnandis et al., 2018; Cosenza & Krämer, 2016; Levine et al., 2017; Prakash et al., 2022). PLK4 expression was also included in the development of the CA20 score, a value based on genes involved in CA and which has prognostic value in breast cancer (Ogden et al., 2017). That *PLK4* was not a DEG in OMM2.5 cells compared with Mel270 cells indicates that there are multiple molecular routes to CA.

The work in this chapter and in this thesis is based on three cell lines: Mel270, OMM2.3 and OMM2.5 cells. The use of these patient matched cell lines helps with the RNA-Seq analysis. The cells are genetically similar so there is less noise in the analysis and any changes in gene expression are more likely to have had functional consequences in the development of metastatic disease. However, this examines just two incidences of CA in one patient, so it is important to consider what the wider relevance that this research might have in the field of CA. In an effort to address this, the expression of genes to be included in the siRNA screen was examined in other cells of known CA status. The 2018 study by Marteil et al. classified NCI-60 cell lines as either having or not having CA. Using data available on the online database cBioPortal, relative expression of the shortlist genes could be found for each of the NCI-60 cell lines. These values were grouped for cells with CA and cells without CA, so that

the average relative expression could be compared with the average log_2(fold change) of OMM2.3 and OMM2.5 vs Mel270. There was a significant positive correlation between relative expression of shortlisted gene in NCI-60 cells with CA and average log_2(fold change) of OMM2.3 and OMM2.5 vs Mel270. The relative expression of genes is given in cBioPortal as a mRNA z-score, which compares the expression of a gene against that of a reference population. However, it is worth noting that the averaged z-scores were low in value, as a z-score of +/- 1.96 is considered statistically significant.

The next steps for this work that will be covered in the following chapter focus on the siRNA screen. Before performing the screen, conditions and analysis methods needed to be optimised. Then, using genes identified in this chapter, an siRNA screen was carried out and the effects on CA in Mel270 and OMM2.3 cells were measured. Top results from the siRNA screen went through a validation process in order to select which genes to carry forwards to the next stage of experiments.

Chapter 4.

Knockdown of Aurora A or HSP90B1 Reduces Centrosome Amplification in OMM2.3 Cells

4.1. Introduction

In the previous chapter, the use of Mel270, OMM2.3 and OMM2.5 cells was established as a model to study centrosome amplification (CA) that had occurred in a patient setting. Following this, RNA-Seq was used to select a shortlist of genes to be tested in an siRNA screen to identify genes whose knockdown has an effect on the level of CA in Mel270 and OMM2.3 cells. In this chapter, conditions for the siRNA screen are developed and the siRNA screen is carried out.

4.1.1. Design Features of an siRNA Screen

siRNA screens have been successfully used to identify genes contributing to biological processes such as infection, obesity, aging and cancer (Mohr & Perrimon, 2012). The design of an siRNA screen can be put into one of two main camps: hypothesis driven screens and discovery driven screens. Hypothesis driven screens take readily available information from, for example, publications or online databases, and use this information to refine the genes that are included in the siRNA screen. An example of such a screen can be seen in the 2015 study by Sacco et al., which identified BAP1 from a screen of de-ubiquitylases as a cellular target that sensitises mesothelioma cells to HDAC inhibitors. Discovery driven screens take a wider stance, screening the whole genome (Kwon et al., 2008; Leber et al., 2010). This is more time and resource intensive, but yields the possibility of a more unexpected result. For the work in this thesis, a hypothesis driven approach was taken, selecting genes from a list curated using published literature of centrosomes and CA (Fukasawa, 2007; Marteil et al., 2018; Ogden et al., 2017). Selection of genes for the siRNA screen was covered in Chapter 3.

Another important consideration when designing and siRNA screen is the siRNAs themselves. siRNAs can have off target effects, causing knock down of genes other than the intended target (Jackson et al., 2003; Putzbach et al., 2018). It is good practice to show that a phenotypic change can be achieved with at least two different siRNAs targeting the same gene, as it is highly unlikely that two siRNAs would have the same off target effect. Screens will already have a large number of experimental conditions, so multiple siRNAs for each target can be pooled together to minimise the number of conditions for the first phase of a screen. Then, any hits identified in the first phase should go through siRNA deconvolution, testing each siRNA individually to ensure that at least two siRNAs provide the same result seen in the first phase of a screen. This limits the number of false positives that will be

identified in a study. It is also good practice, once siRNAs have been selected from screen results, to check for knockdown efficiency using methods such as qPCR or western blotting.

Another challenge facing siRNA screens is false negatives (Sigoillot & King, 2011). The optimal conditions of an siRNA transfection, such as timings and reagent concentrations, may vary between targets due to mRNA and protein turnover and the properties of different siRNA nucleotide sequences (Arvey et al., 2010; Grimson et al., 2007; Hong et al., 2014; Sigoillot & King, 2011). When working with siRNAs for a new target, these conditions should be optimised. However, it is not feasible to optimise conditions for all individual siRNAs in a screen, as conditions need to be the same across the experiment and the cost and amount of work that would be needed is prohibitive. For the work presented in this thesis, the reverse siRNA transfection method was instead validated in the cell lines of interest for two targets, KIFC1 and PLK4. KIFC1 siRNAs were already being successfully used in the lab, of interest due to KIFC1's role in clustering supernumerary centrosomes (Chavali et al., 2016; Kwon et al., 2008). PLK4 siRNAs were tested as they were also to be included in the siRNA screen. PLK4 overexpression is a well-established experimental technique for establishing CA, and PLK4 was overexpressed in OMM2.3 compared to Mel270 cells (Arnandis et al., 2018; Cosenza & Krämer, 2016; Levine et al., 2017; Prakash et al., 2022). Validating with two targets can at least confirm successful knockdown of those two targets, but doesn't necessarily mean that all siRNAs used in the screen will have achieved a successful knockdown. Therefore, negative results from the screen should not be taken at face value.

4.1.2. Chapter Aims

- Validate reverse siRNA transfection for knockdown of genes in Mel270 and OMM2.3 cells.
- Select immunofluorescence staining panel that is suitable for high-throughput analysis of centrosome amplification.
- Create a high-throughput analysis workflow to measure centrosome amplification in Mel270 and OMM2.3 cells
- Perform an siRNA screen to identify genes that affect centrosome amplification in Mel270 and OMM2.3 cells.
- Validate hits from siRNA screen, including deconvolution of siRNA pools.

4.2. Reverse siRNA Transfection

Reverse siRNA transfection was the method of choice to manipulate gene expression in an siRNA screen to find genes whose differential expression contribute to CA in OMM2.3 cells. Before doing the screen, knockdown was validated at the RNA and protein level in Mel270 and OMM2.3 cells (Figure 4-1). For KIFC1, a single siRNA was tested and knockdown was measured at the mRNA transcript and protein level. For PLK4, a pool of four siRNAs were tested and knockdown was measured at the mRNA transcript level only. Cells were treated with target siRNAs or control siRNA for 48 hours before taking RNA extracts and protein lysates. RNA extracts and protein lysates for KIFC1 knock down were generated from the same experiments.

After 48 hours, there was a significant reduction in target mRNA transcript (Figure 4-1, panels A-D) and, where measured, target protein (Figure 4-1, panels E-F) in both cell lines for both KIFC1 and PLK4 knockdown. One-way ANOVA tests were performed to compare the effects of target siRNA transfection on target mRNA transcript or target protein levels, in both Mel270 and OMM2.3 cells. In all cases, there was significantly less transcript or protein in the target siRNA conditions (PLK4 siRNA or KIFC1 siRNA) compared to either of the control conditions, indicating the siRNA treatment had been successful. These results showed that this method of transfection was suitable for the siRNA screen.

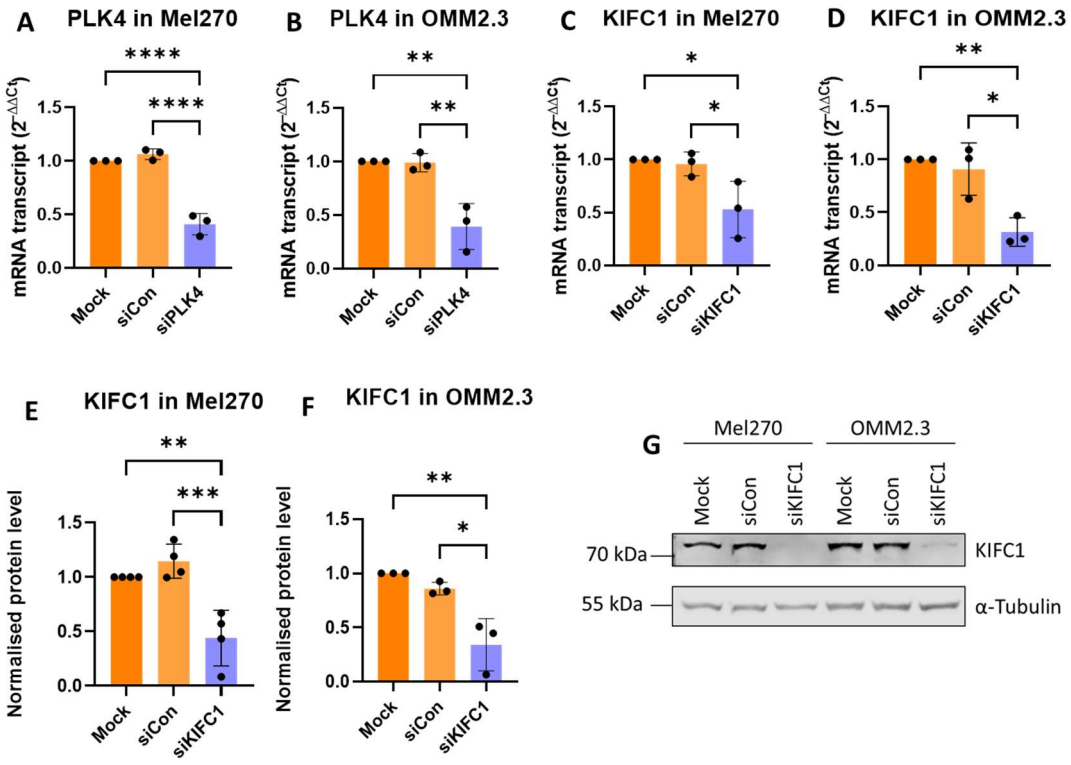

Figure 4-1. Validation of knock down of PLK4 and KIFC1 by reverse siRNA transfection.
PLK4 mRNA transcript levels in (A) Mel270 and (B) OMM2.3 cells, and KIFC1 mRNA transcript levels in (C) Mel270 and (D) OMM23 cells, 48 hours after reverse siRNA transfection with the indicated siRNAs. KIFC1 protein levels, normalised to α-tubulin control, in (E) Mel270 and (F) OMM2.3 cells, 48 hours after reverse siRNA transfection. (G) Western blot showing KIFC1 and α-tubulin protein levels in the indicated cell lines 48 hours after reverse siRNA transfection. n ≥ 3, siCon = Qiagen AllStars negative control siRNA. Means were compared using ordinary one-way ANOVA with Tukey's multiple comparisons post hoc test (* = $p \leq 0.05$, ** = $p \leq 0.01$, *** = $p \leq 0.001$, **** = $p \leq 0.0001$).

4.3. Imaging and Analysis Optimisation

In Chapter 3, CA was measured by searching for individual mitotic cells in a methodical manner and taking high resolution z-stacks of those cells. Images were then analysed individually by eye to record how many centrosomes each cell had. This was an accurate but time intensive approach, making it unsuitable for an siRNA screen. It was necessary to establish a more time efficient approach to compare levels of CA in an siRNA screen. Several methods for semi-automated imaging and quantification of CA have been published (for example, Balestra et al., 2013; Marteil et al., 2018). However, these studies still required time-intensive manual identification of individual mitotic cells to image and were not applicable to this study due to the specific systems and equipment used. Instead, to develop a new appropriate method for this study, a number of experimental setups were tested to optimise the CA assay. These included selection of antibodies for immunofluorescence staining, cell seeding density and image acquisition settings.

4.3.1. Immunofluorescent Staining Panels

Different immunofluorescence staining panels were compared to see which ones could lend themselves well to an image analysis workflow (Figure 4-2).

For the first staining panel, cells were stained with DAPI and antibodies against α-tubulin, pericentrin and centrin (Figure 4-2, panel A and E). These were the antibodies used in chapter 3 when quantifying CA in Mel270, OMM2.3 and OMM2.5 cells. The benefit of this panel is that there are two centrosome markers: pericentrin labels the PCM and centrin labels the centrioles. This panel worked well in chapter 3 to identify centrosomes and also acted as a benchmark to compare the other panels against.

For the second staining panel, cells were stained with DAPI and antibodies against α-tubulin (raised in mouse), and pericentrin (Figure 4-2, panel B and F). The α-tubulin stain has the potential to aid with cell segmentation and/or identification of mitotic cells. There were anecdotal observations from the lab group that the cleanliness of α-tubulin staining was better with the mouse-derived antibody compared to the rat-derived antibody. However, when images were compared, there was no clear difference between cells staining with the mouse-derived versus rat-derived α-tubulin antibody.

For the third staining panel, cells were stained with DAPI and antibodies against α-tubulin, pericentrin and phospho-histone H3 (pHH3) (Figure 4-2, panel C and G). pHH3 is a well-established marker of mitotic cells, and was included to see if it could speed up or even automate the identification of mitotic cells (Kim et al., 2017; L. H. Lee et al., 2014; Tetzlaff et al., 2013). The benefit of analysing mitotic cells is that they are a readily identifiable stage of the cell cycle and so their centrosome status is clear; a normal cell should have two centrosomes, any cell with three or more centrosomes has CA. This contrasts with interphase cells, where a cell with 2 centrosomes could either be a normal cell in G2 or a cell with CA in G1. It was possible to segment mitotic cells using the pHH3 marker. However, the number of mitotic cells in a field of view was low. The number of images that would need to be taken to provide a sufficient number of cells for analysis was impractical for an siRNA screen.

For the fourth staining panel, cells were stained with DAPI and antibodies against α-tubulin, pericentrin and cyclin B1 (Figure 4-2, panel D and H). Cyclin B1 labels cells in late S phase to mitosis, peaking in G2, which coincides with the stages of the cell cycle when 2 centrosomes should be present (Matthews et al., 2021; Pines & Hunter, 1989, 1991). By taking cyclin B1 staining into account, interphase cells could be analysed to measure CA. Out of all staining

panels tested, the images that were produced with this one were the most promising from the point of view of developing an analysis work flow.

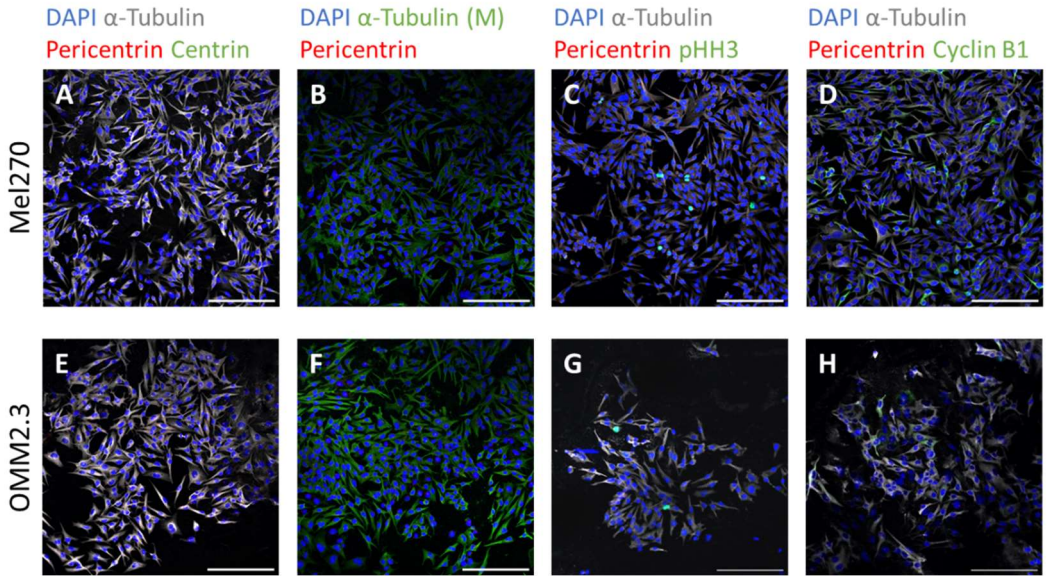

Figure 4-2. Optimisation of staining panel for siRNA screen.
Mel270 cells (top row) and OMM2.3 cells (bottom row) were stained with DAPI and various antibodies, as indicated: (A, E) α-tubulin (white), pericentrin (red) and centrin (green); (B, F) α-tubulin (green) and pericentrin (red); (C, G) α-tubulin (white), pericentrin (red) and phospho-histone H3 (pHH3) (green); (D, H) α-tubulin (white), pericentrin (red) and cyclin B1 (green). Scale bars are 200 µm.

4.3.2. Seeding Density

The density of cells must be considered, as high cell density will affect growth and densely growing cells can be more difficult to segment during image analysis. However, if cells are seeded too sparsely it can also impede cell growth and reduces the number of cells available to analyse.

Three different seeding densities were trialled for both Mel270 and OMM2.3 cells (Figure 4-3). Cells were reverse transfected with negative control siRNA at the time of seeding in order to mimic growth conditions of the siRNA screen. Media was changed 24 hours after seeding. After a total of 72 hours following siRNA transfection, cells were fixed and stained with the fourth staining panel trialled in Figure 4-2.

The low (Figure 4-3, panels C and F) and medium (Figure 4-3, panels B and E) densities for both cell lines resulted in cell growth that was too sparse. The high densities (Figure 4-3, panels A and D) for both cell lines produced the best images and those densities (12,000 and 6,000 cells per well for Mel270 and OMM2.3 cells, respectively) were selected for use in the siRNA screen.

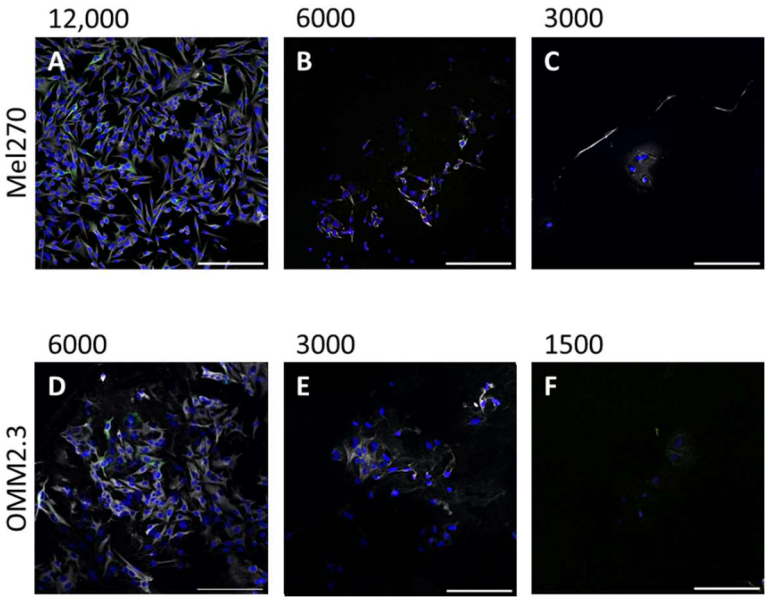

Figure 4-3. Optimisation of seeding density for siRNA screen.
Mel270 cells (top row) and OMM2.3 cells (bottom row) were seeded into a 96 well plate at three different seeding densities each and fixed after 72 hours of growth. The number of cells that were seeded are indicated by the numbers above each image. Cells were stained with DAPI (blue) and with antibodies against α-tubulin (white), pericentrin (red) and cyclin B1 (green). Scale bars are 200 µm.

4.3.3. Image Acquisition

Imaging and analysing centrosomes is a difficult task, as their size is close to the limit of optical resolution. Additionally, there is a balance to be struck between image resolution and imaging time. Performing an siRNA screen requires many images to be taken, which makes it impractical to have long image acquisition times. Low, medium and high resolution acquisition settings were tested for Mel270 and OMM2.3 cells, the details of which can be found in Table 4-1.

Seeding density	Image size (pixels)	Image resolution (pixels per µm)	Additional information
Low:	512x512	0.72	Images taken as a z-stack
Medium:	1024x1024	1.45	Images taken as a single slice
High:	2048x2048	2.89	Images taken as a single slice

Table 4-1. Image acquisition settings tested for siRNA screen.
For all settings a Plan-Apochromat 20x/0.8 M27 objective was used, at 0.6x zoom with the pinhole opened to give a 15 µm slice.

Example images can be seen in Figure 4-4. The short acquisition time of the low resolution setting meant that a z-stack covering the depth of the cells could be taken in a similar time to the mid/ high resolution images. This had the potential to more accurately capture the number of centrosomes in the cells. However, the resolution made it very difficult to distinguish nearby centrosomes. As centrosome clustering is common in cells with CA, this made the low resolution z-stack setup unsuitable. The medium resolution images allowed for better distinction between nearby centrosomes, and the high resolution image was better still. As a result of this analysis, the high resolution settings were identified as being the best but, at the 0.6x zoom used here, centrosomes in cells on the edge of the field of view were not in good focus. Therefore, it was decided to use the high resolution setting but with a 0.8x zoom for the screen. This made the image acquisition time more manageable for the screen and gave a resolution of 3.85 pixels per µm.

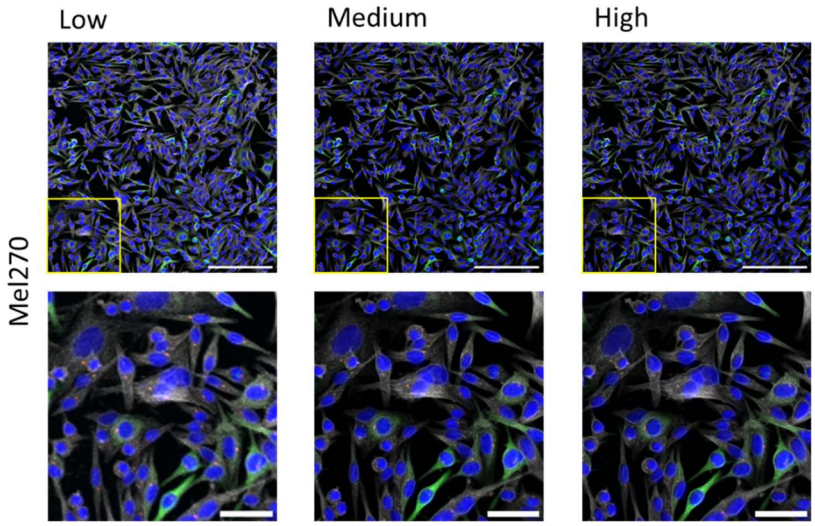

Figure 4-4. Optimisation of image acquisition for siRNA screen.
Mel270 cells stained with DAPI (blue) and with antibodies against α-tubulin (white), pericentrin (red) and cyclin B1 (green). Low (512x512 pixels, 0.72 pixels/µm, z-stack), medium (1028x1028 pixels, 1.45 pixels/µm, single slice) and high (2048x2048 pixels, 2.89 pixels/µm, single slice) are presented, all taken at 0.6x zoom. Yellow inserts (top) indicate zoomed in area (bottom). Scale bars on the top row are 200 µm, scale bars on the bottom row are 50 µm.

4.4. Development of an Image Analysis Workflow

Ideally, an image analysis workflow will be automated, as this eliminates the risk of human error and makes the analysis more reproducible. This automated analysis should also provide accurate results. Several different workflows were tested, the details of which can be found in Table 4-2.

		Analysis steps
Nuclei	Method 1	• Median blur, kernel 1 • Find maxima prominence = X, where X was a value that gave 1 point per nucleus, as examined by eye.
	Method 2	• Median blur, kernel 2 • Find maxima prominence = X, where X was a value that gave 1 point per nucleus, as examined by eye.
	Method 3	• Gaussian blur, kernel 1 • Threshold 20/225 • Watershed • Analyse particles (size 80 - inf, circularity 0 - 1, show overlay masks, all options except record starts and in situ show).
	Method 4	• Median blur, kernel 5 • Threshold X/225, where X was a value that selected all nuclei and no background, as examined by eye. • Fill holes • Watershed • Analyse particles (size 50 - inf, circularity 0 - 1, show overlay masks, all options except record starts and in situ show).
Pericentrin foci	Method 1	• Median blur, kernel 1 • Find maxima, prominence = X where X was a value that gave 1 point per pericentrin foci, as examined by eye.
	Method 2	• Gaussian blur, kernel 1 • Math: Min = 20 • Find maxima, prominence = 30
	Method 3	• Threshold 130/255 • Analyse particles (2-25 pixel units, circularity 0-1, overlay masks, everything selected except record starts and in situ show).

Table 4-2. Methods to count nuclei and pericentrin foci.
The steps of several different analysis workflows that were tested are outlined.

4.4.1. Common Steps in the Analysis Workflow

Most methods began with applying a blur filer, either gaussian blur or median blur. The blur step smoothens the image, helping to remove noise. The median blur filter was better at conserving edges of objects, which was especially beneficial in the case of the small pericentrin foci. The kernel size effects the "strength" of the filter, a larger kernel will result in a more heavily blurred image.

Thresholding is another step that was present in some of the different methods in Table 4-2. Thresholding will create a binary image, which is a prerequisite for some analysis steps such as "analyse particles". Thresholding will colour a pixel either black or white, depending on the pixel's original value and the thresholding settings that are chosen. Due to image variability, analysis methods with "set" parameters for thresholding (nuclei method 3 and pericentrin foci method 3) generating results of varying accuracy, as these settings were not appropriate for all images. Nuclei method 4 had a variable thresholding step, which meant that appropriate thresholding settings were selected for each image. This resulted in a more accurate analysis.

"Analyse particles" and "Find maxima" were both used as final steps to count objects of interest. Analyse particles has the benefit of being able to set parameters to filter out particles depending on their size and circularity. However analyse particles requires a binary image, which requires accurate thresholding. Find maxima identifies pixels within an area of the image that "stand out" from the surrounding pixels. It doesn't require a binary image, and can pick out multiple maxima within an object depending on the setting of the prominence parameter.

4.4.2. Comparison of Analysis Workflows

To assess the efficacy of different analysis workflows, their results were compared with "absolute counts" of nuclei and pericentrin foci, made by carefully counting manually. The results of these different analysis workflows can be seen in Figure 4-5.

To count nuclei, method 1,2 and 4 all worked well. However, method 1 and 2, which relied on measuring prominence to identify nuclei, had no way of excluding fragmented nuclear debris from dead cells from the analysis. Method 4 could exclude objects under a certain size, solving this problem. Method 4 was selected for analysis of siRNA screen images.

To count pericentrin foci only method 1 gave values that were consistently similar to the absolute counts so this method was selected for analysis of screen images.

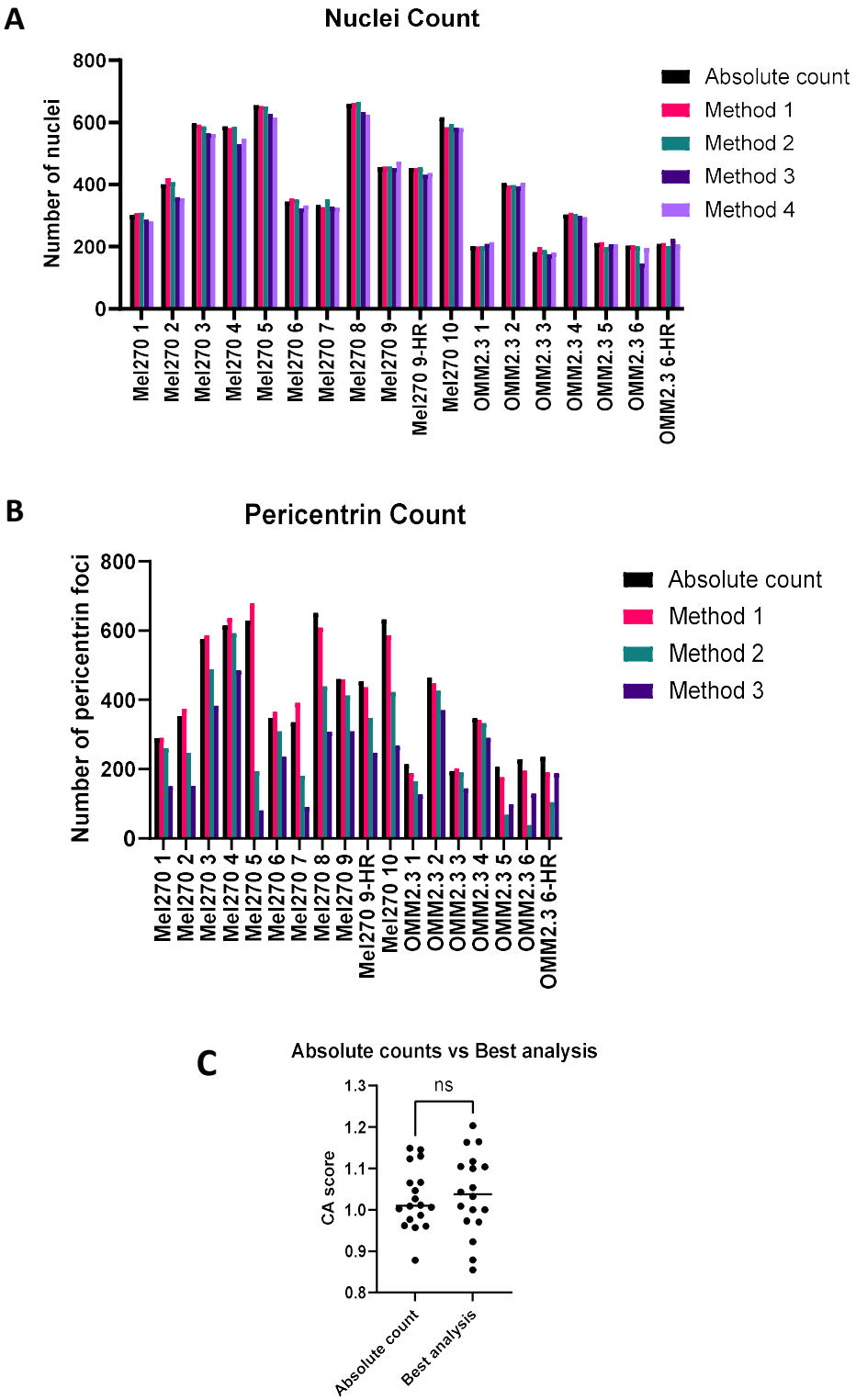

Figure 4-5. Comparison of image analysis workflows.
Immunofluorescence images of Mel270 and OMM2.3 cells grown, stained and imaged as for an siRNA screen were analysed in ImageJ. “Absolute” counts, i.e. image analysis by eye, were made for nuclei and pericentrin foci. These values were compared against those generated by several different image analysis workflows to count nuclei (A) and pericentrin foci (B). Comparison between absolute counts and the best analysis (using the nuclei count and pericentrin foci methods selected for future work) revealed no significant difference between the calculated CA scores (C). Two tailed paired t test, $t(17) = 0.3865$, $p = 0.7039$.

4.5. siRNA Screen to Identify Genes with a Role in Centrosome Amplification

Thousands of genes were identified as being differentially expressed between Mel270 and OMM2.3 or OMM2.5 cells. To narrow this number down, a list of genes was curated to cross reference with the DEG list. This narrowed the DEGs to 107 genes. Out of these 107, the genes which had the highest fold change, plus genes of special interest such as *PLK4*, were shortlisted to be tested in an siRNA screen. This process, from identification of thousands of DEGs to the shortlisting of genes to be included in the siRNA screen, was discussed in Chapter 3. Six mock and six scrambled siRNA control wells were randomised into the screen. This enabled the establishment of a strong "baseline" CA score for each cell line to compare the screen siRNA CA scores against. Cells were stained, imaged and analysed as outlined in sections 2.2 and 2.3.3. Figure 4-6 illustrates the screening process as a diagram.

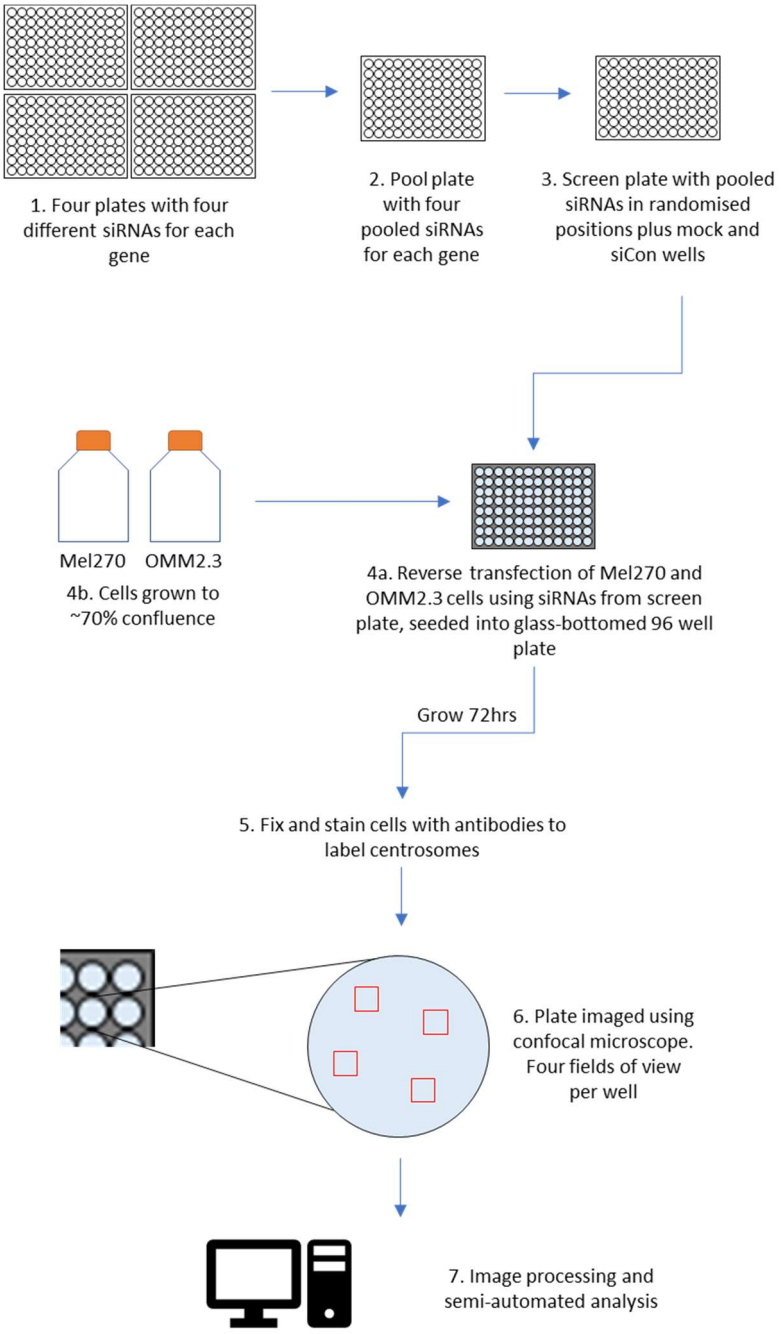

Figure 4-6. Workflow of siRNA screen.
The siRNAs to be screened were spread across four different plates (1), as there were four different siRNAs for each gene in the screen. The location of each siRNA was arranged so that so that an siRNA targeting Gene A was in the same well on each plate. In a new plate, for each gene, the four different siRNAs were pooled into a single well (2). The pool plate had the same siRNA layout as the four original plates. A screen plate was made using the pool plate (3), which took pooled siRNA and put it into a well according to a plate plan. The screen plate also had mock, positive control and negative control wells. The plate plan for the screen plate randomised the location of siRNAs, mock and control wells. To set up the screen, well contents were taken from the screen plate and added to the corresponding well of a glass bottomed 96 well plate (4a). Transfection reagents were added to the wells, followed by Mel270 and OMM2.3 cell suspension (4b) to perform a reverse transfection. 72 hours after transfections, the plate was fixed and stained for immunofluorescence imaging (5). Cells were stained for tubulin, pericentrin, cyclin B1 and with DAPI. Several fields of view, most often 4, were taken of each well on a confocal microscope (6). The images were then processed and analysed in a semi-automated manner using ImageJ (7).

23 genes were tested in this siRNA screen to determine their effects of the level of CA in Mel270 or OMM2.3 cells. 72 hours after reverse transfection, cells were fixed, stained, imaged and analysed as described in sections 2.2 and 2.3.3. Cells in the mock and siCon -ve wells had a similar appearance, and cells in the siCon +ve wells appeared dead, whilst cells in siRNA treated wells ranged in appearance (Figure 4-7, panel A). The mock and siCon -ve wells were expected to be similar in appearance, as the siCon -ve sequence doesn't target any genes. This means that the transfection procedure per se didn't have an effect of the cells. The siCon +ve siRNA used was AllStars Hs Cell Death control, which combines siRNAs that target ubiquitously expressed genes that are essential for cell survival. Therefore, the death of the cells treated with this control siRNA indicates a successful transfection procedure. Due to the variety of functions of genes that were selected for the siRNA screen, the range in appearance of siRNA treated cells was not unexpected.

To assess the effect of siRNA treatment on cells, CA scores were calculated. The CA score = (number of pericentrin foci)/(number of nuclei – number cyclin B1 positive cells). This returns the number of centrosomes per cell, adjusting for the number of cells in G2. The CA scores were normalised against the combined average CA scores of the Mock and siCon wells, allowing comparison between cell lines and repeat experiments. Values have been logged, too, to allow for comparison between treatments that decreased CA and treatments that increased CA. The results from the initial screen can be found in Figure 4-7, panel B.

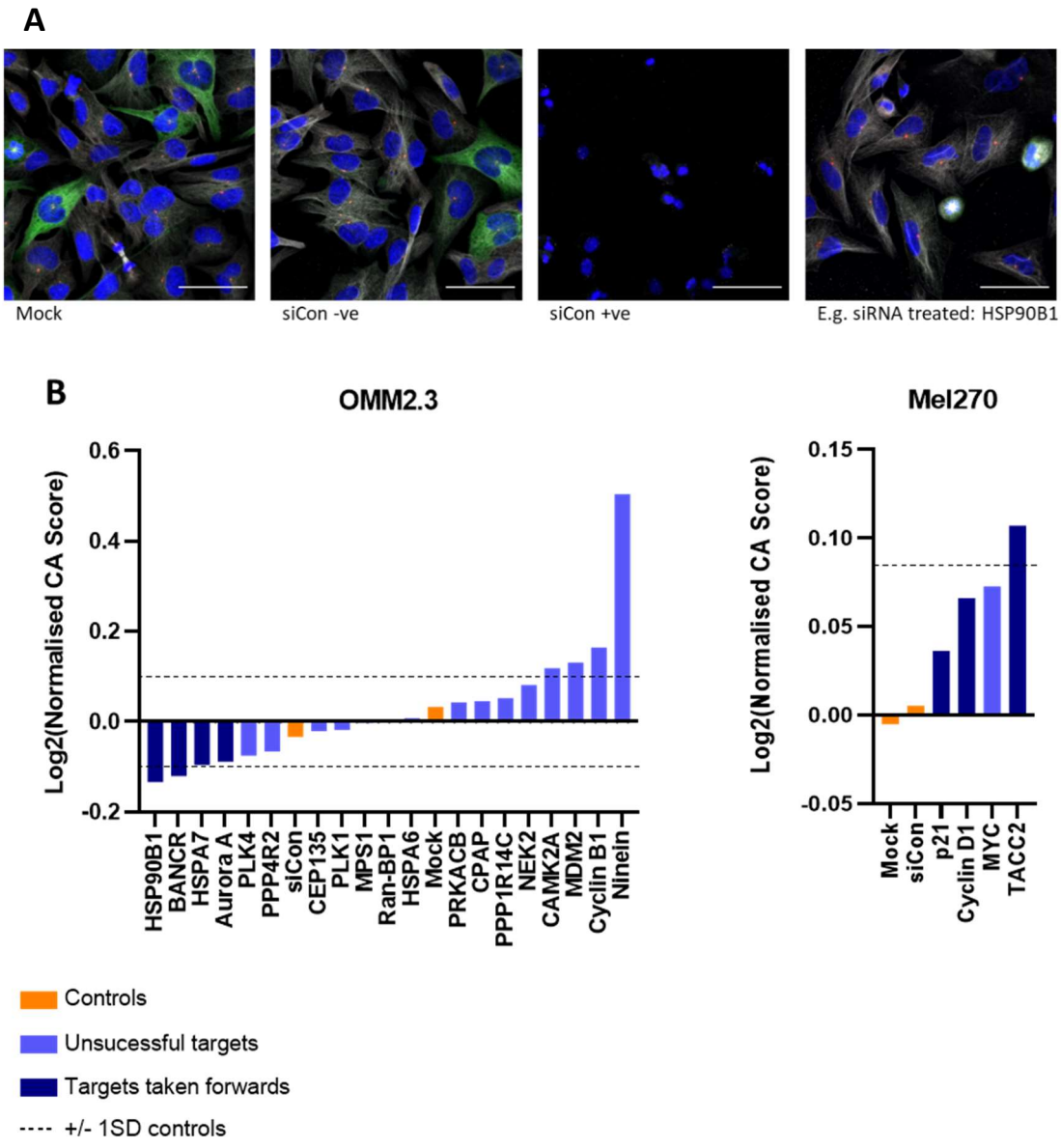

Figure 4-7. Results from the siRNA screen.
Mel270 cells (not shown) and OMM2.3 cells (A), transfected with siRNAs as indicated in the figure, and stained with DAPI (blue) and with antibodies against α-tubulin (white), pericentrin (red) and cyclin B1 (green). Scale bars are 50 µm. Results of the siRNA screen are summarised in the graphs in panel B. A dotted line shows +/- 1 standard deviation (S.D.) of the control wells (mock and siCon-ve wells).

siRNA treatments that caused the largest decrease in CA in OMM2.3 cells and the largest increase in CA in Mel270 cells were taken forwards for siRNA pool deconvolution. These were siRNAs targeting HSP90B1, BANCR, HSPA7 or Aurora A in OMM2.3 cells and TACC2, Cyclin D1 or p21 in Mel270 cells. The MYC siRNA treatment in Mel270 cells also caused an increase in CA score but was not taken forwards. This was due to an analytical error at the time of planning the subsequent deconvolution experiment.

4.5.1. Deconvolution of siRNA Pools

Seven targets were taken forwards from the initial siRNA screen for siRNA deconvolution. Experimental set up and analysis of siRNA deconvolution was similar to the siRNA screen, except individual siRNAs were tested additionally to pooled siRNAs. Using pools of siRNAs for a screen is standard practice, as using multiple different siRNAs increases the chance of successful knockdown of the target. A caveat of siRNA knockdown is that the siRNAs can have off target effects, silencing genes other than the intended target. It is highly unlikely that two siRNAs would have the same off target effect, which is why it is good practice to test individual siRNAs to see whether at least two siRNAs cause the same phenotype.

Results of the siRNA deconvolution can be found in Figure 4-8. In OMM2.3 cells, there were ≥2 individual siRNAs for both Aurora A and HSP90B1 that caused a decrease in CA score as with the pooled siRNAs (Figure 4-8, panel A). In Mel270 cells, only TACC2 had ≥2 siRNAs that caused an increase in the CA score (Figure 4-8, panel B). However, only one TACC2 siRNA gave a strong increase in CA, 2 TACC2 siRNAs caused a small decrease, and the pooled siRNA result from the deconvolution experiment also only gave a small increase. For these reasons, Aurora A and HSP90B1 were selected for further investigation. Knockdown of Aurora A or HSP90B1 with siRNA pools consistently reduced CA score in OMM2.3 cells (Figure 4-8, panel C). One-way ANOVA revealed statistically significant difference between at least two siRNA treatments ($F(3, 8) = [9.644]$, $p = 0.0049$). Dunnett's multiple comparisons test found that the mean CA score for siAuroraA treated cells was significantly lower than mock treated cells ($p = 0.0055$, 95% C.I. = [0.048, 0.226]). The mean CA score for siHP90B1 treated cells was not significantly lower than mock treated cells, but was close to significance ($p = 0.055$, 95% C.I. = -0.002, 0.175]). Though this difference was not significant, it was decided that HP90B1 would still be followed up in later work.

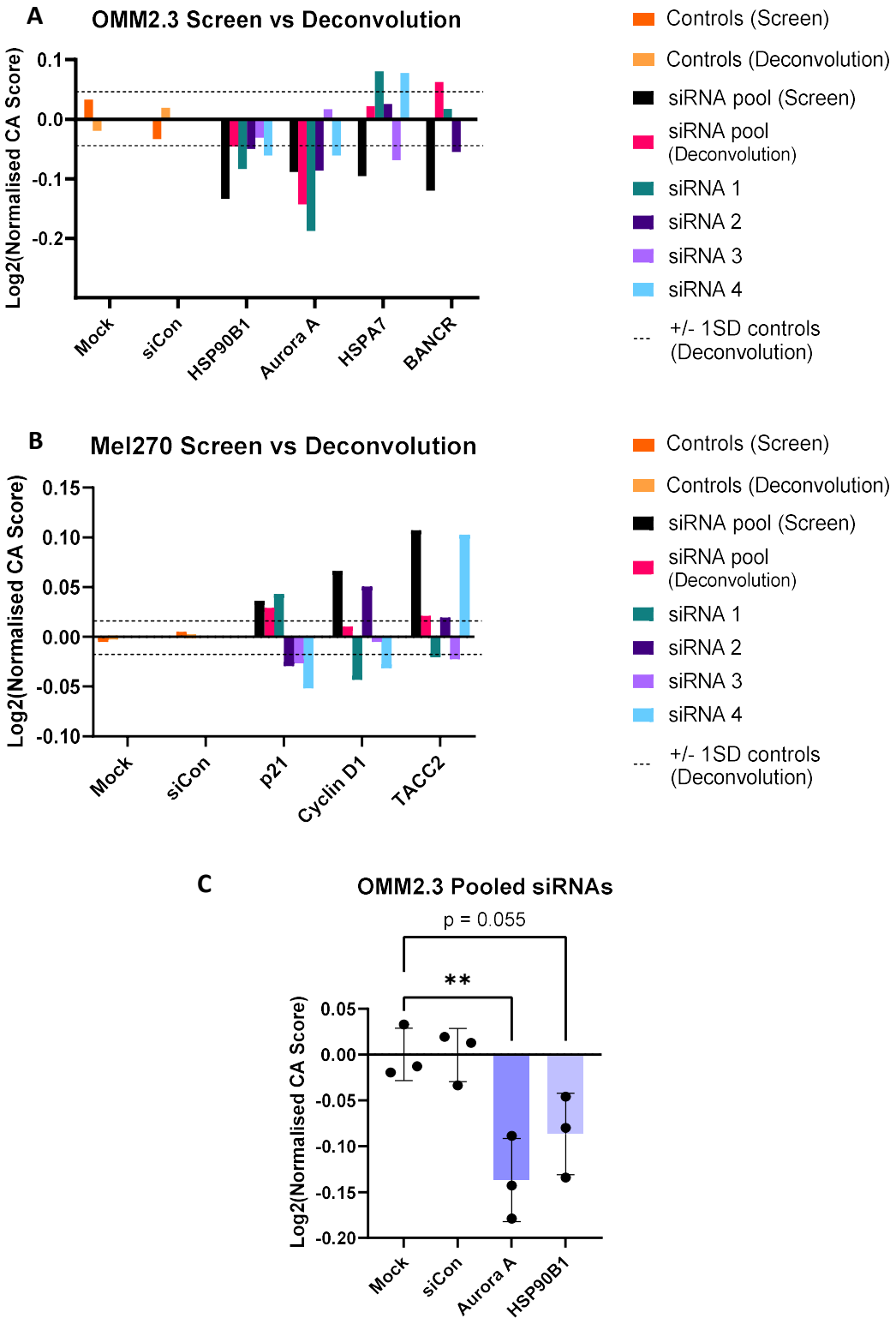

Figure 4-8. Knockdown of Aurora A or HSP90B1 reduces CA score in OMM2.3 cells.
Deconvolution of pooled siRNAs identified in the siRNA screen that decreased CA score in OMM2.3 cells (A) and increased CA score in Mel270 cells (B). A dotted line shows +/- 1 standard deviation (S.D.) of the control wells from the deconvolution experiments (mock and siCon-ve wells). Pooled siRNAs for Aurora A and HSP90B1 were tested in OMM2.3 cells for their effects on CA score, n = 3 (C). siCon = All Stars negative control, error bars in C show the mean ± 1S.D. Means in panel C have been compared with a one-way ANOVA and Dunnett's multiple comparisons post hoc test (** = p ≤ 0.005).

4.5.2. Selection of siRNAs for Aurora A and HSP90B1 by qPCR

After an siRNA screen and subsequent siRNA pool deconvolution, *Aurora A* and *HSP90B1* were identified as interesting genes with a role in CA in OMM2.3 cells. The next step was to check mRNA levels of *Aurora A* and *HSP90B1* after siRNA transfection. This step, along with siRNA deconvolution, demonstrated that siRNAs are causing a knockdown in the target gene. As well as looking at target gene knockdown, the effects of siRNAs targeting *Aurora A* on *HSP90B1* mRNA levels and vice versa were checked. The results of this work helped with selection of siRNAs for subsequent experiments.

OMM2.3 cells were treated with one of the 4 siRNAs, or a pool of the 4 siRNAs for *Aurora A* or *HSP90B1*. Also included were a mock treatment and a negative siRNA control, which in this case was siGFP-22. 48 hours after transfection, RNA extracts were taken (see section 2.5). RNA was reverse transcribed into cDNA and used in qPCR assays (see sections 2.6.1 and 2.6.4). The results can be seen in Figure 1-1Figure 4-9.

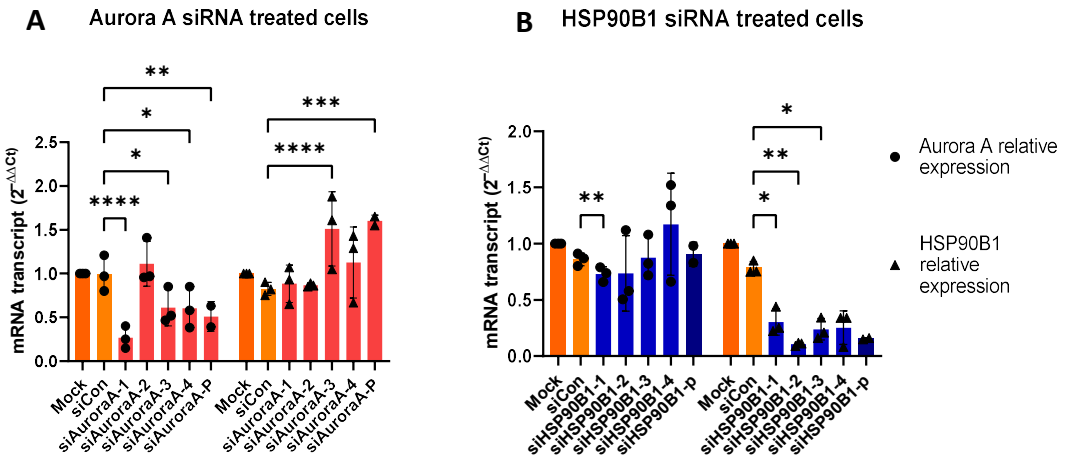

Figure 4-9. Aurora A and HSP90B1 mRNA expression in siAuroraA and siHSP90B1 treated OMM2.3 cells.
Relative expression of *Aurora A* (circles) and *HSP90B1* (triangles) mRNA in OMM2.3 cells 48 hours after transfection with individual (numbered) and pooled (P) siRNA targeting either *Aurora A* (A) or *HSP90B1* (B). A mixed effects analysis with Dunnett's multiple comparisons post-hoc test was used to compare means against the siCon mean (* = $p \leq 0.05$, ** = $p \leq 0.01$, *** = $p \leq 0.001$, **** = $p \leq 0.0001$). siCon = siGFP-22. N = 2 for pooled siRNAs, n = 3 for all other conditions.

Of the *Aurora A* siRNAs, three caused a statistically significant reduction in *Aurora A* mRNA levels (Figure 4-9, A). There was a slight, statistically insignificant increase in *Aurora A* mRNA after treatment with siAuroraA-2, so this siRNA was not chosen. siAuroraA-3 caused a statistically significant increase in *HSP90B1* signal, so this siRNA was not chosen. This was also the only *Aurora A* siRNA that didn't reduce CA score in OMM2.3 cells. siAuroraA-1,

which caused the greatest reduction in *Aurora A* mRNA, also caused the greatest reduction in CA score (Figure 4-8, panel B).

Of the *HSP90B1* siRNAs, all four caused a reduction in *HSP90B1* mRNA levels. However this was not statistically significant in siHSP90B1-4, and siHSP90B1-1 also caused a slight, but statistically significant, reduction in *Aurora A* mRNA levels, so these siRNAs were not chosen.

For future experiments, siAuroraA-1, siAuroraA-4, siHSP90B1-2 and siHSP90B1-3 were selected to use. These siRNAs caused the greatest reduction in their target mRNA and all reduced the CA score in OMM2.3 cells during the deconvolution experiments. Additionally, neither of the selected siRNAs targeting *Aurora A* had an effect on *HSP90B1* mRNA expression, and vice versa.

4.6. Chapter Discussion

The aims of this chapter can be split into three main groups. The first group of aims concern preparation for the siRNA screen. The method of reverse siRNA transfection was validated, both at the RNA and protein level. The immunofluorescence staining panel and image acquisition settings for the siRNA screen were selected. Finally, the image analysis workflow for the siRNA screen was developed. The second main aim was to perform the siRNA screen itself and analyse the images. Finally, the third main aim was to validate the initial results of the siRNA screen to select target genes to follow up. This was achieved by deconvolving the siRNA pools, testing individual siRNAs for their effect on CA score and target gene knockdown at the mRNA level.

When validating the reverse siRNA transfection, two targets were tested: KIFC1 and PLK4. A single siRNA targeting KIFC1 was used, as it was an siRNA that had previously and successfully been used in the lab. A pool of siRNAs targeting PLK4 was used, as these were one of the pools of siRNAs that would be used in the siRNA screen. Although the majority of siRNAs selected for use in the siRNA screen were validated as being functional in certain cell lines by Qiagen, ideally all siRNAs should be validated in the cell lines of interest (Mel270 and OMM2.3 in this case). This isn't practical to do for 23 pools of siRNA but, by validating with siRNAs targeting KIFC1 and PLK4, it was at least possible to show that the siRNA transfection was effective for those two targets in Mel270 and OMM2.3 cells. Western blot and qPCR assays showed a good knock down of KIFC1, with and PLK4 also showing successful depletion by qPCR 48 hours after transfection. A 72 hour timeframe was decided on for the

siRNA screen as it was thought that this would give time to see some effects of the transfections on CA.

To develop the parameters for the siRNA screen, antibodies for immunofluorescence and image acquisition settings were considered. CA had been robustly measured in Chapter 3 (see section 3.2) but that method was not suitable for an siRNA screen setting. Several different combinations of antibodies were tested for immunofluorescence staining panels, which lent themselves to different styles of analysis. For example, the pHH3 marker aided identification of mitotic cells and the cyclin B1 marker allowed for analysis of interphase cells through labelling G2 cells (Kim et al., 2017; Matthews et al., 2021). After examining the different images, the DAPI/ α-tubulin/ pericentrin/ cyclin B1 panel seemed most promising for high-throughput imaging and analysis. As well as the staining panel, different cell seeding densities and image resolutions were also tested.

The next aim was to develop an automated workflow. Having an automated workflow provides benefits such as speeding up analysis, removing human error or bias and making the analysis repeatable (Aeffner et al., 2017). Several workflows were developed and tested that were fully automated (method 3 for nuclei and methods 2 and 3 for pericentrin). However, inaccuracies were always introduced because there was no “once size fits all” value for thresholding or find maxima prominence, due to variability in the images. Another study which involved the development of high throughput automated image analysis of centrosomes applied a correction profile to images to account for uneven illumination between imaging plates (Balestra et al., 2013). Rather than take a similar approach to that, the methods that were eventually selected for the siRNA screen were semi-automated, but required human input to set the image threshold and find maxima prominence. This gave the opportunity to visually inspect image analysis as it was going along, whilst still using some macros to consistently apply the other steps of the analysis, as well as using tools to count objects rather than having the timely task of counting objects manually. The semi-automated analysis presented in this work shares similarities with other published workflows, which also include manual curation steps (Dittrich et al., 2019; Marteil et al., 2018).

Once the immunofluorescence staining panel, image acquisition and analysis workflow had been developed, it was possible to perform the first siRNA screen with pooled siRNAs. As well as the target siRNAs, “AllStars Hs Cell Death” siRNA was included as a positive control for successful transfection. This is a combination of siRNAs that, when transfected, leads to

cell death. In the absence of validating individual siRNAs, this is an alternative measure to show that transfection has been successful. Additionally, 6 mock and 6 scrambled siRNA controls were included for each cell line. This allowed the calculation of a very strong baseline CA score to compare the siRNA treated wells results to. ±1SD of the controls were plotted on the graphs in Figure 4-7 panel B and Figure 4-8 panels A and B. The standard deviation is quite wide, however the average CA scores for mock wells and for siCon wells were consistent throughout this series of experiments. This indicates a number of things. Firstly, it indicates that conditions across experiments were repeatable. Secondly, it highlights the importance of having so many control wells, as this will have generated a more accurate baseline of CA to compare against. Conversely, siRNA treatments were measured in one well only, which could raise some doubt in those results. However, pooled siRNAs for Aurora A and HSP90B1 consistently reduced CA score over three experiments (Figure 4-8, panel C).

Looking at the results of the siRNA screen, for the Mel270 cells, all siRNAs changed the CA score in the expected direction, i.e. knockdown of those targets all increased the CA score. Looking at OMM2.3 cells, there were some targets whose knockdown increased CA score, which is the opposite to what was expected.

A striking result was for the OMM2.3 cells treated with siRNAs targeting *Ninein*, which greatly increased the CA score. In fact, it caused the biggest change in CA score from the whole screen. Ninein is a sub-distal appendage protein on mature centrioles, where it aids in anchoring the minus end of microtubules to the centrosome (Blanco-Ameijeiras et al., 2022; Moss et al., 2007). *Ninein* was included in the screen for its role in centriole elongation, a proposed route to CA (Marteil et al., 2018). Depletion of ninein reduced centriole elongation induced by treatment with the proteasome inhibitor Z-L3VS in U-2 OS cells (Korzeniewski et al., 2010). Depletion of ninein was also shown to cause fragmentation of PCM, leading to multipolar spindles (Maiato & Logarinho, 2014). Conversely, elevated levels of ninein caused ninein aggregates to form outside of the centrosome, and these aggregates recruited γ-tubulin ring complexes, but not centrin or pericentrin (Stillwell et al., 2006). In the siRNA screen, OMM2.3 cells (which express high levels of ninein, as determined by RNA-Seq analysis) were treated with siRNAs targeting ninein in order to reduce ninein levels, perhaps to those of Mel270 cells which don't display CA. However the siRNA treatment may have reduced ninein levels so much so as to cause PCM fragmentation, as seen in a previous study (Maiato & Logarinho, 2014). As pericentrin, a PCM component, was used to label centrosomes in the screen, PCM fragmentation would lead to increased pericentrin foci and

therefore an increased CA score. This result was not followed up but it would be interesting to see if the same result could be repeated.

After testing pooled siRNAs, it was important to deconvolve the pools and test individual siRNAs. There can be off target effects of an siRNA if its sequence closely matches that of another gene (Jackson et al., 2003; Putzbach et al., 2018). However it is highly unlikely for two different siRNAs to have the same off target effect. Therefore, if two different siRNAs targeting the same gene have the same phenotypic effect, it is accepted that the phenotype is due to a knockdown of that target gene. After the initial screen, several genes were selected for follow up with deconvolution. These were *HSP90B1*, *BANCR*, *HSPA7* and *Aurora A* in OMM2.3 cells and *p21*, *cyclin d1* and *TACC2* in Mel270 cells. A similar immunofluorescence experiment was set up with the same controls, but this time individual siRNAs were tested as well as pooled siRNAs. Interestingly, the pooled siRNA results from the deconvolution experiments didn't always concur with the results from the initial screen. For *HSPA7* and *BANCR*, the pooled siRNAs caused a decrease in CA score of OMM2.3 cells in the screen, but an increase in the deconvolution experiment. The pooled siRNAs for *cyclin D1* and *TACC2* caused an increase in CA score of Mel270 cells in both the screen and deconvolution, but in the deconvolution the change in CA score was much more subtle. The pooled siRNAs for *p21* caused a moderate increase in CA score of Mel270 cells in both the screen and deconvolution, however only one of the *p21* siRNAs caused an increase when looking at the siRNAs individually. This points to the observed change in CA score being the result of an off target effect (Jackson et al., 2003; Putzbach et al., 2018). siRNAs for *Aurora A* and *HSP90B1* were the only ones where at least two siRNAs resulted in the desired change in CA score, therefore those two targets were taken forwards for further investigation.

qPCR assays of individual and pooled siRNAs targeting *Aurora A* or *HSP90B1* confirmed that all the siRNAs did indeed cause a reduction in target RNA levels. Two siRNAs for each target were selected using the qPCR results.

One of the targets identified by the siRNA screen and deconvolution was *Aurora A*. Aurora A is a kinase that localises to the centrosome, and whose activity plays a key role in the regulation of centrosome duplication, maturation and separation (Blanco-Ameijeiras et al., 2022; X. Lin et al., 2020; Lukasiewicz & Lingle, 2009). Aurora A is also a mitotic kinase, and loss of function can lead to a range of mitotic defects (Asteriti et al., 2014; Carvalhal et al., 2015; Glover et al., 1995; Macůrek et al., 2008; Marumoto et al., 2003). Overexpression of Aurora A has been reported in many cancers such as breast cancer, lung cancer and prostate

cancer, and this is often of prognostic significance (Du et al., 2021). Aurora A has been identified as a therapeutic target in the treatment of cancer, several Aurora A inhibitors such as Alisertib (MLN8237) and ENMD-2076 are currently undergoing clinical trials (Mou et al., 2021). The potential CA reversing effect of these Aurora A inhibitors may be another mechanism by which they could provide a therapeutic effect.

There have been numerous studies linking Aurora A overexpression and CA. Early work to understand the function of Aurora A revealed that its over expression in NIH 3T3 or MCF10A cells resulted in CA (Zhou et al., 1998). A further study revealed that overexpression of Aurora A lead to mitotic defects, tetraploidy and subsequent CA, a phenotype that was exacerbated in a *-/-p53* setting (Meraldi et al., 2002). Overexpression of Aurora A in mice also lead to a moderate increase in CA compared to WT mice, as well as increasing the incidence of tumours (X. Wang et al., 2006). As with the previous in vitro studies, loss of p53 exacerbated the Aurora A induced CA (X. Wang et al., 2006). Aurora A related CA has not only been observed in an Aurora-A-overexpression setting. GADD45a is a protein involved in the genotoxic stress pathway that inhibits Aurora A activity, and increased CA was observed in *-/-GADD45a* mice compared to WT mice (Shao et al., 2006). Additionally, treatment with methylnitrosourea or oestrogen saw a correlative increase in CA, Aurora A expression and tumourigenesis in rats (Goepfert et al., 2002; Li et al., 2004). Taken together with the other studies mentioned above, it is likely that these carcinogenic treatments caused Aurora A overexpression that was followed by CA. However neither study had experimental conditions when the carcinogenic agent (methylnitrosourea or oestrogen) was administered in conjunction with, for example, an Aurora A inhibitor to elucidate the cause of CA in these cases (Goepfert et al., 2002; Li et al., 2004).

Cells with CA may also have a dependence of Aurora A to survive. A study found that induction of CA (either by PLK4 overexpression or triggering cytokinesis failure following cytochalasin B treatment) increased sensitivity to Aurora A inhibition, which in cells with CA caused multipolar or disorganised cell divisions whose progeny failed to proliferate, whereas cells with normal CA number were unaffected in their ability to proliferate (Navarro-Serer et al., 2019). Additionally, the Acute Myeloid Leukaemia (AML) cell line K562, which naturally displays high levels of CA, displayed an increase in multipolar mitoses and aneuploidy after Aurora A inhibition. In contrast, other AML cell lines with low levels of CA responded to Aurora A inhibition with an increase in the number of “collapsed” mitoses, but no change in ploidy (Navarro-Serer et al., 2019).

Given the strong evidence for the role of Aurora A in CA that comes from previous studies, it is reassuring that the screen was able to identify Aurora A as a hit – in other words, it can act to show that the method for the screen and analysis works. Previous work has shown that OE of Aurora A can induce CA, that cells with CA may have an increased dependence of Aurora A, and that shRNA knockdown of Aurora A was able to eliminate CA induced by p53 abrogation and genotoxic treatments (Leontovich et al., 2013). However this work is to our knowledge the first that demonstrates a reduction of Aurora A can reverse CA that occurred naturally.

Aurora A has been studied extensively in cancers such as breast, lung and prostate cancer, but there is less work on Aurora A in the context of uveal melanoma. As with other cancers, high expression of Aurora A may be indicative of poor prognosis in uveal melanoma (Du et al., 2021). Probing TCGA data for uveal melanoma using cBioPortal revealed that Aurora A expression is most highly correlated with FAM83D, whose over expression is also associated with a poor prognosis in UM (Yu et al., 2022). FAM83D is a protein that plays a role in chromosomal alignment during mitosis involved by recruiting targets such as KID and CK1α, and has been co-immunoprecipitated with Aurora A (Fulcher et al., 2019; Huang et al., 2017; Santamaria et al., 2008). Aurora A was also identified as a key member of the kinome that is down regulated by FOXP1 in UM cells that were sensitive to treatment with the BET inhibitor, JQ1, linking high Aurora A expression to UM survival (Bailey et al., 2018). Finally, the senescence of UM cell line 92.1 cells after exposure to ionising radiation was linked to underexpression of Aurora A and subsequent slippage from G2 arrest into G1 and then senescence (C. Ye et al., 2013).

There are likely different molecular routes to CA. Several different mechanisms leading to CA have been observed, from centriole overduplication to mitotic failure and tetraploidisation (Denu et al., 2018; Meraldi et al., 2002). PLK4 overexpression is often used to artificially induce CA, but results from RNA-Seq analysis presented in this thesis in Chapter 3 revealed that PLK4 is not differentially expressed in OMM2.5 cells compared to Mel270 cells, but OMM2.5 cells still have CA. With this in mind, it would be interesting to see if knockdown of Aurora A in other cell lines with CA also induces reversal of CA. This would be an important result to see when considering Aurora A inhibition as a therapeutic target against CA.

The other target identified through the siRNA screen and deconvolution experiments was *HSP90B1*. Whereas the link between CA and Aurora A is well established, the link between CA and *HSP90B1* is less clear. The protein encoded by *HSP90B1* is known by several names:

Endoplasmin, GRP94 or HSP90B1; HSP90B1 will be used herein. HSP90B1 is a heat shock protein in the HSP90 family. This family has five members: HSP90AA1, HSP90AA2 and HSP90AB1 are the three cytosolic isoforms; TRAP-1 functions in the mitochondria and the aforementioned HSP90B1 functions in the endoplasmic reticulum (ER) (B. Chen et al., 2005). Due to their similarity, HSP90AA1, HSP90AA2 and HSP90AB1 are often not distinguished, simply being referred to as HSP90 instead (B. Chen et al., 2005; Hoter et al., 2018). The majority of HSP90 family research that is published is focussed on the cytosolic isoforms, with "HSP90" OR "HSP90AA" OR "HSP90AB" returning >13,000 results on PubMed, versus <1500 results for "HSP90B1" OR "GRP94" OR "GRP-94" and just over 500 results for "TRAP1" OR "TRAP-1". Cytosolic HSP90 is able to localise to the centrosome, where it stabilises PLK1, a kinase with key roles in centrosome duplication, separation and function (De Cárcer et al., 2001). Additionally, HSP90AB1 was identified as a high confidence interactor with Aurora A (Arslanhan et al., 2021). In contrast, HSP90B1 in its ER location is primarily responsible for the proper folding of secreted and membrane bound proteins (Hoter et al., 2018). This raises the question, why was expression of *HSP90B1* raised in OMM2.3 and OMM2.5 cells, and why did *HSP90B1* knockdown induce CA reversal?

Another role of HSP90B1 is Ca^{2+} homeostasis within the ER (Barton et al., 2012; Biswas et al., 2007). Having 15 Ca^{2+} binding sites, HSP90B1 is the main Ca^{2+} binding protein in the ER, with the ability to sequester Ca^{2+} in a high-capacity low-affinity manner (Marzec et al., 2012). Ca^{2+} localisation to centrosomes is required for successful mitosis, with a strong likelihood that this Ca^{2+} comes from the ER pool (Helassa et al., 2019). It is proposed that this plays a role in mitotic spindle polarity, and that the Ca^{2+} release is governed by IP3 receptors (Lagos-Cabré et al., 2020). Ca^{2+}-activated calcineurin colocalises at the centrosome with POC5, which is involved in centriole elongation; POC5 levels at the centrosome were reduced in cells treated with a calcineurin inhibitor (Tsekitsidou et al., 2022). HSP90B1 is overexpressed in some cancers, where its expression correlates with aggressive phenotypes and poor prognosis (Duan et al., 2021). It is also over expressed in oocytes, being the 7th most abundant protein in mouse oocytes (Duan et al., 2021; P. Zhang et al., 2009). Using a mouse model, HSP90B1 was discovered as being essential for the first mitosis of a developing zygote, as loss of the maternal copy of *HSP90B1* prevented the zygote from reaching the 2 cell stage (Audouard et al., 2011). This study also observed abnormal actin localisation and multipolar spindles in the absence of a maternal copy of HSP90B1 (Audouard et al., 2011). The role of Ca^{2+} in centrosomal function is an emerging field, surely more roles will be discovered in the future. The link between HSP90B1 and Ca^{2+} provides a compelling link

between HSP90B1 and centrosomes. Increased expression of HS90B1 could increase the Ca^{2+} capacity of the ER (Biswas et al., 2007). This increased capacity may be required for correct mitotic spindle alignment and cytoskeletal arrangement under challenging conditions such as the first zygotic mitosis or in a CA environment. Reduction of HSP90B1 in OMM2.3 cells may have led to a reduced ER-Ca^{2+} capacity, perturbing Ca^{2+} localisation to centrosomes in cells with CA, causing multipolar mitoses and cell death.

In this chapter, a method for setting up and analysing an siRNA screen into the effects on CA was designed and performed. Aurora A and HSP90B1 were identified through the siRNA screen as targets whose knockdown reduced the CA score of OMM2.3 cells. The next chapter will focus on other effects that Aurora A or HSP90B1 knockdown has on OMM2.3 cells.

Chapter 5.

Characterisation of Centrosome Amplification-reversed OMM2.3 Cells

5.1. Introduction

In the previous chapter, Aurora A and HSP90B1 were identified through an siRNA screen as proteins required to maintain CA in metastatic uveal melanoma, as knockdown of either of these caused a reduction in the CA score of OMM2.3 cells. In this chapter, the overarching aim is to assess the effects of Aurora A or HSP90B1 knockdown induced CA reversal, on OMM2.3 cells. CA has been shown to increase oncogenicity in cells, including by having cell-autonomous and non-autonomous effects on cell motility and has also been shown to be associated with poor prognosis (Chan, 2011; De Almeida et al., 2019; Ganem et al., 2009; Godinho et al., 2014). The hypothesis is that reversal of CA also reverses oncogenic features of OMM2.3 cells.

This chapter will examine the effect of Aurora A or HSP90B1 knockdown induced CA reversal on both cell cycle and, in particular, cell migration. CA has been shown to affect cell invasion via cell-autonomous and non-autonomous mechanism (Ganem et al., 2009; Godinho et al., 2014). However, whether CA affects cell migration, particularly at a single-cell level, has not been determined. In this chapter I design and test a **C**orrelative **L**ive imaging and **I**mmuno**f**luorescence (CLIF) experimental and analysis method, capable of examining cell migration, cell-cycle and their relationship to CA. I use uveal melanoma cells expressing the cell cycle reporter H2B-FUCCI2a to track cell migration in live cells, over multiple cell cycles, followed by immunofluorescence to determine the centrosome amplification (CA) status of individual tracked cells. An automated tracking and quantification workflow utilising Trackmate and Stardist plugins in FIJI allow for analysis of cell migration parameters of hundreds of individual cells. We call this method FUCCI-CLIF.

5.1.1. FUCCI Biosensors

The FUCCI biosensors are a series of cell cycle biosensors, allowing for live detection of the cell cycle progression, through the expression of fluorescently tagged genes. FUCCI stands for **F**luorescent **U**biquitination based **C**ell **C**ycle **I**ndicator. The system is based on fluorescently tagged Cdt1 and Geminin, both having roles in the regulation of DNA replication (Melixetian et al., 2004; Vaziri et al., 2003). These proteins accumulate in the cell nucleus in an oscillating fashion, partly due to E3 ligase mediated proteolysis (X. Li et al., 2003; McGarry & Kirschner, 1998). Cdt1 and Geminin are direct substrates of the E3 ligases APC^{Cdh1} and SCF^{Skp2}, which also have oscillating activity throughout the cell cycle (Bashir et al., 2004; Benmaamar & Pagano, 2005; Wei et al., 2004). Cdt1 accumulates in the nucleus during G1. In S/G2, SCF^{Skp2} activity causes degradation of Cdt1. Meanwhile, Geminin

accumulates in the nucleus in S/G2, moving to the cytoplasm during mitosis. In late M/G1, APC^{Cdh1} activity causes degradation of Geminin. In the FUCCI system, Cdt1 is tagged with a red spectrum probe such as mCherry and Geminin is tagged with a green spectrum probe such as mVenus. This results in cells fluorescing red throughout G1, a brief period of cells fluorescing yellow (due to both fluorescently tagged proteins being expressed) at the G1/S transition, to cells fluorescing green throughout S/G2/M.

There have been several iterations of the FUCCI biosensor since it was first developed, each improving on issues such as spectral overlap of probes, inconsistent transgene expression between cells and tissue types due to random integration into the genome and, uneven expression of the tagged Cdt1 and tagged Geminin due to their constructs being on two separate transgenes and the lack of a S/G2 transition marker (Abe et al., 2013; Mort et al., 2014; Sakaue-Sawano et al., 2008, 2017).

In this work, H2B-FUCCI2a has been used, which is a modified version of FUCCI2a. FUCCI2a was developed using the *Thosea asigna* virus 2a peptide to fuse mCherry-hCdt1 and mVenus-hGem to make a bicistronic construct. This leads to roughly equimolar expression of the tagged proteins (Mort et al., 2014). H2B is a nuclear marker that is present in all stages of the cell cycle and, in the H2B-FUCCI2a construct, H2B has been tagged with mCerulean. This helps to track cells throughout the cell cycle, including in late stages of mitosis, when both Cdt1 and Geminin are degraded. Use of the H2B-FUCCI2a system in this work was kindly facilitated by the Mort Lab based at Lancaster University, who developed and provided the H2B-FUCCI2a plasmid. OMM2.3 cells stably expressing the H2B-FUCCI2a construct had previously been generated in the Fielding lab (see section 2.1.4).

5.2. Aurora A and HSP90B1 Protein Expression in Mel270, OMM2.3 and OMM2.5 Cells

Aurora A and *HSP90B1* were both differentially expressed genes in OMM2.3 and OMM2.5 cells compared to Mel270 cells, as determined by RNA-Seq. A higher mRNA expression makes it likely that protein expression will also be higher, however this cannot be taken as a given and therefore it is important to establish protein expression levels (Y. Guo et al., 2008). Aurora A and HSPB90B1 protein levels were measured in Mel270, OMM2.3 and OMM2.5 cells by SDS-PAGE and western blot (Figure 5-1). Similar expression patterns can be seen for Aurora A and HSP90B1 in the RNA-Seq and western blot results. For both genes, protein expression was significantly higher in OMM2.3 and OMM2.5 cells compared to

Mel270 cells, with the exception of HSP90B1 protein levels in OMM2.5 cells which were close to significance ($p = 0.058$).

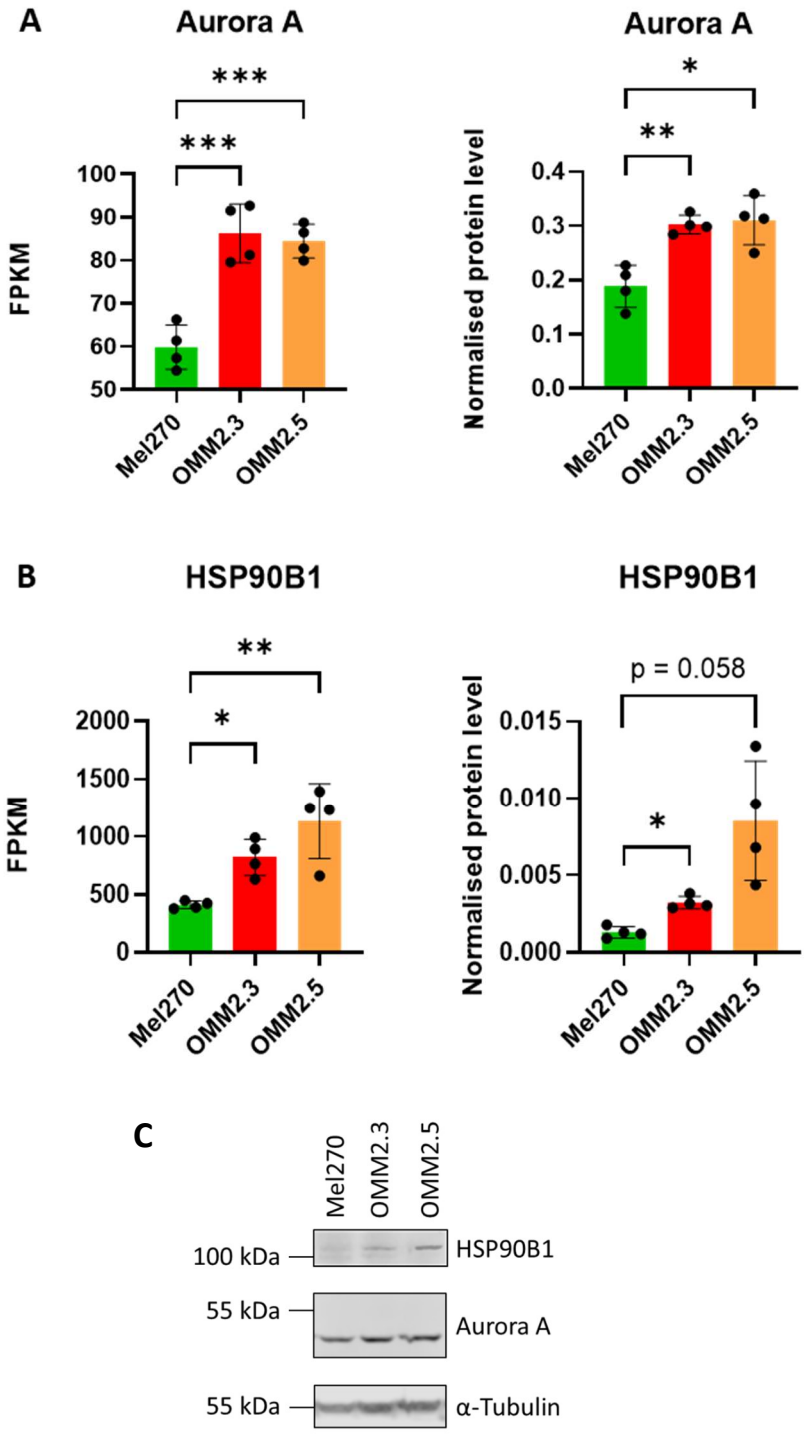

Figure 5-1. Aurora A and HSP90B1 protein expression in Mel270, OMM2.3 and OMM2.5 cells. Western blots were used to measure the levels of Aurora A and HSP90B1 in Mel270, OMM2.3 and OMM2.5 cells, and confirm RNA-Seq results of their differential expression. Panel A shows the RNA-Seq (left) and western blot (right) results for Aurora A expression. Panel B shows the RNA-Seq (left) and western blot (right) results for HSP90B1 expression. Panel C shows a representative western blot. An ordinary one-way ANOVA with Tukey's multiple comparisons post hoc test was used to compare Aurora A and HSP90B1 expression, both at the RNA and protein level. Asterisks have been used to indicate p values (* = $p \leq 0.05$, ** = $p \leq 0.01$, *** = $p \leq 0.001$, **** = $p \leq 0.0001$). N = 4 for both RNA-Seq and western blot results.

5.3. Aurora A Knockdown increases G2, 4n+ and 8N populations in OMM2.3 Cells

During the siRNA screen, the effect of siRNA treatments on CA was measured by analysing all cells in the images that were taken. Centrosome number varies during the cell cycle, so a variation in cell cycle population would have an effect on analysis. This was mitigated by adjusting for cyclin B1 positive cells, which labels cells in late S phase to early mitosis. To get a more holistic picture of the effects of siRNA treatment on cell cycle, propidium iodide staining and flow cytometry was used (see section 2.8). OMM2.3 cells were treated with pooled siRNAs targeting Aurora A or HSP90B1. Mock transfected and negative control siRNA (siGFP-22) conditions were also included. Cells were grown for 72 hours, the same timeframe as the siRNA screen, before being fixed and stained with propidium iodide to run on a flow cytometer. Results from this, along with example flow scatterplots, can be seen in Figure 5-2.

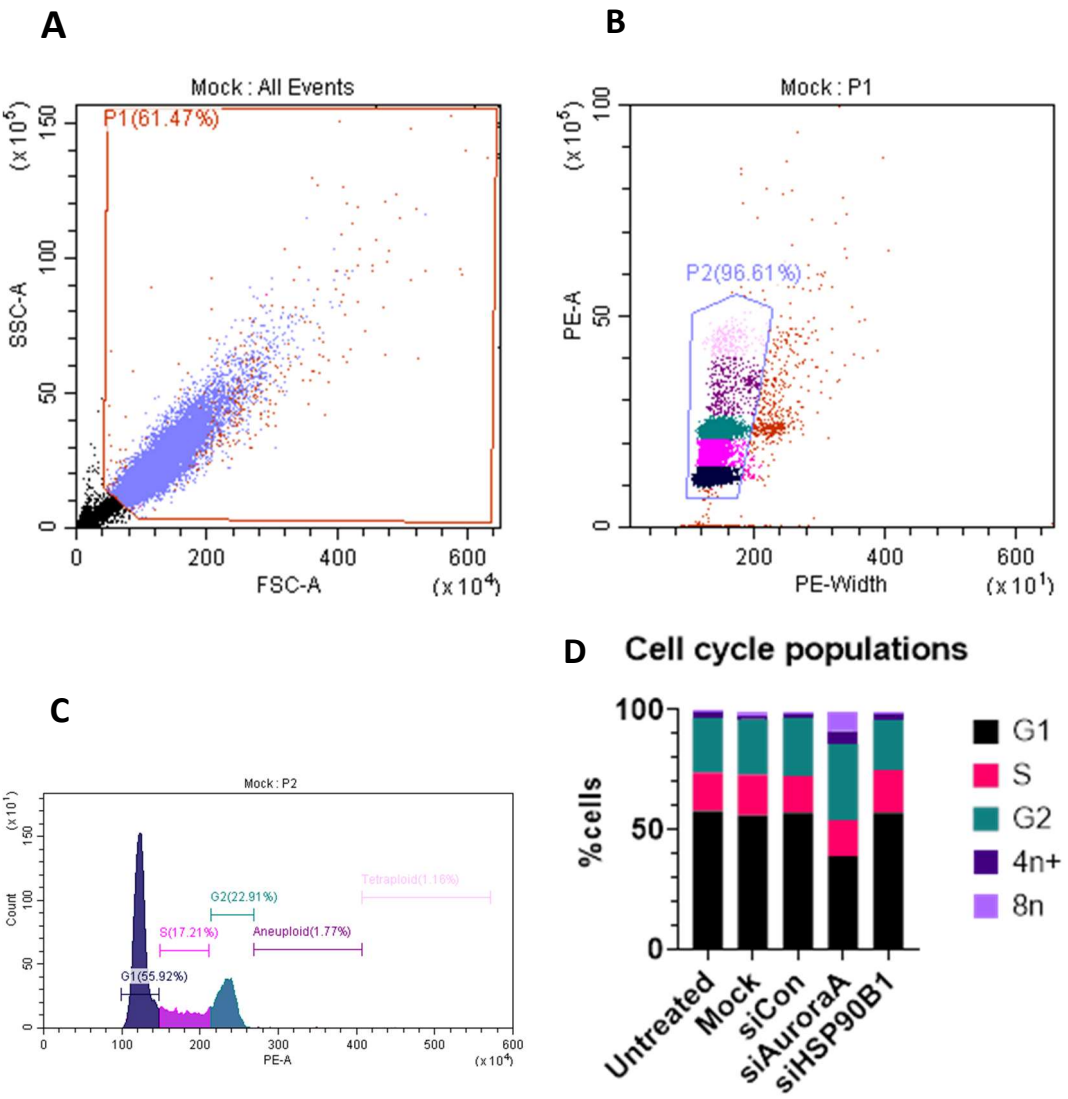

Figure 5-2. Cell cycle populations of siAuroraA and siHSP90B1 treated OMM2.3 cells.
OMM2.3 cells were treated with pooled siRNA targeting either Aurora A or HSP90B1. 72 hours after transfection, cells were stained with propidium iodide and analysed using flow cytometry. Panels A-C show example gates and a histogram from the mock sample. Panel D shows the proportion of cells in each phase of the cell cycle. The siRNA used for siCon was siGFP-22. N = 1.

The cell cycle profile of mock, siCon and siHSP90B1 treated cells is comparable. HSP90B1 isn't known to play any direct roles in cell cycle progression, so this result is expected (B. Chen et al., 2005; Hoter et al., 2018). Cells treated with siAuroraA have increased G2, 4n+ and 8n populations. This indicates there is a build-up of cells stalling in G2/ mitosis, failing mitosis and reduplicating DNA to become octoploid. Aurora A plays a key role in mitotic progression, so this is an expected result (X. Lin et al., 2020; Marumoto et al., 2002). However, this result seems paradoxical as you would expect to see increased CA with the

occurrence of failed mitoses. Indeed, failed mitosis is a proposed route to CA (Godinho & Pellman, 2014). Despite this, during the siRNA screen, siRNA knockdown of Aurora A caused a decrease in CA.

Treatment	% cyclin B1 +ve	% G2 by flow cytometry
Mock	5.6	22.8
siAuroraA-pool	10.7	31.7
siHSP90B1-pool	5.7	20.9

Table 5-1. Comparison of G2 populations in siRNA treated cells as determined by cyclin B1 immunofluorescence staining and propidium iodide flow cytometry.
OMM2.3 cells were treated with pooled siRNA targeting Aurora A or HSP90B1. G2 populations of these cells were compared against control cells, treated with mock conditions. In one set of experiments, cyclin B1 immunofluorescence staining was used to identify cells in G2. In another experiment, propidium iodide was used to stain DNA followed by flow cytometry analysis. Mock and siHSP90B1 treated cells had similar G2 populations to each other by both methods. siAuroraA treated cells had an increased G2 population by both methods, though this was more pronounced in the flow cytometry analysis.

The flow cytometry results can be compared to the cyclin B1 staining in the screen and deconvolution experiments (Table 5-1). Taking results from all mock, siAuroraA-pool, and siHSP90B1-pool immunofluorescence images, the number of cells that that were stained positively for cyclin B1 (therefore were in G2/early M) were 5.6%, 10.7% and 5.7% respectively. This compares with 22.8%, 31.7% and 20.9% cells in G2/M by flow cytometry in mock, siAuroraA-pool, and siHSP90B1-pool treated cells respectively. These numbers show the same trend, with siAuroraA-pool having ~2x the number of cyclin B1 +ve cells and ~1.5X the number of cells in G2 when compared to mock or siHSP90B1 treated cells.

5.4. Aurora A and HSP90B1 Protein Recovery After siRNA Knockdown

For the siRNA screen, cells were analysed 72 hours after transfection. This was deemed an appropriate time frame to see any potential effects on levels of CA. To design experiments looking into the effects of CA reversal on cell behaviour, it would be useful to know when target protein levels recover after siRNA transfection, so that any changes in cell behaviour could be attributed solely to a change in CA status. This is especially the case for Aurora A, which has many functions within the cell (X. Lin et al., 2020). By choosing a timeframe that allows target protein levels to recover, the results are more likely to show the effect of CA reversal, as opposed to any other effects that Aurora A or HSP90B1 knockdown might have.

OMM2.3 cells were transfected with a single siRNA targeting Aurora A or HSP90B1. A mock condition and control siRNA (siGFP-22) was also included. Lysates were taken every day for 4 days after transfection and analysed by SDS-PAGE and western blot. Additionally, it was hypothesised that siRNA knockdown of Aurora A could have an effect on HSP90B1 protein levels and vice versa. Lysates were blotted for the protein that had been knocked down and the reciprocal protein (see section 2.9). Signal of α-tubulin was used to normalise between samples for Aurora A and HSP90B1 protein quantification.

This experiment was carried out twice. A representative blot can be seen in Figure 5-3, panel A. Aurora A and HSP90B1 protein quantification has been presented as graphs in Figure 5-3, panels B-E.

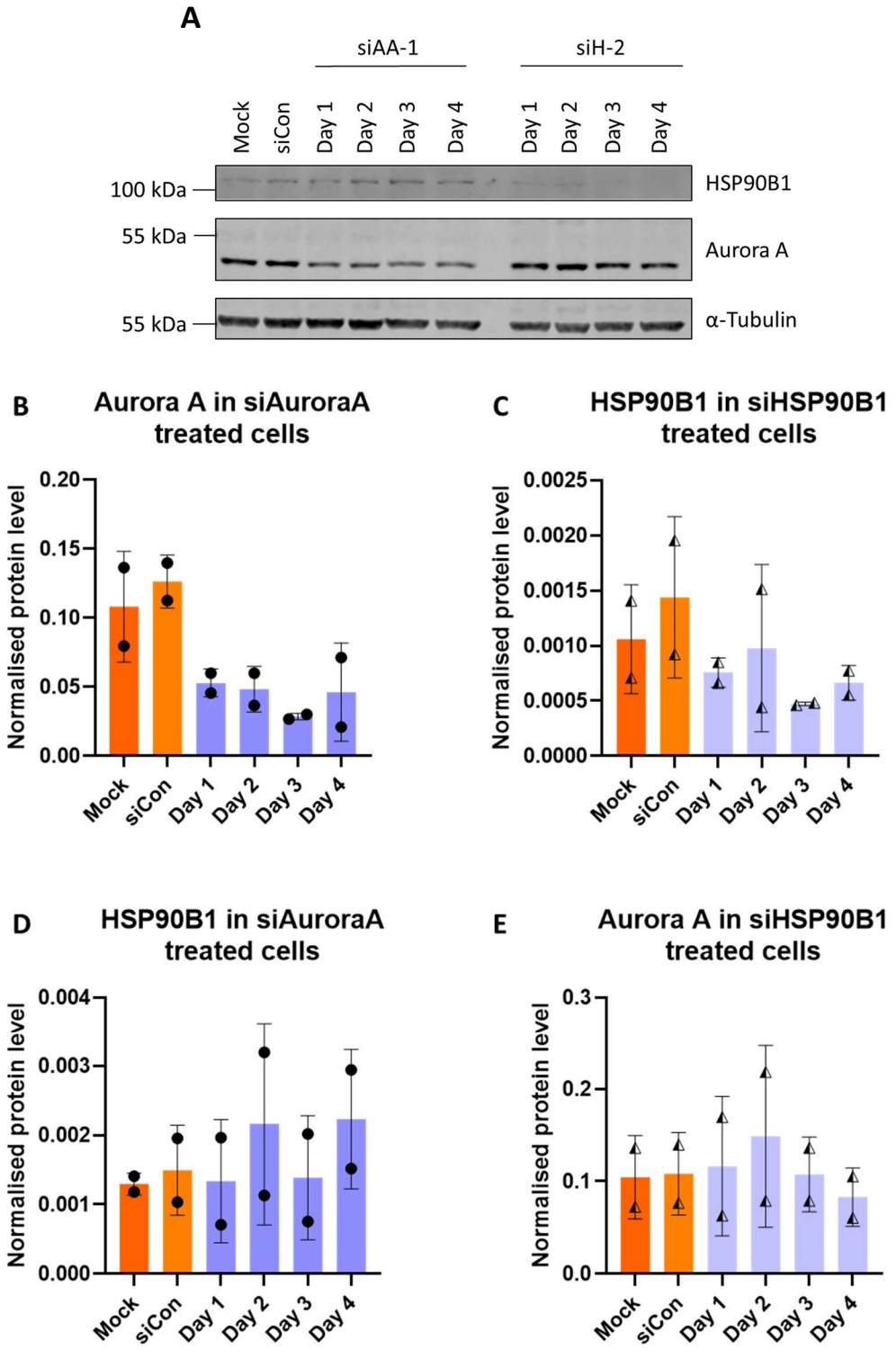

Figure 5-3. Protein recovery of Aurora A and HSP90B1 after siRNA treatment.
Representative western blot of OMM2.3 cells treated with siRNA targeting Aurora A (siAA-1) or HSP90B1 (siH-2) (A). The membrane has been blotted for HSP90B1 and Aurora A, with α-Tubulin used to normalise signals. Normalised protein levels for Aurora A (B) and HSP90B1 (D) in siAuroraA treated OMM2.3 cells up to 4 days post transfection. Normalised protein levels for HSP90B1 (C) and Aurora A (E) in siHSP90B1 treated OMM2.3 cells up to 4 days post transfection. siCon = siGFP-22, n = 2.

Knockdown of Aurora A caused approximately a 50% reduction in Aurora A protein levels from days 1-4 (Figure 5-3, panel A, lanes 2-6 and panel B). HSP90B1 protein levels didn't appear to be consistently affected across the timecourse after Aurora A knockdown (Figure 5-3, panel D).

Knockdown of HSP90B1 caused approximately a 40% reduction in HSP90B1 protein levels from days 1-4 (Figure 5-3, panel A, lanes 8-13 and panel C). Aurora A protein levels in siHSP90B1 treated cells were similar to that of control conditions (Figure 5-3, panel E).

One aim of these experiments was to find the timeframe in which protein levels would recover. After 4 days, both proteins showed indications of starting to recover but this was not statistically significant. In the interest of progressing the research, subsequent experiments were designed with 72 hours, as this was the timeframe used for the siRNA screen experiments and produced a repeatable reduction in CA (Figure 4-8, panel C).

The other aim of these experiments was to see if siRNA knockdown of Aurora A effected HSP90B1 protein levels, and vice versa. Currently, there are no reports of HSP90B1 interacting with Aurora A. However, HSP90AB1, another heat shock 90 family protein, and HSPA8, a member of the heat shock 70 family, are predicted interactors of Aurora A (Arslanhan et al., 2021). From the results presented in Figure 5-3, it doesn't appear that Aurora A knockdown has any effect on HSP90B1 levels and vice versa, indicating that neither protein regulated the abundance of the other.

5.5. Matched mRNA and Protein Expression of Aurora A and HSP90B1 After siRNA Knockdown

The previous protein recovery experiment indicated that knockdown of either Aurora A or HSP90B1 had no effect on levels of the other protein, but that target protein levels may start to recover more than 4 days post siRNA transfection. A further experiment was set up to acquire matched RNA and protein samples at 3 and 5 days post siRNA transfection.

Two siRNAs for each target were tested and, additional to the protein lysates, RNA samples were taken for qPCR assays to allow comparison between RNA and protein expression after treatment. Mock and siCon samples were taken at day 3 and day 5, rather than at day 1, to allow for a more direct comparison with the siAuroraA and siHSP90B1 treated cells.

Results can be seen in Figure 5-4, these data represent an n of 1.

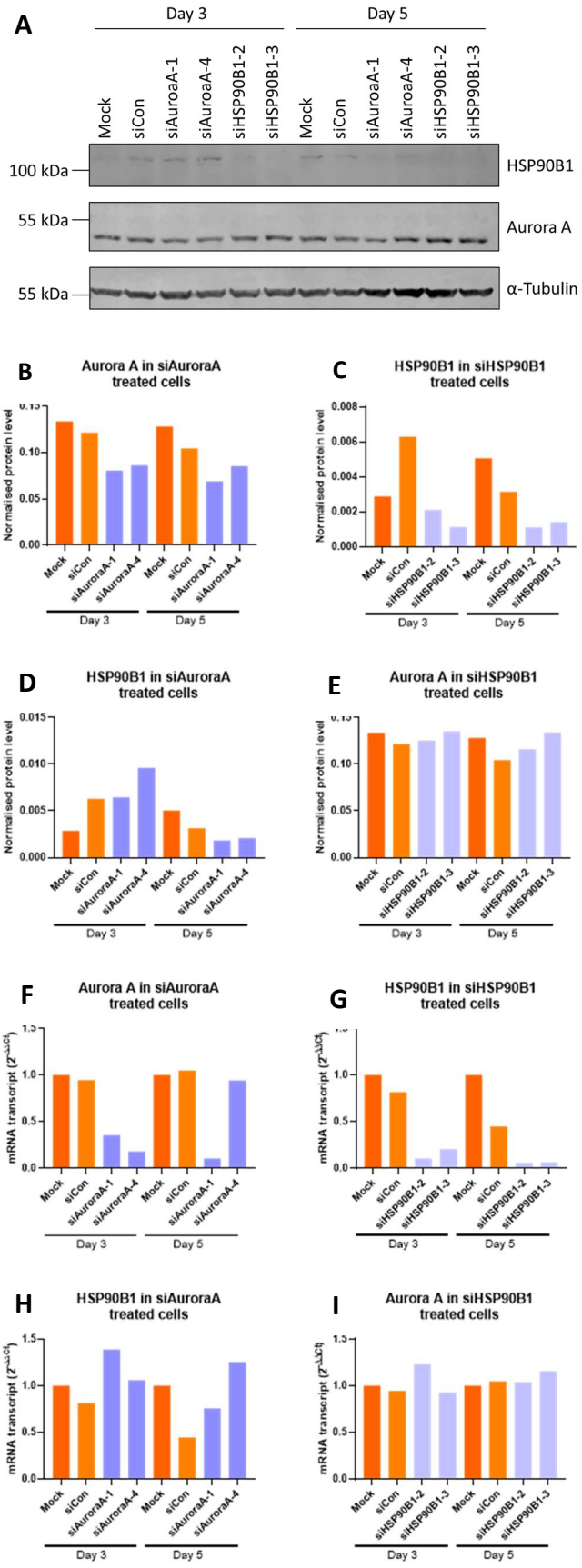

Figure 5-4. Matched mRNA and protein expression of Aurora A and HSP90B1 after siRNA treatment.

Western blot of OMM2.3 cells treated with two different siRNAs for Aurora A or two different siRNAs targeting HSP90B1 (A). The membrane has been blotted for HSP90B1 and Aurora A, with α-Tubulin used to normalise signals. Normalised protein levels of Aurora A (B) and HSP90B1 (D) in siAuroraA treated OMM2.3 cells. Normalised protein levels of HSP90B1 (C) and Aurora A (E) in siHSP90B1 treated OMM2.3 cells. Relative mRNA transcript of Aurora A (F) and HSP90B1 (H) in siAuroraA treated OMM2.3 cells. Relative mRNA transcript of HSP90B1 (G) and Aurora A (I) in siHSP90B1 treated OMM2.3 cells. N = 1, siCon = siGFP-22.

At the protein level, siRNA treatment reduced target protein expression at days 3 and 5 for both Aurora A and HSP90B1 (Figure 5-4, panels B and C). From the quantification, siAuroraA appears to modestly reduce HSP90B1 protein expression at day 5 (Figure 5-4, panel D). However, looking at the blot, the HSP90B1 signal is very weak for all day 5 samples (Figure 5-4, panel A, lanes 7-12) and so it is inconclusive as to whether the normalised signal values represent a true reduction in HSP90B1. siHSP90B1 treatment had no effect on Aurora A protein expression at day 3 or day 5 (Figure 5-4, panel E).

Both siRNAs resulted in reduced target mRNA expression at both timepoints, with the exception of siAuroraA-4 at day 5 (Figure 5-4, panels F and G). Aurora A mRNA levels had recovered by day 5 after treatment with siAuroraA-4. This was reflected in the western blot, where a slightly stronger Aurora A band can be seen for the siAuroraA-4 day 5 sample (Figure 5-4, panel A, lane 10). This suggests that, at least in some cases, mRNA and protein levels can recover or begin to recover 5 days post siRNA transfection.

5.6. Cell Migration in OMM2.3-H2B-FUCCI2a Cells After Aurora A or HSP90B1 Knockdown or Inhibition

CA has been implicated in oncogenic phenotypes in cancer cells such as increased invasiveness, although this has not been examined at the single-cell level. In Chapter 4, it was shown that siRNA knockdown of Aurora A or HSP90B1 reduced CA in OMM2.3 cells. The next step is to see how, if at all, CA reversal effects the oncogenic phenotypes that CA has been attributed to. The ability for a cell to migrate is a prerequisite for invasiveness. The following work investigates the effects of Aurora A or HSP90B1 knockdown or inhibition on the migration of OMM2.3-FUCCI2a cells.

5.6.1. FUCCI-Correlative Live and Immunofluorescent Microscopy Assay Development

A modified scratch assay, combining live imaging, a FUCCI2a biosensor and immunofluorescence, was developed and used to measure migration (Figure 5-5). Scratch

assays are a simple assay to measure cell migration (Liang et al., 2007). Cells are grown to confluency before making a “scratch” in the monolayer. Cells are left to grow for the desired time, then the scratch is imaged to see how far cells have migrated into the wound. One drawback of this technique is that the wound can be filled in by cells either migrating, or by cells dividing into the gap. Taking a timelapse, rather than a single image at the beginning and end of the experiment, counters this issue, as it allows cell movement to be tracked. The other significant advantage of live cell imaging is that it allows the behaviour of individual cells within the population to be monitored, giving a richer insight into cell behaviour.

H2B-FUCCI2a is a biosensor that allows tracking of a cell’s progression through the cell cycle. By using cells that have been transfected with this biosensor, another layer of information is added to the timelapse scratch assay.

Finally, at the end of the timepoint, cells can be fixed and processed for immunofluorescence. By using pericentrin and centrin to label centrosomes and imaging the same field of view as the timelapse, it is possible to determine the CA status of the cells from the timelaspe. This assay provides information on the cell cycle, cell migration and CA status and can be analysed in many different ways depending on what question is being asked.

Cell tracking was performed in ImageJ using TrackMate and Stardist (see section 2.3.4).

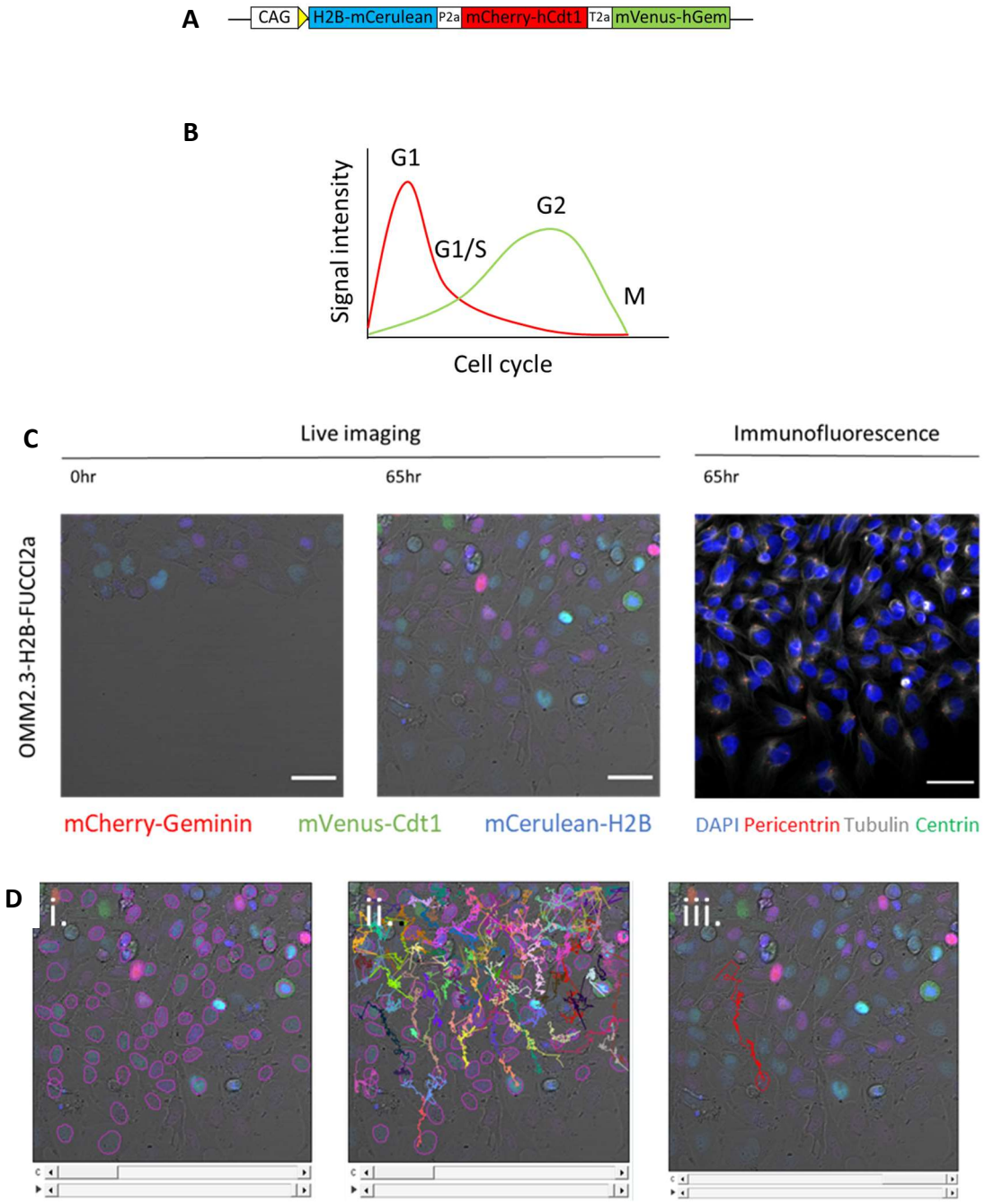

Figure 5-5. FUCCI-CLIF: Live imaging scratch-immunofluorescence assay with H2B-FUCCI2a transfected cells.

Schematic of the H2B-FUCCI2a construct, developed by the Mort Lab at Lancaster University (A). The whole construct is driven by a single synthetic CAG promoter. Eukaryotic ribosomes fail to insert a peptide bond between Gly and Pro residues in the viral P2a and T2a peptides, resulting in the fluorescently tagged genes being synthesised as separate polypeptides. A representation of FUCCI2a fluorophore expression throughout the cell cycle (B). H2B-mCerulean is constitutively expressed. Example images from left to right: the beginning of live imaging, the end of live imaging and a corresponding immunofluorescence image (C). H2B-FUCCI2a cells are labelled with mCherry (red), mVenus (green) and mCerulean (blue). Immunofluorescence image is of cells stained with DAPI (blue) and with antibodies against α-tubulin (white), pericentrin (red) and centrin (green). Scale bars are 50 µm. Example nuclear segmentation and track detection with Stardist and TrackMate (D). Segmented nuclei after filtering for quality is shown in Di, overlayed tracks with at least 100 "spots" are shown in Dii, and an individual spot and its corresponding track are shown in Diii.

5.6.2. Experimental Setup

Aurora A or HSP90B1 were targeted either for knockdown using one of two siRNAs for each target, or targeted with inhibitors. Alisertib (ALS) was used to inhibit Aurora A, GRP94 inhibitor-1 (iGRP94) was used to inhibit HSP90B1. Drug concentrations were chosen following MTS cell viability assays (Appendix item E). Pre-treated OMM2.3-H2B-FUCCI2a cells were prepared for a scratch assay by seeding into glass bottomed plates, creating a scratch with a pipette tip and recording a live imaging timelapse. To pre-treat cells, OMM2.3-H2B-FUCCI2a cells were treated on day 1 with either with siRNAs (40 nM) or inhibitors (100 nM ALS or 5 µM iGRP94). Media on siRNA treated cells was changed on day 2, there was no media change for inhibitor treated cells. On day 4, cells were reseeded onto a glass bottomed 24 well plate at a density of 130,000 cells per well. Cells were left to adhere overnight before starting the live scratch assay on day 5 and therefore the live cell imaging was performed in the absence of either siRNAs or inhibitors. A wound was made in each well by scratching a straight line with a pipette tip immediately before recording the live imaging timelapse. The timelapse was taken over 66 hours. After the timelapse, cells were fixed and stained with antibodies as previously described (see section 2.2) for immunofluorescence imaging. Timelapse footage was analysed using Stardist and Trackmate plugins for ImageJ as described in section 2.3.4. The data output from Trackmate was analysed in two main ways: looking at "bulk" migration, i.e. taking the data from all cells that were recorded; and looking at individual cell migration, selected using immunofluorescence images to identify CA status.

5.6.3. siRNA Knockdown or Aurora A or HSP90B1 Reduces Mean Straight Line Speed of the Fastest Cells

The first analysis of tracked cells looked at the mean straight line speed, taking data from all cells that were recorded. The mean straight line speed (MSLS) is the net distance travelled by a cell divided by the time it took to travel this distance. Some cell tracks didn't last for the entire timelapse, so normalising by track times allows for a better comparison between cells than if net distance travelled alone was analysed. As mean straight line speed is calculated with the net distance travelled, it puts an emphasis on the overall distance travelled by a cell in a certain direction. For example, a cell that moves around quickly but randomly and finishes near to its start point will have a lower MSLS than another cell that moves more slowly but in a persistent direction. Data for MSLS from hundreds of individual cells in each condition is shown in Figure 5-6.

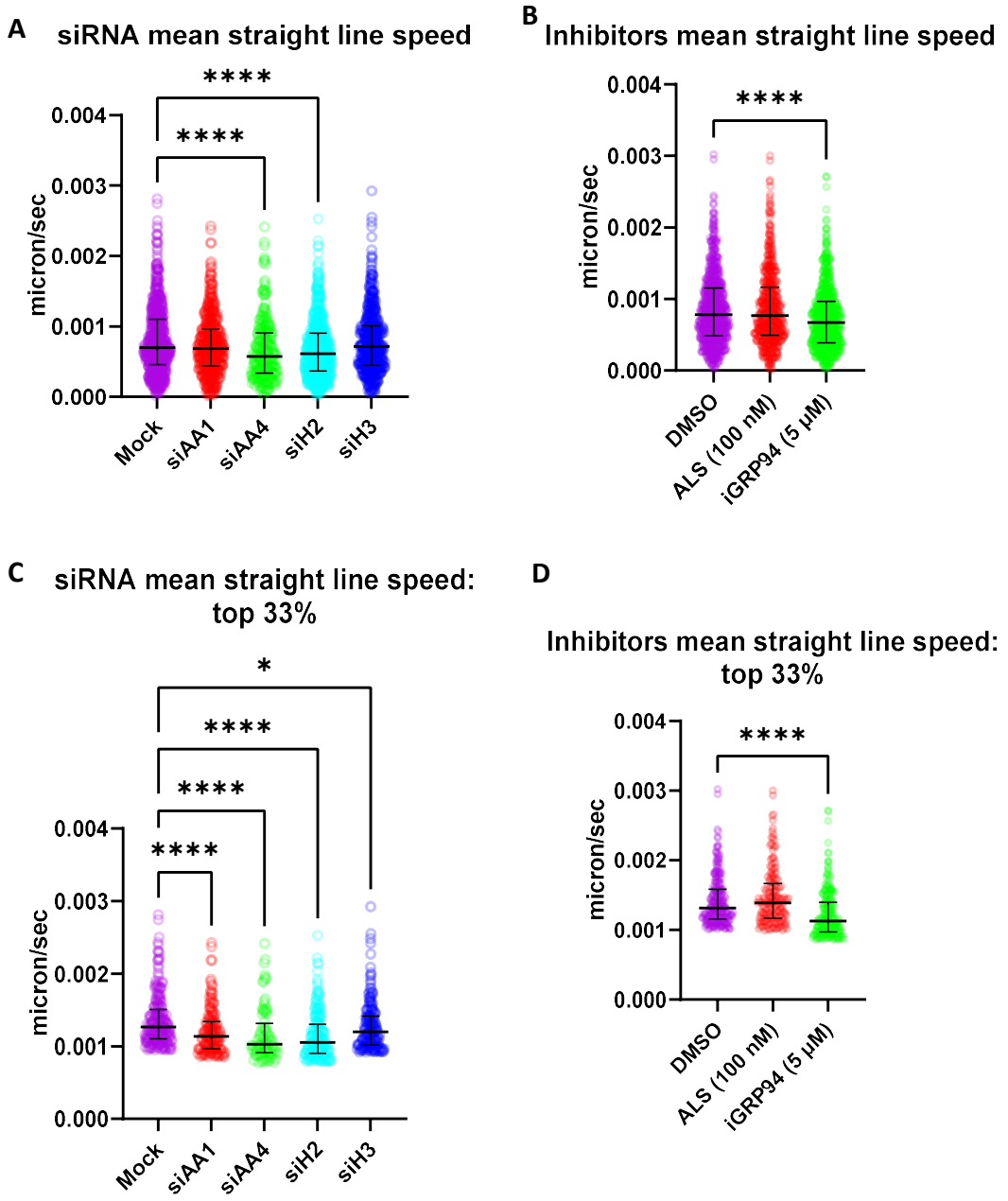

Figure 5-6. Mean straight line speed of FUCCI2a-OMM2.3 cells.
Mean straight line speed (MSLS) of OMM2.3-H2B-FUCCI2a cells treated with siRNAs (A) or inhibitors (B) targeting Aurora A or HSP90B1. ALS = Alisertib, an Aurora A inhibitor. iGRP94 = GRP94 inhibitor-1, an HSP90B1 inhibitor. The number of cells identified and analysed for each condition were as follows: Mock n = 683, siAA-1 n = 472, siAA-4 n = 255, siH-2 n = 603, siH-3 n = 532, DMSO n = 778, ALS n = 535, iGRP94 n = 682. DMSO = vehicle control. MSLS of the fastest 33% OMM2.3-H2B-FUCCI2a cells, as determined by MSLS, treated with siRNAs (C) or inhibitors (D) targeting Aurora A or HSP90B1. Error bars show median and interquartile range. Median speeds were compared using the Kruskal-Wallis test, with Dunn's multiple comparisons test being used as a post hoc test. * = $p<0.05$, **** = $p<0.0001$.

When looking at all the cells, siAuroraA-4, siHSP90B1-2 and iGRP94 caused a subtle but highly significant reduction in MSLS compared to the relevant control (Figure 5-6, panels A and B). Looking at the spread of data, the differences between treatments appeared to be in

the cells with the fastest MSLS. The data were filtered to include the fastest (as determined by MSLS) 33% cells, this percentage was selected as previous work showed that 33% OMM2.3 cells had CA (Figure 3-3, panel D). When looking at the fastest 33% cells by MSLS, all siRNA treatments caused a subtle but significant reduction in MSLS, with siAuroraA-1, siAuroraA-4 and siHSP90B1-2 being highly significant (Figure 5-6, panel C). With the inhibitor treated cells and filtering for the fastest 33% cells, it was still only the iGRP94 treated cells that were significantly slower (Figure 5-6, panel D).

The rationale for filtering for the fastest 33% of cells was that, in the mock condition at least, 33% cells could be expected to have CA. It was hypothesised that CA would affect migration in a cell-autonomous manner such that cells with CA had a faster MSLS. After filtering MSLS data for the fastest 33% cells, all four siRNA treatments became statistically significantly slower than the mock condition. This could point to a cell-autonomous effect of CA on migration.

5.6.4. Migration is Affected More by siRNA Knockdown of Aurora A than by Individual Centrosome Amplification Status of Cells

The previous section looked at the migration of all cells in the timelapse. In this section, individual cells were selected using the immunofluorescence images to select pairs of cells with and without CA. Pairs of cells had a similar distance from the wound edge, as it could be expected that cells near the wound edge will have migrated more persistently than cells far away from the wound edge. Mock and siAuroraA-4 cells were selected for this analysis, as they had the biggest difference in MSLS (Figure 5-6, panels A and C).

After selecting the cells using the immunofluorescence images, tracking data was collated for each cell individually. The results from this analysis can be seen in Figure 5-7. Tracks of individual cells (Figure 5-7, panels A-D) show their migration for the entire timelapse. This makes comparison between cells clearer as each track represents migration over the same timeframe. Graphs in Figure 5-7, panels E and F represent data that was clipped after the first mitosis of each cell going backwards through the timelapse. This was to ensure that cells had the same CA status as seen in the immunofluorescence images.

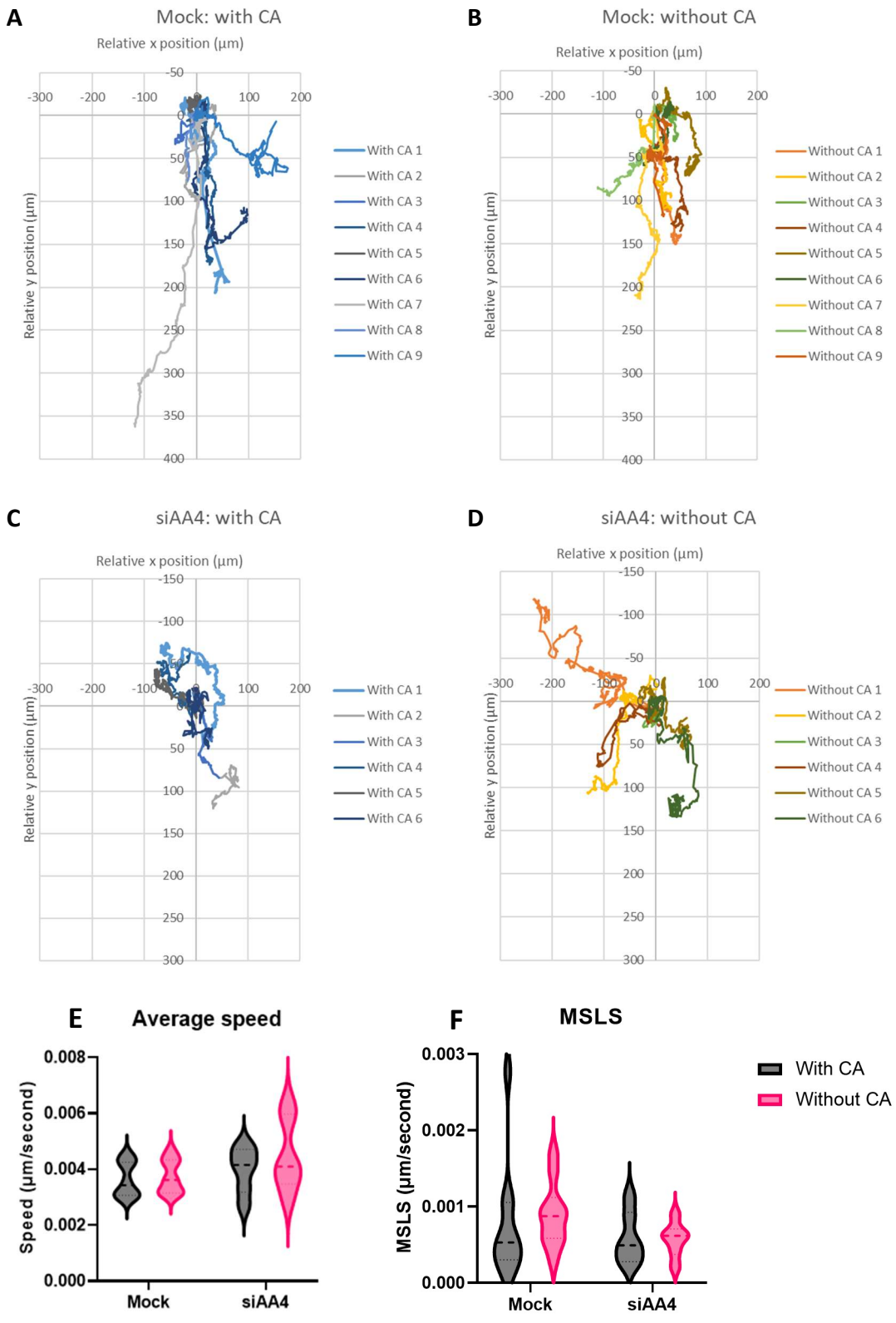

Figure 5-7. Migration of OMM2.3 cells with and without centrosome amplification.
Track of individual mock treated cells with (A) and without (B) CA. Tracks of individual siAuroraA-4 (siAA-4) treated cells with (C) and without (D) CA. Tracks of individual cells represent data from the whole timelapse. Average speed (E) and MSLS (F) of mock and siAA-4 treated cells with and without CA. Graphs in panels E and F use cell tracking data up until the first mitosis going backwards through the timelaspe. Dashed line = median, dotted lines = quartiles.

Looking at the tracks of individual cells (Figure 5-7, A-D), most cell migration is generally in the direction of the wound which was on the bottom edge of the field of view. siAuroraA-4 without CA cell 1 is an exception, it migrated in the opposite direction (Figure 5-7, panel D). Within treatments, there isn't an obvious difference between the migration of cells with or without CA. Comparing between treatments, siAuroraA-4 treated cells seem to have travelled a shorter distance. This translates to a slower MSLS, which mirrors what was seen looking at bulk migration (Figure 5-6, panels A and C).

The CA status of each cell is known at the end of the timelapse due to the immunofluorescence image. As the cells were tracked back through the timelapse, they often went through at least one mitosis. Once the cell has gone through a mitosis, it is not possible to know the CA status with certainty. For example, a cell that had normal centrosome number could be a daughter of a cell with CA that segregated the centrosomes unevenly during mitosis, such that one daughter received one centrosome and the other daughter received more than one centrosome. For this reason, analysis was also performed on the tracks of cells up until their first mitosis, going backwards through the timelapse (Figure 5-7, panels E and F). Both average speed and MSLS have been plotted.

Looking at average speed, the violin plots within a treatment group look similar, regardless of CA status. Comparing treatment groups, there was a wider range of average speeds in the siAuroraA-4 treated cells compared to the mock cells. 2 way ANOVA analysis reveals that treatment was the only significant source of variation in the data ($F = 6.77$, $Dfn = 1$, $DFd = 14$, $p = 0.021$). Cells treated with siAuroraA-4 had a significantly faster average speed than mock cells. Previous analysis showed that siAuroraA-4 treated cells had a slower MSLS than mock cells (Figure 5-6, panels A and C). Taking these two results together, it could be inferred that the siAuroraA-4 treated cells are moving around their environment at a faster speed but with less persistence than the mock cells. 2 way ANOVA analysis of the MSLS of cells up until their first mitosis revealed that there was no significant source of variation between any of the conditions (Figure 5-7, panel F).

5.7. Chapter Discussion

In the previous chapter, siRNA knockdown of either Aurora A or HSP90B1 induced a reduction of the level of CA seen in OMM2.3 cells. In this chapter, we sought to examine the functional effects that this CA reversal had on OMM2.3 cells. This work is important to test the rationale that reversal of CA will reverse the CA related oncogenic phenotypes, to see

whether targeting CA reversal could be a promising new therapeutic target for hard to treat cancers such at metastatic uveal melanoma. A new assay was developed which we call "FUCCI-CLIF", which has the capacity to provide information about cell cycle, migration and CA status, in single cells.

Before moving onto functional studies, endogenous levels of Aurora A and HSP90B1 protein were measured in Mel270, OMM2.3 and OMM2.5 cells. This confirmed that the protein expression showed the same pattern of expression as seen by RNA-Seq analysis, which cannot necessarily be assumed (Y. Guo et al., 2008; Schwanhüusser et al., 2011). We also wanted to check to see if there was any effect of Aurora A knockdown on HSP90B1 protein levels and vice versa. This might point to some regulatory interplay between the two, perhaps providing an explanation as to why HSP90B1 knockdown induced a reduction in CA in OMM2.3 cells. HSP90AB1, a relative of HSP90B1, and HSPA8, another heat shock protein, were identified as high confidence interactors of Aurora A through a proximity interactome screen (Arslanhan et al., 2021). Initially, it appeared that Aurora A protein levels were not affected by HSP90B1 knockdown and vice versa (Figure 5-3, panels A, D and E). A further experiment was set up with altered seeding densities, additional control samples were added for comparison as well as including extra samples for RNA extraction, to enable parallel western blot and qPCR assays. The results from this alternative experimental setup showed mRNA recovery and a slight protein recovery of Aurora A 5 days after siAuroraA-4 treatment. One thing that wasn't tested was levels of Aurora A phosphorylation, which indicates increased Aurora A kinase activity (C. C. Lin et al., 2018; Ohashi et al., 2006).

The effects of siRNA knockdown of Aurora A or HSP90B1 on the cell cycle were checked by flow cytometry. In Chapter 4, both interphase and mitotic cells were included in the siRNA screen analysis, using cyclin B1 staining to adjust for G2 cells which should contain two centrosomes. The proportion of cells in G2 as determined by cyclin B1 staining and by flow cytometry showed the same trend: mock and siHSP90B1 treated OMM2.3 cells had similar G2 proportions, whilst the levels of cells in G2 was elevated in siAuroraA treated OMM2.3 cells. This is not unexpected, as HSP90B1 doesn't have any reported role for cell cycle progression, whereas loss of proper Aurora A function is implicated in a range of mitotic defects (Asteriti et al., 2014; Carvalhal et al., 2015; Glover et al., 1995; Hoter et al., 2018; Macůrek et al., 2008; Marumoto et al., 2003). Cells treated with siAuroraA also had an increased 4n+ and 8n population, pointing towards instances of cytokinesis failure in these cells. This result may seem paradoxical, as failed cytokinesis is a proposed route to CA (Meraldi et al., 2002; Sabat-Pośpiech et al., 2019). This result could be explained if the 4n+

and 8n populations don't survive after an extended period of time. Indeed, inhibition of Aurora A lead to mitotic defects and subsequent failure to proliferate in cells with high levels of CA, whereas inhibition of Aurora A in cells with normal centrosome number continued to proliferate (Navarro-Serer et al., 2019).

CA has been causally linked to increased invasiveness, chromosomal instability and increased tumourigenic potential of cells (Arnandis et al., 2018; Basto et al., 2008; Ganem et al., 2009; Godinho et al., 2014; Levine et al., 2017; Prakash et al., 2022). The final section of work in this thesis begins to explore the idea that reversal of CA may reduce these oncogenic phenotypes, and would therefore be a novel therapeutic strategy for aggressive cancers with CA. The work presented focusses on the effects of CA reversal on cell migration.

Previous studies into the invasive properties of cells with CA have used 3D culture and *in ovo* models (Arnandis et al., 2018; Godinho et al., 2014; Prakash et al., 2022). Here, we develop and use a new assay named FUCCI-CLIF which allows for the tracking of individual cell migration whilst also providing information on cell cycle progression and CA status. The ability to extract data for individual cells allows for identification of more subtle changes in cell behaviour that may be masked when looking at entire cell populations. Using two different imaging techniques on the same field of view is also used in **C**orrelative **L**ight and **E**lectron **M**icroscopy (CLEM) (Begemann & Galic, 2016). Both the established technique of CLEM and the FUCCI-CLIF setup presented here combine two different imaging modalities, making it possible to gain a deeper understanding of the imaged structures. In this work, migration was compared in OMM2.3 cells treated with siRNAs or inhibitors targeting Aurora A or HSP90B1. Migration was compared looking at data from all cells identified, and looking at data for individual pairs of cells with and without CA.

When looking at migration, some siRNA treatments significantly reduced mean straight line speed (MSLS). The data were heavily skewed towards slower cells, so the data were filtered to include only the fastest 33% by MSLS. This filtering made the differences between mock and siRNA treated cells more obvious, with all siRNA treatments being statistically slower than the mock treated cells. It was hypothesised that CA was having a cell-autonomous effect on migration (Godinho et al., 2014). 33% of cells could be expected to have CA in the mock treated cells and may be migrating faster. A reduction in CA in siRNA treated cells would mean that there are fewer cells with CA in that top 33%, leading to a reduction in MSLS.

However, when looking at individual cells with and without CA, there was not a clear difference in migration. Instead, the difference in migration could be seen between treatments. Cells treated with siAA-4 seemed to be migrating faster (Figure 5-7, panel E) but with less persistence overall (Figure 5-7, panels C and D). The results from this analysis pointed towards non-cell-autonomous effects of CA on migration.

The original rationale behind looking at the fastest 33% cells by MSLS was that these cells may be expected to have CA. The reduction in MSLS in siRNA treated cells in this dataset could still be explained by a non-cell-autonomous effect of CA on migration (Arnandis et al., 2018). Rather than treating the 33% as a way to look at cells with CA, instead it was a way to look at the fastest cells where a difference in migration is more obvious, due to the heavy skew of the original dataset.

The FUCCI-CLIF assay can be used to measure cell migration but provides no insight into the invasive characteristics of cells. Transwell tissue culture inserts coated with a substance to mimic the extra-cellular matrix, such as Matrigel, are a well-established invasion assay (Godinho et al., 2014; Mittal et al., 2022; Pijuan et al., 2019). Some preliminary experiments were started to look at invasion of OMM2.3 and Mel270 cells, however no invasion was observed (Appendix F). Further optimisation, such as co-culture with fibroblasts or a longer incubation time, is required for the future.

In this chapter, some of the functional effects of siRNA knockdown of Aurora A or HSP90B1 were assessed. The work in previous chapters focussed mainly on RNA expression of these target genes. In this chapter, expression patterns of Aurora A and HSP90B1 were confirmed at the protein level, as well as looking at whether Aurora A knockdown would affect HSP90B1 protein levels and vice versa (Figure 5-1, Figure 5-3 and Figure 5-4). Such a relationship could indicate that the knockdown induced CA reversal seen after Aurora A or HSP90B1 siRNA treatment is affected through the same molecular pathway. Results on a potential relationship between HSP90B1 and Aurora A expression levels were inconclusive, and more work is required to test this potential link.

The effects of siAuroraA or siHSP090B1 on cell cycle populations was examined using flow cytometry (Figure 5-2). These results followed the same pattern as seen by cyclin B1 positive immunofluorescence staining from work in Chapter 4, giving confidence to the CA score calculations from that chapter.

Lastly, cell migration was investigated in a newly designed assay which we name “FUCCI-CLIF” (Figure 5-5). The analysis of results from this assay showed significantly reduced, likely

cell non-autonomous effects, of Aurora-A or HSP90B1 depletion on cell migration (Figure 5-6 and Figure 5-7).

Overall, this suggests that reversing CA by depleting or inhibiting proteins required for CA in a specific cancer setting, can reduce the oncogenic properties of aggressive cancer cells, and is therefore a new potential therapeutic approach.

Chapter 6.

General Discussion

6.1. Recap of Study Aims and Findings

How does centrosome amplification (CA) develop naturally in a patient setting? Is it possible to reverse the CA status of cells? If so, would that have any therapeutic benefit, reversing the CA-driven oncogenic phenotypes? These questions shaped the aims of this thesis, a recap of how these aims were addressed and the accompanying findings follows.

Mel270, OMM2.3 and OMM2.5 were developed as a model to study CA that had developed during the progression of uveal melanoma (UM). This work helped to show, for the first time, that CA is present in UM in a manner that is associated with poor prognosis (Sabat-Pośpiech et al., 2022). The degree of CA seen in OMM2.3 and OMM2.5 cells was comparable with that of other cell lines sometimes used to study CA, such as BT549 (Kawamura et al., 2013; Morris et al., 2017). Mel270, OMM2.3 and OMM2.5 cells were all derived from the same patient so are genetically similar despite their differing CA statuses. These cell lines can be used as a new tool to study CA without having to artificially induce CA, as is often seen in other studies examining this phenomenon (Godinho et al., 2014; Levine et al., 2017; Saatci et al., 2022). Previous works to understand CA often induce it using one of or a combination of the following: loss of p53, overexpression of PLK4, DNA damaging treatments or inducing cytokinesis failure (Coelho et al., 2015; Löffler et al., 2013; Meraldi et al., 2002; Navarro-Serer et al., 2019; Prosser et al., 2009). RNA-Seq analysis and sequencing of the p53 gene showed that CA in these cells was not driven by p53 mutation or dysregulation, though *p21* which acts downstream of p53 was highly downregulated, and *MDM2* which has inhibitory effects on p53 was upregulated (Hou et al., 2019; L. Wang et al., 2021). This is in line with previous observations that sometimes a p53 null setting is required to maintain experimentally induced CA (Adon et al., 2010; Lopes et al., 2018; Marin Navarro et al., 2020; Serçin et al., 2016). However, p53 loss or mutation is not always observed in cells with CA, it may be that in those cases p53 signalling has been modulated in some other way as seen in OMM2.3 and OMM2.5 cells here (Marteil et al., 2018). *PLK4* was overexpressed in OMM2.3 cells, but not OMM2.5 cells, indicating multiple molecular routes to CA can be experienced in a patient setting. The use of cells such as these where CA has developed naturally in a patient setting may help to discover new proteins involved in CA that are more clinically relevant.

Following RNA-Seq and analysis, and then development and execution of the siRNA screen, *Aurora A* and *HSP90B1* were identified as genes whose knockdown induced a reduction in

CA in OMM2.3 cells (see section 4.5). Knockdown of *p21* in Mel270 wasn't sufficient to increase CA scores when the siRNA pools were deconvolved to test siRNAs individually (Figure 4-8). We hypothesise that p21 under expression, seen in OMM2.3 cells and mimicked in Mel270 cells with siRNA knockdown of *p21*, sets a permissive state for CA to be maintained. However, expression of CA driver genes are required to establish CA in the first place. This corroborates other research where loss of p53 signalling is required to maintain cells with CA (Fava et al., 2017; Holland et al., 2012; Meraldi et al., 2002). The screen itself was designed very carefully. Though manual analysis is still the gold standard for histopathological analysis (Aeffner et al., 2017), it was not practical for the large volume of images generated in the screen. Thus we sought to automate analysis where possible, an approach that has been taken into other studies concerning centrosome biology (Balestra et al., 2013; Dittrich et al., 2019; Marteil et al., 2018). During the development of an image analysis method, semi-automated image analysis was rigorously tested against a set of training images. The CA scores generated by "absolute counts" (i.e. measured manually) and the CA scores generated by the "best analysis" (i.e. the semi-automated method selected for the siRNA screen) were not significantly different as determined by two tailed paired t test (Figure 4-5, panel C). Though the screen was developed carefully, it may have potential for improvement, and it also has its limitations. Other centrosomal markers, such as CEP135, could be considered (M. Wang, Knudsen, et al., 2019). Pericentrin is a protein in the pericentriolar material (PCM) and was used here as a centrosomal marker, but it is possible (especially after knockdown of key centrosomal components) for cells to form acentrosomal PCM aggregates or for PCM to undergo fragmentation (Dzhindzhev et al., 2010; Kalkan et al., 2022; G. Wang et al., 2014). Both of these would result in additional pericentrin foci that don't reflect an increase in centrosome number. A limitation of the screen is that it doesn't provide any information as to how CA score was reduced. Reduced CA score could be through a "true reversal", where cells with CA lose additional centrosomes, it could be that cells with CA have reduced proliferative ability do get outcompeted by cells with normal centrosome number, or it could be that cells with CA die, leaving behind a higher proportion of cells with a normal CA number (Figure 6-1). As it stands, we don't know which of these three scenarios were the case for Aurora A or HSP90B1 knockdown induced CA reversal. Further work to elucidate the mechanism for Aurora A or HSP90B1 knockdown induced CA reversal would help us to better understand the role these genes play in CA.

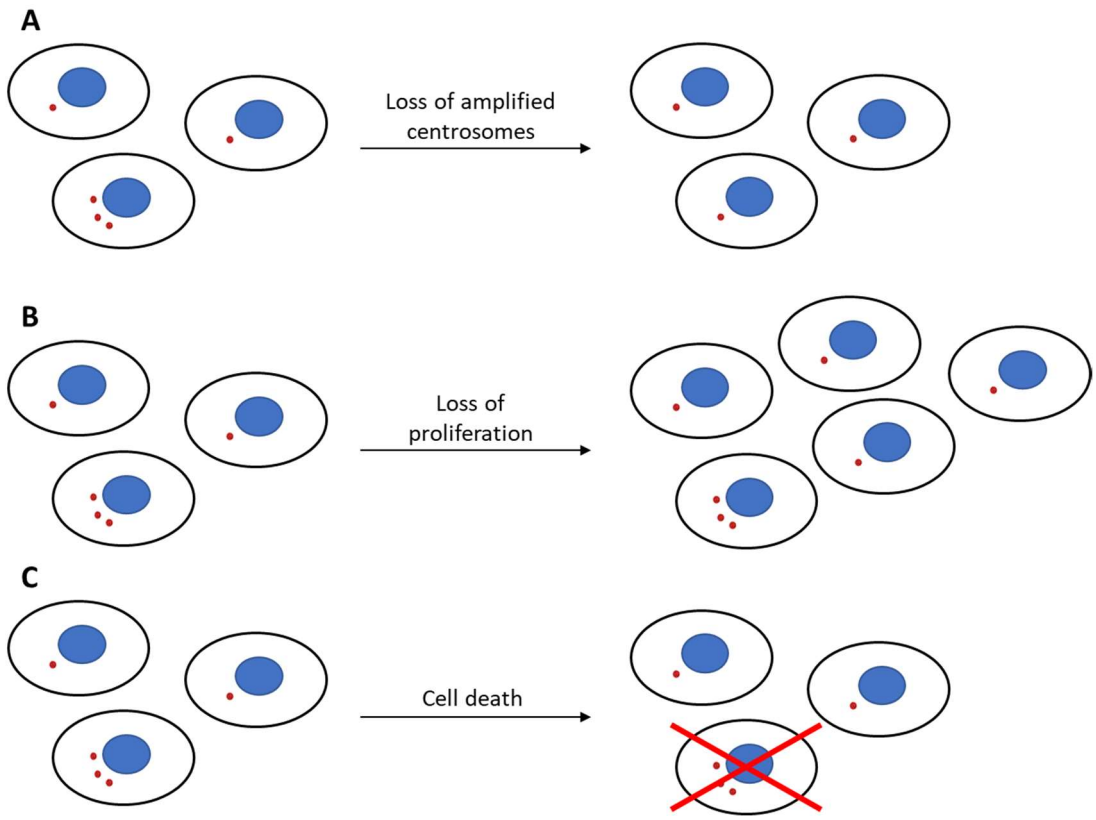

Figure 6-1. Possible routes to reversal of centrosome amplification.
Three possible routes to reversal of centrosome amplification that could have occurred during the siRNA screen are illustrated above. Reversal could occur through cells with centrosome amplification losing their additional centrosomes, returning to a normal centrosome state (A). Reversal could occur through a centrosome amplification associated loss of proliferative ability, resulting a cell population that has a reduced level of centrosome amplification as cells with normal centrosome number continue to proliferate (B). Reversal could occur though death of cells with centrosome amplification, so that only cells with normal centrosome number remain (C).

The work up until this point addressed the first main aim of reversing CA, and ultimately identified Aurora A and HSP90B1 as genes whose knockdown reduced CA score in OMM2.3 cells. The second main aim was to see whether CA reversal also reversed the oncogenic phenotypes of cells with CA. This aim was partially addressed, exploring a possible regulatory interaction between Aurora A and HSP90B1, measuring cell cycle effects of Aurora A or HSP90B1 knockdown and quantifying cell migration parameters.

Seeing as knockdown of either Aurora A or HSP90B1 both induced a reduction in CA, we wondered whether knockdown of one of these targets effected the expression of the other. HSP90AB1, a relative of HSP90B1, and HSPA8, another heat shock protein, were both identified as high confidence interactors of Aurora A (Arslanhan et al., 2021). To test a possible relationship between Aurora A and HSP90B1 we used reciprocal western blots and qPCR assays. No reduction of Aurora A was observed after HSP90B1 knockdown or vice

versa. Therefore, we see no evidence that Aurora A or HSP90B1 act on each other in a regulatory manner.

The effects of Aurora A or HSP90B1 knockdown on the cell cycle was also investigated using propidium iodide staining and flow cytometry. The flow cytometry results showed a similar pattern of cells in G2 as seen by cyclin B1 positive staining in the siRNA screen and related follow up experiments. In both cases, siHSP90B1 treated cells had a similar cell cycle profile to control conditions but siAuroraA treatment increased the G2 population. This similar pattern was reassuring, as cyclin B1 positive staining had been used during the siRNA screen to adjust for the extra centrosome that is present in G2 cells, allowing for comparison between siRNA treatments that may or may not have had an effect on the cell cycle. Flow cytometry analysis was also able to show that siAuroraA treatment increased 4n+ and 8n populations. This may seem paradoxical, as 8n cells formed though a failed mitosis would increase CA, but we hypothesise that these cells may not survive. This is supported by the fact that cells with CA were shown to be vulnerable to Aurora A inhibition, which disturbed mitosis and resulted in cells that failed to proliferate (Navarro-Serer et al., 2019).

FUCCI-CLIF (**F**luorescent **U**biquitination based **C**ell **C**ycle **I**ndicator-**C**orrelative **L**ive imaging and **I**mmuno**f**luorescence) was a new assay developed and used to study cell migration from the single cell level to population level, whilst also providing data on cell cycle and CA status. The amount of data generated by these experiments is huge, but analysis presented in this thesis focussed on the effects of Aurora A or HSP90B1 knockdown on “mean straight line speed” (MSLS), which is a measure that combines Euclidean migration and duration of migration. Looking at the migration of entire populations, which we named “bulk” migration, initially revealed a slight reduction in MSLS upon siRNA treatment. This reduction was more significant when looking at the fastest third of migrating cells. Next, pairs of cells with and without CA were analysed after treatment with an siRNA targeting Aurora A, or under control conditions. There was no perceivable difference between CA statuses, but the tracks of cells treated with siAuroraA-4 appeared to cover less distance overall (shorter Euclidean migration). Interestingly, when looking at migration data of these cells only up until the first mitosis going backwards through the timelaspe (when true CA status could be known), siAuroraA-4 treatment appeared to increase average speed, but not MSLS, regardless of CA status. This implies that, for siAuroraA-4 treated cells at least, cells are moving around their environment faster but with less persistence than the control conditions. The lack of a difference between pairs of cells with and without CA indicates that the differences in MSLS seen when analysing bulk migration may be down to non-cell-autonomous effects on CA. In

the future it would be useful to see if these CA reversal induced changes in migration translate to changes in invasion, which may be measured using coated Transwell assays, or observation of cellular structures grown in a 3D matrix (Godinho et al., 2014; Prakash et al., 2022).

6.2. The Role of Aurora A in Centrosome Amplification

Aurora A is a kinase whose overexpression has been well documented in driving cancer progression, as well as being linked to cells with CA (Du et al., 2021; Lukasiewicz & Lingle, 2009; Ogden et al., 2017). Overexpression of Aurora A has been shown to induce CA via cytokinesis failure and tetraploidy (Meraldi et al., 2002). Several other studies have also demonstrated that overexpression of Aurora A can induce CA in an experimental setting (Lentini et al., 2007; X. Wang et al., 2006). The fact that the siRNA screen presented in this thesis was also able to identify Aurora A as a gene whose overexpression was linked to high CA in OMM2.3 cells gives credence to screen setup and analysis methods. Cells with CA are more sensitive to Aurora A inhibition (Navarro-Serer et al., 2019), and Aurora A activity has been linked to centrosomal localisation of TACC3 (Mori et al., 2007), which works in conjunction with KIFC1 to achieve centrosome clustering (Saatci et al., 2022). With this in mind, Aurora A activity may also be required for cell survival once CA has been established.

6.3. The Role of HSP90B1 in Centrosome Amplification

HSP90B1 is an endoplasmic reticulum heat shock protein with no prior links to centrosomes, so the identification of HSP90B1 in a CA siRNA screen provides a novel link between HSP90B1 and centrosomes (Hoter et al., 2018). HSP90, the cytosolic relative of HSP90B1, has been linked to centrosome function through stabilisation of PLK1 (De Cárcer et al., 2001). HSP90AB1, one of the cytosolic isoforms, was identified as a high confidence interactor of Aurora A but the function of this interaction is unknown (Arslanhan et al., 2021). Results from western blots and qPCR assays ultimately indicated that knockdown of HSP90B1 had no effect on Aurora A at the RNA or protein level, and vice versa. HSP90B1 is unusual in that is has very few client proteins, which include several immune related membrane bound and secreted proteins (Hoter et al., 2018; Marzec et al., 2012). As HSP90B1 is also able to sequester Ca^{2+}, higher levels of HSP90B1 could increase the ER-Ca^{2+} pool (Biswas et al., 2007). It was recently discovered that Ca^{2+} localisation from the ER to centrosomes during mitosis is essential for cell division, playing a role in spindle orientation (Helassa et al., 2019;

Lagos-Cabré et al., 2020). We hypothesise that cells with CA require a larger ER- Ca^{2+} pool, either to properly supply the additional centrosomes with Ca^{2+} or that there is a greater requirement for this Ca^{2+} signal in the challenging environment of CA to maintain mitotic fidelity. A similar dependence on HSP90B1 was identified specifically during the first mitosis of the developing mouse zygote, where the cell has two nuclear structures (the maternal and paternal pro-nuclei) (Audouard et al., 2011). It would be interesting to examine centrosomal Ca^{2+} localisation in OMM2.3 cells, or other cells with CA, after siRNA knockdown or chemical inhibition of HSP90B1.

Due to the nature of the way the siRNA screen was carried out, it can't be said for certain whether HSP90B1 overexpression has a causative role in CA, or whether cells with CA have a dependency on high HSP90B1 levels. One way to approach this would be to see if HSP90B1 overexpression in a CA permissive setting (for example, knocking out p53) is sufficient to induce CA in a cell line such as Mel270.

6.4. FUCCI-CLIF: A Novel Assay to Study Cell Behaviour

FUCCI-CLIF (**F**luorescent **U**biquitination based **C**ell **C**ycle **I**ndicator - **C**orrelative **L**ive imaging and **I**mmuno**f**luorescence) is the name we give to the novel assay that was presented and used in this thesis. It combines the use of a FUCCI biosensor (Mort et al., 2014; Sakaue-Sawano et al., 2017) with the well established scratch assay, sometimes called a wound healing assay (Pijuan et al., 2019), and immunofluorescent imaging. The manner in which these techniques are combined enables live measurement of the cell cycle and cell migration, and also a feature of choice that can be detected by immunofluorescent imaging (centrosomes/ CA status in this case), as well as potential relationships between these cell behaviours and features (Figure 6-2). The benefit of using a FUCCI biosensor is that cell cycle data can be collected from live cells over an extended period of time, as opposed to the cell cycle "snapshot" provided by flow cytometry. Another strength of the FUCCI-CLIF approach is that analysis can be performed at the single cell level, perhaps using the immunofluorescence images to select cells of interest. We believe this will allow subsequent analysis to better reflect the heterogeneity of cancers (Hanahan, 2022). As well as providing single cell resolution, FUCCI-CLIF can also return data points from hundreds of cells. A vast amount and variety of data is generated by the FUCCI-CLIF assay, which means that one experiment could be used to ask a wide variety of questions. For more information on the FUCCI-CLIF method, see thesis sections 2.1.4, 2.3.4 and 5.6.

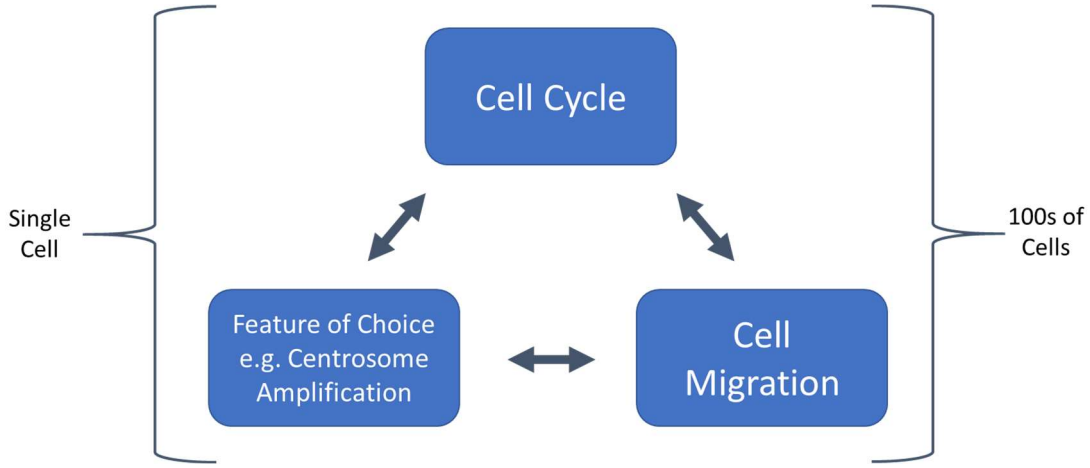

Figure 6-2. Multiparametric data available from FUCCI-CLIF analysis
The FUCCI-CLIF assay allows for detailed analysis of cell cycle progression, cell migration and a feature of choice shown by immunofluorescent imaging. In this thesis that feature was labelling centrosomes, which allowed determination of centrosome amplification status. Relationships between these three features can be examined, as shown by the double ended arrows. Data for all of these features can be collected at the single cell level for hundreds of cells in one experimental setup.

6.5. Therapeutic Potential of Targeting Aurora A or HSP90B1

The expression of Aurora A and HSP90B1 do not seem to be linked (Figure 5-4). It could be inferred from this that Aurora A and HSP90B1 are involved in different pathways in relation to CA. However, knockdown of either gene was sufficient to induce reduction of CA in OMM2.3 cells. This is promising when considering the potential therapeutic value of targeting Aurora A or HSP90B1. Different mechanisms have been shown to contribute to CA e.g. cytokinesis failure and tetraploidisation, centriole over elongation, centriole overduplication (Denu et al., 2018; Marteil et al., 2018; Meraldi et al., 2002). This means that there are probably multiple different molecular pathways that can lead to CA in a patient setting. Given this, it is unlikely that we can find a "silver bullet" that can prevent all cases of CA from occurring. However the data here show that, regardless of how the CA occurred, OMM2.3 cells were vulnerable to knockdown of either Aurora A or HSP90B1. Therefore, in a wider setting, different cancers that have developed CA in different ways might still share a common vulnerability to Aurora A or HSP90B1 targeting therapies. It would be interesting to see if Aurora A or HSP90B1 knockdown induced CA reversal can also be observed in other cell lines with CA, such as OMM2.5 cells or NCI-60 cell lines that have been identified as having CA (Marteil et al., 2018). It would also be important to check whether these effects are CA specific and/ or cancer specific, for example looking at Aurora A or HSP90B1 knockdown in NCI-60 cells without CA and in non-transformed cell lines such as RPE-1 or MCF10A cells.

6.6. Targeting Centrosome Amplification in Uveal Melanoma

What could the therapeutic benefit of targeting CA in UM be? Treatment of primary uveal melanoma is effective and local recurrence is rare (Kowal et al., 2019); survival outcomes of patients who undergo enucleation versus patients who undergo globe preserving therapy are similar (Aronow et al., 2018; van Beek et al., 2018), and the main cause of death is from metastatic disease (Damato et al., 2014; Kujala et al., 2003). Therefore, to improve patient outcome, treatments must be developed to tackle metastatic disease. Until recently, treatment of metastatic UM has offered limited survival benefits (Rantala et al., 2019), and mortality rates remain high even with new therapies such as tebentafusp (Nathan et al., 2021). One issue is that UM is suspected to metastasise early on during tumour development before diagnosis of the primary tumour (Eskelin et al., 2000). Additionally, it can take many years for metastatic disease to present, with micrometastases lying dormant in the interim (Kujala et al., 2003). The role of CA in UM is unknown: does it drive primary disease, the formation of micrometastases, does it play a role in reversing the dormancy of micrometastases, or growth of metastases? The patient matched cell lines used in this thesis (Mel270, OMM2.3 and OMM2.5 cells) formed a model to study CA that had occurred during the progression of uveal melanoma. Mel270 cells from the primary tumour had low levels of CA, whereas OMM2.3 and OMM2.5 from liver metastases had high levels of CA. However, CA has also been found in primary UM tumours, where it was associated with high metastatic risk monosomy-3 tumours (Sabat-Pośpiech et al., 2022). It has been reported that there might be a decrease in the level of CA observed in cancer cell lines when compared to the level of CA found in primary material (Mittal et al., 2021). Therefore it is plausible that the negligible levels of CA seen in Mel270 cells may have translated to a moderate level of CA in the primary tumour it was derived from, with the level of CA in the metastases that were used to generate OMM2.3 and OMM2.5 cells being higher still. As CA increases invasiveness of cells, we hypothesise that primary UM cells with CA may be more prone to metastasise. The resulting metastases that these cells seed would be enriched for cells with CA, leaving the metastases vulnerable to treatments that target CA.

6.7. Proposed Model for Centrosome Amplification Reversal Through Aurora A or HSP90B1 Inhibition

Here we propose a model for the role of Aurora A and HSP90B1 with regards to CA, based on results from the work in this thesis and supported by other published works (Figure 6-3). Firstly, an increase in Aurora A expression can induce CA. OMM2.3 cells, which display a high level of CA, overexpress *Aurora A* compared to Mel270 cells, which have negligible CA (Figure 3-3). Additionally, siRNA knockdown of *Aurora A* reduced the level of CA in OMM2.3 cells (Figure 4-8). Numerous other studies have also observed CA in relation to Aurora A overexpression (J. J. Li et al., 2004; Meraldi et al., 2002; X. Wang et al., 2006). Secondly, a decrease in p53 pathway signalling creates a permissive setting for cells to maintain CA and continue proliferating. OMM2.3 cells overexpress *MDM2* compared to Mel270 cells (Table 3-2), which would have the effect of dampening the p53 response (Hou et al., 2019). Additionally, OMM2.3 cells under-express *p21*, a downstream effector of p53 that is involved in cell cycle arrest (Engeland, 2022; L. Wang et al., 2021). Knockdown of *p21* in Mel270 cells wasn't sufficient to induce CA, strengthening the argument that abrogation of the p53 pathway per se is not sufficient to cause CA, and that other driver genes such as Aurora A are required. Next, we propose that Aurora A and HSP90B1 activity is important in cells with CA, as knockdown of either target leads to a reduction in CA levels. We hypothesise that cells with CA have a dependency on both Aurora A and HSP90B1 and that knockdown of either results in reduced CA, perhaps through cell death or loss of proliferative ability. For Aurora A, this dependency might be related to centrosome clustering, as Aurora A activity can localise TACC3 to the centrosome, where it works in conjunction with KIFC1 to cluster centrosomes (Burgess et al., 2018; Saatci et al., 2022). Indeed, cells with CA have been shown to have an increased sensitivity to Aurora A inhibition (Navarro-Serer et al., 2019). For HSP90B1, this dependency might be related to ER-Ca^{2+} stores, which is the source of centrosomal Ca^{2+} required for mitosis (Helassa et al., 2019; Lagos-Cabré et al., 2020). Further work is required to confirm the nature by which Aurora A or HSP90B1 knockdown leads to reduced CA. Aurora A or HSP90B1 knockdown induced CA reversal has a subtle but significant effect on cell migration, reducing the mean straight line speed of the fastest cells (Figure 5-6).

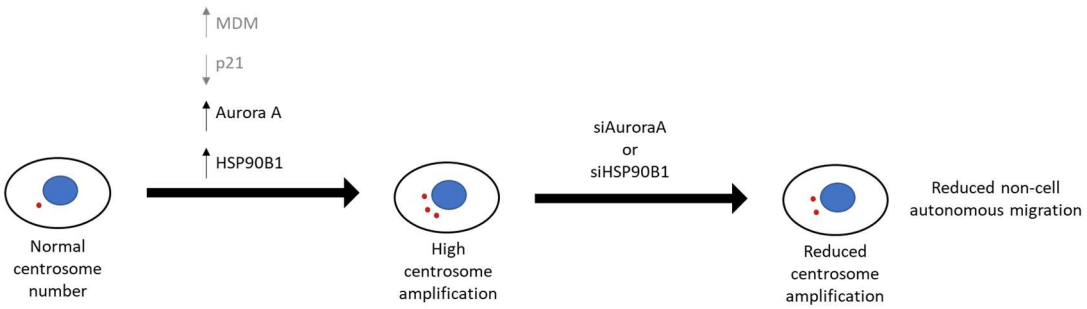

Figure 6-3. Proposed model for development and reversal of centrosome amplification.
A cell with normal centrosome number will develop centrosome amplification after a permissive setting is created by down regulation of p53 pathway components, and by upregulation of CA driver and CA maintenance genes such as Aurora A and HSP90B1. Knockdown of these CA driver/maintenance genes leads to reduced or reversed centrosome amplification, which is accompanied by a reduction in non-cell-autonomous migration.

6.8. Concluding Remarks

Centrosome amplification (CA) drives oncogenic phenotypes in aggressive cancers with a poor prognosis, but may also present cancer specific weaknesses that can be targeted for therapeutic gain. One such cancer that may benefit from CA targeted therapy is metastatic uveal melanoma, which has no curative treatment and high mortality rates. Along with collaborators, we reported for the first time the observation of CA in UM with high-metastatic risk. In this thesis, the use of the patient matched cell lines Mel270, OMM2.3 and OMM2.5 was developed as a new model to study CA. As these cell lines exhibit CA that developed naturally as part of disease progression in a patient setting, they may be more clinically relevant than earlier models that rely on artificial induction of CA. Following RNA-Seq analysis of these cell lines, an siRNA screen approach was taken to identify genes involved in the development or maintenance of CA. Knockdown of either Aurora A or HSP90B1 reversed CA in OMM2.3 cells. Aurora A has already been implicated for its role in CA in several other previous works, so the fact that this screen was able to identify Aurora A can be considered as similar to a positive control, providing assurance for the experimental set up and analysis of the siRNA screen. HSP90B1 was a novel discovery from the siRNA screen, as it currently has no reported roles in relation to centrosomes. The identification of novel CA related genes such as HSP90B1 will be important for the development of CA-related therapies as thus far, current approaches have only proven semi-successful. We hypothesised that CA reversal may have an effect on CA driven oncogenic phenotypes such as invasion. We began to test this hypothesis by developing and using a new assay, “FUCCI-CLIF”, to examine the effects of CA status on cell migration from the single cell level to population level. Depletion of Aurora A or HSP90B1 significantly reduced cell migration as

measured by mean straight line speed in a manner that is likely non-cell-autonomous. Therefore, depleting proteins required for CA may offer new therapeutic approaches for aggressive, hard to treat cancers such as metastatic uveal melanoma.

References

Abe, T., Sakaue-Sawano, A., Kiyonari, H., Shioi, G., Inoue, K. I., Horiuchi, T., Nakao, K., Miyawaki, A., Aizawa, S., & Fujimori, T. (2013). Visualization of cell cycle in mouse embryos with Fucci2 reporter directed by Rosa26 promoter. *Development*, *140*(1), 237–246. https://doi.org/10.1242/DEV.084111

Adon, A. M., Zeng, X., Harrison, M. K., Sannem, S., Kiyokawa, H., Kaldis, P., & Saavedra, H. I. (2010). Cdk2 and Cdk4 regulate the centrosome cycle and are critical mediators of centrosome amplification in p53-null cells. *Molecular and Cellular Biology*, *30*(3), 694–710. https://doi.org/10.1128/MCB.00253-09

Aebersold, R., Agar, J. N., Amster, I. J., Baker, M. S., Bertozzi, C. R., Boja, E. S., Costello, C. E., Cravatt, B. F., Fenselau, C., Garcia, B. A., Ge, Y., Gunawardena, J., Hendrickson, R. C., Hergenrother, P. J., Huber, C. G., Ivanov, A. R., Jensen, O. N., Jewett, M. C., Kelleher, N. L., … Zhang, B. (2018). How many human proteoforms are there? *Nature Chemical Biology 2018 14:3*, *14*(3), 206–214. https://doi.org/10.1038/nchembio.2576

Aeffner, F., Wilson, K., Martin, N. T., Black, J. C., Hendriks, C. L. L., Bolon, B., Rudmann, D. G., Gianani, R., Koegler, S. R., Krueger, J., & Young, G. D. (2017). The Gold Standard Paradox in Digital Image Analysis: Manual Versus Automated Scoring as Ground Truth. *Archives of Pathology & Laboratory Medicine*, *141*(9), 1267–1275. https://doi.org/10.5858/ARPA.2016-0386-RA

Altschul, S. F., Madden, T. L., Schäffer, A. A., Zhang, J., Zhang, Z., Miller, W., & Lipman, D. J. (1997). Gapped BLAST and PSI-BLAST: a new generation of protein database search programs. *Nucleic Acids Research*, *25*(17).

Andreassen, P. R., Lohez, O. D., Lacroix, F. B., & Margolis, R. L. (2001). Tetraploid state induces p53-dependent arrest of nontransformed mammalian cells in G1. *Molecular Biology of the Cell*, *12*(5), 1315–1328. https://doi.org/10.1091/mbc.12.5.1315

Aprile, M., Costa, V., Cimmino, A., & Calin, G. A. (2023). Emerging role of oncogenic long noncoding RNA as cancer biomarkers. *International Journal of Cancer*,

152(5), 822–834. https://doi.org/10.1002/IJC.34282

Arnandis, T., Monteiro, P., Adams, S. D., Bridgeman, V. L., Rajeeve, V., Gadaleta, E., Marzec, J., Chelala, C., Malanchi, I., Cutillas, P. R., & Godinho, S. A. (2018). Oxidative Stress in Cells with Extra Centrosomes Drives Non-Cell-Autonomous Invasion. *Developmental Cell*, *47*(4), 409-424.e9. https://doi.org/10.1016/J.DEVCEL.2018.10.026

Aronow, M. E., Topham, A. K., & Singh, A. D. (2018). Uveal Melanoma: 5-Year Update on Incidence, Treatment, and Survival (SEER 1973-2013). *Ocular Oncology and Pathology*, *4*(3), 145–151. https://doi.org/10.1159/000480640

Arquint, C., & Nigg, E. A. (2016). The PLK4-STIL-SAS-6 module at the core of centriole duplication. *Biochemical Society Transactions*, *44*(5), 1253–1263. https://doi.org/10.1042/BST20160116

Arslanhan, M. D., Rauniyar, N., Yates, J. R., & Firat-Karalar, E. N. (2021). Aurora Kinase A proximity map reveals centriolar satellites as regulators of its ciliary function. *EMBO Reports*, *22*(8). https://doi.org/10.15252/EMBR.202051902

Arvey, A., Larsson, E., Sander, C., Leslie, C. S., & Marks, D. S. (2010). Target mRNA abundance dilutes microRNA and siRNA activity. *Molecular Systems Biology*, *6*, 363. https://doi.org/10.1038/MSB.2010.24

Asteriti, I. A., Cesare, E. Di, Mattia, F. De, Hilsenstein, V., Neumann, B., Cundari, E., Lavia, P., & Guarguaglini, G. (2014). The Aurora-A inhibitor MLN8237 affects multiple mitotic processes and induces dose-dependent mitotic abnormalities and aneuploidy. *Oncotarget*, *5*(15), 6229. https://doi.org/10.18632/ONCOTARGET.2190

Audouard, C., le Masson, F., Charry, C., Li, Z., & Christians, E. S. (2011). Oocyte–Targeted Deletion Reveals That Hsp90b1 Is Needed for the Completion of First Mitosis in Mouse Zygotes. *PLoS ONE*, *6*(2). https://doi.org/10.1371/JOURNAL.PONE.0017109

Aydogan, M. G., Hankins, L. E., Steinacker, T. L., Mofatteh, M., Saurya, S., Wainman, A., Wong, S. S., Lu, X., Zhou, F. Y., & Raff, J. W. (2022). Centriole distal-end

proteins CP110 and Cep97 influence centriole cartwheel growth at the proximal end. *Journal of Cell Science*, *135*(14). https://doi.org/10.1242/JCS.260015/VIDEO-3

Aydogan, M. G., Steinacker, T. L., Mofatteh, M., Wilmott, Z. M., Zhou, F. Y., Gartenmann, L., Wainman, A., Saurya, S., Novak, Z. A., Wong, S. S., Goriely, A., Boemo, M. A., & Raff, J. W. (2020). An Autonomous Oscillation Times and Executes Centriole Biogenesis. *Cell*, *181*(7), 1566. https://doi.org/10.1016/J.CELL.2020.05.018

Aydogan, M. G., Wainman, A., Saurya, S., Steinacker, T. L., Caballe, A., Novak, Z. A., Baumbach, J., Muschalik, N., & Raff, J. W. (2018). A homeostatic clock sets daughter centriole size in flies. *The Journal of Cell Biology*, *217*(4), 1233. https://doi.org/10.1083/JCB.201801014

Bahe, S., Stierhof, Y. D., Wilkinson, C. J., Leiss, F., & Nigg, E. A. (2005). Rootletin forms centriole-associated filaments and functions in centrosome cohesion. *Journal of Cell Biology*, *171*(1), 27–33. https://doi.org/10.1083/jcb.200504107

Bailey, F. P., Clarke, K., Kalirai, H., Kenyani, J., Shahidipour, H., Falciani, F., Coulson, J. M., Sacco, J. J., Coupland, S. E., & Eyers, P. A. (2018). Kinome-wide transcriptional profiling of uveal melanoma reveals new vulnerabilities to targeted therapeutics. *Pigment Cell & Melanoma Research*, *31*(2), 253–266. https://doi.org/10.1111/PCMR.12650

Bakhoum, M. F., & Esmaeli, B. (2019). Molecular characteristics of uveal melanoma: Insights from the cancer genome atlas (TCGA) project. In *Cancers* (Vol. 11, Issue 8). MDPI AG. https://doi.org/10.3390/cancers11081061

Balczon, R., Bao, L., Zimmer, W. E., Brown, K., Zinkowski, R. P., & Brinkley, B. R. (1995). Dissociation of centrosome replication events from cycles of DNA synthesis and mitotic division in hydroxyurea-arrested Chinese hamster ovary cells. *Journal of Cell Biology*, *130*(1), 105–115. https://doi.org/10.1083/jcb.130.1.105

Balestra, F. R., Strnad, P., Flückiger, I., & Gönczy, P. (2013). Discovering regulators of

centriole biogenesis through siRNA-based functional genomics in human cells. *Developmental Cell*, *25*(6), 555–571. https://doi.org/10.1016/j.devcel.2013.05.016

Barton, E. R., Park, S., James, J. K., Makarewich, C. A., Philippou, A., Eletto, D., Lei, H., Brisson, B., Ostrovsky, O., Li, Z., & Argon, Y. (2012). Deletion of muscle GRP94 impairs both muscle and body growth by inhibiting local IGF production. *The FASEB Journal*, *26*(9), 3691. https://doi.org/10.1096/FJ.11-203026

Bashir, T., Dorello, H. V., Amador, V., Guardavaccaro, D., & Pagano, M. (2004). Control of the SCF(Skp2-Cks1) ubiquitin ligase by the APC/C(Cdh1) ubiquitin ligase. *Nature*, *428*(6979), 190–193. https://doi.org/10.1038/NATURE02330

Basto, R., Brunk, K., Vinadogrova, T., Peel, N., Franz, A., Khodjakov, A., & Raff, J. W. (2008). Centrosome amplification can initiate tumorigenesis in flies. *Cell*, *133*(6), 1032–1042. https://doi.org/10.1016/j.cell.2008.05.039

Begemann, I., & Galic, M. (2016). Correlative light electron microscopy: Connecting synaptic structure and function. *Frontiers in Synaptic Neuroscience*, *8*(AUG), 28. https://doi.org/10.3389/FNSYN.2016.00028/BIBTEX

Benmaamar, R., & Pagano, M. (2005). Cell Cycle Involvement of the SCF Complex in the Control of Cdh1 Degradation in S-phase. *Cell Cycle*, *4*(9), 9. https://doi.org/10.4161/cc.4.9.2048

Bhullar, K. S., Lagarón, N. O., McGowan, E. M., Parmar, I., Jha, A., Hubbard, B. P., & Rupasinghe, H. P. V. (2018). Kinase-targeted cancer therapies: progress, challenges and future directions. *Molecular Cancer 2018 17:1*, *17*(1), 1–20. https://doi.org/10.1186/S12943-018-0804-2

Biswas, C., Ostrovsky, O., Makarewich, C. A., Wanderling, S., Gidalevitz, T., & Argon, Y. (2007). The peptide-binding activity of GRP94 is regulated by calcium. *Biochemical Journal*, *405*(Pt 2), 233. https://doi.org/10.1042/BJ20061867

Blanco-Ameijeiras, J., Lozano-Fernández, P., & Martı, E. (2022). Centrosome maturation – in tune with the cell cycle. *Journal of Cell Science*, *135*(2). https://doi.org/10.1242/JCS.259395/274149

Blangy, A., Lane, H. A., D'Hérin, P., Harper, M., Kress, M., & Nigg, E. A. (1995). Phosphorylation by p34cdc2 regulates spindle association of human Eg5, a kinesin-related motor essential for bipolar spindle formation in vivo. *Cell*, *83*(7), 1159–1169. https://doi.org/10.1016/0092-8674(95)90142-6

Bouaoun, L., Sonkin, D., Ardin, M., Hollstein, M., Byrnes, G., Zavadil, J., & Olivier, M. (2016). TP53 Variations in Human Cancers: New Lessons from the IARC TP53 Database and Genomics Data. *Human Mutation*, *37*(9), 865–876. https://doi.org/10.1002/HUMU.23035

Bronkhorst, I. H. G., Jehs, T. M. L., Dijkgraaf, E. M., Luyten, G. P. M., Van Der Velden, P. A., Van Der Burg, S. H., & Jager, M. J. (2014). Effect of Hypoxic Stress on Migration and Characteristics of Monocytes in Uveal Melanoma. *JAMA Ophthalmology*, *132*(5), 614–621. https://doi.org/10.1001/JAMAOPHTHALMOL.2014.43

Brown, N. R., Lowe, E. D., Petri, E., Skamnaki, V., Antrobus, R., & Johnson, L. N. (2007). Cyclin B and Cyclin A Confer Different Substrate Recognition Properties on CDK2. *Http://Dx.Doi.Org/10.4161/Cc.6.11.4278*, *6*(11), 1350–1359. https://doi.org/10.4161/CC.6.11.4278

Brownlee, C. W., & Rogers, G. C. (2013). Show me your license, please: Deregulation of centriole duplication mechanisms that promote amplification. In *Cellular and Molecular Life Sciences* (Vol. 70, Issue 6, pp. 1021–1034). Springer. https://doi.org/10.1007/s00018-012-1102-6

Burgess, S. G., Mukherjee, M., Sabir, S., Joseph, N., Gutiérrez-Caballero, C., Richards, M. W., Huguenin-Dezot, N., Chin, J. W., Kennedy, E. J., Pfuhl, M., Royle, S. J., Gergely, F., & Bayliss, R. (2018). Mitotic spindle association of TACC3 requires Aurora-A-dependent stabilization of a cryptic α-helix. *The EMBO Journal*, *37*(8). https://doi.org/10.15252/EMBJ.201797902

Burigotto, M., Mattivi, A., Migliorati, D., Magnani, G., Valentini, C., Roccuzzo, M., Offterdinger, M., Pizzato, M., Schmidt, A., Villunger, A., Maffini, S., Luca, &, & Fava, L. (2021). Centriolar distal appendages activate the centrosome-

PIDDosome-p53 signalling axis via ANKRD26. *The EMBO Journal*, *40*(4), e104844. https://doi.org/10.15252/EMBJ.2020104844

Bykov, V. J. N., Issaeva, N., Shilov, A., Hultcrantz, M., Pugacheva, E., Chumakov, P., Bergman, J., Wiman, K. G., & Selivanova, G. (2002). Restoration of the tumor suppressor function to mutant p53 by a low-molecular-weight compound. *Nature Medicine*, *8*(3), 282–288. https://doi.org/10.1038/nm0302-282

Cai, Y., Liu, Y., Yang, H., & Lu, H. (2009). [The p53-p21(waf1) pathway and centrosome amplification in oral squamous cell carcinomas]. *Zhonghua Kou Qiang Yi Xue Za Zhi = Zhonghua Kouqiang Yixue Zazhi = Chinese Journal of Stomatology*, *44*(6), 332–335. http://www.ncbi.nlm.nih.gov/pubmed/19953948

Carvalhal, S., Ribeiro, S. A., Arocena, M., Kasciukovic, T., Temme, A., Koehler, K., Huebner, A., & Griffis, E. R. (2015). The nucleoporin ALADIN regulates Aurora A localization to ensure robust mitotic spindle formation. *Molecular Biology of the Cell*, *26*(19), 3424. https://doi.org/10.1091/MBC.E15-02-0113

Chakraborty, S., Hosen, M. I., Ahmed, M., & Shekhar, H. U. (2018). Onco-Multi-OMICS Approach: A New Frontier in Cancer Research. *BioMed Research International*, *2018*. https://doi.org/10.1155/2018/9836256

Chan, J. Y. (2011). A clinical overview of centrosome amplification in human cancers. In *International Journal of Biological Sciences* (Vol. 7, Issue 8, pp. 1122–1144). Ivyspring International Publisher. https://doi.org/10.7150/ijbs.7.1122

Chaudhary, K., Poirion, O. B., Lu, L., & Garmire, L. X. (2018). Deep Learning based multi-omics integration robustly predicts survival in liver cancer. *Clinical Cancer Research : An Official Journal of the American Association for Cancer Research*, *24*(6), 1248. https://doi.org/10.1158/1078-0432.CCR-17-0853

Chavali, P. L., Chandrasekaran, G., Barr, A. R., Tátrai, P., Taylor, C., Papachristou, E. K., Woods, C. G., Chavali, S., & Gergely, F. (2016). A CEP215–HSET complex links centrosomes with spindle poles and drives centrosome clustering in cancer. *Nature Communications*, *7*. https://doi.org/10.1038/NCOMMS11005

Chen, B., Piel, W. H., Gui, L., Bruford, E., & Monteiro, A. (2005). The HSP90 family of

genes in the human genome: insights into their divergence and evolution. *Genomics*, *86*(6), 627–637. https://doi.org/10.1016/J.YGENO.2005.08.012

Chen, E. A., Souaiaia, T., Herstein, J. S., Evgrafov, O. V, Spitsyna, V. N., Rebolini, D. F., & Knowles, J. A. (2014). *Effect of RNA integrity on uniquely mapped reads in RNA-Seq*. https://doi.org/10.1186/1756-0500-7-753

Chen, P. W., Murray, T. G., Uno, T., Salgaller, M. L., Reddy, R., & Ksander, B. R. (1997). Expression of MAGE genes in ocular melanoma during progression from primary to metastatic disease. *Clinical and Experimental Metastasis*, *15*(5), 509–518. https://doi.org/10.1023/A:1018479011340

Chen, T. Y., Syu, J. S., Lin, T. C., Cheng, H. L., Lu, F. L., & Wang, C. Y. (2015). Chloroquine alleviates etoposide-induced centrosome amplification by inhibiting CDK2 in adrenocortical tumor cells. *Oncogenesis*, *4*(12), e180. https://doi.org/10.1038/oncsis.2015.37

Choe, M. H., Kim, J., Ahn, J., Hwang, S. G., Oh, J. S., & Kim, J. S. (2018). Centrosome Clustering Is a Tumor-selective Target for the Improvement of Radiotherapy in Breast Cancer Cells. *Anticancer Research*, *38*(6), 3393–3400. https://doi.org/10.21873/ANTICANRES.12606

Coelho, P. A., Bury, L., Shahbazi, M. N., Liakath-Ali, K., Tate, P. H., Wormald, S., Hindley, C. J., Huch, M., Archer, J., Skarnes, W. C., Zernicka-Goetz, M., & Glover, D. M. (2015). Over-expression of Plk4 induces centrosome amplification, loss of primary cilia and associated tissue hyperplasia in the mouse. *Open Biology*, *5*(12). https://doi.org/10.1098/rsob.150209

Comartin, D., Gupta, G. D., Fussner, E., Coyaud, É., Hasegan, M., Archinti, M., Cheung, S. W. T., Pinchev, D., Lawo, S., Raught, B., Bazett-Jones, D. P., Lüders, J., & Pelletier, L. (2013). CEP120 and SPICE1 cooperate with CPAP in centriole elongation. *Current Biology*, *23*(14), 1360–1366. https://doi.org/10.1016/j.cub.2013.06.002

Cosenza, M. R., & Krämer, A. (2016). Centrosome amplification, chromosomal instability and cancer: mechanistic, clinical and therapeutic issues. *Chromosome*

Research, *24*(1), 105–126. https://doi.org/10.1007/s10577-015-9505-5

D'Angiolella, V., Donato, V., Vijayakumar, S., Saraf, A., Florens, L., Washburn, M. P., Dynlacht, B., & Pagano, M. (2010). SCF Cyclin F controls centrosome homeostasis and mitotic fidelity through CP110 degradation. *Nature*, *466*(7302), 138–142. https://doi.org/10.1038/nature09140

Damato, B. E., Heimann, H., Kalirai, H., & Coupland, S. E. (2014). Age, Survival Predictors, and Metastatic Death in Patients With Choroidal Melanoma: Tentative Evidence of a Therapeutic Effect on Survival. *JAMA Ophthalmology*, *132*(5), 605–613. https://doi.org/10.1001/JAMAOPHTHALMOL.2014.77

Dammermann, A., Maddox, P. S., Desai, A., & Oegema, K. (2008). SAS-4 is recruited to a dynamic structure in newly forming centrioles that is stabilized by the γ-tubulin-mediated addition of centriolar microtubules. *Journal of Cell Biology*, *180*(4), 771–785. https://doi.org/10.1083/jcb.200709102

De Almeida, B. P., Vieira, A. F., Paredes, J., Bettencourt-Dias, M., & Barbosa-Morais, N. L. (2019). Pan-cancer association of a centrosome amplification gene expression signature with genomic alterations and clinical outcome. *PLOS Computational Biology*, *15*(3), e1006832. https://doi.org/10.1371/JOURNAL.PCBI.1006832

De Cárcer, G., Do Carmo Avides, M., Lallena, M. J., Glover, D. M., & González, C. (2001). Requirement of Hsp90 for centrosomal function reflects its regulation of Polo kinase stability. *The EMBO Journal*, *20*(11), 2878. https://doi.org/10.1093/EMBOJ/20.11.2878

Decatur, C. L., Ong, E., Garg, N., Anbunathan, H., Bowcock, A. M., Field, M. G., Harbour, J. W., & Author, J. O. (2016). *Driver Mutations in Uveal Melanoma: Associations With Gene Expression Profile and Patient Outcomes HHS Public Access Author manuscript*. *134*(7), 728–733. https://doi.org/10.1001/jamaophthalmol.2016.0903

Denu, R. A., Kaur, G., Sass, M. M., Lakkaraju, A., & Burkard, M. E. (2019). Centrosome amplification in cancer disrupts autophagy and sensitizes to autophagy

inhibition. *Molecular Cancer Research*, molcanres.0509.2019. https://doi.org/10.1158/1541-7786.mcr-19-0509

Denu, R. A., Shabbir, M., Nihal, M., Singh, C. K., Longley, B. J., Burkard, M. E., & Ahmad, N. (2018). Centriole Overduplication is the Predominant Mechanism Leading to Centrosome Amplification in Melanoma. *Molecular Cancer Research : MCR*, *16*(3), 517–527. https://doi.org/10.1158/1541-7786.MCR-17-0197

Diener-West, M., Reynolds, S. M., Agugliaro, D. J., Caldwell, R., Cumming, K., Earle, J. D., Hawkins, B. S., Hayman, J. A., Jaiyesimi, I., Jampol, L. M., Kirkwood, J. M., Koh, W. J., Robertson, D. M., Shaw, J. M., Straatsma, B. R., & Thoma, J. (2005). Development of metastatic disease after enrollment in the COMS trials for treatment of choroidal melanoma: Collaborative Ocular Melanoma Study Group Report No. 26. *Archives of Ophthalmology*, *123*(12), 1639–1643. https://doi.org/10.1001/archopht.123.12.1639

Dittrich, T., Schorb, M., Haberbosch, I., Bausch, E., Börmel, M., Cosenza, M., Goldschmidt, H., Müller-Tidow, C., Raab, M. S., Hegenbart, U., Schönland, S. O., Schwab, Y., & Krämer, A. (2019). High-Throughput Immunofluorescence and Electron Tomography to Characterize Centrosomal Aberrations in Plasma Cell Neoplasia. *Blood*, *134*(Supplement_1), 3077–3077. https://doi.org/10.1182/blood-2019-130713

Dou, Z., Ding, X., Zereshki, A., Zhang, Y., Zhang, J., Wang, F., Sun, J., Huang, H., & Yao, X. (2004). TTK kinase is essential for the centrosomal localization of TACC2. *FEBS Letters*, *572*(1–3), 51–56. https://doi.org/10.1016/j.febslet.2004.06.092

Du, R., Huang, C., Liu, K., Li, X., & Dong, Z. (2021). Targeting AURKA in Cancer: molecular mechanisms and opportunities for Cancer therapy. *Molecular Cancer 2021 20:1*, *20*(1), 1–27. https://doi.org/10.1186/S12943-020-01305-3

Duan, X., Iwanowycz, S., Ngoi, S., Hill, M., Zhao, Q., & Liu, B. (2021). Molecular Chaperone GRP94/GP96 in Cancers: Oncogenesis and Therapeutic Target. *Frontiers in Oncology*, *11*. https://doi.org/10.3389/FONC.2021.629846

Duensing, S. (2015). Analysis of centrosomes in human cancer. *Methods in Cell Biology*, *129*, 51–60. https://doi.org/10.1016/BS.MCB.2015.03.002

Duensing, S., Darr, S., Cuevas, R., Melquiot, N., Brickner, A. G., Duensing, A., & Münger, K. (2010). Tripeptidyl peptidase II is required for c-MYC-induced centriole overduplication and a novel therapeutic target in c-MYC-associated neoplasms. *Genes and Cancer*, *1*(9), 883–892. https://doi.org/10.1177/1947601910389605

Dupree, E. J., Jayathirtha, M., Yorkey, H., Mihasan, M., Petre, B. A., & Darie, C. C. (2020). A Critical Review of Bottom-Up Proteomics: The Good, the Bad, and the Future of This Field. *Proteomes 2020, Vol. 8, Page 14*, *8*(3), 14. https://doi.org/10.3390/PROTEOMES8030014

Dzhindzhev, N. S., Tzolovsky, G., Lipinszki, Z., Schneider, S., Lattao, R., Fu, J., Debski, J., Dadlez, M., & Glover, D. M. (2014). Plk4 phosphorylates Ana2 to trigger Sas6 recruitment and procentriole formation. *Current Biology : CB*, *24*(21), 2526–2532. https://doi.org/10.1016/j.cub.2014.08.061

Dzhindzhev, N. S., Yu, Q. D., Weiskopf, K., Tzolovsky, G., Cunha-Ferreira, I., Riparbelli, M., Rodrigues-Martins, A., Bettencourt-Dias, M., Callaini, G., & Glover, D. M. (2010). Asterless is a scaffold for the onset of centriole assembly. *Nature*, *467*(7316), 714–718. https://doi.org/10.1038/nature09445

Engeland, K. (2022). Cell cycle regulation: p53-p21-RB signaling. *Cell Death & Differentiation 2022 29:5*, *29*(5), 946–960. https://doi.org/10.1038/s41418-022-00988-z

Ershov, D., Phan, M.-S., Pylvänäinen, J. W., Rigaud, S. U., Blanc, L. Le, Charles-Orszag, A., Conway, J. R. W., Laine, R. F., Roy, N. H., Bonazzi, D., Duménil, G., Jacquemet, G., & Tinevez, J.-Y. (2021). Bringing TrackMate into the era of machine-learning and deep-learning. *BioRxiv*, 2021.09.03.458852. https://doi.org/10.1101/2021.09.03.458852

Eskelin, S., Pyrhönen, S., Summanen, P., Hahka-Kemppinen, M., & Kivelä, T. (2000). Tumor doubling times in metastatic malignant melanoma of the uvea: tumor

progression before and after treatment. *Ophthalmology*, *107*(8), 1443–1449. https://doi.org/10.1016/S0161-6420(00)00182-2

Evans, L. T., Anglen, T., Scott, P., Lukasik, K., Loncarek, J., & Holland, A. J. (2021). ANKRD26 recruits PIDD1 to centriolar distal appendages to activate the PIDDosome following centrosome amplification. *The EMBO Journal*, *40*(4), e105106. https://doi.org/10.15252/EMBJ.2020105106

Fang, C.-T., Kuo, H.-H., Hsu, S.-C., & Yih, L.-H. (2019). HSP70 is required for the proper assembly of pericentriolar material and function of mitotic centrosomes. *Cell Division*, *14*(1), 4. https://doi.org/10.1186/s13008-019-0047-7

Fang, Y., & Fullwood, M. J. (2016). Roles, Functions, and Mechanisms of Long Non-coding RNAs in Cancer. In *Genomics, Proteomics and Bioinformatics* (Vol. 14, Issue 1, pp. 42–54). Beijing Genomics Institute. https://doi.org/10.1016/j.gpb.2015.09.006

Farrukh, U. B., Bilal, A., Zahid, H., Iqbal, M., Manzoor, S., Firdous, F., Furqan, M., Azeem, M., Emwas, A.-H., Alazmi, M., Gao, X., Saleem, R. S. Z., & Faisal, A. (2022). Synthesis and Evaluation of Novel Carboxamides Capable of Causing Centrosome Declustering and Apoptosis in Breast Cancer Cells. *ChemistrySelect*, *7*(15), e202104218. https://doi.org/10.1002/SLCT.202104218

Fava, L. L., Schuler, F., Sladky, V., Haschka, M. D., Soratroi, C., Eiterer, L., Demetz, E., Weiss, G., Geley, S., Nigg, E. A., & Villunger, A. (2017). The PIDDosome activates p53 in response to supernumerary centrosomes. *Genes and Development*, *31*(1), 34–45. https://doi.org/10.1101/gad.289728.116

Feng, L. yuan, Yan, B. bing, Huang, Y. zhi, & Li, L. (2021). Abnormal methylation characteristics predict chemoresistance and poor prognosis in advanced high-grade serous ovarian cancer. *Clinical Epigenetics*, *13*(1), 141. https://doi.org/10.1186/S13148-021-01133-2

Fry, A. M., O'Regan, L., Sabir, S. R., & Bayliss, R. (2012). Cell cycle regulation by the NEK family of protein kinases. *Journal of Cell Science*, *125*(19), 4423. https://doi.org/10.1242/JCS.111195

Fry, A. M., Sampson, J., Shak, C., & Shackleton, S. (2017). Recent advances in pericentriolar material organization: ordered layers and scaffolding gels. *F1000Research*, *6*, 1622. https://doi.org/10.12688/F1000RESEARCH.11652.1

Fu, J., Hagan, I. M., & Glover, D. M. (2015). The centrosome and its duplication cycle. *Cold Spring Harbor Perspectives in Medicine*, *5*(1). https://doi.org/10.1101/cshperspect.a015800

Fujiwara, T., Bandi, M., Nitta, M., Ivanova, E. V., Bronson, R. T., & Pellman, D. (2005). Cytokinesis failure generating tetraploids promotes tumorigenesis in p53-null cells. *Nature*, *437*(7061), 1043–1047. https://doi.org/10.1038/nature04217

Fukasawa, K. (2007). Oncogenes and tumour suppressors take on centrosomes. *Nature Reviews Cancer*, *7*(12), 911–924. https://doi.org/10.1038/nrc2249

Fukasawa, K., Choi, T., Kuriyama, R., Rulong, S., & Vande Woude, G. F. (1996). Abnormal centrosome amplification in the absence of p53. *Science*, *271*(5256), 1744–1747. https://doi.org/10.1126/science.271.5256.1744

Fulcher, L. J., He, Z., Mei, L., Macartney, T. J., Wood, N. T., Prescott, A. R., Whigham, A. J., Varghese, J., Gourlay, R., Ball, G., Clarke, R., Campbell, D. G., Maxwell, C. A., & Sapkota, G. P. (2019). FAM83D directs protein kinase CK1α to the mitotic spindle for proper spindle positioning. *EMBO Reports*, *20*(9). https://doi.org/10.15252/EMBR.201847495

Galofré, C., Asensio, E., Ubach, M., Torres, I. M., Quintanilla, I., Castells, A., & Camps, J. (2020). Centrosome reduction in newly-generated tetraploid cancer cells obtained by separase depletion. *Scientific Reports 2020 10:1*, *10*(1), 1–12. https://doi.org/10.1038/s41598-020-65975-1

Ganapathi Sankaran, D., Stemm-Wolf, A. J., & Pearson, C. G. (2019). CEP135 isoform dysregulation promotes centrosome amplification in breast cancer cells. *Molecular Biology of the Cell*, *30*(10), 1230–1244. https://doi.org/10.1091/mbc.E18-10-0674

Ganem, N. J., Godinho, S. A., & Pellman, D. (2009). A mechanism linking extra centrosomes to chromosomal instability. *Nature*, *460*(7252), 278–282.

https://doi.org/10.1038/nature08136

Gartel, A. L., & Radhakrishnan, S. K. (2005). Lost in Transcription: p21 Repression, Mechanisms, and Consequences. *Cancer Research*, *65*(10), 3980–3985. https://doi.org/10.1158/0008-5472.CAN-04-3995

Gill, V. T., Sabazade, S., Herrspiegel, C., Ewens, K. G., Opalko, A., Dan, N., Christersdottir, T., Berg Rendahl, A., Shields, C. L., Seregard, S., Ganguly, A., & Stålhammar, G. (2022). A prognostic classification system for uveal melanoma based on a combination of patient age and sex, the American Joint Committee on Cancer and the Cancer Genome Atlas models. *Acta Ophthalmologica*. https://doi.org/10.1111/AOS.15210

Glover, D. M., Leibowitz, M. H., McLean, D. A., & Parry, H. (1995). Mutations in aurora prevent centrosome separation leading to the formation of monopolar spindles. *Cell*, *81*(1), 95–105. https://doi.org/10.1016/0092-8674(95)90374-7

Godinho, S. A., Kwon, M., & Pellman, D. (2009). Centrosomes and cancer: how cancer cells divide with too many centrosomes. *Cancer and Metastasis Reviews*, *28*(1–2), 85–98. https://doi.org/10.1007/s10555-008-9163-6

Godinho, S. A., & Pellman, D. (2014). Causes and consequences of centrosome abnormalities in cancer. *Philosophical Transactions of the Royal Society of London. Series B, Biological Sciences*, *369*(1650). https://doi.org/10.1098/rstb.2013.0467

Godinho, S. A., Picone, R., Burute, M., Dagher, R., Su, Y., Leung, C. T., Polyak, K., Brugge, J. S., Théry, M., & Pellman, D. (2014). Oncogene-like induction of cellular invasion from centrosome amplification. *Nature*, *510*(7503), 167–171. https://doi.org/10.1038/nature13277

Goepfert T.M., Adigun Y.E., Zhong L., Gay J., Medina D., B. W. R. (2002). Centrosome amplification and overexpression of aurora A are early events in rat mammary carcinogenesis. *Cancer Research*, *62*(14), 4115–4122. https://aacrjournals.org/cancerres/article/62/14/4115/509017/Centrosome-Amplification-and-Overexpression-of

Gomes, C. C., Diniz, M. G., Orsine, L. A., Duarte, A. P., Fonseca-Silva, T., Conn, B. I., De Marco, L., Pereira, C. M., & Gomez, R. S. (2012). Assessment of TP53 Mutations in Benign and Malignant Salivary Gland Neoplasms. *PLoS ONE*, *7*(7), e41261. https://doi.org/10.1371/journal.pone.0041261

Gönczy, P., & Hatzopoulos, G. N. (2019). Centriole assembly at a glance. *Journal of Cell Science*, *132*(4), jcs228833. https://doi.org/10.1242/jcs.228833

Gräf, R., Euteneuer, U., Ho, T. H., & Rehberg, M. (2003). Regulated Expression of the Centrosomal Protein DdCP224 Affects Microtubule Dynamics and Reveals Mechanisms for the Control of Supernumerary Centrosome Number. *Molecular Biology of the Cell*, *14*(10), 4067. https://doi.org/10.1091/MBC.E03-04-0242

Green, M. R., & Sambrook, J. (2022). Preparation of Labeled DNA, RNA, and Oligonucleotide Probes. *Cold Spring Harbor Protocols*, *2022*(1), pdb.top100578. https://doi.org/10.1101/PDB.TOP100578

Grimson, A., Farh, K. K. H., Johnston, W. K., Garrett-Engele, P., Lim, L. P., & Bartel, D. P. (2007). MicroRNA Targeting Specificity in Mammals: Determinants Beyond Seed Pairing. *Molecular Cell*, *27*(1), 91. https://doi.org/10.1016/J.MOLCEL.2007.06.017

Gruss, O. J. (2018). Animal Female Meiosis: The Challenges of Eliminating Centrosomes. *Cells*, *7*(7). https://doi.org/10.3390/CELLS7070073

Gudi, R., Zou, C., Li, J., & Gao, Q. (2011). Centrobin-tubulin interaction is required for centriole elongation and stability. *Journal of Cell Biology*, *193*(4), 711–725. https://doi.org/10.1083/jcb.201006135

Guo, M., Rever, J., Nguyen, P. N. U., Akella, N. M., Reid, G. S. D., & Maxwell, C. A. (2023). Centrosome Amplification Is a Potential Molecular Target in Paediatric Acute Lymphoblastic Leukemia. *Cancers*, *15*(1). https://doi.org/10.3390/CANCERS15010154/S1

Guo, Y., Xiao, P., Lei, S., Deng, F., Xiao, G. G., Liu, Y., Chen, X., Li, L., Wu, S., Chen, Y., Jiang, H., Tan, L., Xie, J., Zhu, X., Liang, S., & Deng, H. (2008). How is mRNA expression predictive for protein expression? A correlation study on human

circulating monocytes. *Acta Biochimica et Biophysica Sinica*, *40*(5), 426–436. https://doi.org/10.1111/J.1745-7270.2008.00418.X

Hanahan, D. (2022). Hallmarks of Cancer: New Dimensions. *Cancer Discovery*, *12*(1), 31–46. https://doi.org/10.1158/2159-8290.CD-21-1059

Harrison, L. E., Bleiler, M., & Giardina, C. (2018). A look into centrosome abnormalities in colon cancer cells, how they arise and how they might be targeted therapeutically. *Biochemical Pharmacology*, *147*, 1–8. https://doi.org/10.1016/j.bcp.2017.11.003

Hata, S., Pastor Peidro, A., Panic, M., Liu, P., Atorino, E., Funaya, C., Jäkle, U., Pereira, G., & Schiebel, E. (2019). The balance between KIFC3 and EG5 tetrameric kinesins controls the onset of mitotic spindle assembly. *Nature Cell Biology*, *21*(9), 1138–1151. https://doi.org/10.1038/s41556-019-0382-6

Hatano, T., & Sluder, G. (2012). The interrelationship between APC/C and Plk1 activities in centriole disengagement. *Biology Open*, *1*(11), 1153–1160. https://doi.org/10.1242/bio.20122626

Heijkants, R., Willekens, K., Schoonderwoerd, M., Teunisse, A., Nieveen, M., Radaelli, E., Hawinkels, L., Marine, J.-C., Jochemsen, A., Heijkants, R., Willekens, K., Schoonderwoerd, M., Teunisse, A., Nieveen, M., Radaelli, E., Hawinkels, L., Marine, J.-C., & Jochemsen, A. (2017). Combined inhibition of CDK and HDAC as a promising therapeutic strategy for both cutaneous and uveal metastatic melanoma. *Oncotarget*, *9*(5), 6174–6187. https://doi.org/10.18632/ONCOTARGET.23485

Helassa, N., Nugues, C., Rajamanoharan, D., Burgoyne, R. D., & Haynes, L. P. (2019). A centrosome-localized calcium signal is essential for mammalian cell mitosis. *The FASEB Journal*, *33*(12), 14602. https://doi.org/10.1096/FJ.201901662R

Helgadottir, H., & Höiom, V. (2016). *The Application of Clinical Genetics Dovepress The genetics of uveal melanoma: current insights*. https://doi.org/10.2147/TACG.S69210

Heo, Y. J., Hwa, C., Lee, G. H., Park, J. M., & An, J. Y. (2021). Integrative Multi-Omics

Approaches in Cancer Research: From Biological Networks to Clinical Subtypes. *Molecules and Cells*, *44*(7), 433. https://doi.org/10.14348/MOLCELLS.2021.0042

Hinchcliffe, E. H., Li, C., Thompson, E. A., Maller, J. L., & Sluder, G. (1999). Requirement of Cdk2-cyclin E activity for repeated centrosome reproduction in xenopus egg extracts. *Science*, *283*(5403), 851–854. https://doi.org/10.1126/science.283.5403.851

Holland, A. J., Fachinetti, D., Zhu, Q., Bauer, M., Verma, I. M., Nigg, E. A., & Cleveland, D. W. (2012). The autoregulated instability of Polo-like kinase 4 limits centrosome duplication to once per cell cycle. *Genes and Development*, *26*(24), 2684–2689. https://doi.org/10.1101/gad.207027.112

Hong, S. W., Jiang, Y., Kim, S., Li, C. J., & Lee, D. K. (2014). Target Gene Abundance Contributes to the Efficiency of siRNA-Mediated Gene Silencing. *Nucleic Acid Therapeutics*, *24*(3), 192. https://doi.org/10.1089/NAT.2013.0466

Horsman, D. E., Sroka, H., Rootman, J., & White, V. A. (1990). Monosomy 3 and isochromosome 8q in a uveal melanoma. *Cancer Genetics and Cytogenetics*, *45*(2), 249–253. http://www.ncbi.nlm.nih.gov/pubmed/2317773

Horsthemke, B., Prescher, G., Bornfeld, N., & Becher, R. (1992). Loss of chromosome 3 alleles and multiplication of chromosome 8 alleles in uveal melanoma. *Genes, Chromosomes & Cancer*, *4*(3), 217–221. http://www.ncbi.nlm.nih.gov/pubmed/1382562

Hoter, A., El-Sabban, M. E., & Naim, H. Y. (2018). The HSP90 Family: Structure, Regulation, Function, and Implications in Health and Disease. *International Journal of Molecular Sciences*, *19*(9). https://doi.org/10.3390/IJMS19092560

Hou, H., Sun, D., & Zhang, X. (2019). The role of MDM2 amplification and overexpression in therapeutic resistance of malignant tumors. *Cancer Cell International*, *19*(1), 1–8. https://doi.org/10.1186/S12935-019-0937-4/TABLES/1

Huang, M., Ma, X., Shi, H., Hu, L., Fan, Z., Pang, L., Zhu, F., Yang, X., Xu, W., Liu, B., Zhu, Z., & Li, C. (2017). FAM83D, a microtubule-associated protein, promotes

tumor growth and progression of human gastric cancer. *Oncotarget*, *8*(43), 74479. https://doi.org/10.18632/ONCOTARGET.20157

Hut, H. M. J., Kampinga, H. H., & Sibon, O. C. M. (2005). Hsp70 protects mitotic cells against heat-induced centrosome damage and division abnormalities. *Molecular Biology of the Cell*, *16*(8), 3776–3785. https://doi.org/10.1091/mbc.E05-01-0038

Jackson, A. L., Bartz, S. R., Schelter, J., Kobayashi, S. V., Burchard, J., Mao, M., Li, B., Cavet, G., & Linsley, P. S. (2003). Expression profiling reveals off-target gene regulation by RNAi. *Nature Biotechnology 2003 21:6*, *21*(6), 635–637. https://doi.org/10.1038/nbt831

Jelluma, N., Brenkman, A. B., van den Broek, N. J. F., Cruijsen, C. W. A., van Osch, M. H. J., Lens, S. M. A., Medema, R. H., & Kops, G. J. P. L. (2008). Mps1 Phosphorylates Borealin to Control Aurora B Activity and Chromosome Alignment. *Cell*, *132*(2), 233–246. https://doi.org/10.1016/j.cell.2007.11.046

Kalkan, B. M., Ozcan, S. C., Quintyne, N. J., Reed, S. L., & Acilan, C. (2022). Keep Calm and Carry on with Extra Centrosomes. *Cancers 2022, Vol. 14, Page 442*, *14*(2), 442. https://doi.org/10.3390/CANCERS14020442

Karczewski, K. J., & Snyder, M. P. (2018). Integrative omics for health and disease. *Nature Reviews Genetics 2018 19:5*, *19*(5), 299–310. https://doi.org/10.1038/nrg.2018.4

Kashihara, H., Chiba, S., Kanno, S. ichiro, Suzuki, K., Yano, T., & Tsukita, S. (2019). Cep128 associates with Odf2 to form the subdistal appendage of the centriole. *Genes to Cells*, *24*(3), 231–243. https://doi.org/10.1111/gtc.12668

Kawamura, E., Fielding, A. B., Kannan, N., Balgi, A., Eaves, C. J., Roberge, M., & Dedhar, S. (2013). Identification of novel small molecule inhibitors of centrosome clustering in cancer cells. *Oncotarget*, *4*(10), 1763. https://doi.org/10.18632/ONCOTARGET.1198

Khodjakov, A., Rieder, C. L., Sluder, G., Cassels, G., Sibon, O., & Wang, C. L. (2002). De novo formation of centrosomes in vertebrate cells arrested during S phase.

Journal of Cell Biology, *158*(7), 1171–1181. https://doi.org/10.1083/jcb.200205102

Kim, J. Y., Jeong, H. S., Chung, T., Kim, M., Lee, J. H., Jung, W. H., & Koo, J. S. (2017). The value of phosphohistone H3 as a proliferation marker for evaluating invasive breast cancers: A comparative study with Ki67. *Oncotarget*, *8*(39), 65064. https://doi.org/10.18632/ONCOTARGET.17775

Kleylein-Sohn, J., Pöllinger, B., Ohmer, M., Hofmann, F., Nigg, E. A., Hemmings, B. A., & Wartmann, M. (2012). Acentrosomal spindle organization renders cancer cells dependent on the kinesin HSET. *Journal of Cell Science*, *125*(22), 5391–5402. https://doi.org/10.1242/jcs.107474

Kodani, A., Salomé Sirerol-Piquer, M., Seol, A., Manuel Garcia-Verdugo, J., & Reiter, J. F. (2013). Kif3a interacts with Dynactin subunit p150Glued to organize centriole subdistal appendages. *The EMBO Journal*, *32*(4), 597–607. https://doi.org/10.1038/emboj.2013.3

Kodani, A., Yu, T. W., Johnson, J. R., Jayaraman, D., Johnson, T. L., Al-Gazali, L., Sztriha, L., Partlow, J. N., Kim, H., Krup, A. L., Dammermann, A., Krogan, N. J., Walsh, C. A., & Reiter, J. F. (2015). Centriolar satellites assemble centrosomal microcephaly proteins to recruit CDK2 and promote centriole duplication. *ELife*, *4*(AUGUST2015). https://doi.org/10.7554/eLife.07519

Kohlmaier, G., Lončarek, J., Meng, X., McEwen, B. F., Mogensen, M. M., Spektor, A., Dynlacht, B. D., Khodjakov, A., & Gönczy, P. (2009). Overly Long Centrioles and Defective Cell Division upon Excess of the SAS-4-Related Protein CPAP. *Current Biology*, *19*(12), 1012–1018. https://doi.org/10.1016/j.cub.2009.05.018

Korzeniewski, N., Cuevas, R., Duensing, A., & Duensing, S. (2010). Daughter centriole elongation is controlled by proteolysis. *Molecular Biology of the Cell*, *21*(22), 3942–3951. https://doi.org/10.1091/mbc.E09-12-1049

Kowal, J., Markiewicz, A., Debicka-Kumela, M., Bogdali, A., Jakubowska, B., Karska-Basta, I., & Romanowska-Dixon, B. (2019). Analysis of local recurrence causes in uveal melanoma patients treated with 125I brachytherapy – a single institution

study. *Journal of Contemporary Brachytherapy*, *11*(6), 554. https://doi.org/10.5114/JCB.2019.90985

Kujala, E., Mäkitie, T., & Kivelä, T. (2003). Very Long-Term Prognosis of Patients with Malignant Uveal Melanoma. *Investigative Ophthalmology and Visual Science*, *44*(11), 4651–4659. https://doi.org/10.1167/iovs.03-0538

Kukurba, K. R., & Montgomery, S. B. (2015). RNA Sequencing and Analysis. *Cold Spring Harbor Protocols*, *2015*(11), 951. https://doi.org/10.1101/PDB.TOP084970

Kwon, M., Godinho, S. A., Chandhok, N. S., Ganem, N. J., Azioune, A., Thery, M., & Pellman, D. (2008). Mechanisms to suppress multipolar divisions in cancer cells with extra centrosomes. *Genes and Development*, *22*(16), 2189–2203. https://doi.org/10.1101/gad.1700908

Lacey, K. R., Jackson, P. K., & Stearns, T. (1999). Cyclin-dependent kinase control of centrosome duplication. *Proceedings of the National Academy of Sciences of the United States of America*, *96*(6), 2817–2822. https://doi.org/10.1073/pnas.96.6.2817

Lagos-Cabré, R., Ivanova, A., & Taylor, C. W. (2020). Ca2+ Release by IP3 Receptors Is Required to Orient the Mitotic Spindle. *Cell Reports*, *33*(11). https://doi.org/10.1016/J.CELREP.2020.108483

Lange, B. M. H., Bachi, A., Wilm, M., & Cayetano, G. (2000). Hsp90 is a core centrosomal component and is required at different stages of the centrosome cycle in Drosophila and vertebrates. *The EMBO Journal*, *19*(6), 1252–1262. https://doi.org/10.1093/emboj/19.6.1252

Leber, B., Maier, B., Fuchs, F., Chi, J., Riffel, P., Anderhub, S., Wagner, L., Ho, A. D., Salisbury, J. L., Boutros, M., & Krämer, A. (2010). Proteins required for centrosome clustering in cancer cells. *Science Translational Medicine*, *2*(33). https://doi.org/10.1126/SCITRANSLMED.3000915/SUPPL_FILE/2-33RA38_SM.PDF

Lee, J. M., Hammarén, H. M., Savitski, M. M., & Baek, S. H. (2023). Control of protein

stability by post-translational modifications. *Nature Communications*, *14*(1). https://doi.org/10.1038/S41467-023-35795-8

Lee, K., & Rhee, K. (2011). PLK1 phosphorylation of pericentrin initiates centrosome maturation at the onset of mitosis. *Journal of Cell Biology*, *195*(7), 1093–1101. https://doi.org/10.1083/jcb.201106093

Lee, L. H., Yang, H., & Bigras, G. (2014). Current breast cancer proliferative markers correlate variably based on decoupled duration of cell cycle phases. *Scientific Reports*, *4*(1), 1–8. https://doi.org/10.1038/srep05122

Lentini, L., Amato, A., Schillaci, T., & Di Leonardo, A. (2007). Simultaneous Aurora-A/STK15 overexpression and centrosome amplification induce chromosomal instability in tumour cells with a MIN phenotype. *BMC Cancer*, *7*(1), 1–13. https://doi.org/10.1186/1471-2407-7-212/FIGURES/6

Leontovich, A. A., Salisbury, J. L., Veroux, M., Tallarita, T., Billadeau, D., McCubrey, J., Ingle, J., Galanis, E., & D'Assoro, A. B. (2013). Inhibition of Cdk2 activity decreases Aurora-A kinase centrosomal localization and prevents centrosome amplification in breast cancer cells. *Oncology Reports*, *29*(5), 1785–1788. https://doi.org/10.3892/OR.2013.2313/HTML

Levine, M. S., Bakker, B., Boeckx, B., Moyett, J., Lu, J., Vitre, B., Spierings, D. C., Lansdorp, P. M., Cleveland, D. W., Lambrechts, D., Foijer, F., & Holland, A. J. (2017). Centrosome Amplification Is Sufficient to Promote Spontaneous Tumorigenesis in Mammals. *Developmental Cell*, *40*(3), 313-322.e5. https://doi.org/10.1016/j.devcel.2016.12.022

Li, J., D'Angiolella, V., Seeley, E. S., Kim, S., Kobayashi, T., Fu, W., Campos, E. I., Pagano, M., & Dynlacht, B. D. (2013). USP33 regulates centrosome biogenesis via deubiquitination of the centriolar protein CP110. *Nature*, *495*(7440), 255–259. https://doi.org/10.1038/nature11941

Li, J. J., Weroha, S. J., Lingle, W. L., Papa, D., Salisbury, J. L., & Li, S. A. (2004). Estrogen mediates Aurora-A overexpression, centrosome amplification, chromosomal instability, and breast cancer in female ACI rats. *Proceedings of*

the National Academy of Sciences of the United States of America, *101*(52), 18123–18128. https://doi.org/10.1073/pnas.0408273101

Li, X., Zhao, Q., Liao, R., Sun, P., & Wu, X. (2003). The SCFSkp2 Ubiquitin Ligase Complex Interacts with the Human Replication Licensing Factor Cdt1 and Regulates Cdt1 Degradation. *Journal of Biological Chemistry*, *278*(33), 30854–30858. https://doi.org/10.1074/JBC.C300251200

Liang, C. C., Park, A. Y., & Guan, J. L. (2007). In vitro scratch assay: a convenient and inexpensive method for analysis of cell migration in vitro. *Nature Protocols 2007 2:2*, *2*(2), 329–333. https://doi.org/10.1038/nprot.2007.30

Lin, C. C., Kitagawa, M., Tang, X., Hou, M. H., Wu, J., Qu, D. C., Srinivas, V., Liu, X., Thompson, J. W., Mathey-Prevot, B., Yao, T. P., Lee, S. H., & Chi, J. T. (2018). CoA synthase regulates mitotic fidelity via CBP-mediated acetylation. *Nature Communications*, *9*(1). https://doi.org/10.1038/S41467-018-03422-6

Lin, X., Xiang, X., Hao, L., Wang, T., Lai, Y., Abudoureyimu, M., Zhou, H., Feng, B., Chu, X., & Wang, R. (2020). The role of Aurora-A in human cancers and future therapeutics. *American Journal of Cancer Research*, *10*(9), 2705. /pmc/articles/PMC7539775/

Lin, Y.-C., Chang, C.-W., Hsu, W.-B., Tang, C.-J. C., Lin, Y.-N., Chou, E.-J., Wu, C.-T., & Tang, T. K. (2013). Human microcephaly protein CEP135 binds to hSAS-6 and CPAP, and is required for centriole assembly. *The EMBO Journal*, *32*(8), 1141–1154. https://doi.org/10.1038/emboj.2013.56

Lin, Y. N., Wu, C. T., Lin, Y. C., Hsu, W. Bin, Tang, C. J. C., Chang, C. W., & Tang, T. K. (2013). CEP120 interacts with CPAP and positively regulates centriole elongation. *Journal of Cell Biology*, *202*(2), 211–219. https://doi.org/10.1083/jcb.201212060

Lingle, W. L., Barrett, S. L., Negron, V. C., D'Assoro, A. B., Boeneman, K., Liu, W., Whitehead, C. M., Reynolds, C., & Salisbury, J. L. (2002). Centrosome amplification drives chromosomal instability in breast tumor development. *Proceedings of the National Academy of Sciences of the United States of*

America, *99*(4), 1978–1983. https://doi.org/10.1073/pnas.032479999

Löffler, H., Fechter, A., Liu, F. Y., Poppelreuther, S., & Krämer, A. (2013). DNA damage-induced centrosome amplification occurs via excessive formation of centriolar satellites. *Oncogene*, *32*(24), 2963–2972. https://doi.org/10.1038/onc.2012.310

Löffler, H., Fechter, A., Matuszewska, M., Saffrich, R., Mistrik, M., Marhold, J., Hornung, C., Westermann, F., Bartek, J., & Krämer, A. (2011). Cep63 recruits Cdk1 to the centrosome: Implications for regulation of mitotic entry, centrosome amplification, and genome maintenance. *Cancer Research*, *71*(6), 2129–2139. https://doi.org/10.1158/0008-5472.CAN-10-2684

Loncarek, J., & Bettencourt-Dias, M. (2018). Building the right centriole for each cell type. *The Journal of Cell Biology*, *217*(3), 823. https://doi.org/10.1083/JCB.201704093

Lončarek, J., Hergert, P., & Khodjakov, A. (2010). Centriole reduplication during prolonged interphase requires procentriole maturation governed by plk1. *Current Biology*, *20*(14), 1277–1282. https://doi.org/10.1016/j.cub.2010.05.050

Lopes, C. A. M., Jana, S. C., Cunha-Ferreira, I., Zitouni, S., Bento, I., Duarte, P., Gilberto, S., Freixo, F., Guerrero, A., Francia, M., Lince-Faria, M., Carneiro, J., & Bettencourt-Dias, M. (2015). PLK4 trans-Autoactivation Controls Centriole Biogenesis in Space. *Developmental Cell*, *35*(2), 222–235. https://doi.org/10.1016/j.devcel.2015.09.020

Lopes, C. A. M., Mesquita, M., Cunha, A. I., Cardoso, J., Carapeta, S., Laranjeira, C., Pinto, A. E., Pereira-Leal, J. B., Dias-Pereira, A., Bettencourt-Dias, M., & Chaves, P. (2018). Centrosome amplification arises before neoplasia and increases upon p53 loss in tumorigenesis. *Journal of Cell Biology*, *217*(7), 2353–2363. https://doi.org/10.1083/jcb.201711191

Lovén, J., Orlando, D. A., Sigova, A. A., Lin, C. Y., Rahl, P. B., Burge, C. B., Levens, D. L., Lee, T. I., & Young, R. A. (2012). Revisiting global gene expression analysis. *Cell*, *151*(3), 476–482. https://doi.org/10.1016/j.cell.2012.10.012

Lukasiewicz, K. B., & Lingle, W. L. (2009). Aurora A, centrosome structure, and the centrosome cycle. In *Environmental and Molecular Mutagenesis* (Vol. 50, Issue 8, pp. 602–619). https://doi.org/10.1002/em.20533

Maat, W., Beiboer, S. H. W., Jager, M. J., Luyten, G. P. M., Gruis, N. A., & Van Der Velden, P. A. (2008). Epigenetic Regulation Identifies RASEF as a Tumor-Suppressor Gene in Uveal Melanoma. *Investigative Ophthalmology & Visual Science*, *49*(4), 1291–1298. https://doi.org/10.1167/IOVS.07-1135

Macůrek, L., Lindqvist, A., Lim, D., Lampson, M. A., Klompmaker, R., Freire, R., Clouin, C., Taylor, S. S., Yaffe, M. B., & Medema, R. H. (2008). Polo-like kinase-1 is activated by aurora A to promote checkpoint recovery. *Nature 2008 455:7209*, *455*(7209), 119–123. https://doi.org/10.1038/nature07185

Magescas, J., Zonka, J. C., & Feldman, J. L. (2019). A two-step mechanism for the inactivation of microtubule organizing center function at the centrosome. *ELife*, *8*. https://doi.org/10.7554/ELIFE.47867

Maiato, H., & Logarinho, E. (2014). Mitotic spindle multipolarity without centrosome amplification. *Nature Cell Biology 2014 16:5*, *16*(5), 386–394. https://doi.org/10.1038/ncb2958

Manandhar, G., Schatten, H., & Sutovsky, P. (2005). Centrosome Reduction During Gametogenesis and Its Significance. *Biology of Reproduction*, *72*(1), 2–13. https://doi.org/10.1095/BIOLREPROD.104.031245

Mardin, B. R., Agircan, F. G., Lange, C., & Schiebel, E. (2011). Plk1 controls the Nek2A-PP1γ Antagonism in centrosome disjunction. *Current Biology*, *21*(13), 1145–1151. https://doi.org/10.1016/j.cub.2011.05.047

Mariappan, A., Soni, K., Schorpp, K., Zhao, F., Minakar, A., Zheng, X., Mandad, S., Macheleidt, I., Ramani, A., Kubelka, T., Dawidowski, M., Golfmann, K., Wason, A., Yang, C., Simons, J., Schmalz, H., Hyman, A. A., Aneja, R., Ullrich, R., … Gopalakrishnan, J. (2019). Inhibition of <scp>CPAP</scp> –tubulin interaction prevents proliferation of centrosome-amplified cancer cells. *The EMBO Journal*, *38*(2). https://doi.org/10.15252/embj.201899876

Marin Navarro, A., Pronk, R. J., van der Geest, A. T., Oliynyk, G., Nordgren, A., Arsenian-Henriksson, M., Falk, A., & Wilhelm, M. (2020). p53 controls genomic stability and temporal differentiation of human neural stem cells and affects neural organization in human brain organoids. *Cell Death and Disease*, *11*(1). https://doi.org/10.1038/s41419-019-2208-7

Marteil, G., Guerrero, A., Vieira, A. F., de Almeida, B. P., Machado, P., Mendonça, S., Mesquita, M., Villarreal, B., Fonseca, I., Francia, M. E., Dores, K., Martins, N. P., Jana, S. C., Tranfield, E. M., Barbosa-Morais, N. L., Paredes, J., Pellman, D., Godinho, S. A., & Bettencourt-Dias, M. (2018). Over-elongation of centrioles in cancer promotes centriole amplification and chromosome missegregation. *Nature Communications*, *9*(1), 1258. https://doi.org/10.1038/s41467-018-03641-x

Marthiens, V., Rujano, M. A., Pennetier, C., Tessier, S., Paul-Gilloteaux, P., & Basto, R. (2013). Centrosome amplification causes microcephaly. *Nature Cell Biology*, *15*(7), 731–740. https://doi.org/10.1038/ncb2746

Martinez-Campos, M., Basto, R., Baker, J., Kernan, M., & Raff, J. W. (2004). The Drosophila pericentrin-like protein is essential for cilia/flagella function, but appears to be dispensable for mitosis. *Journal of Cell Biology*, *165*(5), 673–683. https://doi.org/10.1083/jcb.200402130

Marumoto, T., Hirota, T., Morisaki, T., Kunitoku, N., Zhang, D., Ichikawa, Y., Sasayama, T., Kuninaka, S., Mimori, T., Tamaki, N., Kimura, M., Okano, Y., & Saya, H. (2002). Roles of aurora-A kinase in mitotic entry and G2 checkpoint in mammalian cells. *Genes to Cells*, *7*(11), 1173–1182. https://doi.org/10.1046/J.1365-2443.2002.00592.X

Marumoto, T., Honda, S., Hara, T., Nitta, M., Hirota, T., Kohmura, E., & Saya, H. (2003). Aurora-A Kinase Maintains the Fidelity of Early and Late Mitotic Events in HeLa Cells. *Journal of Biological Chemistry*, *278*(51), 51786–51795. https://doi.org/10.1074/jbc.M306275200

Marzec, M., Eletto, D., & Argon, Y. (2012). GRP94: an HSP90-like protein specialized

for protein folding and quality control in the Endoplasmic Reticulum. *Biochimica et Biophysica Acta*, *1823*(3), 774. https://doi.org/10.1016/J.BBAMCR.2011.10.013

Matthews, H. K., Bertoli, C., & de Bruin, R. A. M. (2021). Cell cycle control in cancer. *Nature Reviews Molecular Cell Biology 2021 23:1*, *23*(1), 74–88. https://doi.org/10.1038/s41580-021-00404-3

McGarry, T. J., & Kirschner, M. W. (1998). Geminin, an Inhibitor of DNA Replication, Is Degraded during Mitosis. *Cell*, *93*(6), 1043–1053. https://doi.org/10.1016/S0092-8674(00)81209-X

Melixetian, M., Ballabeni, A., Masiero, L., Gasparini, P., Zamponi, R., Bartek, J., Lukas, J., & Helin, K. (2004). Loss of Geminin induces rereplication in the presence of functional p53. *The Journal of Cell Biology*, *165*(4), 473. https://doi.org/10.1083/JCB.200403106

Meraldi, P. (2016). Centrosomes in spindle organization and chromosome segregation: a mechanistic view. *Chromosome Research*, *24*(1), 19–34. https://doi.org/10.1007/s10577-015-9508-2

Meraldi, P., Honda, R., & Nigg, E. A. (2002). Aurora-A overexpression reveals tetraploidization as a major route to centrosome amplification in p53-/- cells. *EMBO Journal*, *21*(4), 483–492. https://doi.org/10.1093/emboj/21.4.483

Mittal, K., Kaur, J., Jaczko, M., Wei, G., Toss, M. S., Rakha, E. A., Janssen, E. A. M., Søiland, H., Kucuk, O., Reid, M. D., Gupta, M. V., & Aneja, R. (2021). Centrosome amplification: a quantifiable cancer cell trait with prognostic value in solid malignancies. *Cancer Metastasis Reviews*, *40*(1), 319. https://doi.org/10.1007/S10555-020-09937-Z

Mittal, K., Kaur, J., Sharma, S., Sharma, N., Wei, G., Choudhary, I., Imhansi-Jacob, P., Maganti, N., Pawar, S., Rida, P., Toss, M. S., Aleskandarany, M., Janssen, E. A., Søiland, H., Gupta, M. V., Reid, M. D., Rakha, E. A., & Aneja, R. (2022). Hypoxia Drives Centrosome Amplification in Cancer Cells via HIF1α-dependent Induction of Polo-Like Kinase 4PLK4 is HIF1α Target Gene. *Molecular Cancer Research*,

20(4), 596–606. https://doi.org/10.1158/1541-7786.MCR-20-0798

Mohr, S. E., & Perrimon, N. (2012). RNAi Screening: New Approaches, Understandings and Organisms. *Wiley Interdisciplinary Reviews. RNA*, *3*(2), 145. https://doi.org/10.1002/WRNA.110

Mori, D., Yano, Y., Toyo-oka, K., Yoshida, N., Yamada, M., Muramatsu, M., Zhang, D., Saya, H., Toyoshima, Y. Y., Kinoshita, K., Wynshaw-Boris, A., & Hirotsune, S. (2007). NDEL1 Phosphorylation by Aurora-A Kinase Is Essential for Centrosomal Maturation, Separation, and TACC3 Recruitment. *Molecular and Cellular Biology*, *27*(1).

Morris, E. J., Kawamura, E., Gillespie, J. A., Balgi, A., Kannan, N., Muller, W. J., Roberge, M., & Dedhar, S. (2017). Stat3 regulates centrosome clustering in cancer cells via Stathmin/PLK1. *Nature Communications*, *8*. https://doi.org/10.1038/NCOMMS15289

Mort, R. L., Ford, M. J., Sakaue-Sawano, A., Lindstrom, N. O., Casadio, A., Douglas, A. T., Keighren, M. A., Hohenstein, P., Miyawaki, A., & Jackson, I. J. (2014). Fucci2a: a bicistronic cell cycle reporter that allows Cre mediated tissue specific expression in mice. *Cell Cycle (Georgetown, Tex.)*, *13*(17), 2681–2696. https://doi.org/10.4161/15384101.2015.945381

Moss, D. K., Bellett, G., Carter, J. M., Liovic, M., Keynton, J., Prescott, A. R., Lane, E. B., & Mogensen, M. M. (2007). Ninein is released from the centrosome and moves bi-directionally along microtubules. *Journal of Cell Science*, *120*(17), 3064–3074. https://doi.org/10.1242/JCS.010322

Mou, P. K., Yang, E. J., Shi, C., Ren, G., Tao, S., & Shim, J. S. (2021). Aurora kinase A, a synthetic lethal target for precision cancer medicine. *Experimental & Molecular Medicine 2021 53:5*, *53*(5), 835–847. https://doi.org/10.1038/s12276-021-00635-6

Mountain, V., Simerly, C., Howard, L., Ando, A., Schatten, G., & Compton, D. A. (1999). The kinesin-related protein, HSET, opposes the activity of Eg5 and cross-links microtubules in the mammalian mitotic spindle. *Journal of Cell Biology*,

147(2), 351–365. https://doi.org/10.1083/jcb.147.2.351

Nathan, P., Cohen, V., Coupland, S., Curtis, K., Damato, B., Evans, J., Fenwick, S., Kirkpatrick, L., Li, O., Marshall, E., Mcguirk, K., Ottensmeier, C., Pearce, N., Salvi, S., Stedman, B., Szlosarek, P., & Turnbull, N. (2015). *Uveal Melanoma UK National Guidelines*. https://doi.org/10.1016/j.ejca.2015.07.013

Nathan, P., Hassel, J. C., Rutkowski, P., Baurain, J.-F., Butler, M. O., Schlaak, M., Sullivan, R. J., Ochsenreither, S., Dummer, R., Kirkwood, J. M., Joshua, A. M., Sacco, J. J., Shoushtari, A. N., Orloff, M., Piulats, J. M., Milhem, M., Salama, A. K. S., Curti, B., Demidov, L., … Piperno-Neumann, S. (2021). Overall Survival Benefit with Tebentafusp in Metastatic Uveal Melanoma. *New England Journal of Medicine*, *385*(13), 1196–1206. https://doi.org/10.1056/NEJMOA2103485/SUPPL_FILE/NEJMOA2103485_DATA-SHARING.PDF

Navarro-Serer, B., Childers, E. P., Hermance, N. M., Mercadante, D., & Manning, A. L. (2019). Aurora A inhibition limits centrosome clustering and promotes mitotic catastrophe in cells with supernumerary centrosomes. *Oncotarget*, *10*(17), 1649. https://doi.org/10.18632/ONCOTARGET.26714

Nigg, E. A. (2002). Centrosome aberrations: cause or consequence of cancer progression? *Nature Reviews Cancer*, *2*(11), 815–825. https://doi.org/10.1038/nrc924

Nigg, E. A., & Holland, A. J. (2018). Once and only once: Mechanisms of centriole duplication and their deregulation in diseases. In *Nature Reviews Molecular Cell Biology* (Vol. 19, Issue 5, pp. 297–312). Nature Publishing Group. https://doi.org/10.1038/nrm.2017.127

Nigg, E. A., & Raff, J. W. (2009). Centrioles, centrosomes, and cilia in health and disease. *Cell*, *139*(4), 663–678. https://doi.org/10.1016/J.CELL.2009.10.036

Nigg, E. A., & Stearns, T. (2011). The centrosome cycle: Centriole biogenesis, duplication and inherent asymmetries. *Nature Cell Biology*, *13*(10), 1154–1160. https://doi.org/10.1038/ncb2345

Novak, Z. A. A., Wainman, A., Gartenmann, L., & Raff, J. W. W. (2016). Cdk1 Phosphorylates Drosophila Sas-4 to Recruit Polo to Daughter Centrioles and Convert Them to Centrosomes. *Developmental Cell*, *37*(6), 545–557. https://doi.org/10.1016/j.devcel.2016.05.022

Ogden, A., Rida, P. C. G., & Aneja, R. (2017). Prognostic value of CA20, a score based on centrosome amplification-associated genes, in breast tumors. *Scientific Reports*, *7*(1), 262. https://doi.org/10.1038/s41598-017-00363-w

Ohashi, S., Sakashita, G., Ban, R., Nagasawa, M., Matsuzaki, H., Murata, Y., Taniguchi, H., Shima, H., Furukawa, K., & Urano, T. (2006). Phospho-regulation of human protein kinase Aurora-A: analysis using anti-phospho-Thr288 monoclonal antibodies. *Oncogene 2006 25:59*, *25*(59), 7691–7702. https://doi.org/10.1038/sj.onc.1209754

Pannu, V., Rida, P. C. G., Ogden, A., Clewley, R., Cheng, A., Karna, P., Lopus, M., Mishra, R. C., Zhou, J., & Aneja, R. (2012). Induction of robust de novo centrosome amplification, high-grade spindle multipolarity and metaphase catastrophe: A novel chemotherapeutic approach. *Cell Death and Disease*, *3*(7), e346–e346. https://doi.org/10.1038/cddis.2012.82

Patel, N., Weekes, D., Drosopoulos, K., Gazinska, P., Noel, E., Rashid, M., Mirza, H., Quist, J., Brasó-Maristany, F., Mathew, S., Ferro, R., Pereira, A. M., Prince, C., Noor, F., Francesch-Domenech, E., Marlow, R., De Rinaldis, E., Grigoriadis, A., Linardopoulos, S., … Tutt, A. N. J. (2018). Integrated genomics and functional validation identifies malignant cell specific dependencies in triple negative breast cancer. *Nature Communications*, *9*(1). https://doi.org/10.1038/S41467-018-03283-Z

Piehl, M., Tulu, U. S., Wadsworth, P., & Cassimeris, L. (2004). Centrosome maturation: Measurement of microtubule nucleation throughout the cell cycle by using GFP-tagged EB1. *Proceedings of the National Academy of Sciences of the United States of America*, *101*(6), 1584–1588. https://doi.org/10.1073/PNAS.0308205100/SUPPL_FILE/8205MOVIE2.MOV

Pijuan, J., Barceló, C., Moreno, D. F., Maiques, O., Sisó, P., Marti, R. M., Macià, A., & Panosa, A. (2019). In vitro cell migration, invasion, and adhesion assays: From cell imaging to data analysis. *Frontiers in Cell and Developmental Biology*, *7*(JUN), 107. https://doi.org/10.3389/FCELL.2019.00107/BIBTEX

Pike, A. N., & Fisk, H. A. (2011). Centriole assembly and the role of Mps1: Defensible or dispensable? *Cell Division*, *6*(1), 1–13. https://doi.org/10.1186/1747-1028-6-9/FIGURES/6

Pines, J., & Hunter, T. (1989). Isolation of a human cyclin cDNA: Evidence for cyclin mRNA and protein regulation in the cell cycle and for interaction with p34cdc2. *Cell*, *58*(5), 833–846. https://doi.org/10.1016/0092-8674(89)90936-7

Pines, J., & Hunter, T. (1991). Human Cyclins A and Bl Are Differentially Located in the Cell and Undergo Cell Cycle-Dependent Nuclear Transport. *The Journal of Cell Biology*, *115*(1), 1–17.

Prakash, A., Paunikar, S., Webber, M., McDermott, E., Vellanki, S. H., Thompson, K., Dockery, P., Jahns, H., Brown, J. A. L., Hopkins, A. M., & Bourke, E. (2022). "Centrosome Amplification promotes cell invasion via cell-cell contact disruption and Rap-1 activation." *BioRxiv*, 2022.05.09.490051. https://doi.org/10.1101/2022.05.09.490051

Prescher, G., Bornfeld, N., & Becher, R. (1990). Nonrandom chromosomal abnormalities in primary uveal melanoma. *Journal of the National Cancer Institute*, *82*(22), 1765–1769. http://www.ncbi.nlm.nih.gov/pubmed/2231772

Prescher, G., Bornfeld, N., & Becher, R. (1994). Two subclones in a case of uveal melanoma. Relevance of monosomy 3 and multiplication of chromosome 8q. *Cancer Genetics and Cytogenetics*, *77*(2), 144–146. http://www.ncbi.nlm.nih.gov/pubmed/7954325

Prescher, G., Bornfeld, N., Hirche, H., Horsthemke, B., Jöckel, K. H., & Becher, R. (1996). Prognostic implications of monosomy 3 in uveal melanoma. *Lancet (London, England)*, *347*(9010), 1222–1225. https://doi.org/10.1016/S0140-6736(96)90736-9

Prosser, S. L., Straatman, K. R., & Fry, A. M. (2009). Molecular Dissection of the Centrosome Overduplication Pathway in S-Phase-Arrested Cells. *Molecular and Cellular Biology*, *29*(7), 1760–1773. https://doi.org/10.1128/mcb.01124-08

Puklowski, A., Homsi, Y., Keller, D., May, M., Chauhan, S., Kossatz, U., Grünwald, V., Kubicka, S., Pich, A., Manns, M. P., Hoffmann, I., Gönczy, P., & Malek, N. P. (2011). The SCF-FBXW5 E3-ubiquitin ligase is regulated by PLK4 and targets HsSAS-6 to control centrosome duplication. *Nature Cell Biology*, *13*(8), 1004–1009. https://doi.org/10.1038/ncb2282

Putzbach, W., Gao, Q. Q., Patel, M., Haluck-Kangas, A., Murmann, A. E., & Peter, M. E. (2018). DISE - A Seed Dependent RNAi Off-Target Effect that Kills Cancer Cells. *Trends in Cancer*, *4*(1), 10. https://doi.org/10.1016/J.TRECAN.2017.11.007

Quintyne, N. J., Reing, J. E., Hoffelder, D. R., Gollin, S. M., & Saunders, W. S. (2005). Spindle multipolarity is prevented by centrosomal clustering. *Science (New York, N.Y.)*, *307*(5706), 127–129. https://doi.org/10.1126/SCIENCE.1104905

Raff, J. W. (2002). Centrosomes and cancer: Lessons from a TACC. In *Trends in Cell Biology* (Vol. 12, Issue 5, pp. 222–225). Elsevier Current Trends. https://doi.org/10.1016/S0962-8924(02)02268-7

Ramani, A., Mariappan, A., Gottardo, M., Mandad, S., Urlaub, H., Avidor-Reiss, T., Riparbelli, M., Callaini, G., Debec, A., Feederle, R., & Gopalakrishnan, J. (2018). Plk1/Polo Phosphorylates Sas-4 at the Onset of Mitosis for an Efficient Recruitment of Pericentriolar Material to Centrosomes. *Cell Reports*, *25*(13), 3618-3630.e6. https://doi.org/10.1016/j.celrep.2018.11.102

Rantala, E. S., Hernberg, M., & Kivelä, T. T. (2019). Overall survival after treatment for metastatic uveal melanoma: a systematic review and meta-analysis. *Melanoma Research*, *29*(6), 561. https://doi.org/10.1097/CMR.0000000000000575

Robertson, A. G., Shih, J., Yau, C., Gibb, E. A., Oba, J., Mungall, K. L., Hess, J. M., Uzunangelov, V., Walter, V., Danilova, L., Lichtenberg, T. M., Kucherlapati, M., Kimes, P. K., Tang, M., Penson, A., Babur, O., Akbani, R., Bristow, C. A., Hoadley,

K. A., … Zmuda, E. (2017). Integrative Analysis Identifies Four Molecular and Clinical Subsets in Uveal Melanoma. *Cancer Cell*, *32*(2), 204-220.e15. https://doi.org/10.1016/j.ccell.2017.07.003

Saatci, O., Akbulut, O., Cetin, M., Sikirzhytski, V., & Sahin, O. (2022). Targeting TACC3 represents a novel vulnerability in highly aggressive breast cancers with centrosome amplification. *BioRxiv*, 2022.05.18.492567. https://doi.org/10.1101/2022.05.18.492567

Sabat-Pośpiech, D., Fabian-Kolpanowicz, K., Kalirai, H., Kipling, N., Coupland, S. E., Coulson, J. M., & Fielding, A. B. (2022). Aggressive uveal melanoma displays a high degree of centrosome amplification, opening the door to therapeutic intervention. *The Journal of Pathology: Clinical Research*, *8*(4), 383–394. https://doi.org/10.1002/CJP2.272

Sabat-Pośpiech, D., Fabian-Kolpanowicz, K., Prior, I. A., Coulson, J. M., & Fielding, A. B. (2019). Targeting centrosome amplification, an Achilles' heel of cancer. *Biochemical Society Transactions*, *47*(5), 1209–1222. https://doi.org/10.1042/BST20190034

Sacco, J. J., Kenyani, J., Butt, Z., Carter, R., Chew, H. Y., Cheeseman, L. P., Darling, S., Denny, M., Urbé, S., Clague, M. J., Coulson, J. M., Sacco, J. J., Kenyani, J., Butt, Z., Carter, R., Chew, H. Y., Cheeseman, L. P., Darling, S., Denny, M., … Coulson, J. M. (2015). Loss of the deubiquitylase BAP1 alters class I histone deacetylase expression and sensitivity of mesothelioma cells to HDAC inhibitors. *Oncotarget*, *6*(15), 13757–13771. https://doi.org/10.18632/ONCOTARGET.3765

Sakaue-Sawano, A., Kurokawa, H., Morimura, T., Hanyu, A., Hama, H., Osawa, H., Kashiwagi, S., Fukami, K., Miyata, T., Miyoshi, H., Imamura, T., Ogawa, M., Masai, H., & Miyawaki, A. (2008). Visualizing Spatiotemporal Dynamics of Multicellular Cell-Cycle Progression. *Cell*, *132*(3), 487–498. https://doi.org/10.1016/j.cell.2007.12.033

Sakaue-Sawano, A., Yo, M., Komatsu, N., Hiratsuka, T., Kogure, T., Hoshida, T., Goshima, N., Matsuda, M., Miyoshi, H., & Miyawaki, A. (2017). Genetically

Encoded Tools for Optical Dissection of the Mammalian Cell Cycle. *Molecular Cell*, *68*(3), 626-640.e5. https://doi.org/10.1016/J.MOLCEL.2017.10.001

Sandinha, M. T., Farquharson, M. A., McKay, I. C., & Roberts, F. (2005). Monosomy 3 Predicts Death but Not Time until Death in Choroidal Melanoma. *Investigative Opthalmology & Visual Science*, *46*(10), 3497. https://doi.org/10.1167/iovs.05-0613

Santamaria, A., Nagel, S., Sillje, H. H. W., & Nigg, E. A. (2008). The spindle protein CHICA mediates localization of the chromokinesin Kid to the mitotic spindle. *Current Biology : CB*, *18*(10), 723–729. https://doi.org/10.1016/J.CUB.2008.04.041

Schmidt, T. I., Kleylein-Sohn, J., Westendorf, J., Le Clech, M., Lavoie, S. B., Stierhof, Y. D., & Nigg, E. A. (2009). Control of Centriole Length by CPAP and CP110. *Current Biology*, *19*(12), 1005–1011. https://doi.org/10.1016/j.cub.2009.05.016

Schmidt, U., Weigert, M., Broaddus, C., & Myers, G. (2018). Cell detection with star-convex polygons. *Lecture Notes in Computer Science (Including Subseries Lecture Notes in Artificial Intelligence and Lecture Notes in Bioinformatics)*, *11071 LNCS*, 265–273. https://doi.org/10.1007/978-3-030-00934-2_30/COVER

Schnittger, A., & De Veylder, L. (2018). The Dual Face of Cyclin B1. *Trends in Plant Science*, *23*(6), 475–478. https://doi.org/10.1016/j.tplants.2018.03.015

Schroeder, A., Mueller, O., Stocker, S., Salowsky, R., Leiber, M., Gassmann, M., Lightfoot, S., Menzel, W., Granzow, M., & Ragg, T. (2006). The RIN: an RNA integrity number for assigning integrity values to RNA measurements. *BMC Molecular Biology*, *7*, 3. https://doi.org/10.1186/1471-2199-7-3

Schwanhüusser, B., Busse, D., Li, N., Dittmar, G., Schuchhardt, J., Wolf, J., Chen, W., & Selbach, M. (2011). Global quantification of mammalian gene expression control. *Nature 2011 473:7347*, *473*(7347), 337–342. https://doi.org/10.1038/nature10098

Serçin, Ö., Larsimont, J.-C., Karambelas, A. E., Marthiens, V., Moers, V., Boeckx, B., Le Mercier, M., Lambrechts, D., Basto, R., & Blanpain, C. (2016). Transient PLK4

overexpression accelerates tumorigenesis in p53-deficient epidermis. *Nature Cell Biology*, *18*(1), 100–110. https://doi.org/10.1038/ncb3270

Shao, S., Wang, Y., Jin, S., Song, Y., Wang, X., Fan, W., Zhao, Z., Fu, M., Tong, T., Dong, L., Fan, F., Xu, N., & Zhan, Q. (2006). Gadd45a interacts with aurora-A and inhibits its kinase activity. *The Journal of Biological Chemistry*, *281*(39), 28943–28950. https://doi.org/10.1074/JBC.M600235200

Sharma, A., Aher, A., Dynes, N. J., Frey, D., Katrukha, E. A., Jaussi, R., Grigoriev, I., Croisier, M., Kammerer, R. A., Akhmanova, A., Gönczy, P., & Steinmetz, M. O. (2016). Centriolar CPAP/SAS-4 Imparts Slow Processive Microtubule Growth. *Developmental Cell*, *37*(4), 362–376. https://doi.org/10.1016/j.devcel.2016.04.024

She, Z.-Y., & Yang, W.-X. (2017). Molecular mechanisms of kinesin-14 motors in spindle assembly and chromosome segregation. *Journal of Cell Science*, *130*(13), 2097–2110. https://doi.org/10.1242/jcs.200261

Shinmura, K., Kurabe, N., Goto, M., Yamada, H., Natsume, H., Konno, H., & Sugimura, H. (2014). PLK4 overexpression and its effect on centrosome regulation and chromosome stability in human gastric cancer. *Molecular Biology Reports*, *41*(10), 6635–6644. https://doi.org/10.1007/s11033-014-3546-2

Sibon, O. C. M., Kelkar, A., Lemstra, W., & Theurkauf, W. E. (2000). DNA-replication/DNA-damage-dependent centrosome inactivation in Drosophila embryos. *Nature Cell Biology 2000 2:2*, *2*(2), 90–95. https://doi.org/10.1038/35000041

Sigoillot, F. D., & King, R. W. (2011). Vigilance and Validation: Keys to Success in RNAi Screening. *ACS Chemical Biology*, *6*(1), 47. https://doi.org/10.1021/CB100358F

Singh, A. D., & Topham, A. (2003). Incidence of uveal melanoma in the United States: 1973-1997. *Ophthalmology*, *110*(5), 956–961. https://doi.org/10.1016/S0161-6420(03)00078-2

Smith, E., Hégarat, N., Vesely, C., Roseboom, I., Larch, C., Streicher, H., Straatman, K., Flynn, H., Skehel, M., Hirota, T., Kuriyama, R., & Hochegger, H. (2011).

Differential control of Eg5-dependent centrosome separation by Plk1 and Cdk1. *EMBO Journal*, *30*(11), 2233–2245. https://doi.org/10.1038/emboj.2011.120

Spektor, A., Tsang, W. Y., Khoo, D., & Dynlacht, B. D. (2007). Cep97 and CP110 Suppress a Cilia Assembly Program. *Cell*, *130*(4), 678–690. https://doi.org/10.1016/j.cell.2007.06.027

Stillwell, E. E., Zhou, J., & Joshi, H. C. (2006). Human Ninein is a Centrosomal Autoantigen Recognized by CREST Patient Sera and Plays a Regulatory Role in Microtubule Nucleation. *Https://Doi.Org/10.4161/Cc.3.7.947*, *3*(7), 921–928. https://doi.org/10.4161/CC.3.7.947

Sumiyoshi, E., Sugimoto, A., & Yamamoto, M. (2002). Protein phosphatase 4 is required for centrosome maturation in mitosis and sperm meiosis in C. elegans. *Journal of Cell Science*, *115*(7), 1403–1410.

Takao, D., Watanabe, K., Kuroki, K., & Kitagawa, D. (2019). Feedback loops in the Plk4–STIL–HsSAS6 network coordinate site selection for procentriole formation. *Biology Open*, *8*(9). https://doi.org/10.1242/bio.047175

Tang, C.-J. C., Lin, S.-Y., Hsu, W.-B., Lin, Y.-N., Wu, C.-T., Lin, Y.-C., Chang, C.-W., Wu, K.-S., & Tang, T. K. (2011). The human microcephaly protein STIL interacts with CPAP and is required for procentriole formation. *The EMBO Journal*, *30*(23), 4790–4804. https://doi.org/10.1038/emboj.2011.378

Tetzlaff, M. T., Curry, J. L., Ivan, D., Wang, W. L., Torres-Cabala, C. A., Bassett, R. L., Valencia, K. M., McLemore, M. S., Ross, M. I., & Prieto, V. G. (2013). Immunodetection of phosphohistone H3 as a surrogate of mitotic figure count and clinical outcome in cutaneous melanoma. *Modern Pathology*, *26*(9), 1153–1160. https://doi.org/10.1038/modpathol.2013.59

Timp, W., & Timp, G. (2020). Beyond mass spectrometry, the next step in proteomics. *Science Advances*, *6*(2). https://doi.org/10.1126/SCIADV.AAX8978/ASSET/897695F4-32D4-46FF-9D1B-984C00442EBE/ASSETS/GRAPHIC/AAX8978-F7.JPEG

Toyo-oka, K., Mori, D., Yano, Y., Shiota, M., Iwao, H., Goto, H., Inagaki, M., Hiraiwa,

N., Muramatsu, M., Wynshaw-Boris, A., Yoshiki, A., & Hirotsune, S. (2008). Protein phosphatase 4 catalytic subunit regulates Cdk1 activity and microtubule organization via NDEL1 dephosphorylation. *Journal of Cell Biology*, *180*(6), 1133–1147. https://doi.org/10.1083/jcb.200705148

Tsekitsidou, E., Wang, J. T., Wong, C. J., Ulengin-Talkish, I., Stearns, T., Gingras, A.-C., & Cyert, M. S. (2022). Calcineurin associates with centrosomes and regulates cilia length maintenance. *BioRxiv*, 2022.06.16.496489. https://doi.org/10.1101/2022.06.16.496489

Uetake, Y., Lončarek, J., Nordberg, J. J., English, C. N., La Terra, S., Khodjakov, A., & Sluder, G. (2007). Cell cycle progression and de novo centriole assembly after centrosomal removal in untransformed human cells. *Journal of Cell Biology*, *176*(2), 173–182. https://doi.org/10.1083/jcb.200607073

van Beek, J. G. M., Buitendijk, G. H. S., Timman, R., Muller, K., Luyten, G. P. M., Paridaens, D., Naus, N. C., & Kiliç, E. (2018). Quality of life: fractionated stereotactic radiotherapy versus enucleation treatment in uveal melanoma patients. *Acta Ophthalmologica*, *96*(8), 841–848. https://doi.org/10.1111/AOS.13823

Vaziri, C., Saxena, S., Jeon, Y., Lee, C., Murata, K., Machida, Y., Wagle, N., Hwang, D. S., & Dutta, A. (2003). A p53-Dependent Checkpoint Pathway Prevents Rereplication. *Molecular Cell*, *11*(4), 997–1008. https://doi.org/10.1016/S1097-2765(03)00099-6

Virgili, G., Gatta, G., Ciccolallo, L., Capocaccia, R., Biggeri, A., Crocetti, E., Lutz, J.-M., & Paci, E. (2007). Incidence of Uveal Melanoma in Europe. *Ophthalmology*, *114*(12), 2309-2315.e2. https://doi.org/10.1016/J.OPHTHA.2007.01.032

Vitre, B., Holland, A. J., Kulukian, A., Shoshani, O., Hirai, M., Wang, Y., Maldonado, M., Cho, T., Boubaker, J., Swing, D. A., Tessarollo, L., Evans, S. M., Fuchs, E., & Cleveland, D. W. (2015). Chronic centrosome amplification without tumorigenesis. *Proceedings of the National Academy of Sciences of the United States of America*, *112*(46), E6321-30.

https://doi.org/10.1073/pnas.1519388112

Wang, C. Y., Huang, E. Y. H., Huang, S. C., & Chung, B. C. (2015). DNA-PK/Chk2 induces centrosome amplification during prolonged replication stress. *Oncogene*, *34*(10), 1263–1269. https://doi.org/10.1038/onc.2014.74

Wang, G., Jiang, Q., & Zhang, C. (2014). The role of mitotic kinases in coupling the centrosome cycle with the assembly of the mitotic spindle. In *Journal of Cell Science* (Vol. 127, Issue 19, pp. 4111–4122). Company of Biologists Ltd. https://doi.org/10.1242/jcs.151753

Wang, L., Failler, M., Fu, W., & Dynlacht, B. D. (2018). A distal centriolar protein network controls organelle maturation and asymmetry. *Nature Communications 2018 9:1*, *9*(1), 1–15. https://doi.org/10.1038/s41467-018-06286-y

Wang, L., Han, H., Dong, L., Wang, Z., & Qin, Y. (2021). Function of p21 and its therapeutic effects in esophageal cancer (Review). *Oncology Letters*, *21*(2), 1–1. https://doi.org/10.3892/OL.2020.12397/HTML

Wang, M., Knudsen, B. S., Nagle, R. B., Rogers, G. C., & Cress, A. E. (2019). A method of quantifying centrosomes at the single-cell level in human normal and cancer tissue. *Molecular Biology of the Cell*, *30*(7), 811–819. https://doi.org/10.1091/MBC.E18-10-0651/ASSET/IMAGES/LARGE/MBC-30-811-G005.JPEG

Wang, M., Rogers, G. C., & Cress, A. E. (2019). Immunofluorescence-based Determination of Centrosome Number in Tissue Samples. *Bio-Protocol*, *9*(20). https://doi.org/10.21769/BIOPROTOC.3396

Wang, X., Zhou, Y. X., Qiao, W., Tominaga, Y., Ouchi, M., Ouchi, T., & Deng, C. X. (2006). Overexpression of aurora kinase A in mouse mammary epithelium induces genetic instability preceding mammary tumor formation. *Oncogene 2006 25:54*, *25*(54), 7148–7158. https://doi.org/10.1038/sj.onc.1209707

Watts, C. A., Richards, F. M., Bender, A., Bond, P. J., Korb, O., Kern, O., Riddick, M., Owen, P., Myers, R. M., Raff, J., Gergely, F., Jodrell, D. I., & Ley, S. V. (2013).

Design, synthesis, and biological evaluation of an allosteric inhibitor of HSET that targets cancer cells with supernumerary centrosomes. *Chemistry and Biology*, *20*(11), 1399–1410. https://doi.org/10.1016/j.chembiol.2013.09.012

Wei, W., Ayad, N. G., Wan, Y., Zhang, G. J., Kirschner, M. W., & Kaelin, W. G. (2004). Degradation of the SCF component Skp2 in cell-cycle phase G1 by the anaphase-promoting complex. *Nature*, *428*(6979), 194–198. https://doi.org/10.1038/NATURE02381

Weigert, M., Schmidt, U., Haase, R., Sugawara, K., & Myers, G. (n.d.). *Star-convex Polyhedra for 3D Object Detection and Segmentation in Microscopy*. Retrieved August 4, 2022, from https://github.com/

Wu, J., Mikule, K., Wang, W., Su, N., Petteruti, P., Gharahdaghi, F., Code, E., Zhu, X., Jacques, K., Lai, Z., Yang, B., Lamb, M. L., Chuaqui, C., Keen, N., & Chen, H. (2013). Discovery and mechanistic study of a small molecule inhibitor for motor protein KIFC1. *ACS Chemical Biology*, *8*(10), 2201–2208. https://doi.org/10.1021/cb400186w

Yang, J., Adamian, M., & Li, T. (2006). Rootletin interacts with C-Nap1 and may function as a physical linker between the pair of centrioles/basal bodies in cells. *Molecular Biology of the Cell*, *17*(2), 1033–1040. https://doi.org/10.1091/mbc.E05-10-0943

Ye, C., Zhang, X., Wan, J., Chang, L., Hu, W., Bing, Z., Zhang, S., Li, J., He, J., Wang, J., & Zhou, G. (2013). Radiation-induced cellular senescence results from a slippage of long-term G2 arrested cells into G1 phase. *Cell Cycle*, *12*(9), 1424. https://doi.org/10.4161/CC.24528

Ye, X., Zeng, H., Ning, G., Reiter, J. F., & Liu, A. (2014). C2cd3 is critical for centriolar distal appendage assembly and ciliary vesicle docking in mammals. *Proceedings of the National Academy of Sciences of the United States of America*, *111*(6), 2164–2169. https://doi.org/10.1073/PNAS.1318737111/-/DCSUPPLEMENTAL

Yoshino, Y., Kobayashi, A., Qi, H., Endo, S., Fang, Z., Shindo, K., Kanazawa, R., & Chiba, N. (2020). RACK1 regulates centriole duplication through promoting the

activation of polo-like kinase 1 by Aurora A. *Journal of Cell Science*, *133*(17). https://doi.org/10.1242/JCS.238931/266530/AM/RACK1-REGULATES-CENTRIOLE-DUPLICATION-THROUGH-THE

Yu, H., Chen, Q., Wang, Z., Qian, X., & Pan, Y. (2022). Pan-cancer and single-cell analysis reveals FAM83D expression as a cancer prognostic biomarker. *Frontiers in Genetics*, *13*. https://doi.org/10.3389/FGENE.2022.1009325/FULL

Yu, H., Cheng, Y., Li, W., Li, Z., Wu, P., Qiu, S., Zeng, B., & Huang, B. (2020). A novel lncRNA–miRNA–mRNA competitive endogenous RNA network for uveal melanoma prognosis constructed by weighted gene co-expression network analysis. *Life Sciences*, *260*. https://doi.org/10.1016/j.lfs.2020.118409

Zhang, C. Z., Spektor, A., Cornils, H., Francis, J. M., Jackson, E. K., Liu, S., Meyerson, M., & Pellman, D. (2015). Chromothripsis from DNA damage in micronuclei. *Nature*, *522*(7555), 179–184. https://doi.org/10.1038/nature14493

Zhang, P., Ni, X., Guo, Y., Guo, X., Wang, Y., Zhou, Z., Huo, R., & Sha, J. (2009). Proteomic-based identification of maternal proteins in mature mouse oocytes. *BMC Genomics*, *10*(1), 1–11. https://doi.org/10.1186/1471-2164-10-348/FIGURES/6

Zhang, W., Zhai, L., Wang, Y., Boohaker, R. J., Lu, W., Gupta, V. V., Padmalayam, I., Bostwick, R. J., White, E. L., Ross, L. J., Maddry, J., Ananthan, S., Augelli-Szafran, C. E., Suto, M. J., Xu, B., Li, R., & Li, Y. (2016). Discovery of a novel inhibitor of kinesin-like protein KIFC1. *Biochemical Journal*, *473*(8), 1027–1035. https://doi.org/10.1042/BJ20150992

Zhao, H., Zhu, L., Zhu, Y., Cao, J., Li, S., Huang, Q., Xu, T., Huang, X., Yan, X., & Zhu, X. (2013). The cep63 paralogue deup1 enables massive de novo centriole biogenesis for vertebrate multiciliogenesis. *Nature Cell Biology*, *15*(12), 1434–1444. https://doi.org/10.1038/ncb2880

Zhou, H., Kuang, J., Zhong, L., Kuo, W. L., Gray, J. W., Sahin, A., Brinkley, B. R., & Sen, S. (1998). Tumour amplified kinase STK15/BTAK induces centrosome amplification, aneuploidy and transformation. *Nature Genetics 1998 20:2*, *20*(2),

189–193. https://doi.org/10.1038/2496

Zubarev, R. A. (2013). The challenge of the proteome dynamic range and its implications for in-depth proteomics. *PROTEOMICS*, *13*(5), 723–726. https://doi.org/10.1002/PMIC.201200451

Appendix A

siRNAs used in siRNA screen

siRNAs were for the siRNA screen were ordered from Qiagen in the Flexi Plate format. Details of the siRNA codes and names can be found in the table.

	Plate 1		**Plate 2**		**Plate 3**		**Plate 4**	
Gene	siRNA code	siRNA name	siRNA code	siRNA name	siRNA code	siRNA name	siRNA code	siRNA name
Ran-BP1	SI04142089	Hs_RANBP1_7	SI03188381	Hs_RANBP1_6	SI00698208	Hs_RANBP1_4	SI00698201	Hs_RANBP1_3
HSP90B1	SI00302008	Hs_TRA1_5	SI02663738	Hs_TRA1_9	SI03044566	Hs_HSP90B1_1	SI02630838	Hs_TRA1_6
PPP4R2	SI04316473	Hs_PPP4R2_8	SI04186266	Hs_PPP4R2_7	SI04170677	Hs_PPP4R2_6	SI04131974	Hs_PPP4R2_5
HSPA6	SI04355113	Hs_HSPA6_8	SI04322353	Hs_HSPA6_7	SI04244219	Hs_HSPA6_6	SI042143399	Hs_HSPA6_5
PRKACB	SI02225468	Hs_PRKACB_10	SI02225461	Hs_PRKACB_9	SI03112900	Hs_PRKACB_16	SI03110569	Hs_PRKACB_15
PPP1R14C	SI03107118	Hs_PPP1R14C_7	SI03030321	Hs_PPP1R14C_6	SI02646231	Hs_PPP1R14C_5	SI00139937	Hs_PPP1R14C_3
CAMK2A	SI02641828	Hs_CAMK2A_6	SI02641821	Hs_CAMK2A_5	SI00112889	Hs_CAMK2A_2	SI00112882	Hs_CAMK2A_1
HSPA7	SI05394676	Hs_HSPA7_10	SI05394669	Hs_HSPA7_9	SI04933467	Hs_HSPA7_7	SI04917024	Hs_HSPA7_5
PLK4	SI02660371	Hs_PLK4_6	SI02758917	Hs_PLK4_7	SI02640358	Hs_PLK4_5	SI00104209	Hs_PLK4_4
CCNB1	SI02653147	Hs_CCNB1_5	SI02653896	Hs_CCNB1_6	SI04381524	Hs_CCNB1_8	SI03035396	Hs_CCNB1_7
MDM2	SI02653392	Hs_MDM2_10	SI00300846	Hs_MDM2_5	SI02652979	Hs_MDM2_9	SI03092607	Hs_MDM2_12
TTK	SI02223207	Hs_TTK_6	SI02223214	Hs_TTK_7	SI04898747	Hs_TTK_12	SI03062745	Hs_TTK_9
PLK1	SI02223837	Hs_PLK1_6	SI02223844	Hs_PLK1_7	SI04376365	Hs_PLK1_11	SI00071638	Hs_PLK1_4
NEK2	SI00605640	Hs_NEK2_5	SI00605647	Hs_NEK2_6	SI03023279	Hs_NEK2_9	SI02628703	Hs_NEK2_7
AURKA	SI02223305	Hs_STK6_5	SI02631384	Hs_STK6_6	SI04380796	Hs_AURKA_4	SI03114111	Hs_AURKA_1
CEP135	SI04306358	Hs_CEP135_4	SI04270175	Hs_CEP135_3	SI04236330	Hs_CEP135_2	SI04182430	Hs_CEP135_1
CPAP	SI04222127	Hs_CENPJ_8	SI04160016	Hs_CENPJ_6	SI04157804	Hs_CENPJ_5	SI05021044	Hs_CENPJ_9
Ninein	SI05392758	Hs_NIN_17	SI05392751	Hs_NIN_16	SI05392744	Hs_NIN_15	SI04288445	Hs_NIN_7
p21	SI00299810	Hs_CDKN1A_5	SI00604898	Hs_CDKN1A_6	SI00604905	Hs_CDKN1A_7	SI03031105	Hs_CDKN1A_9
TACC2	SI04223723	Hs_TACC2_9	SI04194225	Hs_TACC2_8	SI04171454	Hs_TACC2_7	SI04135551	Hs_TACC2_6
MYC	SI00300902	Hs_MYC_5	SI02662611	Hs_MYC_7	SI03101847	Hs_MYC_9	SI03068926	Hs_MYC_8
CCND1	SI02654540	Hs_CCND1_5	SI02654547	Hs_CCND1_6	SI00147833	Hs_CCND1_4	SI00147826	Hs_CCND1_3

Appendix B

Quality control of cDNA library.

An example of each chart has been shown for each cell line. Error rate along reads (**A**). cDNA was synthesised in 150 bp fragments. Higher error rate is seen in the first six bases due to the random hexamers used to prime for cDNA synthesis. Error rate increases further along the read as reagents become more scarce. All samples had an overall error rate of 0.02 – 0.03%. Average A/T/G/C content along reads (**B**). As the library preparation was non-stranded, distribution should be such that A% = T% and G% = C%. Base distribution was also examined to confirm that there was no AT/GC separation, as this would affect gene expression quantification efforts. Charts showing the proportion of raw reads classified as clean or otherwise (**C**). Only clean reads were used for subsequent mapping and analysis. Reads containing N (where uncertain nucleotides were >10% of the total read), reads of low quality (where >50% bases had <99% correct call rate) and reads with adapter contamination were filtered out of subsequent mapping and analysis. All samples had a high proportion of clean reads (96.44% - 98.01%) with the majority of error being adapter related in all cases.

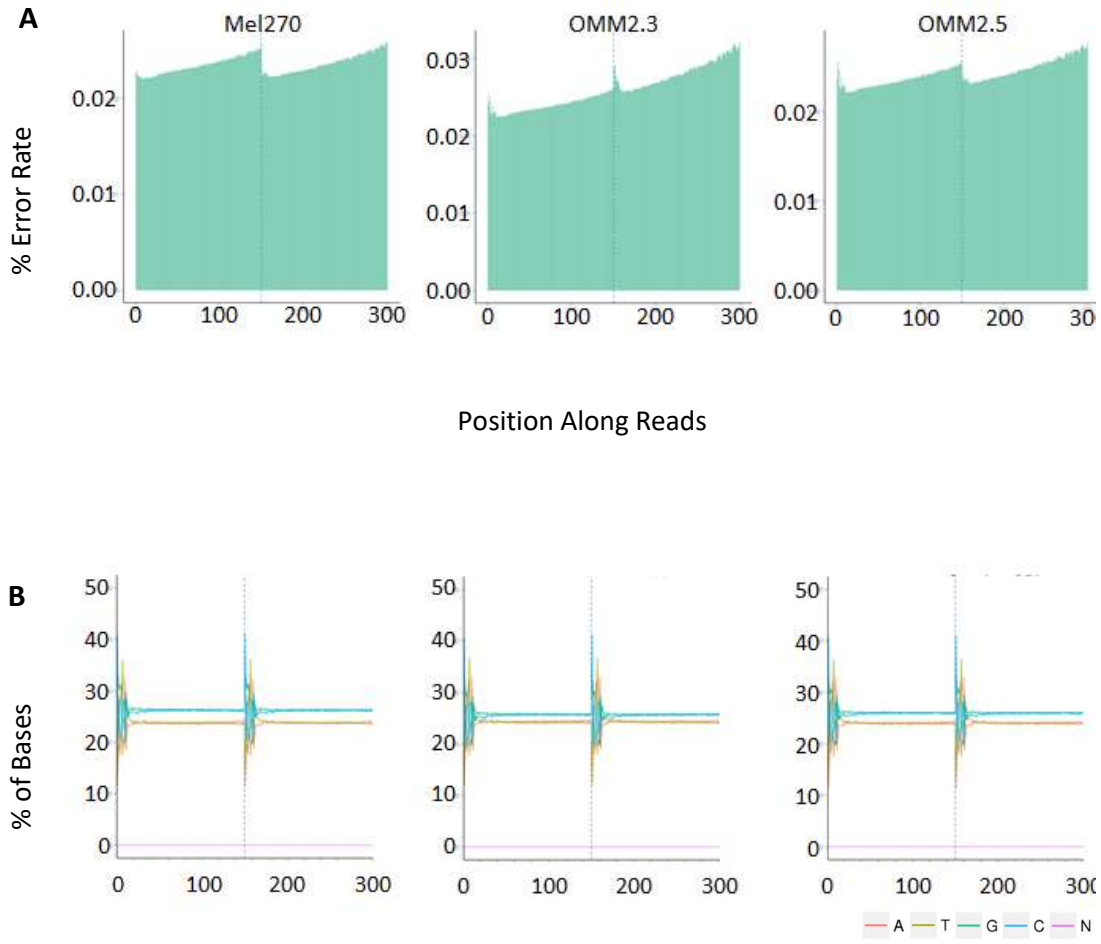
A
Mel270
OMM2.3
OMM2.5
% Error Rate
0.02
0.01
0.00
0.03
0.02
0.01
0.00
0.02
0.01
0.00
0
100
200
300
Position Along Reads
B
% of Bases
50
40
30
20
10
0
A
T
G
C
N
Position Along Reads
C
Mel270
OMM2.3
OMM2.5
97.1%
97.4%
97.7%
Clean Reads
Containing N
Low Quality
Adapter related

Appendix C

Percentage of reads mapped to different genome regions.

An example chart has been shown for each cell line, along with the average percentage of reads mapped to exons for that cell line. The low proportion of intron reads indicates the samples were free of pre-mRNA contamination and the low proportion of intergenic reads is the result of a well annotated reference genome.

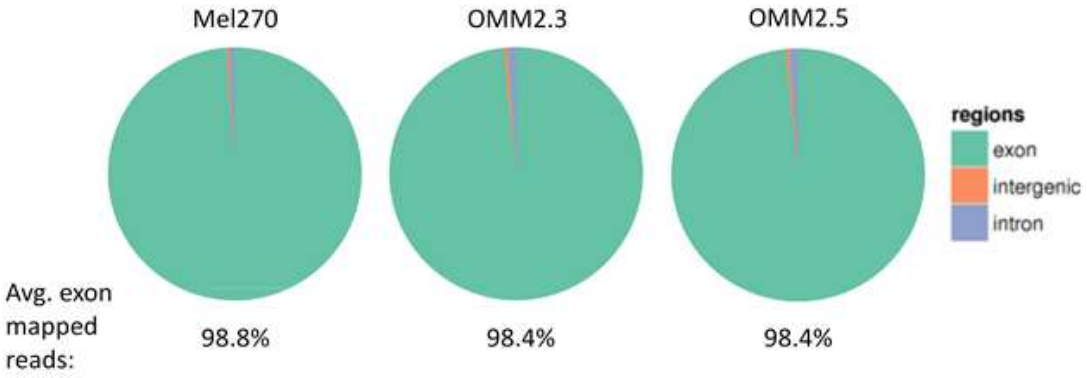

Appendix D

List of genes that were screened against the lists of differentially expressed genes.

A "+" indicates the gene was overexpressed compared to Mel270, a "-" indicates the gene was underexpressed compared to Mel70. "NDE" stands for not differentially expressed, these genes were not present in the list of differentially expressed genes. Entries in bold were shortlisted for the siRNA screen.

Name	Ensemble ID	Differential expression compared to Mel270		References
		OMM2.3	OMM2.5	
ATM	ENSG00000149311	-	NDE	(Fukasawa, 2007)
ATR	ENSG00000175054	NDE	NDE	(Fukasawa, 2007)
Aurora A	ENSG00000087586	+	+	
BANCR	ENSG00000278910	+	+	
BARD1	ENSG00000138376	-	-	(Fukasawa, 2007)
BNIP3	ENSG00000176171	+	+	
BRCA1	ENSG00000012048	NDE	+	(Fukasawa, 2007)
BRCA2	ENSG00000139618	+	+	(Fukasawa, 2007)
BRCC3	ENSG00000185515	+	NDE	
CAMK2A	ENSG00000070808	+	+	(Fukasawa, 2007)
CAMK2D	ENSG00000145349	+	+	
CAMK2G	ENSG00000148660	-	-	
CCDC14	ENSG00000175455	+	+	(Kodani *et al.*, 2015)
CDC20	ENSG00000117399	+	+	(Vidwans, Wong and O'Farrell, 1999)
CDC25A	ENSG00000164045	NDE	-	(Fukasawa, 2007)
CDC25B	ENSG00000101224	+	+	(Fukasawa, 2007)
CDC25C	ENSG00000158402	+	+	(Fukasawa, 2007)
CDK1	ENSG00000170312	NDE	NDE	(Fukasawa, 2007; Ogden, Rida and Aneja, 2017)
CDK2	ENSG00000123374	NDE	+	(Fukasawa, 2007)
CDK2AP2	ENSG00000167797	+	+	
CDK4	ENSG00000135446	+	+	(Fukasawa, 2007)
CDK5RAP2	ENSG00000136861	-	NDE	(Y.-C. Lin *et al.*, 2013; Kodani *et al.*, 2015)
CDK6	ENSG00000105810	+	NDE	(Fukasawa, 2007)
Centrobin	ENSG00000170037	NDE	NDE	(Gudi *et al.*, 2015)
CEP120	ENSG00000168944	+	NDE	(Comartin *et al.*, 2013)

CEP135	ENSG00000174799	+	+	(Y.-C. Lin *et al.*, 2013; Kodani *et al.*, 2015; Ganapathi Sankaran, Stemm-Wolf and Pearson, 2019)
CEP152	ENSG00000103995	+	+	(Ogden, Rida and Aneja, 2017)
CEP192	ENSG00000101639	-	NDE	(Kim *et al.*, 2013; Nasa *et al.*, 2017)
CEP295	ENSG00000166004	NDE	NDE	(Chang *et al.*, 2016)
CEP63	ENSG00000182923	+	+	(Ogden, Rida and Aneja, 2017)
CEP97	ENSG00000182504	+	NDE	(Spektor *et al.*, 2007)
CHK1	ENSG00000149554	NDE	NDE	(Fukasawa, 2007)
CHK2	ENSG00000183765	+	NDE	(Fukasawa, 2007)
CP110	ENSG00000103540	+	NDE	(Chen *et al.*, 2002)
CPAP	ENSG00000151849	+	+	(Mariappan *et al.*, 2019)
Cyclin A2	ENSG00000145386	+	+	(Fukasawa, 2007; Ogden, Rida and Aneja, 2017)
Cyclin B	ENSG00000134057	+	+	(Fukasawa, 2007)
Cyclin D1	ENSG00000110092	-	NDE	(Fukasawa, 2007; Ogden, Rida and Aneja, 2017)
Cyclin D3	ENSG00000112576	+	NDE	(Fukasawa, 2007)
Cyclin E2	ENSG00000175305	NDE	NDE	(Ogden, Rida and Aneja, 2017)
Cyclin G2	ENSG00000138764	-	-	(Fukasawa, 2007)
E2F1	ENSG00000101412	+	+	(Fukasawa, 2007; Ogden, Rida and Aneja, 2017)
E2F2	ENSG00000007968	NDE	NDE	(Ogden, Rida and Aneja, 2017)
E2F3	ENSG00000112242	-	-	(Fukasawa, 2007)
GADD45a	ENSG00000116717	+	+	(Fukasawa, 2007)
HSP90AA1	ENSG00000080824	+	+	(Fukasawa, 2007)
HSP90AB1	ENSG00000096384	NDE	-	
HSP90B1	ENSG00000166598	+	+	
HSPA6	ENSG00000173110	+	+	(Fukasawa, 2007)
HSPA7	ENSG00000225217	+	+	
IPO11	ENSG00000086200	-	NDE	
IPO7	ENSG00000205339	-	-	
KPNB1	ENSG00000108424	+	NDE	(Fukasawa, 2007)
LATS2	ENSG00000150457	-	NDE	(Fukasawa, 2007)
LMO4	ENSG00000143013	+	+	(Ogden, Rida and Aneja, 2017)
MDM2	ENSG00000135679	+	+	(Fukasawa, 2007; Ogden, Rida and Aneja, 2017)
Mortalin	ENSG00000113013	+	+	(Fukasawa, 2007)
MSH2	ENSG00000095002	NDE	NDE	(Fukasawa, 2007)

MTBP	ENSG00000172167	+	+	
MYC	ENSG00000136997	-	-	(Fukasawa, 2007)
MYCN	ENSG00000134323	NDE	NDE	(Ogden, Rida and Aneja, 2017)
NDRG1	ENSG00000104419	NDE	NDE	(Ogden, Rida and Aneja, 2017)
NEK2	ENSG00000117650	+	+	(Fukasawa, 2007; Ogden, Rida and Aneja, 2017)
Ninein	ENSG00000100503	+	+	(Kodani *et al.*, 2015)
NPM1	ENSG00000181163	+	+	(Fukasawa, 2007)
OFD1	ENSG00000046651	NDE	NDE	(Singla *et al.*, 2010)
p16	ENSG00000147889	NDE	NDE	(Fukasawa, 2007)
p21	ENSG00000124762	-	-	(Fukasawa, 2007)
p27	ENSG00000111276	-	NDE	(Fukasawa, 2007)
p53	ENSG00000141510	NDE	NDE	(Fukasawa, 2007)
PAK1	ENSG00000149269	-	-	(Fukasawa, 2007)
PAK1IP1	ENSG00000111845	-	-	
PARP-1	ENSG00000143799	+	NDE	(Fukasawa, 2007)
PARP-3	ENSG00000041880	-	-	(Fukasawa, 2007)
PARPBP	ENSG00000185480	+	+	
PIN1	ENSG00000127445	NDE	NDE	(Ogden, Rida and Aneja, 2017)
PLK1	ENSG00000166851	+	+	(Fukasawa, 2007; Ogden, Rida and Aneja, 2017)
PLK2	ENSG00000145632	+	+	(Fukasawa, 2007)
PLK3	ENSG00000173846	+	+	(Fukasawa, 2007)
PLK4	ENSG00000142731	+	NDE	(Fukasawa, 2007; Ogden, Rida and Aneja, 2017)
PML3	ENSG00000140464	-	-	(Fukasawa, 2007)
POC1B	ENSG00000139323	+	NDE	(Keller *et al.*, 2009)
POC5	ENSG00000152359	NDE	NDE	(Azimzadeh *et al.*, 2009)
PPP1CB	ENSG00000213639	-	-	
PPP1R12A	ENSG00000058272	+	+	(Fukasawa, 2007)
PPP1R14C	ENSG00000198729	+	+	
PPP1R15A	ENSG00000087074	-	-	
PPP1R16B	ENSG00000101445	+	NDE	
PPP1R35	ENSG00000160813	-	-	
PPP1R37	ENSG00000104866	-	NDE	
PPP1R7	ENSG00000115685	-	NDE	
PPP2R4	ENSG00000119383	-	-	(Fukasawa, 2007)
PPP4R2	ENSG00000163605	+	+	
PPP4R3A	ENSG00000100796	+	+	(Fukasawa, 2007)
PRKACB	ENSG00000142875	+	+	(Fukasawa, 2007)
PRKAR2B	ENSG00000005249	NDE	+	

Rad51	ENSG00000051180	NDE	NDE	(Fukasawa, 2007)
Rad51B	ENSG00000182185	NDE	NDE	(Fukasawa, 2007)
Rad51C	ENSG00000108384	+	+	(Fukasawa, 2007)
Rad51D	ENSG00000185379	NDE	NDE	(Fukasawa, 2007)
RAN	ENSG00000132341	-	-	(Fukasawa, 2007)
Ran-BP1	ENSG00000099901	+	+	(Fukasawa, 2007)
RCC1	ENSG00000180198	NDE	NDE	(Fukasawa, 2007)
RHAMM	ENSG00000072571	+	+	(Fukasawa, 2007)
Rint-1	ENSG00000135249	NDE	NDE	(Fukasawa, 2007)
RTTN	ENSG00000176225	-	NDE	(Chen *et al.*, 2017)
SAS6	ENSG00000156876	NDE	NDE	(Ogden, Rida and Aneja, 2017)
SCAPER	ENSG00000140386	NDE	+	
SKP1	ENSG00000113558	NDE	NDE	(Fukasawa, 2007)
SKP2	ENSG00000145604	+	+	(Fukasawa, 2007)
SKP2	ENSG00000145604	+	+	
SPICE1	ENSG00000163611	NDE	NDE	(Comartin *et al.*, 2013)
ST13	ENSG00000100380	+	+	
STIL	ENSG00000123473	NDE	NDE	(Ogden, Rida and Aneja, 2017)
TACC2	ENSG00000138162	-	-	(Fukasawa, 2007)
TACC3	ENSG00000013810	+	NDE	
Tankyrase 1	ENSG00000173273	+	NDE	(Fukasawa, 2007)
TPX2	ENSG00000088325	+	+	(Fukasawa, 2007)
TTK	ENSG00000112742	+	+	(Fukasawa, 2007)
TUBG1	ENSG00000131462	NDE	NDE	(Ogden, Rida and Aneja, 2017)
TUBG2	ENSG00000037042	-	NDE	(Dammermann *et al.*, 2008)
WDR62	ENSG00000075702	NDE	NDE	(Y.-C. Lin *et al.*, 2013; Kodani *et al.*, 2015)
XPO5	ENSG00000124571	-	-	(Fukasawa, 2007)
XPO7	ENSG00000130227	+	NDE	
XRCC1	ENSG00000073050	NDE	NDE	(Fukasawa, 2007)
XRCC2	ENSG00000196584	+	+	(Fukasawa, 2007)
XRCC3	ENSG00000126215	+	+	(Fukasawa, 2007)

Appendix E

MTS assays were used to determine the appropriate concentrations to use for the Aurora A inhibitor Alisertib (ALS) and the HSP90B1 inhibitor GRP94 Inhibitor-1 (iGRP94). Data shown are blank adjusted means of triplicate wells, normalised to a no treatment control for comparison between replicate experiments. An unusual "seagull" shaped curve was seen for increasing ALS concentrations, which may be due to Aurora B inhibition, which ALS will inhibit at higher concentrations. Concentrations that had a moderate effect on OMM2.3 cell viability were selected for future use: 100 nM ALS and 5 µM iGRP94.

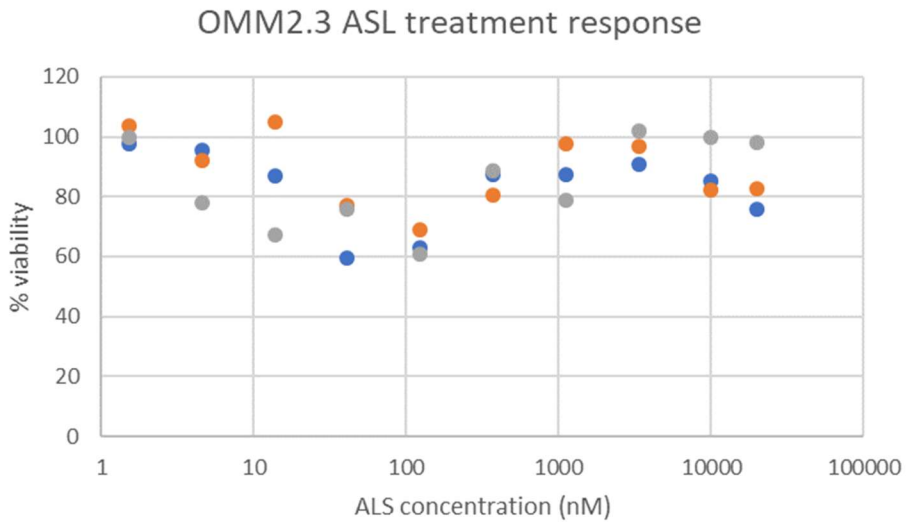

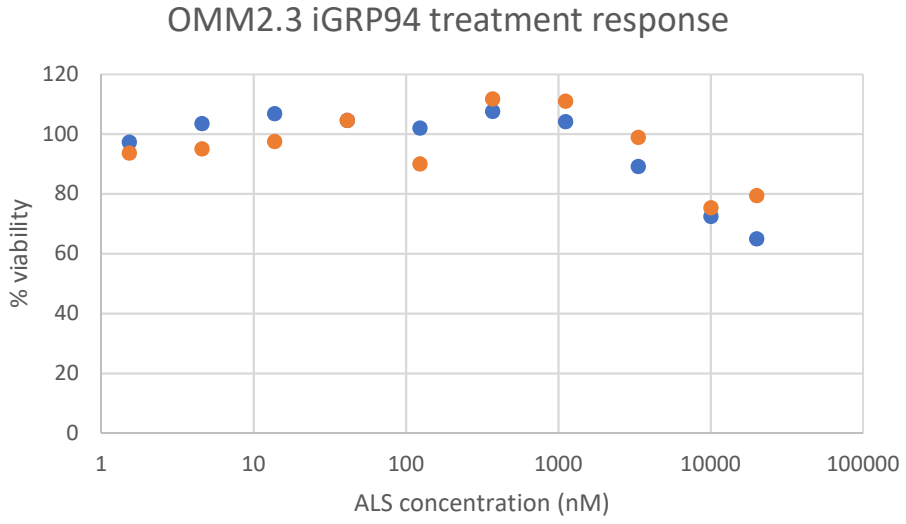

Appendix F

Transwell assay for migration and invasion of siAuroraA and siHSP90B1 treated Mel270 and OMM2.3 cells.

Transwell inserts can be used to measure cell migration or, when coated with a product mimicking the ECM such as Matrigel, to measure cell invasion. Uncoated and Matrigel coated transwells were used in an attempt to measure migration and invasion of Mel270 and OMM2.3 cells treated with siRNAs targeting Aurora A or HSP90B1. The Matrigel coating protocol was optimised before setting up the experiment and, when seeded on a certain thickness and concertation of Matrigel it appeared that cells had invaded. Unfortunately, no invasion was seen in the Matrigel coated inserts during the experimental setup, so only migration data has been presented. Migrated cells were stained with DAPI (**A**), and images were analysed using the StarDist plugin for FIJI (**B, C**). StarDist identified and segmented nuclei (**B**), and nuclei were counted using "Find maxima" (**C**). Nuclei counts for the different conditions has been presented (**D**). The uncoated inserts measuring migration were initially setup to normalise the invasion data to improve comparison between different experimental conditions. Considering the variation in control wells and the different siRNAs targeting the same gene alongside the fact that this data represents an n of 1, the conclusions that can be drawn from the results are very limited. It is possible that during optimisation, artefacts were mistaken for cells, and there were never any cells that had invaded. Further optimisation, such as a longer incubation time or coculture with fibroblasts, is needed to develop this assay with Mel270, OMM2.3 and OMM2.5 cells. Unfortunately, that was outside the scope of this work.

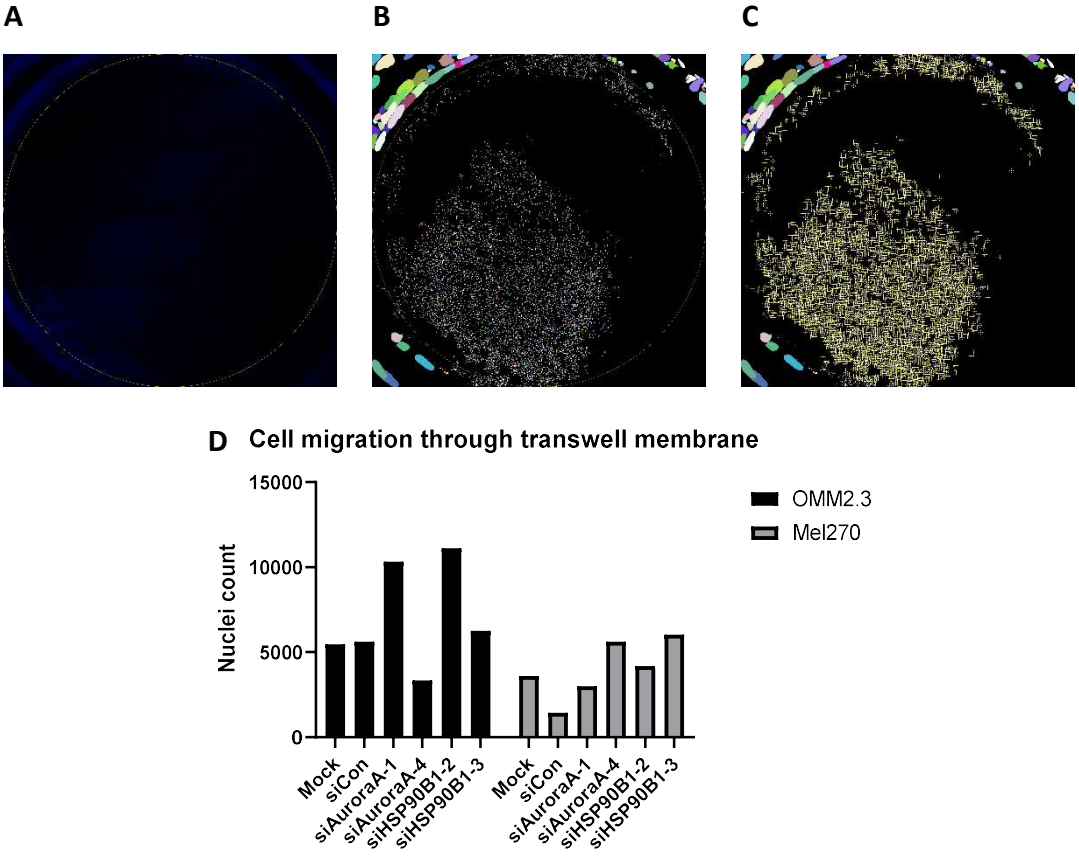
A
B
C
D Cell migration through transwell membrane
Nuclei count
15000
10000
5000
0
OMM2.3
Mel270
Mock
siCon
siAuroraA-1
siAuroraA-4
siHSP90B1-2
siHSP90B1-3
Mock
siCon
siAuroraA-1
siAuroraA-4
siHSP90B1-2
siHSP90B1-3